IRE Transactions

on Microwave Theory and Techniques

Volume MTT-7 OCTOBER, 1959 Number 4

In This Issue

PUBLISHED BY THE
essional Group on Microwave Theory and Techniques

IRE Transactions on Microwave Theory and Techniques

Volume MTT-7 OCTOBER, 1959 Number 4

TABLE OF CONTENTS

CONTRIBUTIONS

CORRESPONDENCE

A. Gardner Fox

A. Gardner Fox (A'40–SM'45–F'56) was born in Syracuse, N. Y. on November 22, 1912. He received the B.S. and M.S. degrees in electrical engineering from the Massachusetts Institute of Technology, Cambridge, in 1935.

In 1936 after a short time with the General Electric Company in Bridgeport, Conn., he joined the technical staff of the Bell Telephone Laboratories, where he was engaged in development work on mobile radio transmitters and an early radar project. In 1939 he transferred to the Radio Research Department of Bell Telephone Laboratories at Holmdel, N. J. and participated in the research on waveguide techniques being carried on under the direction of Dr. G. C. Southworth. For two years during the war, he was concerned with microwave radar antenna design at the Whippany Laboratory. In 1944, he returned to Holmdel, where he took part in the pioneering of the Bell System's first microwave radio-relay system and later engaged in millimeter-wave research. Since 1953, he has been in charge of a microwave physics group doing research on ferrites, dielectrics, and semiconductors. His present interests are concerned with problems of microwave amplification and modulation by means of ferromagnetic materials.

Mr. Fox has been active on the IRE Technical Committee and was chairman of the Committee on Antennas and Waveguides for several years.

The Communications Frontier Between Classical and Quantum Physics

A. G. FOX†

MAN'S sophisticated art of communications has been built upon his ability to generate and detect coherent electromagnetic waves. This art has been pushed to higher and ever higher frequencies, until now important experimental work is being carried on in the neighborhood of one millimeter wavelength.

At this point, however, we seem to have arrived at a barrier. The physical dimensions of vacuum tubes and diodes have been reduced to the limits of practicality, and there is little hope that further progress can be made with these devices. On the other hand, the field has been greatly stimulated by the advent of new concepts of generating, amplifying, and detecting radiation by maser and mavar[1] processes. These concepts offer promise of extending coherent wave techniques into the infrared and optical ranges. It is too soon to say what uses will be made of this part of the spectrum, but there is little doubt that coherent radiation will prove as powerful a tool at these frequencies as it has at lower frequencies. At the moment, however, we stand at a scientific frontier which challenges us with a number of stimulating questions.

What kind of a frontier is this? It might be called an infrared frontier, but this is only true in a narrow sense. It is also the frontier between coherent and incoherent waves. In the broadest sense, it is the frontier between classical and quantum physics.

In the past, classical physics succeeded well with most of the processes involving man-made, coherent radiation. When dealing with natural radiation produced by the random, incoherent emissions of individual atoms and molecules, the statistical approach of quantum mechanics was necessary. Since the two fields seldom overlapped, the fact that they employed different languages was of no great importance.

The comfortable separation which has existed between these two disciplines in the communication field is now dissolving. Masers use the paramagnetic moments of individual atoms to produce coherent waves, and quantum mechanics is the language used to describe their behavior. Ferrites also can produce coherent waves by means of atomic magnetic moments, but because these moments are strongly coupled so that they operate in a coordinated manner, their behavior is best described classically. The only real distinction between the two processes is the presence of the coupling forces. It is becoming very important, then, to break down the barrier between the languages of classical and quantum physics so that physicists and radio engineers can translate freely.

It might be argued that, in the future, radio engineers should learn more about quantum physics. This is certainly true, but it is not enough. The language of quantum physics involves the mathematical formalism of selection rules and density matrices, but it is lacking in the tangible physical pictures of atomic processes which the radio engineer would like to have. In the development of quantum theory, the demand for physical models of complex atomic processes often has seemed hard to fulfill. Useful results could be obtained by sidestepping the models and relying entirely on abstract mathematical symbolism. By now, it is frequently assumed that because the detailed mechanism of atomic processes cannot be absolutely determined, it is futile to seek physical understanding of them. The writer does not believe this. On the contrary, it is important to develop a physical understanding of quantum theory to the fullest extent possible.

This is necessary in order that the knowledge given to us by quantum theory may be fully exploited. The researcher, interested in ferreting out new facts of nature, may be content when he is able to express nature's processes in compact mathematical form, even though such a description may bring no physical understanding. But mathematics is primarily an analytical tool. It can express quantitative relationships, but it cannot tell how to use them to make something new and useful. This requires an act of creative imagination. And while there may be individuals who can create within a framework of mathematical symbolism, they are rare. Most inventors can create effectively only when they have a "physical feel" for the processes they are conjuring with.

As an illustration, it is not sufficient to know the power and frequency relations between the pump and the signals in a ferrite mavar or a ruby maser in order to build an operative microwave amplifier. It is also necessary to know what polarizations of waves will be absorbed and emitted by the atomic reactors when magnetized and pumped in given directions, and how these polarizations can be coupled to the electromagnetic modes of a cavity or waveguide. Thus, a considerable knowledge of spatial relations is necessary, and these can best be remembered and visualized if a physical model is available.

Finally, the attempt to find a physical interpretation of mathematical results has in many instances produced an improved understanding of basic physics.

Since the merging of quantum techniques and microwave techniques appears to be the coming thing, work in this field is particularly challenging today. The accumulated knowledge of atomic physics can be more quickly put to work in creating new devices for communications if a concerted effort is made to bridge language barriers and improve our physical understanding of quantum processes.

† Bell Telephone Labs., Holmdel, N. J.

[1] Also called variable reactance amplification, parametric amplification.

Mechanical Design and Manufacture of Microwave Structures*

A. F. HARVEY†

Summary—**The paper gives an account of the various aspects of the design and manufacture of microwave structures. The presentation of design information such as dimensions and tolerances is first discussed. Machining and other fabrication processes are then examined. Several methods of metal casting and associated techniques are described and the electrodeposition of waveguide components studied. Such final stages as inspection procedure, protective finishing and packaging are considered. The survey concludes with a bibliography.**

Engineering Features

Design Information

RECENT developments in microwave engineering have, to a large extent, been devoted to improved methods of design, manufacture and inspection. The essential parts of microwave structures are the surfaces which carry RF currents and the volumes in or around which the electric and magnetic fields exist. These parts are invariably internal and since they are required to be accurate in dimensions and smooth in surface their manufacture has presented special problems. There are currently a large number of manufacturing processes [68], [99], and several of these have been found [8] satisfactory for microwave structures. In the choice of a suitable method, the technical considerations to be taken into account include complexity and accessibility of replaceable components, reliability, reproducibility, possible multiplicity of techniques, size, and weight.

The bulk and weight of microwave assemblies can be reduced by employing compact types of transmission systems, *e.g.*, strip-line, dielectric-filled, and ridged waveguides. An alternative method consists in the use of topological rearrangement so as to form a compact configuration of components. This can be obtained by the elimination, as far as possible, of couplings, corners, twists, and conversion adaptors, to give an integrated assembly requiring less drawing and office work, and possessing greater robustness and simplicity of manufacture.

Miniaturization and simplification are achieved in the micromaze construction of Lewin [62]. An example is shown in Fig. 1(a). An integrated planar assembly was obtained by milling slots in a base- and cover-plate, into which partitions were inserted, thereby creating several waveguide channels side by side. Such built-in elements as hybrids, directional couplers, and filters, employed multipost construction [22]. The planar integrated assemblies described by Jamieson [52], [53] are suitable for structures containing hybrid rings and directional couplers. They permit several methods of manufacture and are economical for quantities of order of 100 off. An example is shown in Fig. 1(b).

Microwave structures are relatively expensive to manufacture and thus economy of the over-all production process is important. The cost of manufacture can be kept low by methods of mass production, because the special tool costs are spread over a number of items. This implies a degree of standardization of the product while consistency and good technique are obtained from specialization.

The ultimate inspection and testing of the article have an influence on the design. A high production yield, or diminished manufacturing cost can be achieved by relaxation of tolerances as much as possible. On the other hand, if the tolerances specified for individual parts are too lax, then the cost of rejection due to testing of and selection for the final complete assembly becomes high. Thus, it is evident that there is an optimum set of design tolerances. This optimum will, of course, be a function of the method of manufacture, procedure of testing, number of items produced, and other parameters.

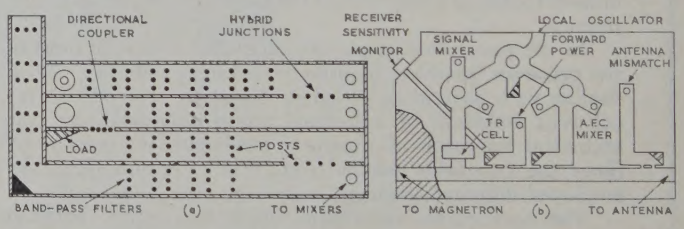

Fig. 1—Planar construction of microwave assemblies; (a) microwave repeater for 4 kmc using $2\times\frac{3}{8}$-inch waveguide, (b) typical RF head for 9.5 kmc using 0.9×0.4-inch waveguide.

Dimensions and Tolerances

To insure that the ultimate electrical performance of a microwave structure is satisfactory, it is necessary that drawings and specifications should state the exact manufacturing requirements in engineering terms. If the drawing merely outlines the conditions of mechanical interchangeability, then only minimum necessary data, often called control information, need be included. For example, in the bolted-type coupling shown in Fig. 2, the control information would include the diameters, the positions and lengths of the clamping holes, the squareness of the mating face, and the calling up of particular mechanical gauges. If, on the other hand, the drawing is intended for manufacturing purposes, addi-

* Manuscript received by the PGMTT, March 30, 1959.
† Royal Radar Establ., Malvern, England.

tional information would, in this instance, include material, secondary dimensions and tolerances, provision of chamfers, and surface finish.

The nominal dimensions in any given design are usually obtained by theoretical calculation and by electrical measurements on a prototype model. The guide wavelength and characteristic impedance of a waveguide depend on its cross section; since microwave structures are often resonant or contain critically spaced admittances, the dimensions of the internal volumes must be closely controlled. In practice, the tolerances required are 1/2000 to 1/10,000 of the free-space wavelength and thus range from 0.001 to 0.00001 inch over the microwave region according to the type of instrument or component. The small radius in the corners of rectangular waveguide modifies slightly the characteristic impedance. If this change is restricted to one part in 1000, then the permissible radii range from 0.002 to 0.050 inch depending upon the guide size.

The effect of a change in a nominal dimension on the electrical performance is not easy to obtain from practical data, and it is necessary to break down a structure into simple elements such as irises, transformers, posts, and teejunctions. The behavior of these can then be examined individually with regard to tolerances and the structure built up again, making due allowance for cancellation effects.

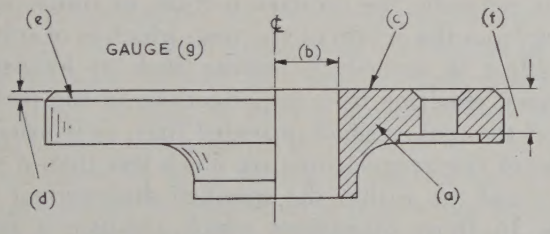

Fig. 2—Typical parameters requested on a drawing; (a) material, (b) toleranced dimensions, (c) surface texture, (d) flatness and squareness, (e) chamfers on mating face, (f) spot facing, and (g) use of inspection gauges.

As an example, Fig. 3 gives the tolerance on the width of an asymmetrical inductive obstacle of zero thickness plotted as a function of this width, both dimensions being expressed in terms of the cross section of the waveguide. The curves are constructed on the assumption that the obstacle is used as a matching device, the performance parameter being a/λ_g times the imaginary part of the reflection coefficient. Tolerances of the same order have been shown, in unpublished work by W. B. W. Alison, to exist for other types of elements and obstacles of both zero and finite thickness.

Tolerances tend to be especially close in structures such as rotating joints and polarizers where more than one mode may be propagated. For example, slight ellipticity in a nominally circular waveguide may cause a relative phase shift of two mutually perpendicular plane TE_{11} modes [80]. This means that both a circularly polarized and a plane polarized wave would be rendered elliptical by an imperfect waveguide. The phase errors have been examined in unpublished work by G. J. Rich and T. B. A. Senior. They may be calculated from the curve of Fig. 4 by taking the value of K and inserting it into

$$\phi = K(a - b)/a \tag{1}$$

where ϕ is the phase slip in terms of the nominal guide-wavelength and a and b are, respectively, the major and minor axes. For example, at a frequency of 9.375 kmc and a tube of diameter 0.875 inch, one meter in length, phase slips of 1.6° and 90° would be obtained for differences of diameter of 0.0001 and 0.005 inch, respectively.

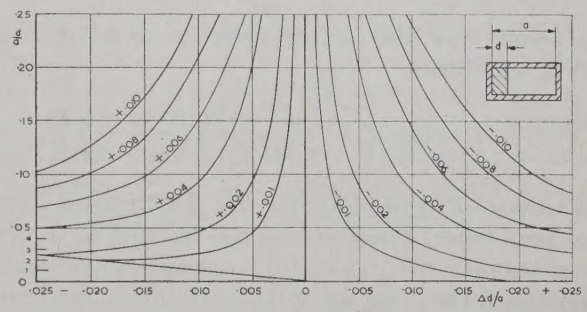

Fig. 3—Effect of dimensional tolerance on electrical performance. The figures on the curves are a/λ_g times the imaginary part of the reflection coefficient.

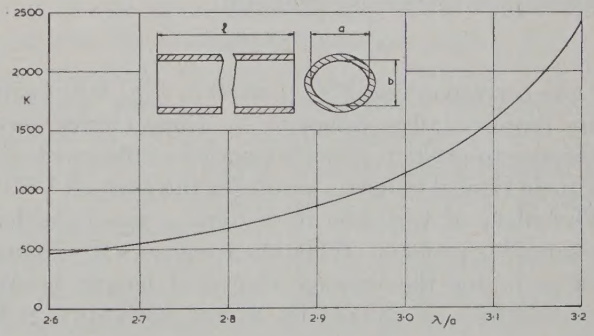

Fig. 4—Computation of phase errors in deformed circular guide.

A microwave structure will normally contain a number of toleranced dimensions and, if allowance were made for the worst case of all tolerances being unfavorable, then they would have to be unnecessarily close. Statistical relations between VSWR and attenuation and the magnitude and spacing of discontinuities in microwave structures were derived by Moore [67] and Mullen and Pritchard [71]. Their analyses assumed that the complex voltage reflection coefficients are small and additive so that

$$\hat{\rho} = \sum_{i=1}^{N} \rho_i e^{2j\theta_i}. \tag{2}$$

It was further assumed that the line lengths between discontinuities are independent of each other, that all values of θ between 0 and 2π are equally probable and

that the total number of discontinuities is large, say, $N>8$. It was shown that the over-all reflection coefficient has the Rayleigh distribution

$$W(\rho) = (\rho/\rho_m{}^2)e^{-\rho^2}/2\rho_m{}^2 \tag{3}$$

where ρ_m is the most probable value of ρ.

If ρ_0 is the rms value of the ρ's, then

$$\rho_m = (N/2)^{1/2}\rho_0. \tag{4}$$

The probability $P(\rho)$ that the reflection factor is less than ρ is given by

$$P(\rho) = \int_0^\rho W(\rho)d\rho = 1 - e^{-\rho^2/2\rho_m{}^2}. \tag{5}$$

This result may also be expressed in terms of S, the VSWR, as follows:

$$P(S) = 1 - \exp\left\{-\frac{1}{2}\left(\frac{S-1}{S+1}\right)^2\left(\frac{S_m+1}{S_m-1}\right)^2\right\}. \tag{6}$$

This value of $P(S)$ is plotted in Fig. 5(a) against S, with S_m as parameter. These curves can be used to compute the probability that, among a large number of possible designs with the same set of discontinuities, the VSWR of a particular design will be less than S.

Further results can be obtained if ρ' is defined as that reflection coefficient which there is only a 10 per cent probability of exceeding. Using (5),

$$\rho' = 1.52N^{1/2}\rho_0 \tag{7}$$

and the corresponding S' is plotted in Fig. 5(b) against S_0 for representative values of N. These curves permit a designer to predict, given a number of discontinuities and their typical values, a result for the over-all VSWR.

The effect of variation of frequency was considered as a sampling problem. When the frequency has changed sufficiently for the average electrical length between discontinuities to change by π, the individual reflection coefficients have changed their phases enough so that their sum can be considered as a new random variable. On this basis N_f, the number of independent frequency points spaced by Δf, is given by

$$N_f = f_b/\Delta f = 2f_b l/f\lambda \tag{8}$$

where f_b, l, f, and λ are, respectively, the bandwidth, line length, frequency, and wavelength. The joint probability that, at the N_f frequency points, there will be N_f cases when the reflection coefficient is less than ρ, is simply $P^{N_f}(\rho)$. The value of $P^{N_f}(\rho)$ is plotted in Fig. 5(c), using the normalized abscissa ρ/ρ_m with N_f a parameter.

In the specification of microwave structures, an upper limit should be given to the roughness [36] of the internal surfaces. The various grades of surface texture have been standardized [122] and are expressed, either as the rms or center-line-average height of the irregularities, in the range of 1–1000 microinches. For the short lengths of transmission line normally encountered in the average microwave equipment or when operation is at relatively low frequencies, a fine surface texture is not necessary. It becomes more important in the case of high Q-factor resonant cavities and in equipment for millimeter wavelengths. For general purposes [109] the surface roughness should not exceed about one half the electrical skin depth and thus, according to the frequency and material employed, values from 2–63 microinches are usually specified.

It is generally the primary texture, or roughness resulting from the action of the tool, which is of concern. The effect of secondary texture such as long-period waviness, resulting from imperfections in the performance of the tool, is small provided that, as is usual, the depths of the irregularities are much less than a wavelength and are within the specified dimensional tolerances. In those operations which produce a surface texture having a directional quality or lay, the method of manufacture should be such that this is parallel to the current flow where the latter is unidirectional.

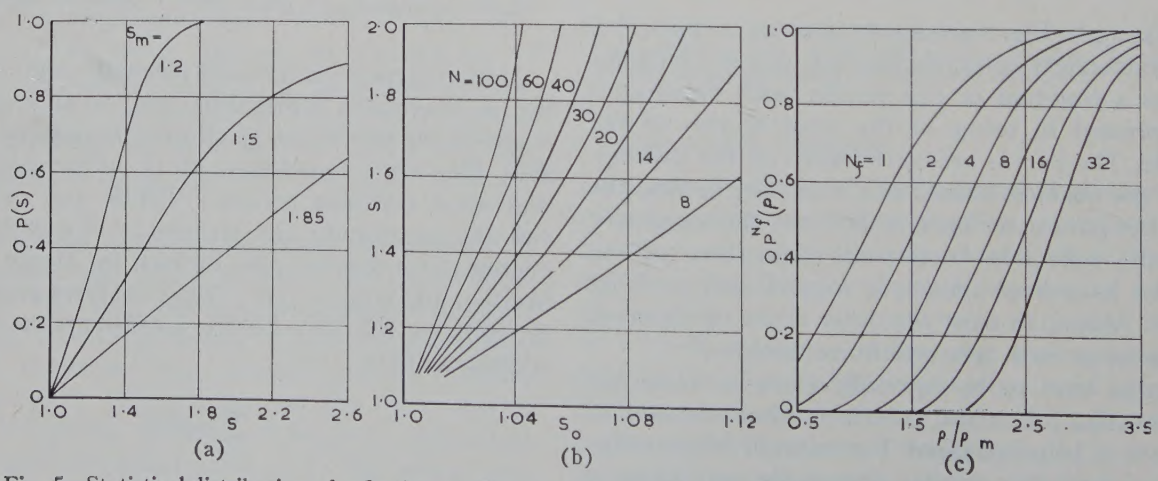

Fig. 5—Statistical distribution of reflection coefficients; (a) cumulative probability of VSWR, (b) VSWR exceeded in only 10 per cent of cases, (c) cumulative probability that the reflection coefficient is less than ρ in a frequency band f_b.

Machining and Allied Processes

Precision Machining

The manufacture of microwave structures, which demand dimensional accuracy and good surface finish, has always relied to a large extent upon precision machining involving skilled labor and high-grade machine tools. Some economy is achieved by the use of copying methods involving jigs or templates; these may take the actual form of the work or may exercise control remotely by mechanical or electronic means. Such tools are special to the particular item produced and their use is justified only for large quantities.

One of the simplest copy tools is a drilling jig for machining accurately-positioned holes. The use of fixtures enables broaching to be employed for the manufacture of microwave components. By commencing with an undersize circular hole, the use of a series of broaches enables parallel-sided sections of a variety of shapes to be obtained with high accuracy and good surface finish. If the teeth are omitted from one or more faces of the broach, then channels can be formed in mating pieces of metal. A machined face with, say, choke and gasket grooves can be turned by the use of a form tool; a similar technique can also be used for milling. Another tool method is copy milling in which the cutters are controlled, by means of a pantograph mechanism, from a master pattern.

Large quantities involving elaborate machining might justify the use of such automation techniques as electronic machine control. In these systems, operations like drilling, turning, or milling are controlled by numerical information supplied by magnetic or paper tape, punched cards, or hand setting on control knobs. This involves an extra process—that of translating the spatial information from the drawing or design into numerical control signals—which, once done, will enable the electronic control system to carry out the various processes with the maximum speed at which the machine tool is capable of operating. While the accuracy of the measuring and positioning devices may be as good as 0.0001 inch, the over-all accuracy of setting depends on other factors as well and may be about 0.0005 inch. The control methods employed fall into two main groups.

In discrete position control, the work piece is brought up to the operating tool in a series of fixed positions. For example, the work table of the machine has to be moved in two dimensions under the control of numerical information on the x and y coordinates of, say, the hole to be drilled. When the required point is under the drilling tool, the worktable is brought to rest by a form of servomechanism operated by an error signal generated by the difference between the control setting and the position of the worktable.

The method of continuous position control in which the work moves continuously past the tool is more complicated. The general principle for, say, milling a piece part to a certain contour is that the numerical input information provides sets of coordinates of marker points defining the contour while a computer interpolates the intervening points in suitable curves. In one design, the output of the computer consists of sets of pulses which specify completely the contour to be machined in terms of increments of distance from a given reference plane.

As an example of the process times involved, some data are given [51] for different methods of milling a planar integrated waveguide assembly. Precise milling operations, with a Kearney-and-Trecker machine, on rolled aluminum sheet required a time of 35 hours, and the use of precast blocks to eliminate the initial rough milling did not appear to be justified economically. The use of a Gorton copy-mill reduced the time to ten hours, while a Tracemaster machine, using hydraulic control and a power feed, reduced the machining time to five hours. Best results were obtained with an electronic-control power-driven milling machine which carried out the operations in a time of two hours. In all cases, the design accuracy of ± 0.001 inch was maintained.

Pressing and Hobbing

Pressing: Several methods of manufacture are based on the shaping of metal. Waveguide tubing of rectangular, circular and ridged cross section is invariably made by a drawing process [100] from a cylindrical billet. A variety of materials can be worked, and a bonded silver-sheath can, for example, be included inside a stainless-steel waveguide to give good conductivity and high mechanical strength. This method of manufacture is employed for sections ranging from 0.080 by 0.040 inch up to 11.50 by 5.75 inches. A small radius is required on the internal and external corners to give a reasonable life to the drawing dies.

Microwave components can be made from thin metal sheet by pressing it into U-shaped sections which are then soldered or riveted together to form the required shape. Contact shims can be made by stamping processes. Hot stamping of brass and other nonferrous metals is often employed. Typical examples are coupling flanges for waveguides of sections 0.50 by 0.25 inch to 6.50 by 3.25 inches.

Extrusion is a hot process carried out at a temperature near the plastic range of the metal. It has been used for the production of aluminum waveguide tubing. In impact extrusion, the component is formed under high pressure and may be used with metals such as magnesium. A pellet or small ingot is placed on the lower half of a hardened press tool which has the inner form of the component. The upper half of the tool takes the shape of the exterior. As the press closes, both the pellet and tool being preheated, the metal is displaced to fill the cavity and thus forms the component.

Hobbing: In the process known as hobbing, a hardened steel tool, termed a hob and machined and ground

to a male replica of the required internal section, is pressed slowly into a metal blank and then withdrawn. The dimensions and form of the master are faithfully reproduced and no additional machining is required. Adequate support against bursting is required around the cavity and, to avoid providing excess material which subsequently has to be removed, it is usual practice to place the blank in a close-fitting bolster or nest made of nickel-chrome or other suitable steel. A typical arrangement is shown in Fig. 6. The press containing the hob should have a double-acting plunger and possess adequate capacity; a 200-ton bridge-press with pneumatic control has been found satisfactory for the hobbing of microwave structures. The length of the blank usually exceeds that of the cavity required in the finished component so that there is no need to force the hob right through the blank.

Microphotographs of etched sections of hobbed blanks have shown that this process involves considerable plastic flow of the material in both radial and axial directions [114]. This flow places limitations on the shapes of cavities that can be hobbed, but, even so, the method can be employed for a variety of sections ranging from the simple to the quite complicated. Only symmetrical structures can be hobbed and, to avoid the risk of tool breakage, the length of the cavity should preferably not exceed eight times the larger cross-sectional dimension.

Although iron and steel can be hobbed, the plastic flow of the material tends to favor the selection of nonferrous metals such as aluminum, brass and copper. Aluminum of 99 per cent purity, such as materials to BSS 1476EIC or 2L34, may be hobbed cold using a mineral-oil lubrication. Copper and brass, in view of their rapid work hardening, require heating to about 800°C before hobbing. This is preferably carried out in an electric muffle furnace, from which the blank is then transferred rapidly to its bolster. After hobbing, a period of 30 seconds is allowed to elapse, after which the blank, with hob in position, is quenched in water. The hob is then extracted cold, a process which gives minimum shrinkage, accurate dimensions, and good surface finish. Suitable materials are oxygen-free copper, and brass to BSS 251 which contains 61 per cent copper and $1/1\frac{1}{2}$ per cent tin; brass containing lead tends to crack and is thus not suitable.

Unless the dimensions are very small, the wear on hobs during use is negligible and they are thus ground to the size of the finished cavity, making a small shrinkage allowance in the case of hot hobbing. A small chamfer of about 0.001 inch is necessary on all sharp exterior angles to prevent cracks and splintering due to stress concentration. The hob is usually provided with a large head fitted with a flat face or collar to take the force applied by the press.

The steel used for the hob must be capable of deep hardening without distortion and must be of a dense, tough structure capable of withstanding compression

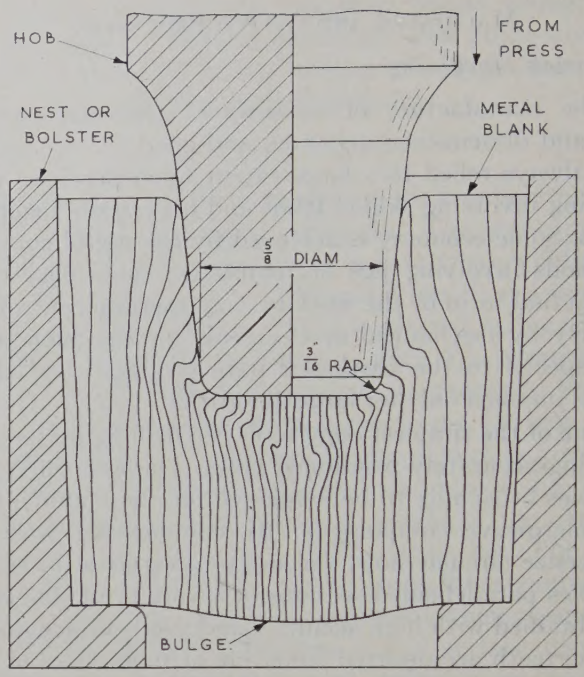

Fig. 6—Hobbing a metal blank. The general arrangement also shows the lines of flow in the metal.

loads up to 200 tons/inch^2. It must not "pick up" the softer metal of the blank and must permit smooth and easy withdrawal of the hob. In hot hobbing the material must be such that its temper is not drawn. A material found suitable for cold hobbing is 18 per cent tungsten high-speed steel; the other constituents being 0.75 per cent carbon, 4.5 per cent chromium, and 1.2 per cent vanadium. After heat treatment in two stages at 400–500°C, it is hardened at 1300°C, quenched in oil and tempered. The hardness figure required is about C62 Rockwell, with an ultimate tensile strength of 135 tons/inch^2. This material may also be used for hot hobbing, where maximum strength is desired, but an alternative for normal hobs, which retains its characteristics for a considerable period under hot working conditions, is an 8.5 per cent tungsten hot-die steel: the other constituents are 0.26 per cent carbon, 3.0 per cent chromium, 0.25 per cent vanadium, 0.5 per cent molybdenum, and 2.5 per cent nickel. After heat treatment at 800–850°C it is hardened at 1050–1100°C, quenched in oil and tempered to a hardness of C47 Rockwell and a tensile strength of 100 tons/inch^2.

Hobbing has found considerable application in the production of hollow structures with parallel, stepped, or tapered sides. The requirement of insertion and withdrawal of the tool does, however, mean that re-entrant shapes cannot be formed. The outside surfaces of the blank are machined to remove surplus metal and correct for the distortion which takes place during hobbing. The accuracy obtainable depends upon the complexity, but 0.001 inch is easily obtained with 0.0002 inch as a lower limit, and the repeatability of the dimensions is usually within 0.0001 inch. The surface finish depends upon the material of the blank but may be as good as

four microinches, while the bulk metal is nonporous and will withstand vacuum or high pressure.

A hob and an 18-vane magnetron anode made from it are shown in Fig. 7(a). In order to obtain a square shoulder, the hob is reduced in section and brazed into its holder. The hob shown in Fig. 7(b) was employed for producing an item containing two blind semicircular choke-grooves, 0.125 inch wide by 0.375 inch deep and 0.687 inch in radius, positioned in relation to the rectangular aperture of 0.90 by 0.40 inch within ± 0.001 inch [118]. A simple taper between rectangular waveguides can be made by means of the hob in Fig. 7(c), while the H-section aperture in Fig. 7(d) is an example of a component which could not otherwise be made.

Spark Machining

The spark-machining or erosion process was developed [63], [82], [111] mainly for producing holes in hard steels, but it has also proved useful in forming small apertures of complicated shape in microwave structures. The general arrangement is shown in Fig. 8, from which it will be seen that the process relies basically on an electrical discharge or spark taking place between an electrode and the workpiece. The discharges occur in rapid succession and the erosive action is greatly intensified by submerging both tool and workpiece in a suitable dielectric such as paraffin or light oil. Apart from cooling, the incompressibility of the liquid restricts energy release to a much smaller space, resulting in a considerable increase in energy density.

The cutting action starts when the gap between the tool electrode and the workpiece is narrowed down to the breakdown voltage. At the point of highest field strength, a spark will pass, pitting the workpiece and, to a smaller extent, the tool. The next spark will similarly discharge at another point where the field strength happens to be highest, and this process will be repeated, the spark always following the locus of the highest field strength.

The energy of the spark is derived from a bank of capacitors which is charged through a resistance from a high-voltage dc supply; the discharge takes place at the optimum voltage. The spark frequency is limited to about 10 kc by de-ionization effects in the gap. The total capacitance of the capacitors determines the intensity of the spark. This intensity affects the speed of cutting and the surface finish—the larger the spark the faster the rate of cutting but the rougher or more pitted the surface. There are a number of machines specially designed for this process. The U.K. examples of the "Sparcatron" made by Impregnated Diamond Products, the "Erodomatic" of Wickman, and the "G.K.N." of Welsh Metal Industries are typical.

In practice, there is a clearance of only 0.003 inch between the electrode and workpiece, and thus quite intricate forms can be produced. The choice of electrode material depends on the metal being machined and is important in view of the considerable wear which takes

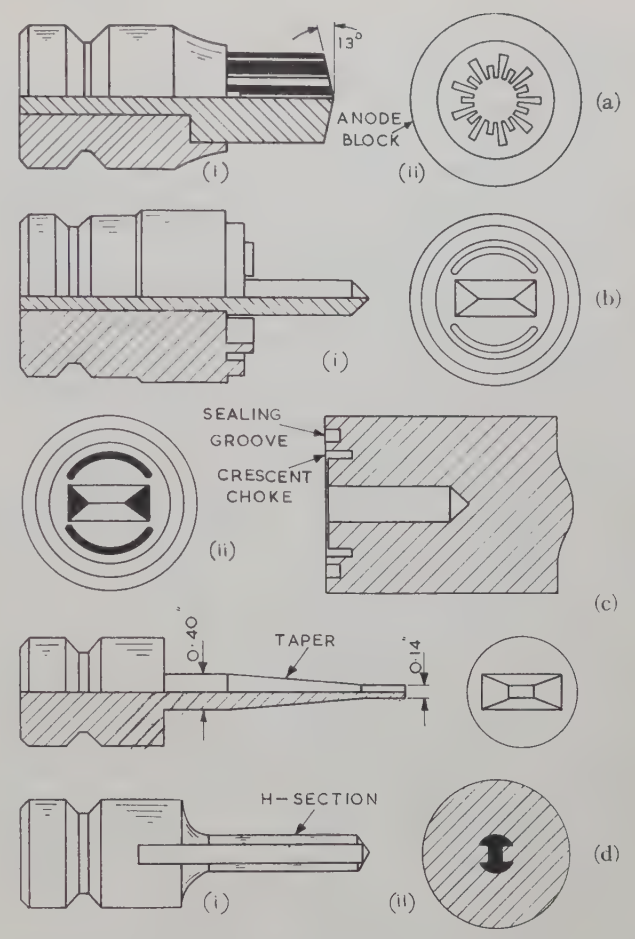

Fig. 7—Typical hobs and finished parts. The hobs are shown in (c) and in (i) of (a), (b), and (d); while the articles so formed are shown in (ii) of (a), (b), and (d).

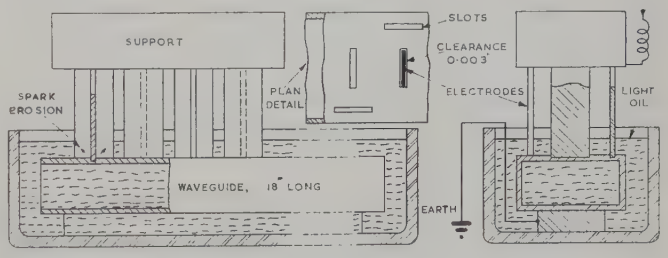

Fig. 8—Manufacture by spark machining. Example shown is a multiple-slot directional-coupler in 0.9- by 0.4-inch ID, 0.05-inch wall, waveguide. The operation is half completed.

place. Normally the electrode wears or erodes at about one sixth the speed of the workpiece, and thus the hole is initially slightly tapered. This is eliminated when the electrode has passed through the work, for the unused portion opens up the hole to the correct size. Dimensional accuracy of the order of ± 0.002 inch/inch with a surface finish of 20–30 microinches can usually be achieved. In the illustration, the small transverse and longitudinal slots in a directional coupler are being spark machined; several are being done at one operation to save time. Spark machining has also proved satisfactory for linear antenna arrays with slots cut in the broad face and anode blocks of millimeter-wave magnetrons.

Methods of Fabrication

Soldering and Brazing

Waveguides in very small sizes, lightly-stressed components-supported inside equipment, and accurate test gear are usually designed for assembly by soft soldering, since the low temperatures involved minimize distortion [65]. Where mechanical strength and fatigue resistance are required, the parts are usually assembled by brazing [11]–[13]; this is a process in which the metals are joined without raising them to their melting point, by the use of a filler alloy of lower melting temperature which is drawn along the joint by capillary action [5]. Copper brazing [98] as well as the medium-temperature Easiflo processes may be employed. For complicated assemblies and production quantities, some suitable methods are furnace brazing, surface heating and induction heating, where temperature and operational times can be closely controlled [24].

Light alloys of aluminum and magnesium are often employed in the construction of microwave components [1], [84]. Such structures may be held together with epoxide resins [35] such as Araldite [70], provided some mechanical pinning is incorporated to give alignment and strength. The soldering and brazing of, for example, aluminum presents difficulties due to the film of oxide which rapidly forms on the surface. This oxide is refractory and requires active fluxes at high temperature for removal.

In one method of assembly, the contact areas are electroplated with copper and, after tinning, joined with soft solder. The oxide film can be removed at low temperatures by various forms of vibratory soldering irons [73], [96], thus enabling tinning and subsequent soft soldering to take place. Such joints, because of the combination of metals present, are liable to corrode; but one example, after being coated with Araldite and cured at 130°C for 7 hours, successfully withstood humidity and salt-spray tests [107].

A number of special aluminium soft solders have been employed for microwave components [6], [112]. Zinc-based alloys have an operating temperature of 450°C to 500°C, but their penetration in lap joints tends to be variable. Another alloy contains 67 per cent cadmium and 33 per cent zinc, but its melting range of 265°C to 310°C puts its operating temperature above the satisfactory range for ultrasonic iron and organic flux application, and it therefore has to be applied to the aluminum surfaces by scratching methods. There are one or two tin-rich solders, *e.g.*, 76 per cent tin, 20 per cent zinc, 4 per cent aluminum, which have given satisfactory corrosion results but, in general, these results become increasingly suspect with solders rich in tin, cadmium, and lead; *i.e.*, the lower melting-range solders. One product, with a working temperature of 200°C, showed signs of corrosion after humidity tests.

Stronger and more reliable joints can be made with processes which employ pure aluminum, such as argon-arc welding [66]. The parts may then be given protection against corrosion [107], [121] by anodizing. A similar advantage exists with brazing processes [57], [91], [102]. The fillter rods used are of an aluminum-silicon alloy with a melting temperature some 50°C below that of the metals to be joined. The parts should be degreased and scratch-brushed to reduce the thickness of oxide. A suitable flux, preferably as a distilled-water suspension, is applied to the surfaces to be joined and also to the filler rod. The joints should preferably be of the lap type, and gaps should be of 0.005–0.015 inch and preferably tapered to assist the capillary flow of the filler. Flame brazing requires skill, but has been employed, for example, in the assembly of coupling flanges on waveguide tubing.

In dip-brazing, the component parts, which must be made of nearly pure aluminum and be suitably supported, are immersed in a bath at brazing temperature. Where jigs or fixtures are used, Wernz recommends that they be designed specifically for dip-brazing, since experience proves that hooked springs with locking bars, springs with key-hole slots, and similar holding devices are the most satisfactory [97]. The fixture body must be adequately braced to avoid warping during heating or cooling and, if necessary, provided with supporting legs. Fixtures should be made of materials such as Inconel, Nimonic, nickel and some stainless steels.

In salt-bath or flux-dip brazing, the joints are filled with a material rich in aluminum [17], [92]. The whole assembly is then immersed in a mixture of salts which acts as a flux and also raises the temperature to a value in excess of the melting point of the filler but below that of the aluminum. In such dip-brazing processes distortion is eliminated and cleaner and more uniform joints are obtained.

In another bath process, the joints are painted with flux and the assembly is immersed in a special alloy containing silicon in solution [104]. The aluminum oxide film is removed under the action of the hot flux, and the metal along the joints takes in silicon from the solution, forming an alloy with a eutectic melting-temperature below that of the bath. The joint is thus made with a molten metallic deposit. The aluminum still continues to absorb silicon and, as the alloy changes in composition, so its melting point eventually rises above the bath temperature, thus enabling the parts to be removed.

A technique of self-jigging of waveguide components, providing lighter and more flexible designs, involves the use of brazing-alloy-clad aluminum sheet [108]. This sheet is punched to the required size and shape and assembled by an interlocking tag-and-slot construction. Tolerances on 0.90 by 0.40 inch waveguide parts can be maintained, after dip-brazing, to within 0.002 inch. Using this technique it has been possible to produce a complicated assembly weighing only one pound. A similar system produced by die casting weighed eight pounds.

Bending and Twisting

In the bending of both circular and rectangular waveguide, care must be taken to avoid distortion. The bent waveguide is thrown partly into compression and partly into tension about a dividing line termed the neutral axis. The part of the tube in tension must stretch, so that it becomes thinner in wall section, and the part in compression must shorten, so that the wall becomes thicker. These changes tend to zero at a short distance along the straight portion and beyond the tangent line of the bend.

Before bending the tubing, it is desirable to bright-anneal it at, for example, 500°C in the case of brass and copper. One simple bending method, requiring manual skill, consists in filling the guide with materials such as hard waxes or fusible alloys like Cerrobend. A draw-bending method is then employed, the tube being gripped by form-and-clamping dies while being allowed to slip between the pressure-and-wiper dies. The tube is constrained by top and bottom plates and its outside surface is lubricated with mixtures containing, say, castor oil, graphite, white lead, or waxes. All surfaces which come into contact with the waveguide should be hardened, ground, and polished, to minimize friction and wear.

Better accuracy is obtainable with the mechanized process [118] shown in Fig. 9. The particular example is an *E*-plane bend of 3-inch radius in 0.90 by 0.40 inch guide. The tubing is formed in a tool which contains, between two side plates, an upper punch and a lower die. During bending, the punch is pressed slowly downward by a fly-press, while being guided by locating surfaces in the die. The waveguide is supported internally by mild steel strips [120] placed normal to the radius of curvature. A suitable material is Chesterman's 0.020-inch thick tape, which is just wide enough to enter the guide. Before they are loaded, the tapes are given a film coating of lubricating oil, and it is usually necessary to pull the last tape through with a motor driven attachment, a device also used for the final extraction after bending.

For even greater accuracy of section, the waveguide is degreased, annealed again and cleaned, the internal bore then being sized by having rollers pushed through it. In practice, a set of 10–20 rollers of varying diameter is employed, the smallest being 0.010–0.020 inch less than the final tube size. Each roller, as it is inserted, swages the metal of the walls and irons out any small irregularities. The rollers may be pushed through by the fly-press or, as illustrated, by a screw attachment to the bending tool.

An articulated drawing mandrel was used by Fuchs for producing bends in rectangular waveguide. This employed a draw-bending technique in conjunction with a hydraulic bender operating on an automatic cycle [34]. As the tube is bent by rotation of the form-and-clamping dies, the articulated links follow the curved

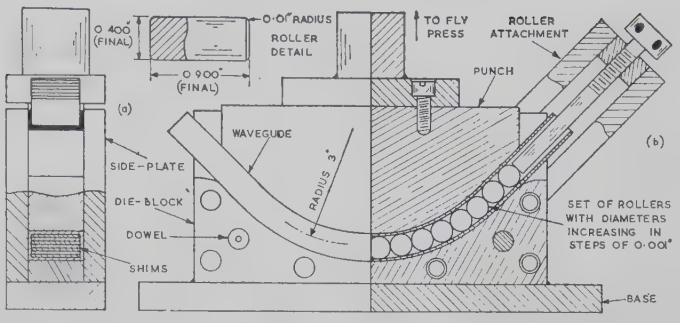

Fig. 9—Press tool for bending waveguides; (a) waveguide tube, with shims in position, during bending, (b) insertion of rollers for final sizing.

form and provide internal support. To avoid wrinkling, the faces of the wiper and form dies are offset by the amount of the increase in wall thickness. By this means, a production rate of 100 bends per hour can be achieved.

In small radius bending, the outer wall is severely stretched and fracture may occur. To reduce this tension, force can be applied to the end of the guide to cause compression. This "boosting" has the effect of shifting the neutral axis towards the outside of the bend. To prevent the tube from leaving the form die, in sharp or zero radius bends, support is given by a chain-like member. This method is also suitable for compound bends and for mitre-shaped tuned corners of various angles.

Rectangular waveguide may be twisted axially by a suitable fixture, distortion being minimized by the use of wax or fusible alloys as a filler. Steel tapes cannot be employed, but accurate sections have been obtained by 0.020-inch thick shims inserted transversely in the guide; after the twisting, these are simply pushed out. Step twists are considered as a small component and may thus be fabricated in any of the usual ways. This also applies to waveguide corners or elbows, whose method of manufacture depends upon the particular design and the quantities involved.

Precision Casting

Permanent-Pattern Processes

Conventional metal casting, in which a sand mold is made with a permanent pattern, is only employed for the larger microwave structures or when some finish-machining can be tolerated. In most cases, the various improved methods known as precision casting are preferred [33]. In one of these, centrifugal casting, the molten metal is poured into a cup or hole in the center of a revolving table and forced through channels into the molds by force [4]. Better quality castings are thus obtained because air pockets and occlusions are not formed.

In another modification, a shell-mold of fine sand and resin may, after removal of the pattern, be backed to form a smooth-surfaced refractory into which the metal can be poured. Such molds are compact and light, being simply placed on the foundry floor for cast-

ing. The risk of slight distortion in the baking process is avoided in the casting method in which the sand is mixed with a chemical so that the mixture sets hard in the presence of carbon dioxide.

Several precision-casting processes are based on the use of ethyl silicate, a colloidal ester of silica and ethyl alcohol [83]. In the presence of a small proportion of water or other reagent, this compound goes through a gelling process, finally condensing to a solid. It is usual to add to this reactive liquid sufficient powdered-refractory filler to form a smooth, easily-poured slurry. In the Shaw process, the slurry is poured over a pattern, preferably of metal, arranged to give the desired parting lines [123], [124]. After a short period, the mixture gels to a tough, rubber-like consistency and stripping is carried out. Complete elastic recovery occurs, so that there is no loss of accuracy, and the gelling process is then allowed to continue until completion. The structure of the mold material is such that there is no appreciable shrinkage during solidification while it is also very permeable. It is inert at temperatures up to 1800°C and is thus suitable for materials with high casting temperatures, especially as it is resistant to thermal shock. Another silicate process employs high-grade refractory fillers such as sillimanite, zirconite or molochite and allows the mold to set dry in position [106]. After removal from the pattern, it is then heated to give a finely-divided amorphous-silica bond with good mechanical properties.

To obtain castings with satisfactory internal surfaces, special attention must be given to the core material. In the Parlanti process the metal is cast around a stainless steel mandrel or core which, of course, can be used a number of times. In another process, plaster cores are used [106]. They are prepared from a standard plaster mixed with a refractory and a special hardening agent. After vibration to remove air bubbles the slurry is poured into highly polished core-boxes made of aluminum bronze.

The dimensions of the core-box allow for shrinkage in the subsequent operations. The cores set in about 20 minutes and are then removed to a stoving oven where they are slowly dried by gentle heating to remove free and combined water. The outside of the casting may be formed by any of the usual methods; and in the casting of corners in the 2.84 by 1.34 inch waveguide illustrated in Fig. 10, ordinary sand molding in boxes was employed.

Plaster cores possess high mechanical strength and have good crushing-resistance and venting properties. Furthermore, when they are wetted, the cores disintegrate freely into a soft mush which is readily flushed away, thus causing little damage to the internal surfaces of the casting. Plaster-core casting is suitable for alloys of copper, aluminum and magnesium; castings containing sections thinner than 3/64 inch are difficult to feed and porosity results, while only core shapes which can be withdrawn from the boxes are practical. The surface

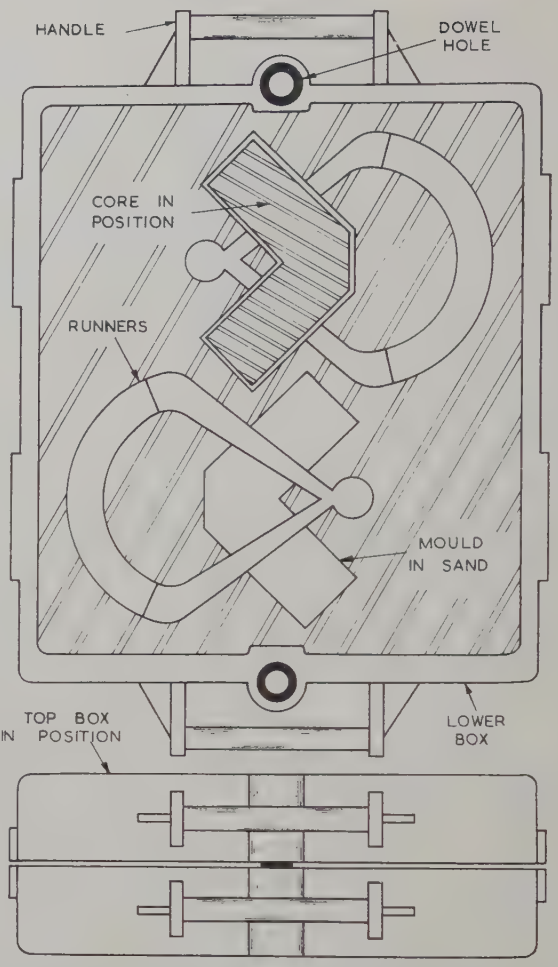

Fig. 10—Sand casting with plaster cores. The sand mold, with one plaster core shown in position, is for producing two waveguide corners at a time in 60/40 brass.

finish of the casting depends upon the plaster but is usually about 30–40 microinches. In aluminum alloys LM6 and LM8, typical tolerances are about ± 0.003 inch/inch with a minimum of ± 0.001 inch and a maximum of ± 0.010 inch.

Disposable Pattern Casting

Lost Wax: Precision casting methods may involve the use of disposable patterns. Such investment casting, as it is sometimes termed, essentially consists in making a pattern of the component to be cast, coating it with a suitable fine-grained refractory material and thus investing it to form a mold [16], [26], [116]. After disposal of the pattern, a cavity is left into which the casting metal is poured. The mold is then broken up to leave the finished article. The process is especially suitable for hollow parts and thus has been much used for microwave structures.

In the lost-wax casting process, the pattern material is simply a suitable wax [27], [29], [93]. This should preferably have a high melting point with narrow softening and melting zones. Production of exact wax models is essential and, although dies can be made of inexpensive materials such as rubber, plastics, low-melting

point alloys and plaster, for long runs and highest accuracy steel dies are advisable.

When liquid wax is injected into metal dies, difficulty arises in the avoidance of "sinks" and "draws" caused by contraction when the material is passing from the liquid to the solid state. It is important that the wax take up faithfully the fine detail of the die, and for small patterns this can be insured by injecting the wax at the lowest possible temperature, under pressures of 1500 to 2000 pounds/inch.[2] Turnbull describes a method for large patterns which consists of injecting the wax at a temperature of 20°C above its solidification point and at a pressure of 100 pounds/inch², and, 30 seconds after injection, removing the wax injector and applying compressed air at 100 pounds/inch² [94]. More complicated patterns can be made by vacuum wax-injection, as shown in Fig. 11(a). After the die is placed in position, the system is evacuated and wax is introduced under pressure through a slide tube on the top plate. Excellent surface finish is obtainable, but the operating cycle times are longer than with simpler methods.

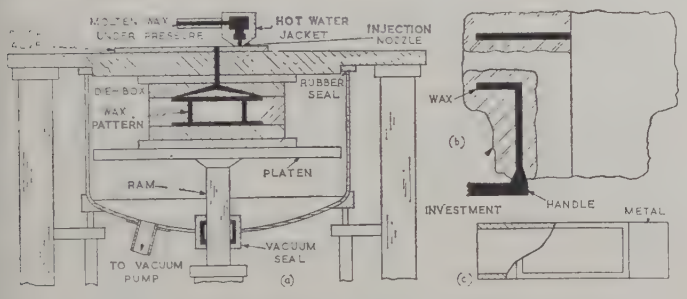

Fig. 11—Lost-wax investment casting; (a) vacuum wax-injection machine, (b) wax pattern with refractory investment, (c) finished cast article—an *H* plane, T junction.

Suitable investment materials include silica or similar refractory oxides suspended in an organic silicate, although others are employed for very-high-melting-point metals. The wax pattern is dipped in the slurry and, after it has been allowed to dry, another dipping is given. This process is repeated until the required thickness—normally $\frac{1}{4}$ to $\frac{1}{2}$ inch, depending upon the size of the casting—is obtained. The appearance is then as shown in Fig. 11(b). Removal of the wax by oven treatment tends to crack the investment shell, and it is preferable to employ a solvent vapor bath containing, for example, trichlorethylene. The wax is then available for reclaiming. The investment is then fired at about 1000°C for two hours to give a hard, strong mold of maximum porosity.

The casting metal is now poured into the mold and such conventional foundry techniques as pressure, centrifugal and suction casting may be employed. In some cases, the shell investments are packed in Nimonic boxes with a refractory mixture to give mechanical support. Aluminum, gunmetal, copper, magnesium and iron alloys can be cast in such molds without any interaction occurring. After cooling the mould is carefully broken away to leave the finished casting as in Fig. 11(c). The accuracy obtainable with the lost-wax casting of microwave structures is about ± 0.003 inch/inch and surface textures are in the range 60–80 microinches.

Lost Mercury: In the Mercast investment process [72], [117] the disposable pattern is made of frozen mercury and is cast in steel dies made to a negative of the finished casting. The die is machined to tolerances better than ± 0.001 inch, and allowance is made for the volumetric expansion of 3.47 per cent on melting. This low expansion of the pattern material means that thin shells, down to 1/16 inch, are usable and large and complex castings can be made. Frozen mercury is resistant to creep, so that mold dimensions are faithfully and consistently reproduced.

In the actual process the pattern die is filled with acetone, which acts as a lubricant, and then liquid mercury is poured in at room temperature, displacing the acetone. The die is now immersed in a freezing mixture of acetone and solid CO_2, the temperature being in the range -65°C to -95°C. The mercury sets because it has a sharply-defined freezing point at about -39°C. In some cases the mercury is poured into the cold die. To provide a convenient means of handling the pattern, a thick wire rod is placed in the filling hole so that it freezes into the mercury.

The die is opened and the pattern removed; it looks like and is about as hard as lead. Frozen mercury has a high rate of self-diffusion, so that when two surfaces are pressed into contact they will weld together. This facility is termed "booking," and advantage is taken of it to produce complicated shapes with intricate cored passages; this is facilitated by using suitably positioned dowels on the mating dies.

The pattern is then coated with the investment material in the usual way and is allowed to dry at room temperature. The mercury runs out and is reclaimed for further use. After firing, the mold is ready for pouring. A typical die, which employs booking, is shown in Fig. 12; the final article is an *E*-plane bend with flanges.

The dimensional tolerances obtainable are about ± 0.002 inch/inch [81]. For example, the cross-section dimensions and deviation of the axes in a component using 0.90 by 0.40 inch guide are about ± 0.003 inch depending on the complexity of the casting. A tolerance of ± 0.008 inch can be held on a 4-inch dimension. The minimum slot that can be incorporated in a casting is 0.040 inch for a maximum depth of 0.060 inch. The surface finish attained on aluminum-alloy waveguide castings is 30 to 40 microinches while corners can have radii as sharp as 0.020 inch.

The types of waveguide components which have been produced by this process include *E*- and *H*-plane bends, rotating-joint parts, hybrid rings, and similar components in copper-base and light alloys. Inserts such as irises and posts can be cast in position. An advantage of

the Mercast process is that in many cases structural features can be incorporated in the waveguide, thus conferring savings in manufacturing space and cost. Castings in light alloy weighing 300 pounds have been produced.

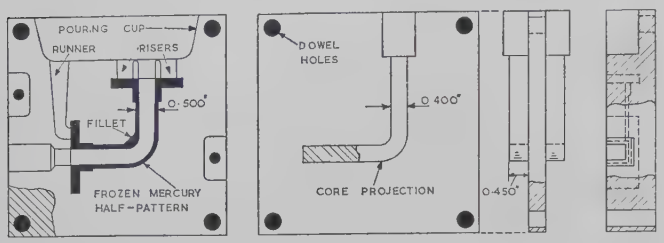

Fig. 12—Typical booking-die for Mercast process. The left- and right-hand die-halves are shown with the central plate. After the mercury is frozen, the plate is removed and the two die-halves booked together so that the two half-patterns become welded into one unit.

Permanent Dies

The casting of metal in permanent dies is a well-known technique [74] and has been employed for the manufacture of accurate waveguide parts. To facilitate extraction of the finished component, it is usually necessary to split it into two or more parts, the division of the waveguide being made, where possible, along the central E plane.

Although gravity-feed of the metal to the die has been used on a limited scale, better results are achieved with pressure die-casting. The tools must be very robust and may weigh as much as 10 cwts; they are also expensive and take several hours to reach operating temperature. Thus, this casting method is best suited to long production runs.

The easiest metals to die cast are low-melting-point zinc alloys such as Mazak, since they cast cleanly with a good surface finish. The electrical resistivity of these materials is not sufficient to eliminate their use for normal microwave components, but they tend to be brittle or have low shock resistance if there is the slightest trace of poisoning from other metals, such as cadmium. Any lack of purity of the zinc also leads to poor corrosion resistance and, although protection can be given by varnishing or chromating, such alloys have not found application in service equipment.

Materials such as brass can, with difficulty, be die cast, but the light alloys have been employed extensively for microwave components. To avoid distortion due to parting of the component from the tool during ejection, a considerable draw or taper must be provided. The larger the taper, the better the surface finish and the longer the life of the tool. While angles of $\frac{1}{2}°$ per side have been found just sufficient, there are advantages in employing a figure of 5°. The casting process is simplified and, if necessary, one of the sides may be made vertical.

Humphreys has designed such a hexagonal waveguide so that it mates with standard rectangular sizes, having the same impedance and cut-off frequency [48]. The geometry is shown in Fig. 13(a). If $\theta=5°$, $a=1.122$ inches, $b=0.497$ inch, then the dimensions of the equivalent hexagon are $a'=1.174$ inches, $b'=0.525$ inch. If $a=0.900$ inch, $b=0.400$ inch, then $a'=0.939$ inch, $b'=0.423$ inch. The effect of a small corner radius is negligible, and moreover it is likely to be present in both types of guide. The junction discontinuity gives a voltage reflection coefficient less than 0.005.

Satisfactory die castings have been made in L33 light alloy, containing 10–13 per cent silicon, with dimensional accuracies ± 0.002 inch/inch, and surface finishes of 10 microinches. A hybrid Tee, designed for die casting, is shown in Fig. 13(b). Both inductive and resonant irises are tapered and the usual post replaced by a tapered web. The shunt arm was made to standard dimensions of 1.122 inches by 0.497 inch, since it was broached to size. It is not practicable to carry the 5° taper along its entire length. The performance of this Tee was equally as good as that made by machining techniques with rectangular sections.

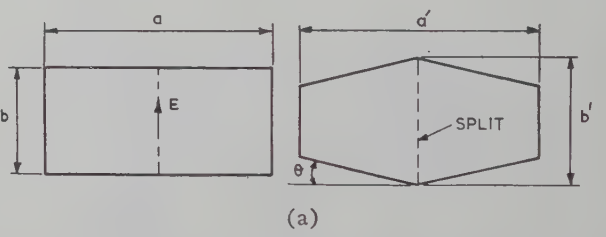

(a)

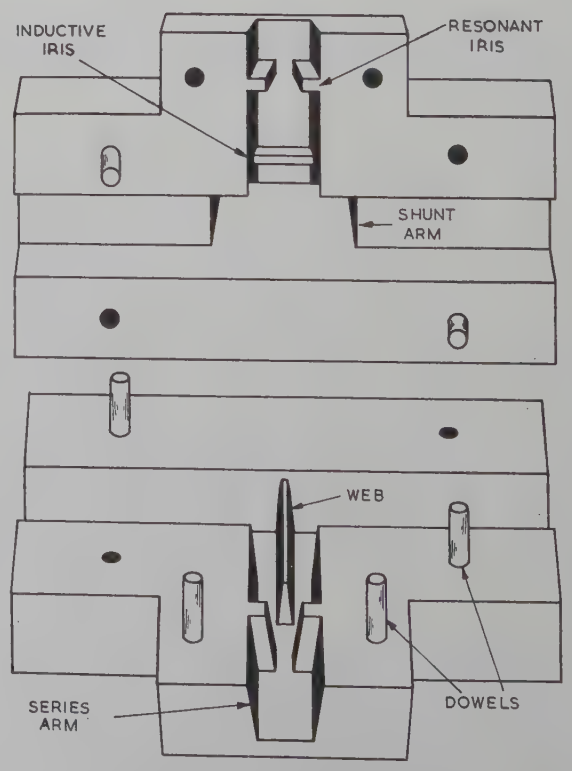

(b)

Fig. 13—Components made by pressure die-casting; (a) equivalent hexagonal guide-section; (b) hybrid-T cast die in aluminium.

Sintering and Spray Techniques

Powder Metallurgy

Sintering or powder metallurgy is a process of molding powdered metals, such as alloys of copper, zinc and aluminum [115], [119]. The finely divided metal is screened and compressed, or briquetted, in a die under pressures of 25–50 tons/inch^2 to form a compact mass. The part is then removed and transferred to a sintering furnace in which it is heated nearly to the melting point, a process that fuses the powder into a hard metal comparable in strength to a casting [60]. The process is practicable for metals such as tungsten which have very high melting temperatures.

The methods employed for the manufacture of metal powders are being improved with the objects of reducing their cost, *e.g.*, by making them direct from metal ores, and of providing better quality in the finished product, especially in strength, density, and ductility. For example, a modern pure iron powder, compressed at 27 tons/inch^2, sintered in dry hydrogen for one hour at 1100°C and then recompressed and resintered under the same conditions gave a density of 6.5 g/cm^3, a tensile strength of 10.8 tons/inch^2 and an elongation of 14.5 per cent. Stainless-steel powder corresponding to A.I.S.I.318, after somewhat similar treatment, gave a tensile strength of 41 tons/inch^2 and an elongation of 36 per cent. Fine-particle sizes are necessary for good physical properties, and grinding is able to produce diameters as low as 60 μ. The sintering atmosphere has an influence on the final product, while infiltration techniques, in which the pores are filled with a metal of lower melting point by capillary action, improve the physical properties.

In powder metallurgy, the costs of the die and of setting up production are high, and thus the process tends to be of use for the manufacture of large quantities of identical parts. The final items are often porous and are not satisfactory where pressurization is required. The high pressures used in molding mean that thin wall sections should be avoided while shapes long compared with the transverse dimensions are not practicable. Dimentional tolerances are about 0.004 inch/inch, and this process has, for example, been employed for wafer-type crystal mounts, a tolerance of ± 0.001 inch being maintained on a 0.280 by 0.140 inch aperture.

Metal Spraying

In the metal-spraying process of manufacture, the material is passed through a flame and blown, in a finely divided state, on to a retractable former until the required thickness of deposit is obtained [105]. The operation is carried out in a spraying booth which should have good air extraction. The available spray guns employ metal in either powder or wire form. A suitable gun is that made by Metallisation which takes 1½-mm diameter wire and contains a high-pressure air turbine. The gun weighs 3½ pounds and, to avoid fatigue to the operator, can be suspended from a support. Acetylene and oxygen are suitable for the flame jets.

The formers can be made of materials such as stainless steel. Before they are used, all traces of oil are removed by a degreasing liquid. To avoid bonding of the initial coat of sprayed metal, the former is coated, in a dust free atmosphere, to a thickness of 0.0003 inch with a synthetic lacquer which is then stoved for 15 minutes at 150°C. This lacquer is usually brightly colored to facilitate the visual observation of uniform thickness.

The metals that can be deposited include zinc, silver-cadmium alloy, silver-tin alloy, brass, copper, aluminum, tin, lead, nickel and its alloys, and steels, including stainless steel. Where silver-cadmium alloy, zinc or tin is employed for the initial deposit, this need only be about 0.010 inch in thickness. This can then be followed by brass, steel or other metal to any required thickness to give greater strength. It is essential that at no time must the temperature of the component rise to the melting temperature of the initial layer, and this is achieved by adjusting the rate of deposition or by air or water cooling of the former. The former can finally be removed by means of a press, and the lacquer dissolved with a suitable solvent.

The structure of the deposited metal tends to be porous, and the tensile strength is only 25 per cent of the wrought metal. Vacuum impregnation with a suitable resin can be used to increase the tensile strength up to the order of 60 per cent of the wrought metal and to render the component vacuum tight. The internal dimensions and finish tend to follow closely those of the original former.

The metal spraying process does not require skilled labor, and a typical taper waveguide of section 0.90 by 0.40 inch would take about twenty minutes. An *E*-plane 90° bend with a socket for waveguide connection can be deposited in 15 minutes, while a twist might take 30 minutes. A circular-section resonant cavity with either silver or gold internal finish has been produced in 0.4 per cent carbon steel, the internal-surface finish being 4 microinches and the bore diameter correct to within 0.0001 inch. Planar components such as hybrid rings and couplers can be made as thin shells, the backs of which are filled with an aluminum casting and an aluminum-powder loaded resin to achieve the required strength with economy of spraying time.

Electroforming

Plating Techniques

Electroplating techniques have proved useful in the manufacture of microwave structures. The conventional method of photoetching enables a thin foil to be produced containing an intricate structure such as the ladder circuit of a backward-wave electron tube or the common wall of a multislot directional coupler. This foil may be made thicker by electroplating, although the fine definition of the process may be impaired if the deposit is too great. Photoetching may be carried out with a number of metals including molybdenum [44].

In electroforming or electrodeposition, a former, in

the shape of the internal volume required, is electroplated to a thickness sufficient to provide adequate strength. The former is then removed to leave an electroformed blank. The material for the former may be of a permanent or expendable nature. The thickness of the deposit, which ranges from 0.04–0.40 inch, means that the electroforming process should have a high plating speed and good throwing power [59], while the deposited metal must be homogeneous, hard but machinable and free from defects.

Many metals can be electroformed [113]. Very hard deposits are obtained with nickel, chromium and nickel-cobalt alloy, but their throwing power tends to be poor. Light weight is provided by aluminum, but special electrolytes are required which must be operated in an atmosphere of dry inert gas. Deposition from fused mixtures of quarternary ammonium salts and an aluminum halide has been achieved [49], [79]. At an operating temperature of 30°C, current densities of $2A/dm^2$ and deposits 0.04 inch thick were obtained. Another electrolyte is based on a complex of sodium fluoride and aluminum tri-ethyl, with an operating temperature of between 80°C and 150°C [101]. Deposits 0.020 inch thick of very pure aluminum have been produced with hardness in the range of 24–33 Brinell. Heritage and Balmer [42], [43] have electroformed waveguide parts, with a bath composition [21] of 300-g aluminum chloride, 6-g lithium hydride and one liter of anhydrous diethyl ether. By employing a sealed vat to keep out moisture, satisfactory operation of the electrolyte was obtained for several months. The rate of deposition at $1A/dm^2$ was 0.0005 inch/hour, and coherent, ductile deposits up to 0.15 thick were obtained on simple cylindrical formers.

In microwave structures, the initial layers are either silver or copper to give maximum conductivity, the metal for the remainder being chosen for other reasons. Most electroforming is, however, carried out with copper, and various techniques have been described [20], [31], [37], [64], [87]. The conventional copper electroplating techniques [10] based on inorganic electrolytes give low throwing power, a metal hardness of B10–B55 Rockwell, and a rough deposit, but, because of their simplicity [3] and economy, they are commonly used.

Improved results [37], but with greater complication and expense, are obtained with the process developed by Jernstedt [54]–[56], which is based on an organic electrolyte containing cyanides of copper and other elements. This process involves periodic-reverse plating in which the article being electroformed is made alternately cathodic and anodic, the net current-time product being, of course, positive. The optimum periods depend upon the shape and size of the formed article but generally lie between 20–100 seconds cathodic and 10–40 seconds anodic, when the respective currents are nearly equal. The anodic cycle deplates any unsound metal and the more sacrificial cycles are required for complicated shapes. A plating speed of 0.006 inch/hour is obtainable with current densities around $8A/dm^2$ at a temperature of 85°C, or 0.002 inch/hour with lower current densities and temperatures down to 50°C. Even and symmetrical deposits are achieved if the former is slowly rotated in the bath, while the solution is agitated and continuously circulated through filters and a purifier containing activated charcoal. The metal deposited is ductile and machinable while photomicrographs have shown freedom from inclusions. The hardness depends upon operating conditions but is within the range of B50–B100 Rockwell.

With any plating process the deposit tends to be less in regions of low electric field as in internal angles. Fig. 14 shows the result of plating on a former with corners of different radii. It will be observed that, with the process described, a constant thickness layer is deposited until the center of the circle is reached, from which point a crack develops. Thus, some radius must always be provided to insure a continuous internal layer of metal. Considerations of mechanical strength require an artificially increased deposit, and suitable methods of achieving this are shown in Fig. 15.

Permanent Formers

Where the shape of the article permits, permanent formers can be employed. These should be made of high-tensile steel, treated by passivation, and coated with a separating medium such as tin or chromium plate. Other materials which have been employed include Invar, molybdenum, titanium, glass, quartz, hard plastics, and stainless steel. The latter material has proved very convenient since it can easily be ground to complicated shapes. For example, a former $\frac{1}{2}$ inch in diameter and 3 inches long was made circular and parallel to within 0.00002 inch with a surface roughness of 4 microinches. After plating to a thickness of $\frac{3}{8}$ inch, the cavity diameter was within 0.00002 inch of that of the former, the ovality being 0.00005 inch and the roughness 5 microinches. These precise measurements show that electroforming is a very accurate method of manufacture for microwave structures.

Formers of cylindrical section are easily ground in the form of blades which are then brazed into stainless-steel heads, as shown in Fig. 16(a), while more complicated shapes are machined and ground in one piece, as in Fig. 16(b). Polythene stops are fitted during plating, and Fig. 17 shows a typical former after electrodeposition. The former or mandrel may be extracted by a simple machine after immersion of the assembly in hot water.

Components involving coupling apertures and slots can be electroformed with the aid of additional pieces, as shown in Fig. 18. These pieces should be of plastic to prevent shielding in the corners. Complicated components need multiple-mandrel assemblies, with support and alignment provided by jigs made of aluminum or stainless steel. Fig. 19 shows an assembly for electroforming a hybrid Tee, with a guide of 0.28 by 0.14 inch,

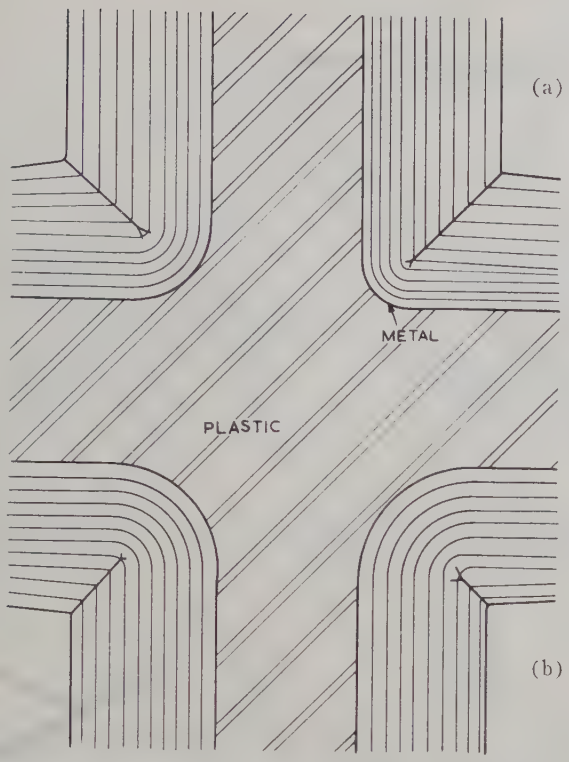

Fig. 14—Electrodesposition in corners of different radii; radii are (a) 0.040 inch, (b) 0.060 inch, (c) 0.100 inch, and (d) 0.120 inch.

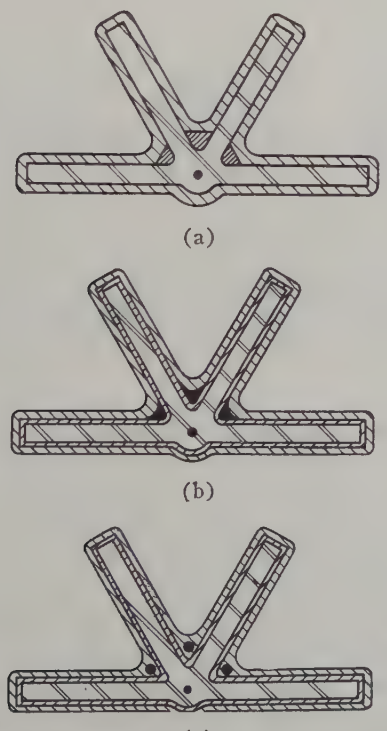

Fig. 15—Methods of increasing thickness of deposit in corners; (a) shaped metal inserts, (b) packing by solder, silver powder, amalgams or sprayed metal, (c) drilling out and plugging.

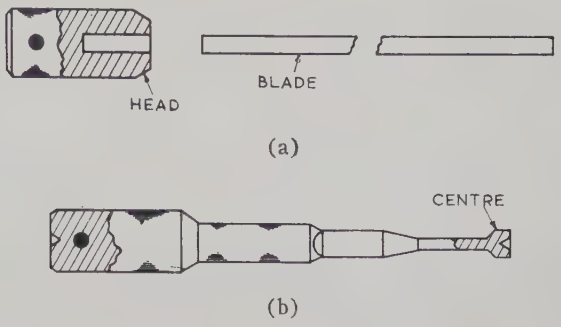

Fig. 16—Manufacture of permanent formers; (a) rectangular mandrel made separately and brazed into its head, (b) complex former with various sections made in one piece. The centre at the free end is removed in a final operation.

Fig. 17—Permanent former with electroformed piece still in position. The polythene stop provides a square face. This former has an extra cylindrical portion to serve as a guide during extraction and as a support for the electroformed piece in subsequent machining.

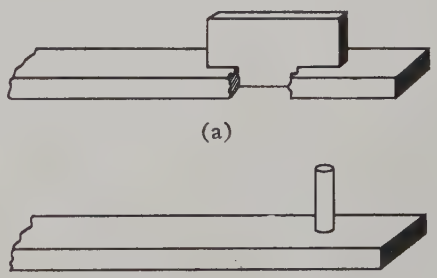

Fig. 18—Formers for the electrodeposition of components with coupling apertures. The strip in (a) and peg in (b) are made of plastic to prevent shielding in the corners thus formed.

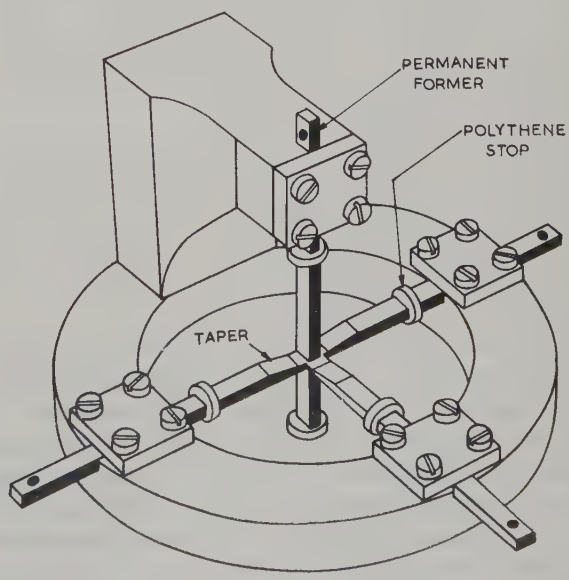

Fig. 19—Assembly jig with formers for producing a hybrid T.

while examples for other components are shown in Fig. 20. It will be noticed that inserts to provide corners or coupling apertures are used freely.

Disposable Formers

Disposable formers impose no restriction on the shape of the article to be electroformed. Suitable materials for these formers include aluminum which can be subsequently dissolved in dilute hydrochloric acid, hard waxes and fusible alloys which can be removed by melting, and plastics which can be removed by organic solvents. Plastic formers may easily be injection-molded and are thus suitable for quantity production. Methacrylate resins, such as Diakon, have a molding shrinkage as low as 1 per cent and small water absorption. By using automatic molding machines, in which the temperature of the die, the injection and cooling times, and other conditions are held constant with pressures of 15 tons/inch^2, dimensional accuracies of 0.0005 inch can be achieved [37]. Some examples of plastic moldings are shown in Fig. 21, where the guide section is 0.28 by 0.14 inch.

The surfaces of the plastic are given a conducting coat by evaporation of a metal in high vacuum or, more usually, by chemical silvering [41]. In the latter process, the former is degreased and then activated by immersion in an acid solution of stannous chloride. The actual silvering involves the reduction of a silver complex by a suitable reagent such as cane sugar, formaldehyde—Rochelle salt and hydrazine sulphate. This process can be carried out by dipping or, more conveniently, by a special gun from the nozzle of which two jets of the constituent solutions emerge to form, on coalescence, a thin adherent film of silver.

In the electroforming process, metal inserts of silver, or silver plate, may be employed which are held in position by simple clips. The shapes of these inserts should be such that sharp corners are avoided and a post, for example, should be shaped as shown in Fig. 22(c) to insure sound bonding and deposition. Flanges which are grown in position should be provided with tapers.

Fabrication of Electroformed Pieces

Although the complete microwave structure can sometimes be electroformed, it is more usual to carry out some additional machining and assembly operations. In such cases, the article should be supported on the locating internal surfaces by a mandrel of hardened steel, machined and ground to the required shape and provided with means for centering and driving.

The assembly of electroformed pieces is preferably carried out by soft-soldering to avoid distortion. The need for a soldered joint may be avoided by electrodeposition. For example, a hybrid ring has been made by machining the channels in a block of copper, temporally filling these with wax or plastic, and then electroforming the fourth side.

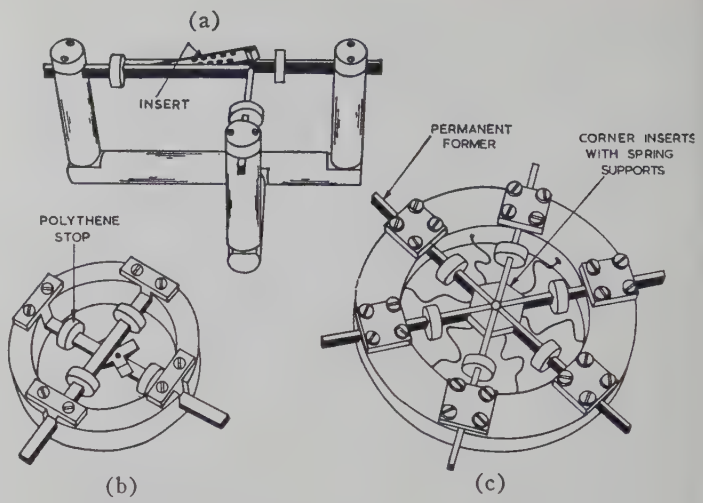

Fig. 20—Miscellaneous assembly jigs; (a) multiple-hole directional coupler, (b) cross-over directional coupler, (c) hybrid ring, two of the arms being finally plugged.

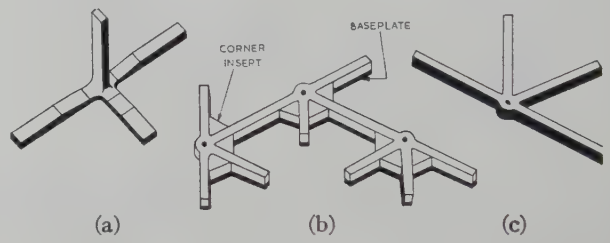

Fig. 21—Disposable formers made in plastic, waveguide size, 0.28 ×0.14 inch. The radii on the various corners are provided to assist electrodeposition. (a) Hybrid T, (b) multiple-ring, (c) single ring.

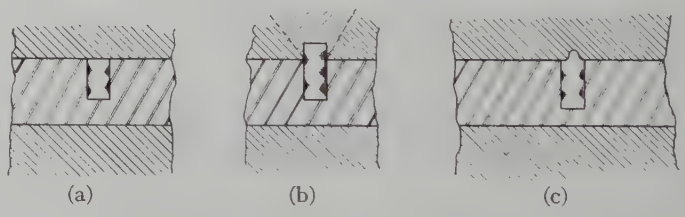

Fig. 22—Electroforming inserts in position using disposable formers. (a) The flush-fitting pin gives sound deposition but poor keying. (b) The protruding pin gives poor deposition but good keying. (c) The shaped protruding pin gives sound deposition and good keying.

Straight waveguides, electroformed to a large diameter, have been machined to form bearings for sliding parts such as post tuners. Locations for side arms in Tee junctions, cross-over connections and directional couplers may be similarly provided, eliminating the complication of strengthening supports. Electroforming is very suitable for the manufacture of taper transitions from one size or type of waveguide to another. Bends, corners and twists are examples of other components which can readily be made by these techniques [7].

The original former can be shaped so that, without any elaborate machining, the electroformed piece can provide proper housing and alignment [38] for such things as micrometer heads. This process has made relatively easy the manufacture of movable short-

circuits, wavemeters and stub-tuners in which plungers, actuated by micrometer heads, are moved along lengths of waveguide. Electroforming has been proven the only satisfactory process of making very small waveguides with sections down to 0.034 by 0.017 inch.

Increased strength can be given to an electroformed structure by metal spraying, using, for example, aluminum or brass, and supporting it in a jig or encapsulation in one of the resins employed in potted circuits [25]. Several components could be so encased to form a subassembly which would withstand mechanical shocks and adverse climatic conditions. Morrison [69] has electroformed the triple hybrid ring shown in Fig. 21(c) to a thickness of 0.040 inch by using periodic-reverse silver plating. The subsequent assembly was secured with Araldite in a stainless steel jig. Measurements on the component gave a loss of about 0.5 db and a discrimination between the arms not worse than 40 db over a 3 per cent bandwidth. Such results compare well with the prototype made by machining.

Inspection and Measurement

Inspection Methods

Inspection of and measurements on microwave structures are an important aspect of their manufacture. A satisfactory method of inspection must take into account the statistics of production. For example, if there are many toleranced dimensions on a component then one of these may be out by as much as 50 per cent of the tolerance without appreciably affecting the electrical performance. As a result, components will be rejected when, in fact, they are quite satisfactory. This is due, of course, to the remainder of the dimensions being well within tolerance and to the fact that the electrical performance is a function of all the critical dimensions involved. If the dimensional errors have a symmetrical distribution, then some waste can be avoided if the design gives the probable tolerances based on standard deviation.

The inspection of microwave structures has been shown in unpublished work by L. V. Byrne to fall into three principal methods: explicit mechanical inspection, implicit mechanical inspection, and electrical inspection. Which one or combination of these three general methods can be used depends upon the type of component, its shape and method of manufacture. Mechanical inspection in its broad sense includes visual inspection for such things as surface defects and faulty manufacture. Such inspection, although very important, is a subjective assessment depending on the skill and experience of the inspector and it is customary in microwave engineering to depend more on the actual measurements.

Explicit mechanical inspection means the direct inspection of the component by measurement of its size, shape, positions, and surface finish. If the inspection of a purely mechanical component such as a drawn waveguide tube is considered, the problems of measurement of size and shape can be readily appreciated. Waveguide couplings are of different types and size, but the basic functional requirement is common and necessitates the verification that features such as fixing holes, waveguide apertures and chokes are within tolerance.

Implicit mechanical inspection means inspection of the former, mandrel or tool from which the part is produced or assembled. Here again the measurement of size, shape, positions, and surface finish are involved. Such implicit inspection is common in microwave manufacture since the measurement of the significant internal dimension is virtually impossible in such components as bends, twists, double tapers, millimeter-wavelength parts and items of complicated shape such as hybrid Tees and rings. In one method of coupling-flange assembly, the two accurately sized and positioned locating holes are drilled after fitting to the waveguide by means of a jig. In such a case, inspection is directed towards checking the jig and insuring that it is properly used.

Electrical inspection involves the measurement of one or more specified electrical characteristics of the component the results of which usually provide the criterion of acceptance. Most routine tests involve measurement of the VSWR at defined points in the specified frequency band and attenuation at a specified, *e.g.*, midband, frequency. The great advantage of electrical inspection is that it gives a positive indication of the functional performance of a component, whereas mechanical inspection by itself, although always necessary in some degree, cannot prove with certainty that a component will fulfill its functional requirements.

The fact that measurements of individual dimensions do not alone insure a satisfactory component is especially true when more than, say, ten variables are involved. Brown has shown that, in these cases, microwave structures must be assembled on an electrical test bench by choosing one part as a central unit and adding others one at a time [14]. In this selective assembly, items which do not cooperate in the phase and amplitude of their reflections and produce a poor over-all performance are rejected until a place is found for them in later assemblies. This process is continued until the combination of tolerances or errors in the complete assembly is such that the test is passed. This process is facilitated if the VSWR meter is provided with some kind of visual display.

Mechanical Dimensions

There are two kinds of dimensional errors: random or accidental errors, and systematic errors. Random errors result from the inability of man and machine to achieve perfect reproducibility of objects made in quantity. These errors can be reduced to almost any desired degree if one is willing to take the time and pay the costs, but they can never be completely eliminated.

Random errors are distributed symmetrically about the "correct" dimension which is to be achieved. Systematic errors are caused by such things as mistakes in design and incorrect calibration of machine tools or measuring equipment. This type of error usually leads to an asymmetrical distribution with respect to the "correct" dimension. In either case, a determination of the actual dimension and its departure from the design value is required. This may be carried out by metrological or gauge methods.

Metrological methods involve the actual measurement of the mechanical dimensions by means of a suitable machine. This is an expensive process which is only employed when extremely high accuracy is required and in the prototype, type-approval or production-sample testing stage of a component in order to verify that such features as wall thickness, rectangularity, radii of inside and outside corners, displacement of rectangles, and internal dimensions are within their permitted tolerance. Typical machines can measure external and internal dimensions to within 0.00002 inch and angles to within 5 seconds of arc. This method may be simplified where larger quantities are involved by a comparator process, the item under test being replaced by a standard.

The usual method of checking mechanical dimensions of microwave structures is by some form of gauging. For example, the dimensions of a waveguide tube would be checked internally by "Go" and "Not-Go" plug gauges and externally by "Go" and "Not-Go" gap gauges. The explicit measurement of internal dimensions of long lengths can be achieved with pneumatic gauges of the Solex type. These consist of a loose-fitting plug fitted with one or more air outlets. The actual internal dimensions determine the amount of clearance and hence of the air pressure in the supply line. Such gauges are very convenient for medium sized waveguides. In order to check that the relative positions of these various features are within tolerance, a more complicated microwave component such as a coupling flange containing a rectangular aperture, fixing holes and a choke would necessitate a receiver or interchangeability gauge. A fixed-type receiver gauge is designed to accept a component in the maximum-metal condition, simultaneously making an allowance for the maximum positional tolerances. This means that all features must be individually checked to insure that they are within limits before the component is offered to the receiver gauge.

Surface Texture

The complete inspection of microwave structures must involve some means of measuring or comparing surface texture. In many instances this measurement can be carried out directly, but where the surface is inaccessible, as on the insides of chokes and very small waveguides, a nondestructive test is possible by making plastic replicas and then measuring their surfaces. In order to show the range of finishes which have to be measured, Table I gives values for a number of typical manufacturing operations.

TABLE I
SURFACE TEXTURE FOR VARIOUS METHODS OF MANUFACTURE

Method of Machining or Fabrication	Microinches
Turning, preliminary finish	63 to 125
Turning, ordinary finish	32 to 63
Turning, fine, ferrous metals	8 to 32
Turning, fine, nonferrous metals	4 to 16
Turning, diamond, nonferrous metals	2 to 8
Boring, ordinary	16 to 32
Boring, fine, ferrous metals	8 to 16
Boring, fine, nonferrous metals	4 to 8
Boring, diamond, nonferrous metals	2 to 4
Planing, ordinary	16 to 63
Planing, fine	8 to 16
Extrusion or drawing, mirror finish	8 to 32
Hobbing	8 to 32
Milling, ordinary	32 to 63
Milling, fine	8 to 32
Reaming, ordinary	16 to 32
Reaming, fine	4 to 16
Broaching, ordinary	16 to 32
Broaching, fine	4 to 16
Scraping	8 to 32
Burnishing	2 to 8
Grinding, ordinary	16 to 32
Grinding, fine	8 to 16
Grinding, super fine	2 to 8
Honing	1 to 8
Lapping	1 to 4
Superfinishing	1 to 4
Polishing	1 to 2
Casting, investment	63 to 125
Casting, polished dies	4 to 32
Powder metallurgy	63 to 125

Most of the listed methods can be put into one of three classes. The first has little or no lay and includes grinding, lapping, honing, superfinishing, and polishing, as well as casting and powder metallurgy methods. The second class is performed with sharp-pointed tools and has a lay in the direction of the movement of the work with respect to the tool, irrespective of which is fixed and whether the motion is in a straight line or in an arc. Operations in this class include turning, boring, flycutting, and planing; similar textures are given by extrusion, drawing and hobbing. In the third class, the tool is broad and the lay tends to be parallel to the width of the tool and at right angles to the relative movement of the work. This class includes roller-milling, broaching, reaming, scraping and burnishing.

An ideal machine for the measurement of surface texture of microwave structures would record the increase in the linear dimensions of the surface. Although this can be achieved by the photography of sectioned items, there appears to be no direct-measuring instrument [2]. In practice, surface finish is assessed in three main ways.

The first is visual and tactile, making use of experience. This is a completely subjective assessment and is liable to large error and much disagreement. The second method employs a measuring instrument and is the most accurate. It is a true comparator inasmuch as it can be calibrated against known standards such as gratings ruled on glass. The normal practice [78], [122]

in the United Kingdom is to traverse a stylus, the radius of whose tip does not exceed 0.0001 inch, over a short sampling length of the surface. The deviations of the stylus are recorded, after amplification, on a moving chart or displayed on an integrating meter. Such a measuring machine gives the center-line-average (cla) height of the irregularities. In the U.S.A., it is more usual to amplify the electrical output of a pick-up traversed over the surface. This gives the rms roughness value, which, for most types of surfaces is 1.11 times the cla figure and this factor can, in practice, be ignored. The principle of this stylus method and a typical record on a paper chart are shown in Fig. 23(a).

Very fine surface textures can also be measured by instruments based on optical interference [86], [88], [89]. As shown in the arrangement of Fig. 23(b), the lack of parallelism of fringes between the surface under test and that of an optically flat glass plate is a measure of the roughness. In one example, the optical system of the microscope is arranged so that the reference surface does not make contact with the specimen [103]. A slight tilt is given to produce the fringes, the difference in level of the specimen between any two of which is one half the wavelength of light chosen for illumination. With green light, an estimate of surface irregularity of 0.1 of a fringe is equivalent to 1 microinch. Such stylus and optical machines [90] are expensive and are hence usually installed in laboratories or standards rooms remote from the workshop.

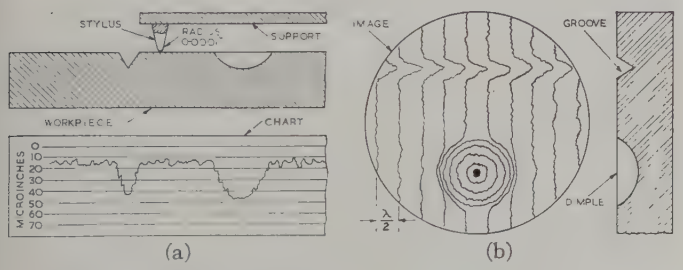

Fig. 23—Measuring surface texture by instruments; (a) mechanical stylus, (b) optical interference. The scale of the texture is exaggerated.

The third method is to employ comparator plates of known surface texture which are compared with the workpiece by appearance and/or sense of touch. It is thus desirable that the plates should include all three classes of finish. The textures shown in the particular example [36] of Fig. 24 are considered appropriate to the manufacture of microwave structures. In the preparation of these scales, the appropriate finishes were put on the ends of stainless steel plugs which were then mounted in an engraved circular copper disk. From this master, a negative copy was made by electrodeposition in nickel and thence positive copies were made in copper. The plates were then backed to give rigidity and given a chromium flash on the face for permanence. Such plates are inexpensive, portable and convenient to use. Errors arise in the texture values because of imperfections in the master and small changes which occur in the reproduction process; while errors in use arise because of possible different materials employed in, and variations of surface texture of, the standard and specimen. Provided care is taken in the visual and tactile estimation, the over-all accuracy is to within one-half of a scale step, which is considered reasonable in such a simple device.

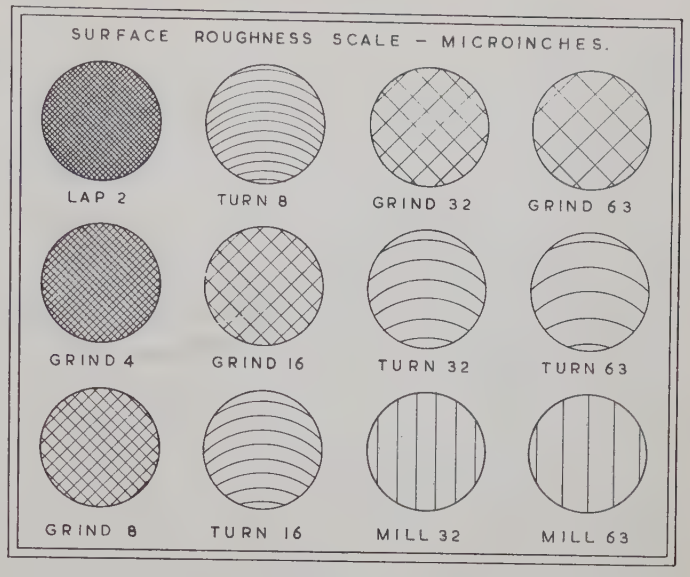

Fig. 24—Surface-texture comparator. The comparator is electrotype-copied in copper, the working surface being flashed with chromium. Over-all size is $4\frac{1}{2}\times3\frac{1}{2}$ inches, thickness $\frac{1}{16}$ inch.

Protection and Packaging

Internal Finishes

The performance of microwave component depends upon the condition [18] and finish of the internal surfaces which are mainly governed by the method of manufacture. The requirement of dimensional accuracy usually excludes any polishing or buffing operations, although these can give very smooth surfaces. Such operations are, in any case, not recommended for microwave surfaces since they tend to form an amorphous low conductivity Beilby layer [9], which may have a thickness up to one microinch.

For some metals, electropolishing provides a good surface finish. The principle is that of selective dissolution under the influence of current, whereby the surface is made progressively smoother and more brilliant. The actual mechanism appears to depend upon the presence of a viscous film of the products of interaction between the metal and the electrolyte [28], [75]. The film-electrolyte junction does not follow the metal surface irregularities so that the film thickness is not constant. This results in a varying current-density and preferential dissolution.

Chemical polishing produces a levelling effect on metals when a thin film of oxide or basic salt is present on the surface during the process [76], [85]. The surface is smoothed because slower diffusion of metal ions

from microdepressions than from microelevations causes the film over the elevations to be dissolved at a greater speed by anions in the polishing solution. The metals which can be chemically polished are copper, brass, bronze, nickel-silver, nickel, zinc, aluminum, iron, steel and most aluminum alloys. To obtain the desired result the total thickness of metal removed must be between 0.001 and 0.0015 inch.

Smooth surfaces are also obtained by bright electroplating which is achieved in silver baths by the addition of sulphur in the form, for example, of turkey-red oil and in copper baths by colloidal material such as gelatine. Electroplating, especially with gold and rhodium, is often employed to give increased protection against corrosion. This flash coating must be much thinner than the skin depth if increased loss is to be avoided.

The internal surfaces of microwave structures can also be protected by nonmetallic finishes. Varnishes that have been used include phenol formaldehyde, cellulose mitrate, varnish DTD Specification X17, seaplane varnish and beeswax dissolved in benzene. In the case of light alloys, anodizing gives good protection with negligible increase of attenuation. In general, it is recommended that the sealing facilities of standard waveguide couplings and fittings be employed, in conjunction with proper desiccator-breathing systems, to maintain the microwave system free from dirt, moisture, and corrosive atmosphere. The open ends of the transmission system should be sealed with polythene tape, windows or covers. More complex assemblies can be fitted inside boxes provided with means for sealing against moisture and variations in external pressure.

External Finishes

A large variety of external finishes are available including paints, varnishes, and resins, while corrosion inhibitors may also have applications [15], [77]. Electrolytic plating should employ a metal giving to the surrounding structures a potential difference not greater than 0.5 volt for ordinary purposes and 0.25 volt when exposure to the weather and salt-spray conditions is likely [110]. Nickel, cadmium, and tin have been found satisfactory under most conditions. For small laboratory instruments, plating with 10^{-4} inch of silver and 2×10^{-6} inch of rhodium [95] gives a hard-wearing and attractive finish which has good resistance to humid conditions. If wearing qualities are not required, gold is also a satisfactory finish.

A method of electrofinishing which is very suitable for microwave components is the Dalic brush-plating process in which metals are deposited from electrolytes held in absorbent pads attached to portable electrodes [45]–[47]. The pad is made the anode of an electrical circuit; the workpiece forms the cathode. The method has the great advantage that the article need not be immersed in an electrolyte and the deposit can be limited to a defined area giving good mechanical properties, high adhesion, and low porosity. The properties of the solution are important and are found only in aqueous solutions of complexed organic salts of the metals concerned. An extensive range of twenty or more metals can be deposited in this manner. The rates of deposition vary from 0.150 inch/hour for copper to 0.004 inch/hour for rhodium. The current densities are of the order of 500 A/dm^2.

The variable thickness of commercial electroplating on intricate shapes is not satisfactory for closely fitting parts such as locating bolts, sleeves and slides, and it is preferable that these should be made from corrosion-resistant alloys such as stainless steel, Tungum, nickel-silver and silver-bronze. Screw threads, especially those in stainless steel and light alloys, should be coated before assembly with graphite or molybdenum disulphide compounds to reduce liability of pick-up after prolonged use. In the standard range of waveguides, couplings and components for service and other arduous use the designs and materials have been chosen to withstand the full relevant specifications [39]. In certain circumstances protection against nuclear radiation may be required [61].

Packaging and Marking

Special care should be taken so that such precision items as microwave components and instruments, which are sometimes delicate, are packed so as to afford protection from damage and distortion during storage, transit, and handling. The open ends of waveguide tubing may be sealed with plastic inserts. In one test, a 24-inch piece of 0.90 by 0.40 inch guide, containing a small amount of silica-gel desiccant and sealed with an approved type of molded-polythene plug, was subjected to cycling between +25°C and +35°C in an atmosphere of 95 per cent relative humidity. After 14 days there was only slight loss of brilliance of the internal surface and an increase in weight of the desiccant, due to moisture absorption, of only 0.4 gm.

Waveguide tubing for service stores is normally packed so that each length is in a separate cleated case from which the guide is removed only when required for use. Small items such as electroformed pieces, dowel bolts and nuts should be enclosed in sealed polythene bags and packed in strong cartons. Coupling flanges, adaptors, bends and twists may, according to their size, be packed in cartons or wooden boxes, the mating faces of any fitted flanges being protected by molded plastic or similar covers.

Measuring instruments are usually supplied by the manufacturer in fitted wooden or plastic cases to which they should be returned when not in use. Equipment destined for use and storage overseas requires more elaborate packing. Such climatic or tropical packing protects the contents from the deteriorating effects of high humidity and extremes of temperature, and also of mold growth and insects.

Identification marking must be carried out so that no damage to the electrical, mechanical, and sealing proper-

ties of the equipment occurs. Light stencil markings or transfers are permissible in positions fulfilling no electrical or essential mechanical function, while transit, packing or instrument cases should be marked or labelled.

Acknowledgment

The author is indebted to the Engineering Unit, Royal Radar Establishment, to his colleagues on the Radio Components Res. and Dev. Waveguide Committee for useful discussion and assistance on this subject, and to J. R. Balmer for reading the manuscript.

References

[1] P. A. Akin, "Light-weight waveguides," *Electrical Mfg.*, vol. 53, p. 112; 1954.
[2] J. Allison and F. A. Benson, "Surface roughness and attenuation of precision drawn, chemically polished, electropolished, electroplated and electroformed waveguides," *Proc. IEE (London)*, vol. 102, pt. B, pp. 251–259; March, 1955.
[3] P. Andrews, "The electroforming of waveguide components," *Electronic Engrg.*, vol. 31, pp. 150–152; March, 1959.
[4] A. G. Arend, "Precision centrifugal casting of small parts," *Machinery*, vol. 68, p. 504; April, 1946.
[5] G. L. Bailey and H. C. Watkins, "The flow of liquid metals on solid metal surfaces and its relation to soldering, brazing and hot dip coating," *J. Inst. Metals*, vol. 80, p. 57; 1951.
[6] J. C. Bailey and J. A. Hirschfield, "Soldering aluminium," *Research (London)*, vol. 7, pp. 320–326; August, 1954.
[7] J. R. Balmer and T. W. A. Bailey, "Electroforming of waveguide components," *Electroplating and Metal Finishing*, to be published.
[8] T. Beardow, "Waveguide manufacturing techniques," *Brit. Commun. and Electronics*, vol. 5, p. 772; 1958.
[9] G. Y. Beilby, "Aggregation and Flow of Solids," Macmillan and Co., Ltd., London, Eng.; 1931.
[10] N. Blum and G. B. Hogaboom, "Principles of Electroplating and Electroforming," McGraw-Hill Book Co., Inc., New York, N. Y.; 1949.
[11] H. R. Brooker and E. V. Beatson, "Industrial Brazing," Iliffe and Sons, Ltd., London, Eng.; 1953.
[12] H. R. Brooker, "Soldering and brazing—their history and development," *Metal Industry*, vol. 60, p. 73; 1942.
[13] "A brief review of brazing processes," *Sheet Metal Industries;* October–December, 1947.
[14] L. W. Brown, "Problems and practice in the production of waveguide transmission systems," *J. IEE (London)*, vol. 93, pt. IIIA, no. 4, pp. 639–646; March–May, 1946.
[15] A. Bukowiecki, "A survey of corrosion inhibitors," *Schweiz. Arch. Wiss. und Tech.*, vol. 20, p. 169; 1954.
[16] E. L. Cady, "Precision investment castings," *Materials and Methods;* March, 1946.
[17] J. B. Campbell, "Brazing in salt baths offers production economics," *Materials and Methods;* January, 1951.
[18] R. G. Chambers and A. B. Pippard, "The Effect of Method of Preparation on the High-Frequency Surface Resistance of Metals," Inst. Metals, London, monog. no. 13, p. 281; 1953.
[19] J. L. Christie and A. M. Setapen, "The inspection and testing of brazed joints," *J. Amer. Welding Soc.*, vol. 26, p. 767; 1947.
[20] R. A. Cole, "Growing components by electroplating," *Aircraft and Missiles Mfg.*, vol. 2, no. 1, p. 29; 1959.
[21] D. E. Couch and A. Brenner, "A hydride bath for the electrodeposition of aluminium," *J. Electrochem. Soc.*, vol. 99, p. 234; June, 1952.
[22] G. Craven and V. H. Knight, "The design and testing of integrally constructed waveguide assemblies," *Proc. IEE (London)*, vol. 106, pt. B, pp. 321–334; May, 1959.
[23] A. E. Crawford, "Ultrasonic tinning techniques for aluminium," *Electronics*, vol. 25, p. 102; January, 1952.
[24] F. W. Curtis, "High-Frequency Induction Heating," McGraw-Hill Book Co., Inc., New York, N. Y.; 1944.
[25] G. W. A. Dummer and D. L. Johnson, "Printed and potted electronic circuits," *Proc. IEE (London)*, vol. 100, pt. III, pp. 177–191; July, 1952.
[26] A. H. Dunlop, "Investment precision casting," *Machinery*, October–November, 1953. See also *Proc. Inst. Brit. Foundrymen*, vol. 38, p. 1; 1945.
[27] "Precision casting by the lost wax process," *Foundry Trades J.*, vol. 75, p. 107; 1945.
[28] W. C. Elmore, "Electrolytic polishing," *J. Appl. Phys.*, vol. 10, pp. 724–727, October, 1939; vol. 11, pp. 797–799, December, 1940.
[29] H. Evans, P. S. Cotton and J. Thexton, "The lost wax process," *Machinery*, vol. 70, p. 645; June, 1947.
[30] A. A. Feldman, "Microwave components: precision casting and electroforming," *Materials and Methods*, vol. 30, p. 70; 1951.
[31] "Techniques for electroforming of precision waveguide components in the millimetre wavelengths," *Rev. Sci. Instr.*, vol. 28, pp. 295–296; April, 1957.
[32] P. Le Franc, "The 'Maproduct' process of precision castings," *La Technique Moderne*, vol. 47, p. 390; 1955.
[33] S. Freedman, "Cast waveguides," *Radio and Electronic Engrg.*, vol. 31, pp. 10–11; February, 1954.
[34] F. J. Fuchs, "Development in precision bending methods for waveguides," *Machinery*, vol. 92, pp. 824–834; April 11, 1958.
[35] A. G. Goodchild, "Epoxide resins in the electronics industry," *Brit. Commun. and Electronics*, vol. 3, p. 293; 1956.
[36] A. F. Harvey, "A surface-texture comparator for microwave structures," *Proc. IEE (London)*, vol. 102, pt. B, pp. 219–222; March, 1955.
[37] "The electroforming of components and instruments for millimetre wavelengths," *Ibid.*, pp. 223–230.
[38] British Patent No. 683246; November 26, 1952.
[39] "Standard waveguides and couplines for microwave equipment," *Proc. IEE (London)*, vol. 102, pt. B, pp. 493–500; July, 1955.
[40] F. Hassell and F. Jenks, "Electroforming microwave components," *Electronics*, vol. 19, no. 3, pp. 134–138; March, 1946.
[41] R. J. Heritage and J. R. Balmer, "Metallizing of glass, ceramic and plastic surfaces," *Metallurgia*, pp. 171–174; April, 1953.
[42] "Recent developments in aluminium electrodeposition," *Product Finishing*, vol. 10, no. 3, p. 54; 1957.
[43] R. J. Heritage, "The electrodeposition of aluminium," *Trans. Inst. Metal Finishing*, vol. 32, p. 106; 1955.
[44] H. A. C. Hogg, "Photo-etching molybdenum foil," *Proc. IEE (London)*, vol. 105, pt. B, suppl. no. 11, pp. 614–616; May, 1958.
[45] H. D. Hughes, "The Dalic plating process," *Machinery*, vol. 83; October 23, 1953.
[46] "Plating small localised areas," *Metal Industry;* February 26, 1953.
[47] "Practical brush-plating," *Trans. Inst. Metal Finishing*, vol. 33, no. 14; 1956.
[48] P. Humphreys, "Waveguide design for die-casting," *Electronic and Radio Engr.*, vol. 34, pp. 441–447; December, 1957.
[49] F. H. Hurley and T. P. Weir, "Electrodeposition of aluminium from nonaqueous solutions at room temperature," *J. Electrochem. Soc.*, vol. 98, pp. 207–212; May, 1951.
[50] A. H. Iverson, "Coupled helix winding machine," IRE Trans. on Electronic Devices, vol. ED-5, p. 317; October, 1958.
[51] E. Jamieson, "Functional integration of microwave components," *L'Ondé Elec.*, suppl. to vol. 1, pp. 266–269; August, 1958.
[52] "Integrated microwave test-bench," *Wireless World*, vol. 60, pp. 351–352; July, 1954.
[53] "Integrated microwave circuits," *Electronic Engrg.*, vol. 27, pp. 60–63; February, 1955.
[54] G. W. Jernstedt, "Periodic-reversal copper plating," *Proc. Amer. Electroplaters Soc.*, vol. 36, p. 63; 1949.
[55] "PR plating—a new tool for electroplaters," *Westinghouse Engr.*, vol. 7, pp. 89–92; May, 1947.
[56] "Better deposits at greater speeds by PR plating," *Plating*, vol. 35, p. 708; 1948.
[57] M. F. Jordan and D. R. Milner, "The removal of oxide from aluminium by brazing fluxes," *J. Inst. Metals*, vol. 85, p. 33; 1956–1957.
[58] T. A. Kaupoi, "Developments in silicones," *Stanki i Instrument*, vol. 36, p. 176; 1945.
[59] J. Kronsbein and L. C. Morton, "Distribution of electrodeposited metal on some simply shaped cathodes," *Proc. Amer. Electroplaters Soc.*, vol. 36, p. 229; 1949.
[60] G. C. Kuczynski, "The mechanism of densification during sintering of metallic particles," *Acta Metallurgica (USA)*, vol. 4, p. 58; 1956.
[61] D. C. Leeser, "The effects of nuclear radiation on engineering materials," *Materials and Methods*, vol. 40, p. 109; 1954.
[62] L. Lewin, "Miniaturization of microwave assemblies," IRE Trans. on Microwave Theory and Techniques, vol. MTT-4, pp. 261–262; October, 1956.
[63] A. L. Livshits and V. Ya Rassokhin, "Electro-machining methods for metals," *Stanki i Instrument*, vol. 25, p. 12, 1954; vol. 28, p. 8, 1957.
[64] W. H. Metzger and V. A. Lamb, "The design of electroformed parts," *Machine Design*, vol. 25, p. 124; 1953.
[65] J. L. Miller, "Modern Assembly Processes," Chapman and Hall, Ltd., London, Eng.; 1946.

[66] M. A. Miller, "Jointing aluminium to other metals," *Welding J.*, vol. 32, p. 730; 1953.
[67] R. K. Moore, "The effect of reflections from randomly spaced discontinuities in transmission lines," IRE TRANS. ON MICROWAVE THEORY AND TECHNIQUES, vol. MTT-5, pp. 121–126; April, 1957.
[68] T. Moreno, "Engineering approach to waveguides," *Electronics*, vol. 19, pp. 99–103; May, 1946.
[69] A. J. Morrison, "Electrojoining of millimetric waveguide components," *L'Onde Elec.*, suppl. to vol. 1, pp. 283–286; August, 1958.
[70] C. J. Moss, "Araldite—a new adhesive, coating and casting resin," *Brit. Plastics*, vol. 20, pp. 521–527; November, 1948.
[71 J. A. Mullen and W. L. Pritchard, "The statistical prediction of voltage standing-wave ratio," IRE TRANS. ON MICROWAVE THEORY AND TECHNIQUES, vol. MTT-5, pp. 127–130; April, 1957.
[72] W. I. Neimeyer, "Precision casting with frozen mercury patterns," *Iron Age;* March 17, 1949.
[73] B. E. Noltingk and E. A. Neppiras, "Ultra-sonic soldering irons," *J. Sci. Instr.*, vol. 28, pp. 50–52; February, 1951.
[74] F. D. Penny, "A Handbook of Die Castings," H.M. Stationery Office, London, Eng.; 1953.
[75] R. Pinner, "Theory of electrolytic polishing," *Electroplating*, vol. 6, p. 444; 1953.
[76] "Theory and practice of chemical polishing, Parts 1 and 2," *Ibid.*, pp. 360, 401.
[77] J. N. Preston, "Corrosion control with organic inhibitors," *Industrial and Engrg. Chem.*, vol. 44, p. 1755; 1952.
[78] R. E. Reason, M. R. Hopkins, and R. I. Garrod, "Report on the Measurement of Surface Finish by Stylus Methods," Taylor, Taylor and Hobson, Ltd., London, Eng.; 1944.
[79] W. H. Safranek, W. C. Schickner, and C. L. Faust, "Electroforming of aluminium waveguides using organo-aluminium plating baths," *J. Electrochem. Soc.*, vol. 99, p. 53; February, 1952.
[80] P. I. Sandsmark, "Effect of ellipticity on dominant-mode axial ratio in nominally circular waveguides," IRE TRANS. ON MICROWAVE THEORY AND TECHNIQUES, vol. MTT-3, pp. 15–20; October, 1955.
[81] H. H. Scholefield, H. H. H. Green, and R. E. Gossett, "Manufacture of waveguide parts by investment casting from frozen mercury patterns," *Proc. IEE (London)*, vol. 106, pt. B, pp. 431–434; July, 1959.
[82] M. G. Seed and H. Drubba, "Some aspects of spark machining," *Engrs. Digest*, vol. 15, pp. 378–380; September, 1954.
[83] C. Shaw, "The application of ethyl silicate to foundry practice," *Foundry Trades J.*, January 10, 1946; January 17, 1946.
[84] R. Sherman, "Aluminium waveguides for lightweight communication equipment," *Commun.*, vol. 27, p. 28; 1947.
[85] J. Sterenguel, "The chemical polishing of aluminium and its alloys," *Rev. Aluminium*, vol. 30, p. 261; 1953.
[86] W. Stray and G. Ogburn, "Measurement of surface roughness with microinterferometer," *Proc. Amer. Electroplaters Soc.*, (37th Annual Conf.), p. 125; 1950.
[87] A. H. Stuart, "Electroforming—practical details of available methods," *Electroplating*, vol. 1, p. 45; 1947.
[88] R. E. Sugg, "An interferometer for examining polished surfaces," *Mech. Engrg.*, vol. 75, p. 629; 1953.
[89] H. Thieisch, "Visual and optical evaluation of metal surfaces," *Metal Finishing*, vol. 49, p. 54; 1951.
[90] C. Timms and C. A. Seeles, "Surface finish measurements: comparison of styles and interference methods," *Metal Treatment*, vol. 18, p. 450; 1951.
[91] E. B. G. Trehearne, "Brazing," Brit. Welding Res. Assoc., London, Eng.; 1956.
[92] J. M. G. Turnbull, "Liquid brazing," *Engr.*, vol. 162, December 11, 1936; December 18, 1936.
[93] J. S. Turnbull, "Lost-wax process of precision casting," *Proc. Inst. Mech. Engrs.*, vol. 162, p. 66; 1950.
[94] "Some recent developments in the lost-wax casting process," *Machinery*, vol. 86, p. 37; 1955.
[95] A. M. Weisberg, "Heavy rhodium plating," *Materials and Methods;* 1953.
[96] P. Wenk and H. Boljahn, "Ultrasonic tinning of aluminium," *Z. Metallkde.*, vol. 43, p. 322; 1952.
[97] D. E. Wernz, "Aluminium dip brazing," *Machinery*, vol. 90, pp. 541–544; March 8, 1957.
[98] G. B. Wilkes, "Properties of copper brazed joints," *Iron Age;* September 30, 1948.
[99] H. Wright-Baker, "Modern Workshop Technology," Cleaver-Hume, Ltd., London, Eng.; 1950.
[100] M. Z. Yermanok and V. F. Kleizmentov, "An efficient technology for the production of rectangular aluminium tubes," *Tsvetnye Metally*, no. 5, p. 85; 1957.
[101] K. Zeigler and H. Lehmkuhl, "The electrolytic separation of aluminium from organic complex compounds," *Z. anorg. und allgem. Chem.*, vol. 283, pp. 414–424; 1956.
[102] "Aluminium Flame Brazing," British Oxygen Gases, Ltd., Tech. Info. Booklet No. 12; May, 1946.
[103] "Baker interference microscope for inspecting surface finish," *Machinery*, vol. 91, pp. 1196–1198; November 22, 1957.
[104] "Brazing of aluminium and its alloys," *Aluminium Dev. Bull.*, vol. 22, pp. 1–36; June, 1957.
[105] Brit. Patent Application No. 32073/56; 1956.
[106] "Casting in semi-permanent ceramic moulds," *Machinery*, vol. 84; March 19, 1954.
[107] "Climatic and Durability Testing of Service Telecommunications Equipment," Wireless Telegraphy Board Spec. No. K114; Issue 2, September, 1950.
[108] "Dip-brazed aluminium waveguide," *Electronic Engrg.*, vol. 30, pp. 354–355; May, 1958.
[109] "Engineering drawing practice," British Standard 308: 1953.
[110] "General Requirements for Service Telecommunication Equipment," H. M. Stationery Office, London, Eng., DEF-5000; 1956.
[111] "High frequency electro-spark machining of hard metals," *Microtechnic*, vol. 9, p. 267; 1955.
[112] "Kynal Aluminium Alloys and Fluxes for Brazing," Imperial Chem. Industries (Metals Div.), Birmingham, Eng.; 1953.
[113] "Materials used in radio and electronic engineering: Part 5—the electrodeposition of metals," *J. Brit. IRE*, vol. 17, no. 1, pp. 35–47; January, 1957.
[114] "Mould hobbing," *Mech. World*, p. 175; February 25, 1938.
[115] "Powder metallurgy: a survey of recent advances," *Engrg.;* December 31, 1954.
[116] "Precision-cast high-speed steel," *Machinery*, vol. 66, p. 641; 1945.
[117] "Precision investment casting by the Mercast process," *Machinery*, vol. 78, p. 396, March 8, 1951; vol. 86, p. 1344, June 17, 1955; vol. 90, pp. 736–742, April 5, 1957; vol. 90, pp. 813–821, April 12, 1957.
[118] "Producing constant-section radar-waveguide connecting tubing," *Machinery*, vol. 87, p. 1518; 1955.
[119] "Recent development in powder metallurgy," *Machinery*, vol. 85, p. 1318; 1954.
[120] "Steel strips for bending waveguides," *Machinery*, vol. 83; October 23, 1953.
[121] "Test Methods for Electronic and Electric Component Parts," U. S. Government, MIL-STD-202.
[122] "The Assessment of Surface Texture," British Standard 1134: 1950.
[123] "The Shaw process of precision casting," *Machinery*, vol. 81, p. 768; October 2, 1952.
[124] "The Shaw process of precision casting," *Machinery*, vol. 87, pp. 577–584, September 2, 1955; vol. 88, pp. 268–275, February 17, 1956.

The Dependence of Reflection on Incidence Angle*

RAYMOND REDHEFFER†

Summary—A lossy dielectric sheet has complex dielectric constant $\epsilon=\epsilon(x)$ and complex permeability $\mu=\mu(x)$, where x is the distance to one interface. This sheet is backed by a conducting surface and used as an absorber. If $|\epsilon(x)\mu(x)| \gg \epsilon_0\mu_0$, so that $(\epsilon/\epsilon_0)(\mu/\mu_0)-\sin^2\theta$ is nearly independent of the incidence angle θ, then the amplitude reflection $R(\theta)$ is wholly determined by $R(0)$. Typical results: When $R(\theta_0)=0$ at one polarization, then at $\theta=\theta_0$ the reflection for the other polarization corresponds to a voltage standing-wave ratio SWR $=\sec^2\theta_0$. At perpendicular polarization max $|R(\theta)|$ on (θ_1, θ_2) is least, for given $|R(0)|$, if $R(0)$ is real and positive; and then $R(\theta)=0$ at $\tan^2\theta/2=R(0)$. But for parallel polarization $R(0)$ must be real and negative to get optimum performance. When the absorber functions at both polarizations the best obtainable result is $|R(\theta)|=\tan^2\theta/2$, no matter what interval (θ_1, θ_2) is specified. The error in the approximation is investigated theoretically and experimentally. A complete set of graphs is included, suitable for design of those absorbers to which the theory applies. The analysis also yields an exact expression for the limiting behavior of the reflection at grazing incidence. This can be used in problems such as computation of the field due to a dipole over a plane earth. Finally, the theory of the Salisbury screen is re-examined as an aid in checking the other developments.

Statement of the Problem

An important problem in electromagnetic theory is the design of absorbers; that is, surfaces which have zero transmission and small reflection. Often it is desired to have these properties not at one incidence angle θ only, but over a range of angles. Since zero reflection cannot be attained over such a range, we are led to a minimax problem: to minimize the maximum reflection over the range.

For a broad class of absorbers (namely, the *thin solid* absorbers of the present article) this problem was solved nearly six years ago. Though a summary of the results was published at that time [1], continuing interest [2] suggests that the method should be made more generally available. Such is the purpose of this paper.

The mathematical formulation depends on a Riccati equation for the reflection [3]. Let $R=R(\theta)=R(\theta, x)$ denote the complex amplitude reflection when the thickness of the absorber is x, and let $e(x)=\epsilon/\epsilon_0$ and $m(x)=\mu/\mu_0$ denote the complex normalized dielectric constant and permeability at a distance x from the terminating interface (Fig. 1). The main point of the present analysis is to introduce a variable y defined by

$$w=\frac{1+R}{1-R}, \quad y_\perp = w_\perp \sec\theta, \quad y_\parallel = w_\parallel \cos\theta. \tag{1}$$

(Here, as elsewhere in this paper, the subscript $\parallel$ or $\perp$ specifies the polarization.) In terms of y the Riccati equations are

$$\begin{cases} \dfrac{dy_\perp}{dx} = -\dfrac{2\pi j}{\lambda}\left[\dfrac{me-\sin^2\theta}{m}\, y_\perp{}^2 - m\right], \\ \dfrac{dy_\parallel}{dx} = -\dfrac{2\pi j}{\lambda}\left[ey_\parallel{}^2 - \dfrac{me-\sin^2\theta}{e}\right]. \end{cases} \tag{2}$$

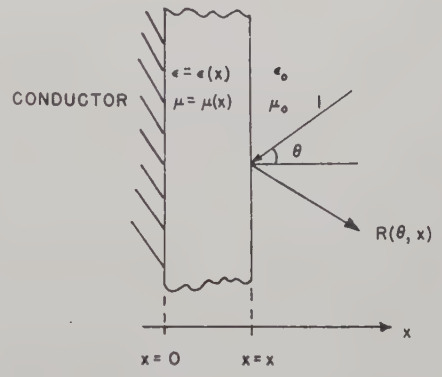

Fig. 1—Stratified medium in cross section.

Analysis of $|R(\theta)|$ is the problem with which we are concerned. Subject to an approximation described in the next paragraph, we answer such questions as: What design minimizes the maximum reflection at a given polarization over a given range (θ_1, θ_2), and what is the minimax reflection so attained? What is the resulting reflection at the other polarization? What design minimizes the maximum reflection when this maximum is considered not only with respect to θ, but also with respect to polarization? What is the optimum reflection so obtained? Though approximate, the analysis applies to a wide variety of cases of practical interest. Besides their relevance to the problem of design, the results obtained yield objective criteria by which the performance of any given absorber can be judged. The furnishing of such criteria is an important part of the absorber problem.

The Approximation

If θ ranges from $\theta_1 \geq 0$ to θ_2, it is possible to replace $\sin^2\theta$ by a constant in such a way that the maximum error committed does not exceed

$$\tfrac{1}{2}(\sin^2\theta_2 - \sin^2\theta_1).$$

For example, on (0, 25°) the error is not more than 0.09, and on (0, 45°) it is, at most, 0.25. Even on the whole range (0, 90°), the error is ≤ 0.5. This fact suggests the approximation

$$m(x)e(x) - \sin^2\theta \cong m(x)e(x) - \sin^2\theta_0 \tag{3}$$

* Manuscript received by the PGMTT, January 14, 1959; revised manuscript received, May 5, 1959. The preparation of this paper was sponsored in part by the McMillan Labs., Inc., Ipswich, Mass., and in part by the Office of Ordnance Res., U. S. Army. Reproduction, in whole or in part, is permitted for any purpose of the U. S. Government.

† Numerical Analysis Res., University of California at Los Angeles.

in (2), where θ_0 is a suitably chosen value between θ_1 and θ_2. The value θ_0 is allowed to depend on θ_1 and θ_2, and on x if desired, but not on θ.

The validity of the approximation is investigated later in this paper. For the present, we note that it is surely justified when Re $(me) \gg 1$. Thus, if the true value of Re (me) is 10, the effect of our approximation on (0, 45°) is similar to that of taking Re (me) somewhere between 9.75 and 10.25. Since few artificial dielectrics of the type used in absorbers can be held to such small tolerances, the approximation seems entirely realistic. Indeed, because of these manufacturing tolerances, the absorber is not really a stratified medium at all; and in the author's opinion the modified equations in (2), resulting from (3), are just as appropriate (or inappropriate) as are those in (2) themselves.

If the thickness x is large, the error may build up in the manner characteristic of differential equations; and when Re $(me) \cong 1$, the approximation is also less easy to justify. (We shall see, nevertheless, that the approximation can be excellent in this latter case.) To keep in mind the situation to which our analysis applies for θ far from 0°, the reader may think of a *thin solid* absorber. The word *solid* suggests Re $(me) \gg 1$, which is not the case for low density foams. If $\theta \doteq 0°$, the approximation is valid regardless of the type of absorber considered.

It should be mentioned, in conclusion, that a given accuracy of approximation for $\sin^2 \theta$ does not usually insure the same accuracy for y. However, the one error can be estimated in terms of the other. For example, let E, F, and M be constants such that for $0 \leq p \leq 1$

$$| e(x) | < E, \quad | 1/e(x) | < F, \quad | m(x) - p/e(x) | < M$$

throughout the dielectric material. If y refers to the value for θ and y_0 to the value for θ_0 at parallel polarization, it can be shown that

$$| y - y_0 | < \frac{2\pi x}{\lambda} | \sin^2 \theta - \sin^2 \theta_0 | F \sec^2 \frac{2\pi x}{\lambda} \sqrt{ME}. \quad (4)$$

The thickness x of the absorber must be such that the argument of the secant is $< \pi/2$. A limitation of this sort will arise in any estimation of y because $|y|$ can be (and generally is) unbounded. (On the other hand, $|R|$ does not depend critically on y when $|y|$ is large; see the section entitled "The Salisbury Screen.")

The Basic Formula for Reflection

In accordance with (3) let θ in (2) be replaced by θ_0. Since $R = -1$ when $x = 0$, the initial conditions are

$$y_\perp = 0, \qquad y_\parallel = 0 \text{ at } x = 0. \quad (5)$$

It is very important that these conditions are independent of θ. This same independence would be observed if $R = +1$ at $x = 0$, the short circuit being replaced by an open circuit; and our analysis applies without change to that case. This remark will be needed later.

Since m, e, $1/m$, and $1/e$ are bounded for any physically realizable materials, the right-hand members of (2) satisfy a Lipschitz condition on y. The uniqueness theorem insures that there is only one solution satisfying the conditions (5). Thus, for each fixed x,

$$w_\perp \sec \theta = \text{constant}, \quad w_\parallel \cos \theta = \text{constant}, \quad (6)$$

independent of θ. These are the fundamental relations for a thin solid absorber. If $w(0) = p \exp(-jq)$ we get the formulas

$$R_\perp(\theta) = \frac{pe^{-iq} \cos \theta - 1}{pe^{-iq} \cos \theta + 1}, \qquad R_\parallel(\theta) = \frac{pe^{-iq} - \cos \theta}{pe^{-iq} + \cos \theta}$$

which admit a physical interpretation [2].

Transforming back from $w(0)$ to $R(0)$ yields the following: *Let the normal-incidence reflection have amplitude a and phase b, so that* $R(0) = a \exp(-jb)$. *Then the reflection* $R(\theta)$ *at incidence* θ *is wholly determined by a and b.* Indeed, with $t = \tan^2 \theta/2$ we have

$$| R_\perp(\theta) |^2 = \frac{t^2 - 2at \cos b + a^2}{1 - 2at \cos b + a^2 t^2} \quad (7)$$

at perpendicular polarization and $| R_\parallel(\theta) |^2$ equals the same, with $+\cos b$ instead of $-\cos b$.

Graphical representation is given in Figs. 2–4. Since absorbers are commonly described in terms of their decibel attenuation, we have plotted the absorption

$$A(\theta) = -\log_{10} | R(\theta) |^2 = \text{db down}$$

rather than the power reflection, $| R(\theta) |^2$. In each figure $a = | R(0) |$ is held constant, while the phase b is a parameter.

According to (7) the same family of curves can be used for both polarizations. In fact, *let two absorbers have the same normal-incidence reflection except for* 180° *change in phase. Then one absorber has the same behavior at perpendicular polarization, as the other has at parallel polarization.* This fact is exploited in the figures by appropriate designation of b.

Optimum Design, Fixed Polarization

With freedom to adjust the two arbitrary complex functions $e(x)$ and $m(x)$, we should have expected a wide variety of possible behaviors, $|R|$ vs θ. But the foregoing considerations show that this expectation is sharply revised when thin, solid absorbers are in question. The angular dependence has a rigidity which is quite unlooked for, in view of the generality of the media considered. We present criteria for optimum design, with due regard to this rigidity.

At a fixed polarization let it be required to minimize the maximum reflection over the given range (θ_1, θ_2). The design is carried out by use of Fig. 5, which gives

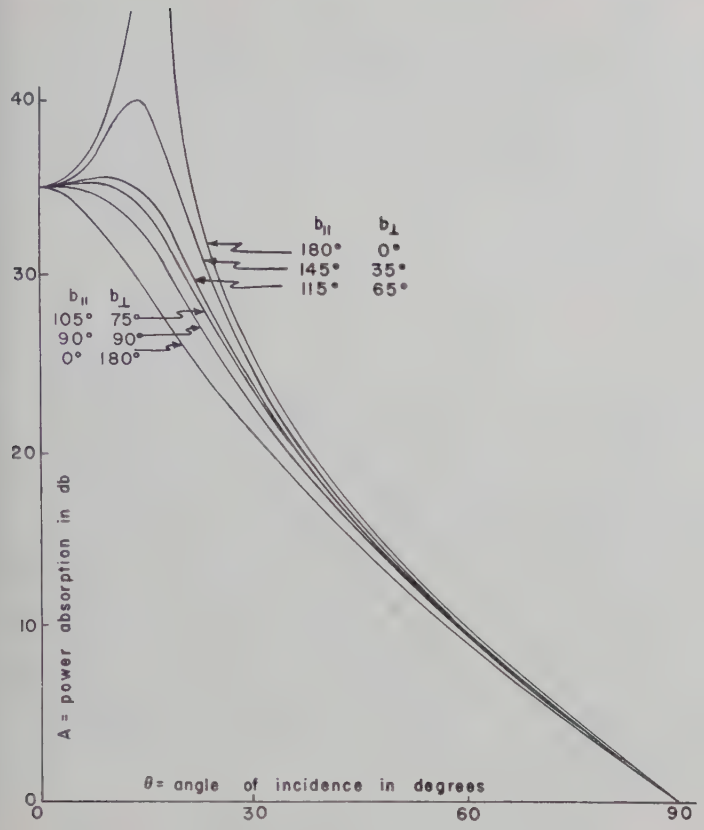

Fig. 2—Power reflection in decibels vs incidence angle when $R(0)=0.0178\ e^{ib}$.

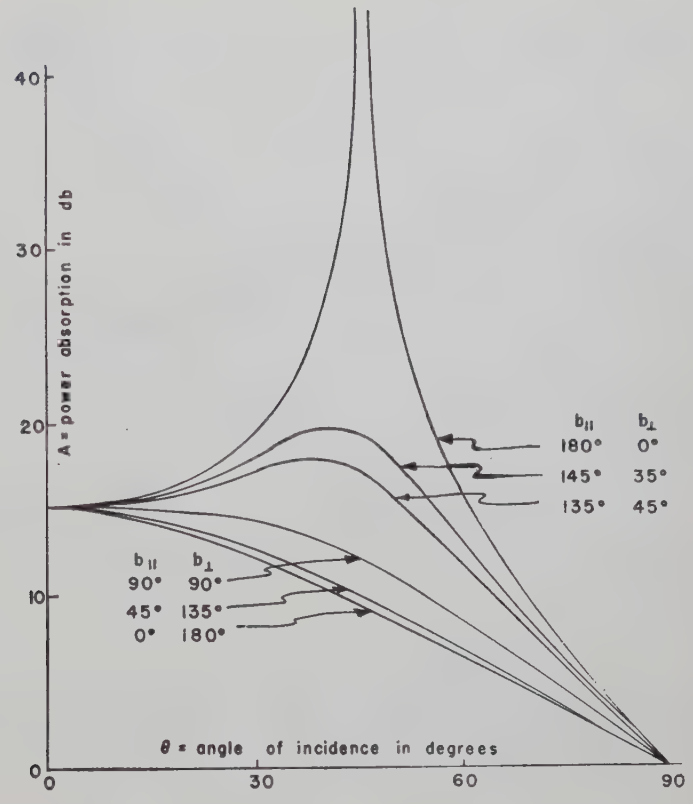

Fig. 4—Same, $R(0)=0.178\ e^{ib}$.

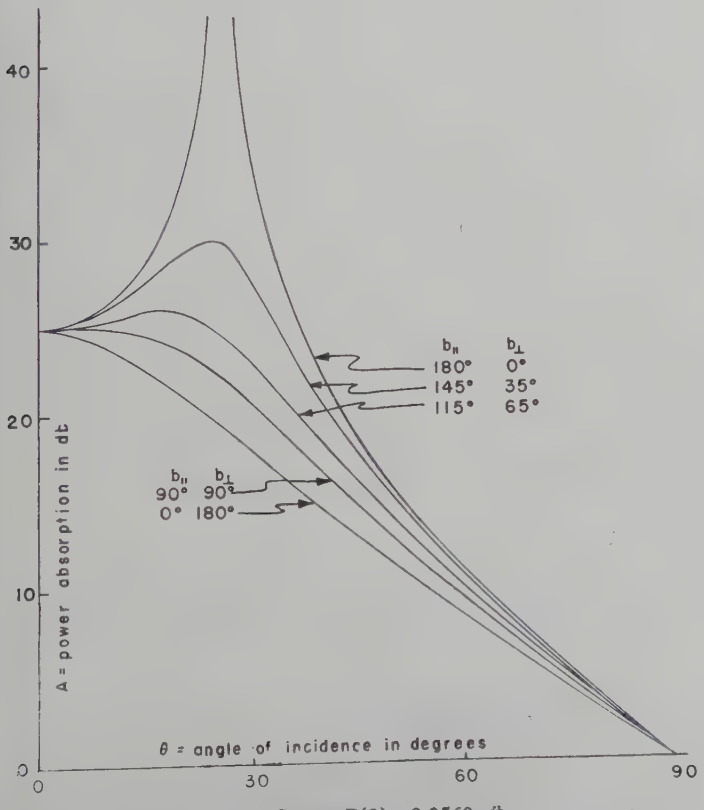

Fig. 3—Same, $R(0)=0.0560\ e^{ib}$.

contours of constant reflection for optimum design vs the incidence angle θ and the design angle, ϕ, at which $R(\theta)=0$. The optimum choice of ϕ is the unique value such that

$$\theta_1 \leq \phi \leq \theta_2 \quad \text{and} \quad A(\theta_1) = A(\theta_2) \tag{8}$$

on the corresponding contour. By considering horizontal line segments extending from θ_1 to θ_2, one readily establishes the ϕ at which (8) holds. Such a segment is shown in the figure for the range $30° < \theta < 60°$. It gives $\phi = 49°$ and the minimax absorption is about 17 db.

The optimum absorber is specified as soon as $R(0)=ae^{-ib}$ is known. Elementary analysis shows that

$$a = \tan^2 \phi/2, \qquad b_\perp = 0°, \qquad b_\parallel = 180°. \tag{9}$$

In summary: *If a thin, solid absorber gives optimum performance for $\theta_1 < \theta < \theta_2$ at a given polarization, then the normal-incidence reflection must have zero phase shift when the given polarization is perpendicular and* 180° *phase shift when it is parallel. The optimum absorber and its performance are given by the relation plotted in Fig. 5, together with* (9).

Here, the absorber is unique only insofar as its behavior is determined by $R(0)$. Many choices of $\epsilon(x)$ and $\mu(x)$ are possible.

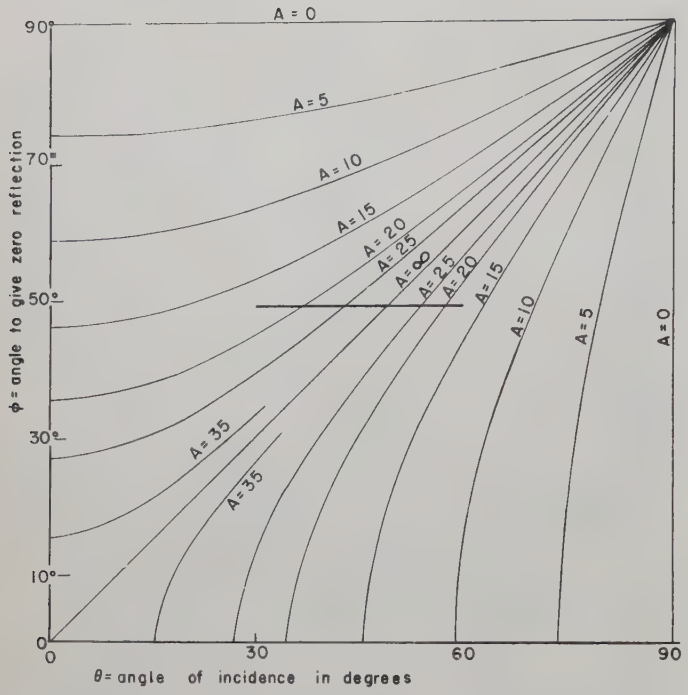

Fig. 5—Contours of constant power reflection in decibels, for a given polarization, vs the incidence angle θ and the design angle ϕ at which the reflection is zero.

Change of Polarization

We have seen that $|R(\theta)|$ must have a minimum between θ_1 and θ_2 if the design is to be optimum at a given polarization. At the other polarization $|R(\theta)|$ cannot have any minimum between 0 and $\pi/2$; indeed, the basic formula readily gives the following: *For a thin, solid absorber, a necessary and sufficient condition that the amplitude reflection* $|R(\theta)|$ *have a minimum at* $\theta=\phi\neq 0$ *is that* $R(\phi)$ *be pure imaginary. This situation arises at perpendicular polarization if, and only if,* $|w(0)|>1$ *(or if* $-\pi/2<R(0)<\pi/2$*, which is the same thing). It arises at parallel polarization in the contrary case.*

Thus, a minimum between 0 and $\pi/2$ [hence, very good performance on (θ_1, θ_2)] is possible for one polarization only, not for both with a given absorber. More detailed analysis yields the following. *For a thin, solid absorber, let the amplitude reflection* $|R(\theta)|$ *have a minimum equal to* $\tan q/2$ *at* $\theta=\phi\neq 0$. *Then the reflection is wholly determined at both polarizations, and at arbitrary incidence, by* ϕ *and* q. We have

$$|R(\theta)|^2=\frac{\cos^2\phi-2\cos\phi\cos\theta\cos q+\cos^2\theta}{\cos^2\phi+2\cos\phi\cos\theta\cos q+\cos^2\theta} \qquad (10)$$

at the given polarization, and the same, with $\sec\theta$ replacing $\cos\theta$, at the other. In particular, suppose $R(\theta)=0$ at one polarization. Then for the standing-wave ratio at the other polarization

$$\mathrm{SWR}\equiv\frac{1+|R(\phi)|}{1-|R(\phi)|}=\sec^2\phi. \qquad (11)$$

Despite these negative results, an absorber may (and generally does) have to perform at both polarizations simultaneously. Since $|R_\perp|$ increases and $|R_\parallel|$ decreases as b increases from 0 to 180°, the value of b which is best for one polarization is worst for the other. We have $|R_\perp|=|R_\parallel|$ if, and only if, $b=\pi/2$; and for optimum design

$$\max(|R_\perp|, |R_\parallel|)=|R_\perp|=|R_\parallel|=\left(\frac{t^2+a^2}{1+t^2a^2}\right)^{1/2}, \qquad (12)$$

where $t=\tan^2\theta/2$. The expression, which is plotted in Fig. 6, increases with a and hence is least at $a=0$. These results may be summarized as follows: *Suppose a thin, solid absorber, intended for use at both polarizations, has prescribed normal incidence reflection, a. Then for any range of* θ *the design is optimum* [*subject to* $|R(0)|=a$] *if and only if* $R(0)$ *is pure imaginary. In that case the reflection is independent of polarization and is given by the relation represented graphically in Fig. 6. The reflection at every angle decreases as* $|R(0)|$ *decreases, and when* $R(0)=0$ *we have* $|R(\theta)|=\tan^2\theta/2$. *This represents the optimum performance possible.*

Experimental Verification

Comparison of theory and experiment leads to satisfactory agreement. The absorbers used were the standard production model F-89-VF, supplied by the McMillan Laboratory, Inc., Ipswich, Mass., where the measurements were made by A. Preston and the author. The theoretical curve showed that the absorbers have approximately the optimum behavior possible (according to our theory) in the range for which they were designed; *viz.*, at perpendicular polarization, and over an interval centered near $\theta=35°$. The constants (a, b) were determined, in fact, by taking $R_\perp(35°)=0$ and using (10). The curve for parallel polarization was determined by the same choice of a and b; it agreed within 3 db out to the last data-point, $\theta=60°$. Since highly accurate data have been presented elsewhere [2] we do not devote much space to the subject here. The point to be emphasized is that the absorbers had a rather complicated internal structure and that *the theory describes their behavior without taking account of this structure.*

Grazing Incidence

The foregoing methods lead to the following: Let $\alpha=\alpha(x)$ satisfy the Riccati equation and boundary condition

$$\frac{d\alpha}{dx}=\frac{-2\pi j}{\lambda}\left[\frac{m(x)e(x)-1}{m(x)}\alpha^2-m(x)\right],\quad \alpha(0)=0. \qquad (13)$$

Let $R_\perp(\theta)$ be the reflection at perpendicular polarization and incidence θ for a medium of thickness x and complex parameters $\epsilon/\epsilon_0=e(x)$, $\mu/\mu_0=m(x)$, backed by a con-

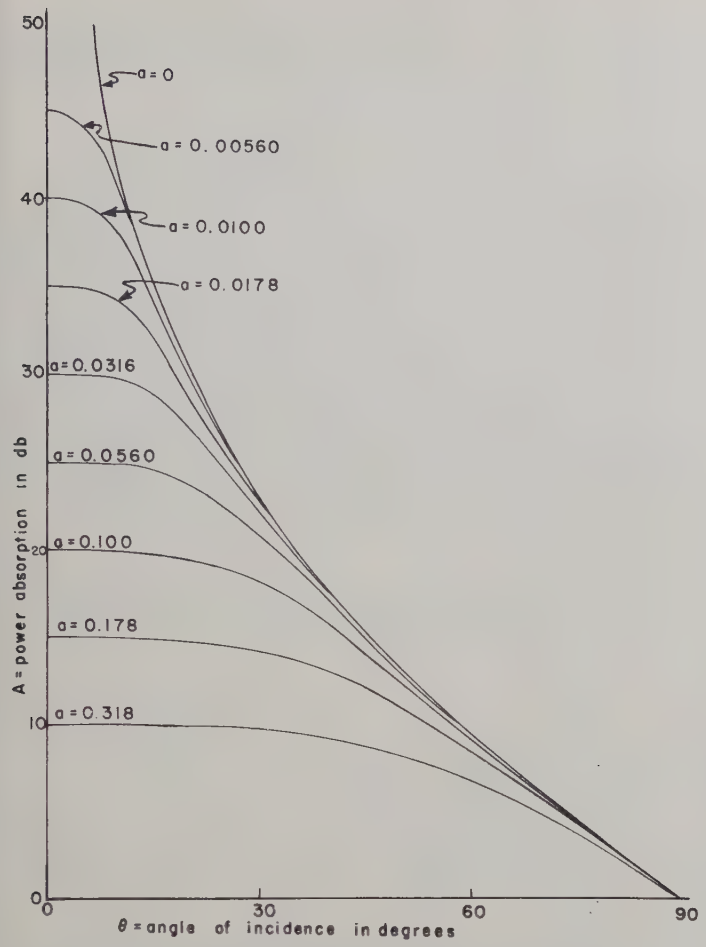

Fig. 6—Power reflection in decibels vs the incidence angle θ, when $\max(|R_\perp|, |R_\parallel|)$ is minimized by suitable choice of arg $R(0)$.

ducting surface. Then

$$\lim_{\theta \to \pi/2} \frac{1 + R_\perp}{\cos \theta} = 2\alpha$$

and

$$\frac{d}{d\theta} |R_\perp|^2 = 4 \operatorname{Re}(\alpha) \text{ at } \theta = \pi/2. \tag{14}$$

Similarly, if $\beta = \beta(x)$ satisfies

$$\frac{d\beta}{dx} = \frac{-2\pi j}{\lambda}\left[e(x)\beta^2 - \frac{m(x)e(x) - 1}{e(x)}\right], \quad \beta(0) = 0 \tag{15}$$

then the complex reflection at parallel polarization satisfies

$$\lim_{\theta \to \pi/2} \frac{1 - R_\parallel}{\cos \theta} = \frac{2}{\beta},$$

$$\frac{d}{d\theta} |R_\parallel|^2 = \operatorname{Re}\left(\frac{4}{\beta}\right) \text{ at } \theta = \pi/2. \tag{16}$$

It should be emphasized that (13)–(16) are exact; that is, they follow from (2) without the approximation (3) used heretofore in this discussion.

The relevance to the problem of θ dependence is as follows. Eqs. (14) and (16) are consequences of the fact that

$$\lim w_\perp \sec \theta = \alpha, \quad \lim w_\parallel \cos \theta = \beta \text{ as } \theta \to 90°. \tag{17}$$

If we take $w \cos \theta = \beta$, we get the approximate formula

$$|R_\parallel|^2 \doteq \frac{P^2 - 2P \cos \theta \cos Q + \cos^2 \theta}{P^2 + 2P \cos \theta \cos Q + \cos^2 \theta} \tag{18}$$

upon setting $\beta = Pe^{iQ}$. This result plays the same role for $\theta \doteq 90°$ as the previous results do for $\theta \doteq 0°$. A similar approximation is true for $R_\perp$.

Since (13) and (15) can be made to yield any desired α and β by appropriate choice of m and e, the results for perpendicular and parallel polarization are independent (in contrast to the behavior near 0°, where they were dependent). Apart from this, the previous discussion and graphs apply here too; for (17) has the same structure as (6).

The Salisbury Screen

An excellent check of this theory is afforded by the Salisbury screen (Fig. 7). If the resistive layer has thickness t_1 and complex parameters

$$e_1 = k_1(1 - j \tan \delta_1), \qquad m_1 = k_1'(1 - j \tan \delta_1'),$$

the reader will recall that its transmission T_1 and reflection R_1 are readily computed under the hypothesis

$$|t_1\sqrt{m_1 e_1}| \ll \lambda, \qquad |e_1/m_1| \gg 1, \qquad |e_1 m_1| \gg 1.$$

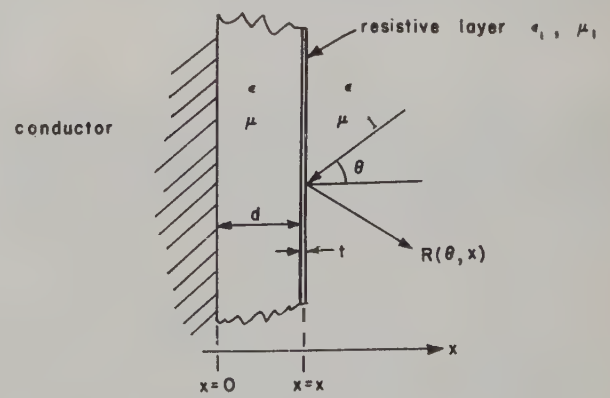

Fig. 7—Salisbury screen in cross section.

The result is

$$T_1 \doteq 1 + R_1 \doteq [1 + \tfrac{1}{2}KN]^{-1} \tag{19}$$

where N is the normalized conductivity and $K = \sec \theta$, or $K = \cos \theta$, at perpendicular, and at parallel polarization, respectively.

If the lossless dielectric separating the resistive and conducting layers has thickness d and real parameter $k = (\epsilon/\epsilon_0)(\mu/\mu_0)$, the reflection of core-plus-metal is very close to $\exp(-2j\psi)$ where

$$\psi = 2\pi d\sqrt{k - \sin^2 \theta}/\lambda. \tag{20}$$

(There is no error in (20) when $k=1$ or when ψ is a multiple of $\pi/2$. This fact will be useful later.)

Without further approximation we get

$$y_\perp = [N - j\cot\psi\cos\theta]^{-1}, \quad y_\parallel = [N - j\cot\psi\sec\theta]^{-1} \tag{21}$$

for the Salisbury screen. If the reflection is 0 at $\theta=\phi$, then

$$\psi = \frac{\pi}{2}\sqrt{\frac{k - \sin^2\theta}{k - \sin^2\phi}}, \quad N_\perp = \cos\phi, \quad N_\parallel = \sec\phi \tag{22}$$

for a first-order, *i.e.*, thinnest possible, structure. The resulting behavior at incidence θ is given by (21). Taking $\phi=0$ as an important and typical case, we get

$$y_\perp = \left[1 - j\cos\theta\cot\frac{\pi}{2}(1 - k^{-1}\sin^2\theta)^{1/2}\right]^{-1}$$

$$y_\parallel = \left[1 - j\sec\theta\cot\frac{\pi}{2}(1 - k^{-1}\sin^2\theta)^{1/2}\right]^{-1}. \tag{23}$$

When $k=1$, the real and imaginary parts are given in Table I as a function of θ. For perpendicular polarization the variation is not excessive, but for parallel polarization the real part varies from 1 to 0. A graph of the real part vs the imaginary part yields very nearly the same curve both times; but the whole curve obtained for perpendicular polarization on (0, 90°) is traced out by the parallel polarization values on (0, 44°). Thus, for our case $|e_1| \gg |m_1|$, the theory for $R_\perp$ is more reliable. just as the experimental work suggests. (If $|m_1| \gg |e_1|$, the theory for $R_\parallel$ is the better.)

According to the general theory

$$|R|^2 = \tan^4\theta/2 \tag{24}$$

at both polarizations when, as in this case, $R(0)=0$. To see how serious an error in $|R|$ is produced by the variation shown in Table I, we have plotted the reflection given by (23) for $k=1$ together with that given by (24). By Fig. 8 the maximum error is about 5 db. In absorber design, an error of 5 db is not as serious as one might think, so that the theory is not wholly vitiated even by the great variation shown in Table I.

If a larger value for k is chosen, the assumption of a *thin solid* absorber is better satisfied, and we expect a smaller error. Table II presents the same calculation as Table I, except that $k=5$. The basic relation (6) is satisfied very accurately at perpendicular polarization on the whole range (0, 90°), and it is satisfied to 70° or 80° for the parallel case. Since the real part will always change from 1 to 0 in the latter case, the equality over the whole range is not possible. However, the effect on $|R|$ is completely negligible even when $\theta \doteq 90°$, as we shall see. The analog of Fig. 8 for Table II leads to three curves that are practically indistinguishable.

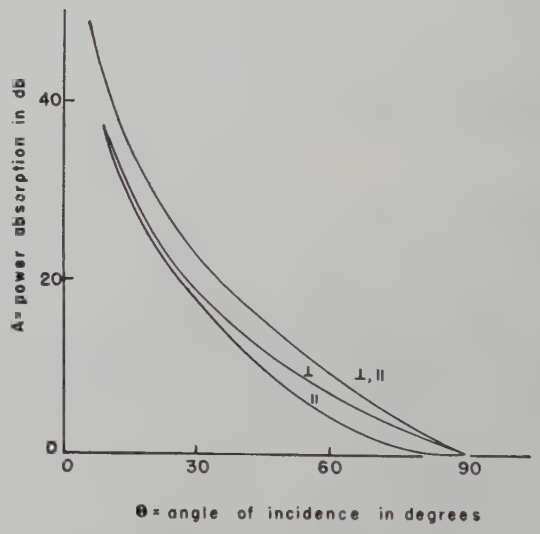

Fig. 8—Comparison of the general theory with the Salisbury screen theory when the core dielectric constant $k=1$ and the resistivity $\Omega=377$ ohms.

TABLE I

SALISBURY SCREEN IMPEDANCE FOR $k=1$, $N=1$, $d/\lambda=\frac{1}{4}$

θ (degrees)	0	10	20	30	40	50	60	70	80	90
Re ($w_\perp \sec\theta$)	1.0000	0.9994	0.992	0.97	0.92	0.86	0.80	0.75	0.72	0.71
Im ($w_\perp \sec\theta$)	0	0.024	0.090	0.18	0.27	0.34	0.40	0.43	0.45	0.45
Re ($w_\parallel \cos\theta$)	1.0000	0.9994	0.990	0.95	0.80	0.51	0.20	0.04	0.002	0
Im ($w_\parallel \cos\theta$)	0	0.024	0.10	0.22	0.40	0.50	0.40	0.20	0.04	0

TABLE II

SALISBURY SCREEN IMPEDANCE FOR $k=5$, $N=1$, $d\sqrt{5}/\lambda=\frac{1}{4}$

θ (degrees)	0	10	20	30	40	50	60	70	80	90
Re ($w_\perp \sec\theta$)	1.0000	0.99998	0.9997	0.9989	0.9972	0.9966	0.9975	0.9976	0.9992	1.000
Im ($w_\perp \sec\theta$)	0	0.0046	0.0713	0.034	0.053	0.059	0.062	0.049	0.028	0
Re ($w_\parallel \cos\theta$)	1.0000	0.99998	0.9996	0.9980	0.9929	0.980	0.942	0.858	0.535	0
Im ($w_\parallel \cos\theta$)	0	0.0048	0.020	0.045	0.090	0.14	0.23	0.36	0.50	0

Further Verification of the General Theory

If $R=0$ at $\theta=\phi$, (21) and (22) yield

$$R(\phi) = \pm \frac{1 - \cos^2 \phi}{1 + \cos^2 \phi} \tag{25}$$

for the reflection at the other polarization. This agrees with (11), so that one major prediction of the theory is precisely verified. But it should be emphasized that (25) follows with no approximation other than (19); in particular, $k \gg 1$ for the core is *not* assumed.[1]

The reason for the success of the theory, even though $k \doteq 1$, is as follows. It happens that core-plus-metal is an exact open circuit at both polarizations, in the circumstances leading to (25). Since the cloth does not know whether this open circuit at $\theta=\phi$ is produced by a low or by a high dielectric constant, we can replace the core by a thinner one having $k \gg 1$ without changing the reflection at the angle in question. But the new absorber satisfies our assumptions, since the cloth does, and since, as we were saying, $k \gg 1$. Thus, its reflection can be computed by (11).

The reader will perceive that we have arrived at a general principle: *Let a thin solid layer, A, be backed by a terminating stratified medium, B, and suppose the over-all reflection is zero at a given angle ϕ and polarization. If there is a thin solid absorber whose complex reflection reproduces that of B at ϕ and at both polarizations, then* (11) *holds for the original composite medium, A plus B.* A mathematical proof of this principle can be based on certain functional equations satisfied by solutions of Riccati's equation, but the physics is so clear that we do not belabor the matter here.

A final check of the theory is given by letting $\theta \to 0$ or $\theta \to 90°$. By (21)

$$|R_\perp|^2 \sim |R_\parallel|^2 \sim [1 + (\pi/2k)^2] \tan^4 \frac{\theta}{2}$$

as $\theta \to 0$, where we write $a \sim b$ to mean $\lim a/b = 1$. Comparing with (24) we see that the general theory is in error by the factor $1+(\pi/2k)^2$, as $\theta \to 0$. For $k=1$ this accounts for the difference of 5.4 db that occurs in Fig. 8. For $k=2$ the error due to this factor is 2.1 db, and it is 1 db for $k=3$.

Since the theory gives the correct result near 0°, the first terms of the Taylor's series for $|R|^2$ must agree, though there is no guarantee of equality of limiting ratios when $R(0)=0$. In the present case the agreement is exact through terms in θ^3, and the ratio of coefficients for θ^4 tends rapidly to 1 as $k \to \infty$.

A similar calculation for θ near 90° gives

$$1 - |R_\perp|^2 \sim 4 \cos \theta$$

$$1 - |R_\parallel|^2 \sim 4\left(1 + \cot^2 \frac{\pi}{2}(1 - k^{-1})^{1/2}\right)^{-1} \cos \theta$$

whereas by (24)

$$1 - |R|^2 \sim 4 \cos \theta$$

at either polarization. Expansion of the radical in powers of $1/k$ yields

$$1 - |R_\parallel|^2 \sim 4[1 + (\pi/4k)^2]^{-1} \cos \theta.$$

Thus, as $\theta \to 90°$ the theory yields the correct behavior for perpendicular polarization regardless of k, and the correct behavior for parallel polarization provided $(\pi/4k)^2 \ll 1$. The theory underestimates the value of $|R_\parallel|$. However, the error in $1-|R_\parallel|^2$ is only 1 db for $k=1.5$ and for $k=5$ as in Table II, the error is only 0.011 db. In practice the important thing is $|R|$, not w; and that Re $(w_\parallel \cos \theta)$ jumps from 0.858 to 0 on the range (70°, 90°) in Table II is without practical significance.

[1] Eq. (25) was noted by Walther [2]. However, he assumes that core-plus-metal has an electrical quarter-wave thickness independently of θ. By (20) this is equivalent to $k \gg \sin^2 \theta$; so that Walther's observation is a direct consequence of the general theory. For the same reason, his analysis of the Salisbury screen does not enable us to compute Tables I and II.

References

[1] Abstract 158t, *Bull. Amer. Math. Soc.*, vol. 60, p. 79; January, 1954. In 1957 the results of sections 3–5 were communicated orally to H. Severin and his co-workers at the Physikalisches Institut der Universität Göttingen.

[2] K. Walther, "Polarisations- und Winkelabhängigkeit des Reflexionsfaktors, von Absorbern für elektromagnetische Zentimeterwellen," *Z. angew. Phys.*, vol. 10, pp. 285–295; June 6, 1958.

[3] R. B. Barrar and R. M. Redheffer, "On nonuniform dielectric media," IRE Trans. on Antennas and Propagation, vol. AP-3, pp. 101–107; July, 1955.

[4] R. Pottel, "Über der Erhöhung der Frequenzbandbreite dünner λ/4-Schicht Absorber für elek. Zentimeterwellen," *Z. angew. Phys.*, vol. 11, pp. 46–51; February, 1959.

[5] H. Haddenhorst, "Durchgang von elektromagnetischen Wellen durch inhomogene Schichten (Teil II: Absorbtion), *Z. angew. Phys.*, vol. 8, pp. 264–267; June, 1956.

Analytical Asymmetry Parameters for Symmetrical Waveguide Junctions*

M. COHEN† AND W. K. KAHN‡

Summary—**This paper presents a systematic approach to the evaluation of (waveguide) junctions from the standpoint of their conformance to certain symmetries. Preferred sets of asymmetry parameters are found which are complete, minimal in number, which go to zero when the junction represented is symmetrical, and which may often be identified with a corresponding structural symmetry defect. The asymmetry parameters are first introduced for general linear junctions, but special attention is given to reciprocal and lossless junctions. The derivation of these preferred sets is based on the theory of group representations hitherto employed in the analysis of ideally symmetric junctions. One of the applications of these preferred parameters yields first-order relations among the defects of a nearly perfect hybrid-T junction which are believed to be new.**

I. Introduction

THIS PAPER presents a systematic approach to the evaluation of waveguide junctions from the standpoint of their conformance to certain symmetries. While ideal symmetrical junctions have received extensive treatment in the recent literature,[1–6] little account is taken, in these papers, of the fact that all actual junctions are, in some degree, asymmetrical. On specialized consideration of a particular junction, engineers have commonly improvised parameters descriptive of junction asymmetries. It generally remained uncertain whether or not such a set of asymmetry parameters, introduced *ad hoc*, was either complete (in the sense that any arbitrary asymmetry could be described) or minimal (in the sense that no linear relations subsisted among elements of the set). Here, these questions are resolved simply and, we believe, naturally in terms of the same theoretical framework which has been successfully employed in the analysis of ideal symmetrical junctions; *i.e.*, the theory of linear transformations and representations of finite point groups.

A procedure is outlined whereby a *preferred set of asymmetry parameters* may be derived for any junction appropriate for description of the degree in which that junction deviates from a given symmetry. The parameters comprised in such a set are complete, minimal in number, and all go to zero if, and only if, the junction is symmetrical (or electrically equivalent to a junction with the required symmetry). They are termed analytical asymmetry parameters because particular structural symmetry defects may often be deduced from them. First obtained for general linear junctions, special attention is given to reciprocal and lossless junctions. Scattering notation has been employed throughout this paper for the network quantities since these are the most convenient for microwave junctions, and moreover they exist for arbitrary passive structures.

The principles by means of which the analytical asymmetry parameters may be derived is sketched in Section II. This sketch may largely be supplemented by reference to the extensive treatments of ideal symmetrical junctions previously cited. A detailed illustration of the procedure is presented in Section III, in which asymmetry parameters appropriate to the H-plane Y junction are derived. This section should also clarify the special case of symmetry degeneracy, which is slighted in Section II for the sake of brevity.

The final section contains two examples illustrating the measurement and theoretical significance of the derived asymmetry parameters. The results of the perturbation calculation performed on a nearly perfect hybrid-T are believed to be new.

II. Symmetry and Asymmetry Parameters

At any frequency the network characteristics of a linear N-port, equivalent to a particular junction (one without "noncontrolled" sources) at reference planes appropriately chosen in perfectly conducting uniform waveguide leads, may be described by N^2 complex parameters. The elements of the conventional (normalized, voltage) scattering matrix,

$$S = (s_{ij}) \qquad i, j = 1, 2, \cdots, N, \tag{1}$$

constitute one such description. This matrix relates the column matrices of terminal quantities $\boldsymbol{a}$ and $\boldsymbol{b}$;

$$\boldsymbol{b} = S\boldsymbol{a}, \tag{2}$$

the elements of which,

$$\boldsymbol{a} = (a_i) \quad \text{and} \quad \boldsymbol{b} = (b_i) \qquad i = 1, 2, \cdots, N, \tag{3}$$

* Manuscript received by the PGMTT, March 12, 1959; revised manuscript received, May 8, 1959. The essentials of this paper were submitted by M. Cohen as a thesis in partial fulfillment of requirements for the M.E.E. degree at the Polytechnic Institute of Brooklyn, N. Y.

† Polytechnic Res. and Dev. Co., Brooklyn, N. Y.

‡ Microwave Res. Inst., Polytechnic Institute of Brooklyn, Brooklyn, N. Y.

[1] B. A. Auld, "Applications of Group Theory in the Study of Symmetrical Waveguide Junctions," Stanford University, Stanford, Calif., MLR-157; March, 1952.

[2] H. A. Folwer, "Reciprocity and the Scattering Matrix of Ferrite Devices," Electronics Res. Lab., Brown University, Providence, R. I.

[3] W. K. Kahn, "Scattering equivalent circuits for common symmetrical junctions," IRE TRANS. ON CIRCUIT THEORY, vol. CT-3, pp. 121–127; June, 1956.

[4] D. M. Kerns, "Analysis of symmetrical waveguide junctions," *J. Res., NBS*, vol. 46, pp. 267–282; April, 1951.

[5] C. G. Montgommery, R. H. Dicke, and E. M. Purcell, "Principles of Microwave Circuits," McGraw-Hill Book Co., Inc., New York, N. Y.; 1948.

[6] A. E. Pannenborg, "On the scattering matrix of symmetrical waveguide junctions," *Phillips Res. Repts.*, vol. 7, pp. 133; April, 1952.

are, respectively, the rms phasors corresponding to the waves incident onto and reflected from the junction at the reference planes chosen. These phasors are so normalized that $\boldsymbol{a}^+\boldsymbol{a}$ and $\boldsymbol{b}^+\boldsymbol{b}$ are, respectively, equal to the power incident onto and the power reflected from the junction. (The symbol $\boldsymbol{a}^+$ denotes the conjugate transpose of $\boldsymbol{a}$.) In this section, alternative (scattering) descriptions will be developed, entirely equivalent in point of generality to the conventional scattering matrix, but especially appropriate to junctions conforming to particular symmetries. The N^2 complex parameters entering into such a description fall into one of two categories: 1) those parameters which *necessarily vanish* when the junction represented actually conforms to the particular symmetries which determined the description; and 2) the parameters which do *not necessarily vanish* in that case. Those in the first category are denoted *asymmetry parameters*, and those in the second, *symmetry parameters*. The elements of the conventional scattering matrix will be expressed (linearly) in terms of the asymmetry and symmetry parameters, and conversely.

Consider a symmetrical structure such as, for example, the waveguide junction shown in Fig. 1. The physical symmetry of such a structure may be described in terms of the operations, *i.e.*, reflections and rotations, which leave the structure invariant. These operations form one representation of a group, the symmetry or point group of the junction. The corresponding electrical symmetry of the network equivalent to the junction may be described in terms of the permutations of the terminal quantities which leave the network relation (2) invariant. The unitary matrices M_k, which perform these permutations of the terminal quantities $\boldsymbol{a}$ and $\boldsymbol{b}$, may be written down by inspection, and these then form another representation of the mentioned group. Thus, if

$$\boldsymbol{b} = S\boldsymbol{a} \tag{4}$$

and

$$\boldsymbol{a}^{(k)} = M_k\boldsymbol{a}, \qquad \boldsymbol{b}^{(k)} = M_k\boldsymbol{b} = M_kS\boldsymbol{a}, \tag{5}$$

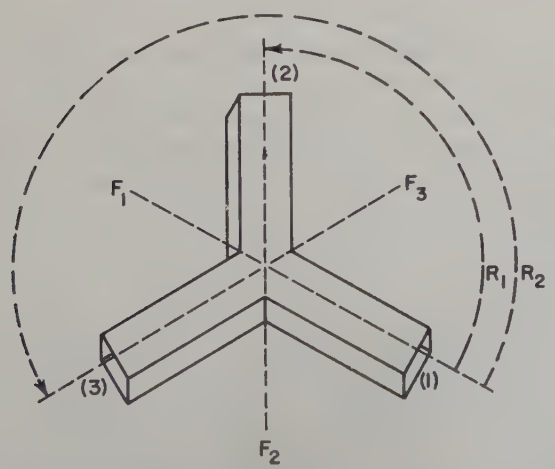

Fig. 1—Symmetrical waveguide junction, H-plane Y. (Symmetry planes marked F, rotational symmetries marked R.)

then

$$\boldsymbol{b}^{(k)} = S\boldsymbol{a}^{(k)} \tag{6}$$

for *arbitrary* $\boldsymbol{a}$. When $\boldsymbol{a}^{(k)}$ and $\boldsymbol{b}^{(k)}$ in (6) are replaced by their equivalents in terms of $\boldsymbol{a}$, there results:

$$M_kS\boldsymbol{a} = SM_k\boldsymbol{a}, \tag{7}$$

which yields the essential connection between M_k and S,

$$M_kS = SM_k. \tag{8}$$

This connection may be utilized directly to find the relations among the conventional scattering coefficients that are a result of the symmetry to which M_k corresponds [Section III, (27)–(29)]. More to the purpose at hand, (8) may also be utilized to find a transformation which reduces the scattering matrix of a symmetrical junction.

Since S and M_k commute, it is known that these two matrices have a common set of invariant subspaces.[7] But the permutation matrix M_k is simple in form and is known (having been deduced from the geometrical symmetry of the junction). Hence, invariant subspaces of S will be found by finding the unique invariant subspaces of M_k, and from these a transformation will be constructed which reduces S.

The eigenvectors $\boldsymbol{m}_k^{(i)}$ belonging to the eigenvalues $\mu_k^{(i)}$ of M_k satisfy the relation

$$(M_k - \mu_k^{(i)})\boldsymbol{m}_k^{(i)} = 0, \qquad i = 1, 2, \cdots. \tag{9}$$

N linearly independent eigenvectors may be arranged as a hermitean orthonormal set since M_k is unitary. Assign consecutive superscripts to any repeated degenerate eigenvalues. The subspaces spanned by all the eigenvectors corresponding to any one value are the unique invariant subspaces of M_k. Then the transformation,

$$T_k = (\boldsymbol{m}_k^{(1)}\boldsymbol{m}_k^{(2)} \cdots \boldsymbol{m}_k^{(N)}), \tag{10}$$

formed with these eigenvectors as columns, is unitary; *i.e.*, $T^{-1} = T^+$. Acting on columns $\boldsymbol{a}_k$ and $\boldsymbol{b}_k$,

$$\boldsymbol{a} = T_k\boldsymbol{a}_k, \qquad \boldsymbol{b} = T_k\boldsymbol{b}_k; \tag{11}$$

T_k expresses $\boldsymbol{a}$ and $\boldsymbol{b}$ as linear combinations of the eigenvectors $\boldsymbol{m}_k^{(i)}$. The column matrices $\boldsymbol{a}_k$ and $\boldsymbol{b}_k$ may be regarded as new or transformed (incident and reflected wave) terminal quantities. The transformed scattering matrix S_k corresponding to these new terminal quantities may be found on substitution for $\boldsymbol{a}$ and $\boldsymbol{b}$ in (2).

$$T_k\boldsymbol{b}_k = ST_k\boldsymbol{a}_k, \tag{12}$$

$$\boldsymbol{b}_k = T_k^{-1}ST_k\boldsymbol{a}_k = T_k^+ST_k\boldsymbol{a}_k, \tag{13}$$

and comparing this result with the defining equation;

$$\boldsymbol{b}_k = S_k\boldsymbol{a}_k; \tag{14}$$

[7] H. L. Hamburger and M. E. Grimshaw, "Linear Transformations in N-Dimensional Vector Space," Cambridge University Press, Cambridge, England, ch. 23, p. 138; 1956.

i.e.,

$$S_k = T_k^+ S T_k. \tag{15}$$

The matrix S_k has the form

$$S_k = \begin{pmatrix} \blacksquare & 0 & \cdots & 0 \\ 0 & \blacksquare & \cdots & 0 \\ \vdots & \vdots & \ddots & \vdots \\ 0 & 0 & \cdots & \blacksquare \end{pmatrix}, \tag{16}$$

where the shaded regions along the principal diagonal of S_k represent square submatrices. The elements of these submatrices will be denoted Q_{ij}. Each submatrix corresponds to an eigenvalue μ_k of M_k; the dimension of the submatrix is equal to the degeneracy of that eigenvalue. The zeros in the remaining rectangles imply that the elements in these submatrices of S_k are *all necessarily zero.*

To recapitulate: if a junction actually possesses the symmetry corresponding to M_k, then its scattering matrix S commutes with M_k and the matrix S_k defined in (15) necessarily has the form (16). The elements Q_{ij} then suffice to describe the junction.

Now consider an *arbitrary* waveguide junction. Its scattering matrix S does not (necessarily) commute with M_k. If, nevertheless, S_k is defined by (15), S_k is entirely general in form with no elements (necessarily) equal to zero. Retain the notation Q_{ij} for those elements with subscripts ij for which it was introduced in the symmetrical case, and denote the remaining elements of S_k q_{ij}. Then the q_{ij} are precisely those scattering parameters which necessarily vanish when the junction represented actually conforms to the particular symmetry corresponding to M_k; *i.e.*, the asymmetry parameters. The Q_{ij} are the corresponding symmetry parameters.

The above theory may readily be extended to include more complex symmetries to which several or a whole group of matrices M_k, $k=1, 2, \cdots$ correspond. An example of the procedure may be found in Section III.

It was suggested in connection with (11)–(15) that the matrix S_k be regarded as an alternative or transformed scattering description with terminal quantities $\boldsymbol{a}_k$ and $\boldsymbol{b}_k$. One way in which this viewpoint may be made useful and, perhaps, more familiar, is by displaying the special forms that this matrix takes when the junction represented is nondissipative and Lorentz reciprocal; a second way is presented in the last section.

When a junction is nondissipative, the conventional scattering matrix S, descriptive of this junction, is unitary. But,

$$S_k^{-1} = (T_k^+ S T_k)^{-1} = T_k^{-1} S^{-1} (T_k^+)^{-1} = T_k^+ S^{-1} T_k, \tag{17}$$

$$S_k^+ = (T_k^+ S T_k)^+ = T_k^+ S^+ T_k, \tag{18}$$

since T_k is unitary; hence, when S is unitary

$$S_k^{-1} = S_k^+, \tag{19}$$

or S_k is also unitary.

When a junction is Lorentz reciprocal, the conventional scattering matrix descriptive of this junction has

$$S = \tilde{S}. \tag{20}$$

($\tilde{S}$ denotes the transpose matrix of S.) Substituting for S its expression in terms of S_k:

$$T_k S_k T_k^+ = \widetilde{T_k S_k T_k^+}, \tag{21}$$

or

$$(\tilde{T}_k T_k) S_k = \tilde{S}_k (\tilde{T}_k T_k). \tag{22}$$

When, in addition to being unitary, the transformation T_k is real, then

$$T_k^{-1} = \tilde{T}_k \tag{23}$$

and (22) reduces to

$$S_k = \tilde{S}_k, \tag{24}$$

i.e., the same formal condition on S_k as was imposed on S.

The general theory of this section separates the N^2 independent parameters descriptive of a linear junction into symmetry and asymmetry parameters. Stipulations in addition to linearity regarding the physical character of the junction, such as reciprocity and the conservation of energy force relations among these parameters or, alternatively phrased, reduce the number of parameters which may be assigned arbitrarily. In the instance of reciprocity, $N(N-1)/2$ linear constraints [(20), (22) or (24)] result, and for all the junctions treated, these are so simple that no difficulty is encountered in selecting $N^2 - N(N-1)/2 = (N+1)N/2$ independent parameters. The nonlinear constraints (19) which result from the conservation of energy are not automatically satisfied by the parameters. An illustration of how these nonlinear constraints may be employed is given in the last section.

III. Illustrative Example

While the general principles by means of which appropriate symmetry and asymmetry parameters may be introduced for any junction were presented in the preceding section, these will now be made concrete by application to the H-plane Y junction shown in Fig. 1. This junction constitutes the simplest example which displays all the idiosyncrasies encountered in the most general case.

The symmetry operations have been indicated by marking the planes of reflection symmetry F_1, F_2, F_3, respectively, and the 120°, 240° rotations by R_1 and R_2, respectively.[8] The unitary matrices which perform per-

[8] Subsequently, the same notation will be employed for the geometrical symmetry, the symmetry operation which leaves the junction invariant, and the corresponding permutation matrix.

mutations of the terminal quantities corresponding to F_1 and R_1 are

$$F_1 = \begin{pmatrix} 1 & 0 & 0 \\ 0 & 0 & 1 \\ 0 & 1 & 0 \end{pmatrix}, \qquad R_1 = \begin{pmatrix} 0 & 0 & 1 \\ 1 & 0 & 0 \\ 0 & 1 & 0 \end{pmatrix}. \tag{25}$$

Note that $F_1^2 = I$ and $R_1^3 = I$.

The remaining matrices may be found from the two given by matrix multiplication in accordance with the multiplication Table A below.

TABLE A

M_i \ M_j	I	R_1	R_2	F_1	F_2	F_3
I	I	R_1	R^2	F_1	F_2	F_3
R_1	R_1	R_2	I	F_2	F_3	F_1
R_2	R_2	I	R_1	F_3	F_1	F_2
F_1	F_1	F_3	F_2	I	R_2	R_1
F_2	F_2	F_1	F_3	R_1	I	R_2
F_3	F_3	F_2	F_1	R_2	R_1	I

This table is to be read:

$$M_j M_i = M_k, \tag{26}$$

where

M_i = the ith element of the first column,
M_j = the jth element of the first row,
M_k = the element at the intersection of the ith row and jth column.

Each entry in Table A may be verified by reference to Fig. 1, where the effect of operation M_i *followed* by operation M_j may be seen geometrically.

In the frequency range in which only one mode propagates in each of the waveguide leads, the scattering matrix S of the Y junction with respect to symmetrically chosen reference planes, may be written:

$$S = \begin{pmatrix} \mathcal{S}_{11} & \mathcal{S}_{12} & \mathcal{S}_{13} \\ \mathcal{S}_{21} & \mathcal{S}_{22} & \mathcal{S}_{23} \\ \mathcal{S}_{31} & \mathcal{S}_{32} & \mathcal{S}_{33} \end{pmatrix}. \tag{27}$$

If the Y Junction truly conforms to the symmetry F_1, we have from (8):

$$F_1 S = S F_1, \tag{28}$$

which, on multiplying out, is seen to imply:

$$\mathcal{S}_{12} = \mathcal{S}_{13}, \quad \mathcal{S}_{21} = \mathcal{S}_{31}, \quad \mathcal{S}_{22} = \mathcal{S}_{33}, \text{ and } \mathcal{S}_{23} = \mathcal{S}_{32}. \tag{29}$$

In order to find the symmetry and asymmetry parameters appropriate to F_1, the transformation T_{F_1} must be constructed from eigenvectors $\boldsymbol{f}_1^{(i)}$ of F_1. Accordingly, consider the eigenvalue problem:

$$(F_1 - \phi_1^{(i)})\boldsymbol{f}_1^{(i)} = 0. \tag{30}$$

The eigenvalues $\phi_1^{(i)}$ are found as the roots of

$$\det (F_1 - \phi_1 I) = 0 = (\phi_1 - 1)(\phi_1^2 - 1), \tag{31}$$

or

$$\phi_1^{(1)} = +1, \quad \phi_1^{(2)} = +1, \text{ and } \phi_1^{(3)} = -1.$$

Since $\phi_1^{(1)} = \phi_1^{(2)}$, the eigenvalue problem is degenerate; *i.e.*, the invariant subspace belonging to the eigenvalue $+1$ is two-dimensional. Many pairs of eigenvectors which span the subspace belonging to the eigenvalue $+1$ may be found. Perhaps the simplest orthonormal set is that given in Table B.

TABLE B

Eigenvalue	$\phi_1^{(1)} = \phi_1^{(2)} = +1$		$\phi_1^{(3)} = -1$
Corresponding eigenvector(s)	$\boldsymbol{f}_1^{(1)} = \frac{1}{\sqrt{2}}\begin{pmatrix} 0 \\ 1 \\ 1 \end{pmatrix}$	$\boldsymbol{f}_1^{(2)} = \begin{pmatrix} 1 \\ 0 \\ 0 \end{pmatrix}$	$\boldsymbol{f}_1^{(3)} = \frac{1}{\sqrt{2}}\begin{pmatrix} 0 \\ 1 \\ -1 \end{pmatrix}$

The transformation T_{F_1} constructed from these eigenvectors is

$$T_{F_1} = \frac{1}{\sqrt{2}}\begin{pmatrix} 0 & \sqrt{2} & 0 \\ 1 & 0 & 1 \\ 1 & 0 & -1 \end{pmatrix}. \tag{32}$$

In accordance with (16), the matrix $S_{F_1} = T_{F_1}{}^{+} S T_{F_1}$ has the form

$$S_{F_1} = \begin{pmatrix} \mathcal{A}_{11} & \mathcal{A}_{12} & 0 \\ \mathcal{A}_{21} & \mathcal{A}_{22} & 0 \\ 0 & 0 & \mathcal{A}_{33} \end{pmatrix}, \tag{33}$$

provided that the Y Junction truly conforms to the symmetry F_1. Therefore, in general, $S_{F_1} = T_{F_1}{}^{+} S T_{F_1}$ is given by

$$S_{F_1} = \begin{pmatrix} \mathcal{A}_{11} & \mathcal{A}_{12} & a_{13} \\ \mathcal{A}_{21} & \mathcal{A}_{22} & a_{23} \\ a_{31} & a_{32} & \mathcal{A}_{33} \end{pmatrix} = \frac{1}{2}\begin{pmatrix} \mathcal{S}_{22} + \mathcal{S}_{32} + \mathcal{S}_{23} + \mathcal{S}_{32} & \sqrt{2}(\mathcal{S}_{21} + \mathcal{S}_{31}) & \mathcal{S}_{22} - \mathcal{S}_{33} + \mathcal{S}_{32} - \mathcal{S}_{23} \\ \sqrt{2}(\mathcal{S}_{12} + \mathcal{S}_{13}) & 2\mathcal{S}_{11} & \sqrt{2}(\mathcal{S}_{12} - \mathcal{S}_{13}) \\ \mathcal{S}_{22} - \mathcal{S}_{33} + \mathcal{S}_{23} - \mathcal{S}_{32} & \sqrt{2}(\mathcal{S}_{21} - \mathcal{S}_{31}) & \mathcal{S}_{22} + \mathcal{S}_{33} - \mathcal{S}_{23} - \mathcal{S}_{32} \end{pmatrix}, \tag{34}$$

where the upper case $\mathcal{A}_{ij}$ are symmetry and the lower case a_{ij} asymmetry, parameters. Inversely, $S = T_{F_1} S_{F_1} T_{F_1}{}^{+}$ is given by

$$S = \begin{pmatrix} s_{11} & s_{12} & s_{13} \\ s_{12} & s_{22} & s_{23} \\ s_{31} & s_{32} & s_{33} \end{pmatrix} = \frac{1}{2}\begin{pmatrix} 2a_{22} & \sqrt{2}(a_{21} - a_{23}) & \sqrt{2}(a_{21} - a_{23}) \\ \sqrt{2}(a_{13} + a_{32}) & a_{11} + a_{33} + a_{13} + a_{31} & a_{11} - a_{33} - a_{13} + a_{31} \\ \sqrt{2}(a_{12} - a_{32}) & a_{11} - a_{33} + a_{13} - a_{31} & a_{11} + a_{22} - a_{13} - a_{31} \end{pmatrix}. \tag{35}$$

These results are also listed in Table I(a).

Returning to the eigenvalue problem, (30), an alternative set of orthonormal eigenvectors which will prove useful subsequently is given in Table C.

TABLE C

Eigenvalues	$\phi_1^{(1)} = \phi_1^{(2)} = +1$		$\phi_1^{(3)} = -1$
Corresponding eigenvector(s)	$\hat{f}_1^{(1)} = \frac{1}{\sqrt{3}}\begin{pmatrix} 1 \\ 1 \\ 1 \end{pmatrix}$	$\hat{f}_1^{(2)} = \frac{1}{\sqrt{6}}\begin{pmatrix} 2 \\ -1 \\ -1 \end{pmatrix}$	$\hat{f}_1^{(3)} = \frac{1}{\sqrt{2}}\begin{pmatrix} 0 \\ 1 \\ -1 \end{pmatrix}$

The transformation $\hat{T}_{F_1}$ now appears as

$$\hat{T}_{F_1} = \begin{pmatrix} \frac{1}{\sqrt{2}} & \frac{2}{\sqrt{6}} & 0 \\ \frac{1}{\sqrt{3}} & -\frac{1}{\sqrt{6}} & \frac{1}{\sqrt{2}} \\ \frac{1}{\sqrt{3}} & -\frac{1}{\sqrt{6}} & -\frac{1}{\sqrt{2}} \end{pmatrix}. \tag{36}$$

Corresponding (but different) symmetry and asymmetry parameters may be introduced to parallel (33)–(35).

In order to find the parameters appropriate to R_1, the transformation T_{R_1} must be constructed from the eigenvectors $r_1^{(i)}$ of R_1. Accordingly, consider the eigenvalue problem

$$(R_1 - \rho_1^{(i)})r_1^{(i)} = 0. \tag{37}$$

The eigenvalues $\rho_1^{(i)}$ are found as the roots of

$$\det (R_1 - \rho_1 I) = 0 = (\rho_1^3 - 1),$$

or

$$\rho_1^{(1)} = 1, \qquad \rho_1^{(2)} = k_1 = -\frac{1}{2} + \frac{\sqrt{3}}{2j},$$

and

$$\rho_1^{(3)} = k_2 = -\frac{1}{2} - \frac{\sqrt{3}}{2j}.$$

Since the three roots are distinct, the normalized eigenvectors are uniquely those given in Table D.

TABLE D

Eigenvalue	$\rho_1^{(1)} = 1$	$\rho_1^{(2)} = k_1$	$\rho_1^{(3)} = k_2$
Corresponding eigenvector	$r_1^{(1)} = \frac{1}{\sqrt{3}}\begin{pmatrix} 1 \\ 1 \\ 1 \end{pmatrix}$	$r_1^{(2)} = \frac{1}{\sqrt{3}}\begin{pmatrix} 1 \\ k_2 \\ k_1 \end{pmatrix}$	$r_1^{(3)} = \frac{1}{\sqrt{3}}\begin{pmatrix} 1 \\ k_1 \\ k_2 \end{pmatrix}$

The transformation T_{R_1} constructed from these eigenvectors is

$$T_{R_1} = \frac{1}{\sqrt{3}}\begin{pmatrix} 1 & 1 & 1 \\ 1 & k_2 & k_1 \\ 1 & k_1 & k_2 \end{pmatrix}. \tag{38}$$

In accordance with (16), the transformed scattering matrix $S_{R_1} = T_{R_1}{}^{+} S T_{R_1}$ has the form

$$S_{R_1} = \begin{pmatrix} D_{11} & 0 & 0 \\ 0 & D_{22} & 0 \\ 0 & 0 & D_{33} \end{pmatrix}, \tag{39}$$

provided that the Y junction truly conforms to the symmetry R_1. The general expressions for S_{R_1} and S in terms of symmetry and asymmetry parameters are listed in Table I(b).

When symmetries F_1 and R_1 obtain simultaneously, then the junction is perfectly symmetrical; *i.e.*, when

$$F_1 S = S F_1 \quad \text{and} \quad R_1 S = S R_1, \tag{40}$$

then similar relations hold for F_2, F_3, and R_2, for these may be expressed in terms of F_1 and R_1; *cf.*, Table A. In order to find the parameters appropriate to this symmetry, the transformation $T_{F_1 \& R_1}$ must be constructed. Both eigenvalue problems (30) and (37) are in point here since the scattering matrix of a perfectly symmetrical junction, by (40), must have a set of eigenvectors in common with each F_1 and R_1. Comparison of the eigenvectors in Tables C and D shows that while the first eigenvectors of F_1 and R_1 listed there agree, the remaining two do not. Hence, the requirements imposed by (40) on the eigenvectors of the scattering matrix of a *perfectly symmetrical junction* may be satisfied only if the eigenvalue problem

$$(S - \sigma^{(i)} I)\mathbf{s}^{(i)} = 0 \tag{41}$$

is degenerate. That the vectors $\hat{f}_1^{(2)}$, $\hat{f}_1^{(3)}$ and $r_1^{(2)}$, $r_1^{(3)}$ span the same subspace follows from their orthogonality (to $\hat{f}_1^{(1)} = r_1^{(1)}$). Hence, if the eigenvector $\mathbf{s}_1^{(1)} = \hat{f}_1^{(1)} = r_1^{(1)}$ corresponds to $\sigma^{(1)}$ then

$$\sigma^{(2)} = \sigma^{(3)} \tag{42}$$

is a necessary and sufficient condition on S to satisfy (40). The eigenvectors corresponding to $\sigma^{(2)} = \sigma^{(3)}$ may then be chosen as $\hat{f}_1^{(2)}$, $\hat{f}_1^{(3)}$; $r_1^{(2)}$, $r_1^{(3)}$; or any other linear combination of these. Selecting the first of these alternatives, it follows that

$$T_{F_1 \& R_1} = \hat{T}_{F_1},$$

and that for a perfectly symmetrical junction, $S_{F_1 \& R_1} = T_{F_1}{}^{+}{}_{\& R_1} S T_{F_1 \& R_1}$ has the form

TABLE I

(a) Symmetrical Nonreciprocal H-Plane Y Junction F_1 Symmetry Plane

$$F_1 = \begin{pmatrix} 1 & 0 & 0 \\ 0 & 0 & 1 \\ 0 & 1 & 0 \end{pmatrix} \qquad T_{F_1} = \frac{1}{\sqrt{2}} \begin{pmatrix} 0 & \sqrt{2} & 0 \\ 1 & 0 & 1 \\ 1 & 0 & -1 \end{pmatrix}$$

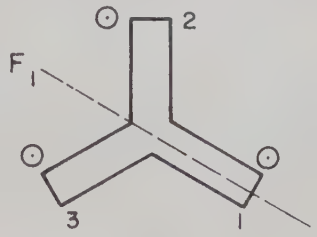

Natural Basis	$S = \begin{pmatrix} \mathcal{S}_{11} & \mathcal{S}_{12} & \mathcal{S}_{13} \\ \mathcal{S}_{21} & \mathcal{S}_{22} & \mathcal{S}_{23} \\ \mathcal{S}_{31} & \mathcal{S}_{32} & \mathcal{S}_{33} \end{pmatrix}$	$S = \frac{1}{2} \begin{pmatrix} 2\mathcal{A}_{22} & \sqrt{2}(\mathcal{A}_{21} + a_{23}) & \sqrt{2}(\mathcal{A}_{21} - a_{23}) \\ \sqrt{2}(\mathcal{A}_{12} + a_{32}) & (\mathcal{A}_{11} + \mathcal{A}_{33} + a_{13} + a_{31}) & (\mathcal{A}_{11} - \mathcal{A}_{33} - a_{13} + a_{31}) \\ \sqrt{2}(\mathcal{A}_{12} - a_{32}) & (\mathcal{A}_{11} - \mathcal{A}_{33} + a_{13} - a_{31}) & (\mathcal{A}_{11} + \mathcal{A}_{33} - a_{13} - a_{31}) \end{pmatrix}$
Transformed Basis	$S_{F_1} = \begin{pmatrix} \mathcal{A}_{11} & \mathcal{A}_{12} & a_{13} \\ \mathcal{A}_{21} & \mathcal{A}_{22} & a_{23} \\ a_{31} & a_{32} & \mathcal{A}_{33} \end{pmatrix}$	$S_{F_1} = \frac{1}{2} \begin{pmatrix} (\mathcal{S}_{22} + \mathcal{S}_{33} + \mathcal{S}_{23} + \mathcal{S}_{32}) & \sqrt{2}(\mathcal{S}_{21} + \mathcal{S}_{31}) & (\mathcal{S}_{22} - \mathcal{S}_{33} + \mathcal{S}_{32} - \mathcal{S}_{23}) \\ \sqrt{2}(\mathcal{S}_{12} + \mathcal{S}_{13}) & 2\mathcal{S}_{11} & \sqrt{2}(\mathcal{S}_{12} - \mathcal{S}_{13}) \\ (\mathcal{S}_{22} - \mathcal{S}_{33} + \mathcal{S}_{23} - \mathcal{S}_{32}) & \sqrt{2}(\mathcal{S}_{21} - \mathcal{S}_{31}) & (\mathcal{S}_{22} + \mathcal{S}_{33} - \mathcal{S}_{23} - \mathcal{S}_{32}) \end{pmatrix}$

(b) Symmetrical Nonreciprocal H-Plane Y Junction R_1 Rotational Symmetry

$$R_1 = \begin{pmatrix} 0 & 0 & 1 \\ 1 & 0 & 0 \\ 0 & 1 & 0 \end{pmatrix} \qquad T_{R_1} = \frac{1}{\sqrt{3}} \begin{pmatrix} 1 & 1 & 1 \\ 1 & k_2 & k_1 \\ 1 & k_1 & k_2 \end{pmatrix}$$

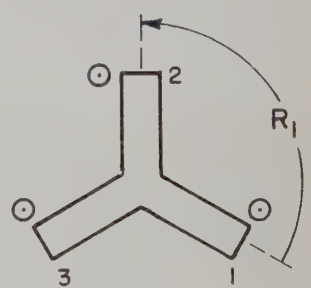

Natural Basis	$S = \begin{pmatrix} \mathcal{S}_{11} & \mathcal{S}_{12} & \mathcal{S}_{13} \\ \mathcal{S}_{21} & \mathcal{S}_{22} & \mathcal{S}_{23} \\ \mathcal{S}_{31} & \mathcal{S}_{32} & \mathcal{S}_{33} \end{pmatrix}$	$\mathcal{S}_{11} = \frac{1}{3}[\mathcal{D}_{11} + \mathcal{D}_{22} + \mathcal{D}_{33} + d_{12} + d_{13} + d_{21} + d_{23} + d_{31} + d_{32}]$ $\mathcal{S}_{12} = \frac{1}{3}[\mathcal{D}_{11} + \mathcal{D}_{22}k_1 + \mathcal{D}_{33}k_2 + k_1(d_{12} + d_{32}) + k_2(d_{13} + d_{23}) + d_{21} + d_{31}]$ $\mathcal{S}_{13} = \frac{1}{3}[\mathcal{D}_{11} + \mathcal{D}_{22}k_2 + \mathcal{D}_{33}k_1 + k_1(d_{13} + d_{23}) + k_2(d_{12} + d_{32}) + d_{21} + d_{31}]$ $\mathcal{S}_{21} = \frac{1}{3}[\mathcal{D}_{11} + \mathcal{D}_{22}k_2 + \mathcal{D}_{33}k_1 + k_1(d_{31} + d_{32}) + k_2(d_{21} + d_{23}) + d_{12} + d_{13}]$ $\mathcal{S}_{22} = \frac{1}{3}[\mathcal{D}_{11} + \mathcal{D}_{22} + \mathcal{D}_{33} + k_1(d_{12} + d_{23} + d_{31}) + k_2(d_{13} + d_{21} + d_{32})]$ $\mathcal{S}_{23} = \frac{1}{3}[\mathcal{D}_{11} + \mathcal{D}_{22}k_1 + \mathcal{D}_{33}k_2 + k_1(d_{13} + d_{21} + d_{32}) + k_2(d_{12} + d_{23} + d_{31})]$ $\mathcal{S}_{31} = \frac{1}{3}[\mathcal{D}_{11} + \mathcal{D}_{22}k_1 + \mathcal{D}_{33}k_2 + k_1(d_{21} + d_{23}) + k_2(d_{31} + d_{32}) + d_{12} + d_{13}]$ $\mathcal{S}_{32} = \frac{1}{3}[\mathcal{D}_{11} + \mathcal{D}_{22}k_2 + \mathcal{D}_{33}k_1 + k_1(d_{12} + d_{21}) + k_2(d_{13} + d_{31}) + d_{23} + d_{32}]$ $\mathcal{S}_{33} = \frac{1}{3}[\mathcal{D}_{11} + \mathcal{D}_{22} + \mathcal{D}_{33} + k_1(d_{13} + d_{21} + d_{32}) + k_2(d_{12} + d_{23} + d_{31})]$
Transformed Basis	$S_{R_1} = \begin{pmatrix} \mathcal{D}_{11} & d_{12} & d_{13} \\ d_{21} & \mathcal{D}_{22} & d_{23} \\ d_{31} & d_{32} & \mathcal{D}_{33} \end{pmatrix}$	$\mathcal{D}_{11} = \frac{1}{3}[\mathcal{S}_{11} + \mathcal{S}_{22} + \mathcal{S}_{33} + \mathcal{S}_{12} + \mathcal{S}_{13} + \mathcal{S}_{21} + \mathcal{S}_{23} + \mathcal{S}_{31} + \mathcal{S}_{32}]$ $d_{12} = \frac{1}{3}[\mathcal{S}_{11} + \mathcal{S}_{22}k_2 + \mathcal{S}_{33}k_1 + k_1(\mathcal{S}_{13} + \mathcal{S}_{23}) + k_2(\mathcal{S}_{12} + \mathcal{S}_{32}) + \mathcal{S}_{21} + \mathcal{S}_{31}]$ $d_{13} = \frac{1}{3}[\mathcal{S}_{11} + \mathcal{S}_{22}k_1 + \mathcal{S}_{33}k_2 + k_1(\mathcal{S}_{12} + \mathcal{S}_{32}) + k_2(\mathcal{S}_{13} + \mathcal{S}_{23}) + \mathcal{S}_{21} + \mathcal{S}_{31}]$ $d_{21} = \frac{1}{3}[\mathcal{S}_{11} + \mathcal{S}_{22}k_1 + \mathcal{S}_{33}k_2 + k_1(\mathcal{S}_{21} + \mathcal{S}_{23}) + k_2(\mathcal{S}_{31} + \mathcal{S}_{32}) + \mathcal{S}_{12} + \mathcal{S}_{13}]$ $\mathcal{D}_{22} = \frac{1}{3}[\mathcal{S}_{11} + \mathcal{S}_{22} + \mathcal{S}_{33} + k_1(\mathcal{S}_{13} + \mathcal{S}_{21} + \mathcal{S}_{32}) + k_2(\mathcal{S}_{12} + \mathcal{S}_{23} + \mathcal{S}_{31})]$ $d_{23} = \frac{1}{3}[\mathcal{S}_{11} + \mathcal{S}_{22}k_2 + \mathcal{S}_{33}k_1 + k_1(\mathcal{S}_{12} + \mathcal{S}_{21}) + k_2(\mathcal{S}_{13} + \mathcal{S}_{31}) + \mathcal{S}_{23} + \mathcal{S}_{32}]$ $d_{31} = \frac{1}{3}[\mathcal{S}_{11} + \mathcal{S}_{22}k_2 + \mathcal{S}_{33}k_1 + k_1(\mathcal{S}_{31} + \mathcal{S}_{32}) + k_2(\mathcal{S}_{21} + \mathcal{S}_{23}) + \mathcal{S}_{12} + \mathcal{S}_{13}]$ $d_{32} = \frac{1}{3}[\mathcal{S}_{11} + \mathcal{S}_{22}k_1 + \mathcal{S}_{33}k_2 + k_1(\mathcal{S}_{13} + \mathcal{S}_{31}) + k_2(\mathcal{S}_{12} + \mathcal{S}_{21}) + \mathcal{S}_{23} + \mathcal{S}_{32}]$ $\mathcal{D}_{33} = \frac{1}{3}[\mathcal{S}_{11} + \mathcal{S}_{22} + \mathcal{S}_{33} + k_1(\mathcal{S}_{12} + \mathcal{S}_{23} + \mathcal{S}_{31}) + k_2(\mathcal{S}_{13} + \mathcal{S}_{21} + \mathcal{S}_{23})]$

$$k_1 = -\frac{1}{2} + \frac{\sqrt{3}}{2j}, \qquad k_2 = -\frac{1}{2} - \frac{\sqrt{3}}{2j}$$

$$S_{F_1\&R_1} = \begin{pmatrix} \mathcal{E}_{11} & 0 & 0 \\ 0 & \mathcal{E}_{22} & 0 \\ 0 & 0 & \mathcal{E}_{22} \end{pmatrix}, \tag{43}$$

where $\sigma^{(1)}$ and $\sigma^{(2)} = \sigma^{(3)}$ have been replaced, respectively, by $\mathcal{E}_{11}$ and $\mathcal{E}_{22}$ to conform to the notation of Section II.

The general expression for $S_{F_1 \& R_1}$ (for *any* three-port) in terms of symmetry and asymmetry parameters takes the form

$$S_{F_1\&R_1} = \begin{pmatrix} \mathcal{E}_{11} & e_{12} & e_{13} \\ e_{21} & \mathcal{E}_{22} + e_{22} & e_{23} \\ e_{31} & e_{32} & \mathcal{E}_{22} - e_{22} \end{pmatrix}. \tag{44}$$

The asymmetry parameter e_{22} is required by the symmetry degeneracy. (More complex combinations of symmetries in junctions with large numbers of ports are more systematically handled by the apparatus of the theory of group representations.)

It is unnecessary to repeat, in each case, for symmetries F_2, F_3 and R_2, discussions equivalent to those just completed for F_1 and R_1. F_1 and R_1 constitute generators of the group, Table A, and hence the parameters for the symmetries F_2 and F_3 may be obtained via, in essence, a relabeling of the ports in Fig. 1. Since R_1 and R_2 commute, the results for S_{R_1} and S_{R_2} are identical. The procedure may be formalized in terms of the symmetry matrices.

Assume that for some symmetry M_k, the eigenvalue problem (9) has been solved; the transformation T_k, (10), has been found, and the form of S_k, (15), determined. From these, it is easy to obtain corresponding results for a matrix M_l.

$$M_k = M_j^{-1} M_l M_j. \tag{45}$$

Substituting for M_k in (9), the expression (45) yields:

$$(M_l - \mu_k^{(i)}) M_j \boldsymbol{m}_k^{(i)} = 0. \tag{46}$$

Thus, the eigenvalues of M_l are precisely those of M_k, namely $\mu_k^{(i)}$, and the corresponding eigenvectors are $M_j \boldsymbol{m}_k^{(i)}$. The transformation T_l is therefore

$$T_l = M_j T_k, \tag{47}$$

and the form of the transformed scattering matrix

$$\begin{aligned} S_l &= T_l^+ S T_l = M_j^+ (T_k^+ S T_k) M_j \\ &= M_j^+ S_k M_j. \end{aligned} \tag{48}$$

To apply (48) for the purpose of finding the additional matrices S_{F_2} and S_{F_3} required to complete the treatment of the symmetrical Y junction, the matrices F_2 and F_3 must be written in the form of (45); M_k may be either F_1 or R_1. As may be verified by employing Table A,

$$F_1 = R_1^{-1} F_2 R_1 = R_2^{-1} F_3 R_2. \tag{49}$$

IV. Applications

Preferred asymmetry parameters may be tabulated for the several common types of waveguide junctions. Convenient tabulations take the form of pairs of equal matrices, comparison of which, element for element, yields the asymmetry parameters in terms of the conventional scattering parameters, and conversely.

Tables are assigned Roman numerals which correspond to the type of symmetrical waveguide junction considered. Within these principal divisions, according to junction type, each particular symmetry, or combination of symmetries, is distinguished by a letter following the Roman numeral. Due to limitations of space, only those tables required in the body of the paper are given. On the extreme right is a drawing of a common form of the type of waveguide junction considered. This drawing should be examined with care as certain information in respect to circuit conventions essential for the use of the tables is given only in this form. First, the pertinent symmetry is indicated. Second, the waveguide leads of the junction are distinguished by circled Arabic numerals; these numerals correspond to the port designations in the equivalent circuit for the junction. Third, reference or terminal planes are indicated simply by truncating the waveguide leads. The arrows across the terminal planes indicate the assigned polarity.

The tables are divided into two columns. Consider the column on the left designated "Natural Basis." The two matrices in this column are both the conventional (normalized voltage) scattering matrix for the junction S. The upper matrix is essentially the definition of $S = (\mathcal{S}_{ij})$ for the junction. If $\mathcal{S}_{ij} = \mathcal{S}_{ji}$, reciprocity constraints have been imposed. The lower matrix is the scattering matrix written in terms of the preferred parameters. The lower case letters are the asymmetry parameters. The remaining parameters, upper case letters, are symmetry parameters.

Now consider the column on the right designated "Transformed Basis." The matrices in this column are both related to the conventional scattering matrix by the transformation T_M (the subscript M stands for the pertinent symmetry in the particular table), *i.e.*,

$$S_M = T_M^+ S T_M. \tag{50}$$

The upper matrix is S_M written in terms of the preferred parameters, while the lower matrix is S_M written in terms of the elements of the conventional scattering matrix.

Eq. (50) may be given a network interpretation.[3] If one defines a $2N$-port with scattering matrix $S\{T_M\}$,

$$S\{T_M\} = \left(\begin{array}{c|c} 0 & T_M^+ \\ \hline T_M & 0 \end{array}\right), \tag{51}$$

then the N-ports represented by S and S_M are related as shown in Fig. 2. The tandem connection of S with $S\{T_M\}$, in accordance with the terminal markings in Fig. 2, yield a network representation for S_M. Note that each line on the circuit diagram represents a waveguide port or terminal *pair*.

The symmetry and asymmetry parameters have a variety of straightforward applications. These will be

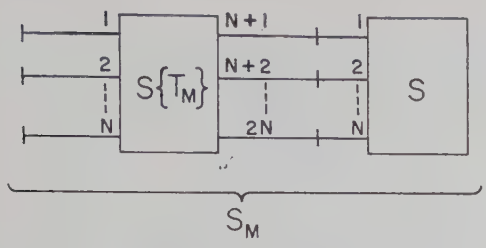

Fig. 2—Network representation of S_M.

illustrated by two examples involving 1) a hybrid-T junction, and 2) a short-slot directional coupler, both frequently encountered in practice.

Consider a hybrid-T junction such as, for example, shown in Table II. The asymmetry parameters for this junction may be determined by measuring the elements of the scattering matrix $S=(s_{ij})$ and then substituting in the second matrix listed in the second column,

$$a_{13} = \frac{1}{2}(s_{11} - s_{22}) = \text{reflection difference},$$

$$a_{14} = \frac{1}{\sqrt{2}}(s_{14} - s_{24}) = H\text{-arm balance depth},$$

$$a_{23} = \frac{1}{\sqrt{2}}(s_{13} - s_{23}) = E\text{-arm balance depth},$$

$$a_{24} = s_{34} = E\text{-}H \text{ arm isolation}.$$

However, Fig. 2 indicates how these asymmetry parameters might be measured directly provided the network $S\{T_F\}$, *cf.* (51),

$$S\{T_F\} = \frac{1}{\sqrt{2}}\left[\begin{array}{cccc|cccc} 0 & 0 & 0 & 0 & 1 & 1 & 0 & 0 \\ 0 & 0 & 0 & 0 & 0 & 0 & \sqrt{2} & 0 \\ 0 & 0 & 0 & 0 & 1 & -1 & 0 & 0 \\ 0 & 0 & 0 & 0 & 0 & 0 & 0 & \sqrt{2} \\ \hline 1 & 0 & 1 & 0 & 0 & 0 & 0 & 0 \\ 1 & 0 & -1 & 0 & 0 & 0 & 0 & 0 \\ 0 & \sqrt{2} & 0 & 0 & 0 & 0 & 0 & 0 \\ 0 & 0 & 0 & \sqrt{2} & 0 & 0 & 0 & 0 \end{array}\right], \quad (52)$$

were available. The equivalent circuit of $S\{T_F\}$, shown in Fig. 3, consists of an ideal hybrid-T and two direct connections, as may be verified by inspection. Thus, if a suitable high-quality hybrid-T junction is available, the asymmetry parameters of a second hybrid-T junction may be measured directly by connecting these two as required by the terminal markings for Fig. 2.

The four asymmetry parameters introduced to describe an arbitrary reciprocal hybrid-T junction are all linearly independent. However, if the hybrid-T junction is also lossless, certain nonlinear relations are forced among these parameters and the symmetry parameters of the junction. Some interesting conclusions for *nearly symmetrical, nearly matched* hybrid-T junctions may be drawn from a simple perturbation calculation.

The condition that the junction be lossless is that the scattering matrix S or S_F be unitary. Partition the matrix S_F;

$$S_F = \left[\begin{array}{cc|cc} \alpha_{11} & \alpha_{12} & a_{13} & a_{14} \\ \alpha_{12} & \alpha_{22} & a_{23} & a_{24} \\ \hline a_{13} & a_{23} & \alpha_{33} & \alpha_{34} \\ a_{14} & a_{24} & \alpha_{34} & \alpha_{44} \end{array}\right] = \left(\begin{array}{c|c} \alpha_{\mathrm{I\,I}} & a_{\mathrm{I\,II}} \\ \hline a_{\mathrm{I\,II}} & \alpha_{\mathrm{II\,II}} \end{array}\right), \quad (53)$$

as shown in (53). Since the junction is *nearly symmetrical*, every element of $a_{\mathrm{I\,II}}$ is small. Neglecting squares of small quantities, the unitary condition $S_F S_F^{+} = I$ yields:

$$\alpha_{\mathrm{I\,I}}\,\alpha_{\mathrm{I\,I}}^{+} = I, \quad (54a)$$

$$\alpha_{\mathrm{II\,II}}\,\alpha_{\mathrm{II\,II}}^{+} = I; \quad (54b)$$

$$\bar{a}_{\mathrm{I\,II}}\,\alpha_{\mathrm{I}}{}^{+}{}_{\mathrm{I}} + \alpha_{\mathrm{II\,II}}\,a_{\mathrm{I}}{}^{+}{}_{\mathrm{II}} = 0, \quad (55a)$$

$$\alpha_{\mathrm{I\,I}}\,a_{\mathrm{I}}{}^{*}{}_{\mathrm{II}} + a_{\mathrm{I\,II}}\,\alpha_{\mathrm{II}}{}^{+}{}_{\mathrm{II}} = 0. \quad (55b)$$

Eqs. (54a) and (54b) state that, to first order, the same relations exist among the symmetry parameters of the hybrid-T junction as would obtain if the junction were perfectly symmetrical. In particular,

$$\begin{aligned} |\alpha_{11}|^2 + |\alpha_{12}|^2 &= 1, & |\alpha_{33}|^2 + |\alpha_{34}|^2 &= 1; \\ |\alpha_{11}| &= |\alpha_{22}|, & |\alpha_{33}| &= |\alpha_{44}|. \end{aligned} \quad (56)$$

From Table II, column 2, it may be seen that

$$s_{33} = \alpha_{22} \quad \text{and} \quad s_{44} = \alpha_{44}, \quad (57)$$

so that if the hybrid-T junction is *nearly matched*, α_{22} and α_{44} are so small that squares of $|\alpha_{ii}|^2$ may be neglected. (This also implies that, to first order, $|\alpha_{12}|^2 = |\alpha_{34}|^2 = 1$.) Eqs. (55a) and (55b) then reduce to

$$\bar{a}_{\mathrm{I\,II}}\,U\alpha_{12}^{*} + \alpha_{34}U a_{\mathrm{I}}{}^{+}{}_{\mathrm{II}} = 0, \quad (58a)$$

$$\alpha_{12}U a_{\mathrm{I}}{}^{*}{}_{\mathrm{II}} + a_{\mathrm{I\,II}}U\alpha_{34}^{*} = 0; \quad (58b)$$

$$U = \begin{pmatrix} 0 & 1 \\ 1 & 0 \end{pmatrix}. \quad (58c)$$

It follows directly from either (58a) or (58b) that

$$|a_{13}| = |a_{24}| \quad \text{and} \quad |a_{14}| = |a_{23}|. \quad (59)$$

For a second example, consider a junction with many symmetries such as a (short-slot) directional coupler. This junction may be asymmetric in many ways and the analytical asymmetry parameters may aid in the determination of where the symmetry defect lies. To avoid the specialty of a purely numerical example, consider that the scattering matrix of a coupler $S=(s_{ij})$ has been measured and was found to be (see Fig. 4)

$$S = (s_{ij}) = \begin{pmatrix} \alpha p^2 & \beta p & \gamma p^2 & \delta p \\ \beta p & \alpha & \delta p & \gamma \\ \gamma p^2 & \delta p & \alpha p^2 & \beta p \\ \delta p & \gamma & \beta p & \alpha \end{pmatrix}. \quad (60)$$

As compared to the somewhat more symmetrical 4-port junction (see Fig. 5) considered in Table III, the short-slot coupler cannot be expected to possess R_1 or F_3 symmetry. However, it is pertinent to compute the asymmetry parameters associated with F_1, F_2 and R_2.

TABLE II

HYBRID T JUNCTION F SYMMETRY PLANE

$$F = \begin{bmatrix} 0 & 1 & 0 & 0 \\ 1 & 0 & 0 & 0 \\ 0 & 0 & 1 & 0 \\ 0 & 0 & 0 & -1 \end{bmatrix} \qquad T = \frac{1}{\sqrt{2}} \begin{bmatrix} 1 & 0 & 1 & 0 \\ 1 & 0 & -1 & 0 \\ 0 & \sqrt{2} & 0 & 0 \\ 0 & 0 & 0 & \sqrt{2} \end{bmatrix}$$

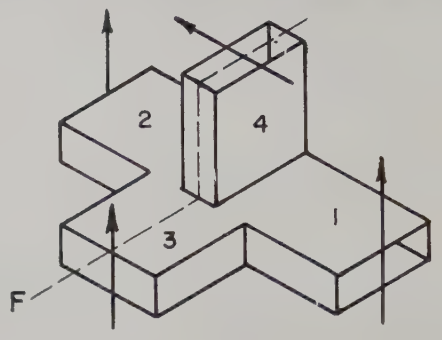

Natural Basis	$S = \begin{bmatrix} \mathcal{S}_{11} & \mathcal{S}_{12} & \mathcal{S}_{13} & \mathcal{S}_{14} \\ \mathcal{S}_{12} & \mathcal{S}_{22} & \mathcal{S}_{23} & \mathcal{S}_{24} \\ \mathcal{S}_{13} & \mathcal{S}_{23} & \mathcal{S}_{33} & \mathcal{S}_{34} \\ \mathcal{S}_{14} & \mathcal{S}_{24} & \mathcal{S}_{34} & \mathcal{S}_{44} \end{bmatrix}$	$S = \frac{1}{2} \begin{bmatrix} (\mathcal{A}_{11} + \mathcal{A}_{33} + 2a_{13}) & (\mathcal{A}_{11} - \mathcal{A}_{33}) & \sqrt{2}(\mathcal{A}_{12} + a_{23}) & \sqrt{2}(\mathcal{A}_{34} + a_{14}) \\ (\mathcal{A}_{11} - \mathcal{A}_{33}) & (\mathcal{A}_{11} + \mathcal{A}_{33} - 2a_{13}) & \sqrt{2}(\mathcal{A}_{12} - a_{23}) & -\sqrt{2}(\mathcal{A}_{34} - a_{14}) \\ \sqrt{2}(\mathcal{A}_{12} + a_{23}) & \sqrt{2}(\mathcal{A}_{12} - a_{23}) & 2\mathcal{A}_{22} & 2a_{24} \\ \sqrt{2}(\mathcal{A}_{34} + a_{14}) & -\sqrt{2}(\mathcal{A}_{34} - a_{14}) & 2a_{24} & 2\mathcal{A}_{44} \end{bmatrix}$
Transformed Basis	$S_F = \begin{bmatrix} \mathcal{A}_{11} & \mathcal{A}_{12} & a_{13} & a_{14} \\ \mathcal{A}_{12} & \mathcal{A}_{22} & a_{23} & a_{24} \\ a_{13} & a_{23} & \mathcal{A}_{33} & \mathcal{A}_{34} \\ a_{14} & a_{24} & \mathcal{A}_{34} & \mathcal{A}_{44} \end{bmatrix}$	$S_F = \frac{1}{2} \begin{bmatrix} (\mathcal{S}_{11} + \mathcal{S}_{22} + 2\mathcal{S}_{12}) & \sqrt{2}(\mathcal{S}_{13} + \mathcal{S}_{23}) & (\mathcal{S}_{11} - \mathcal{S}_{22}) & \sqrt{2}(\mathcal{S}_{14} + \mathcal{S}_{24}) \\ \sqrt{2}(\mathcal{S}_{13} + \mathcal{S}_{23}) & 2\mathcal{S}_{33} & \sqrt{2}(\mathcal{S}_{13} - \mathcal{S}_{23}) & 2\mathcal{S}_{34} \\ (\mathcal{S}_{11} - \mathcal{S}_{22}) & \sqrt{2}(\mathcal{S}_{13} - \mathcal{S}_{23}) & (\mathcal{S}_{11} + \mathcal{S}_{22} - 2\mathcal{S}_{12}) & \sqrt{2}(\mathcal{S}_{14} - \mathcal{S}_{24}) \\ \sqrt{2}(\mathcal{S}_{14} + \mathcal{S}_{24}) & 2\mathcal{S}_{24} & \sqrt{2}(\mathcal{S}_{14} - \mathcal{S}_{24}) & 2\mathcal{S}_{44} \end{bmatrix}$

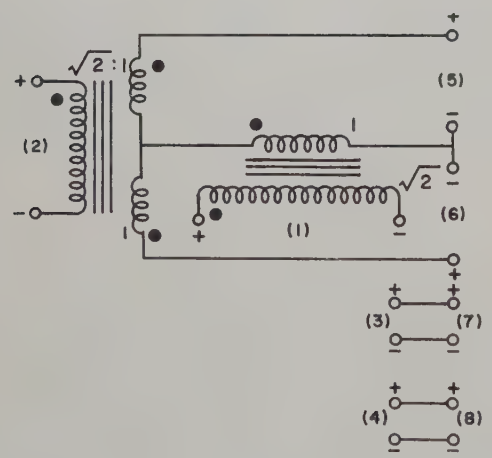

Fig. 3—Equivalent circuit for $S\{T_F\}$ associated with the hybrid-T.

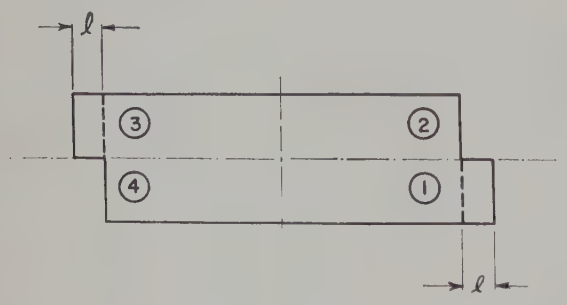

Fig. 4—Symmetry of the coupler described by (60).

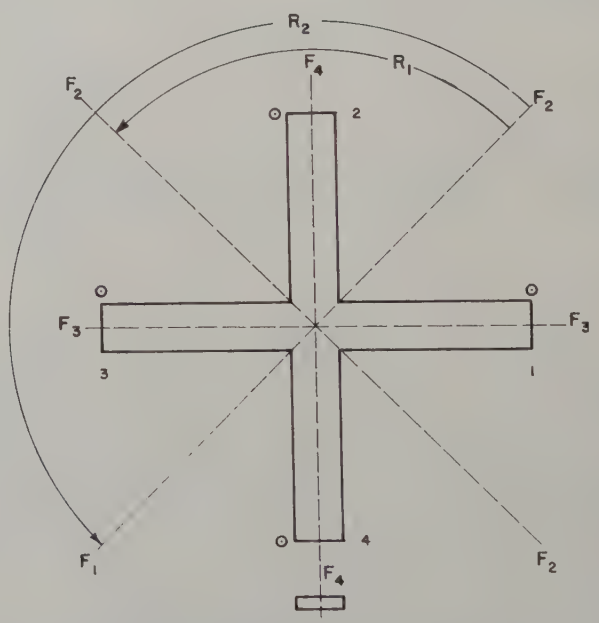

Fig. 5—Symmetrical reciprocal H-plane four-port junction. F_1, symmetry plane; F_2, symmetry plane; F_3, symmetry plane; F_4, symmetry plane; R_1, rotational symmetry; F_1 and R_1 symmetry (implies all remaining operations in group); R_2, rotational symmetry (applicable to short-slot coupler); F_1 and R_2, symmetry (implies all remaining operations in subgroup for short-slot coupler geometry).

TABLE III

(a) Symmetrical H-Plane Four-Port Junction F_1 Symmetry Plane

$$F_1 = \begin{pmatrix} 0 & 1 & 0 & 0 \\ 1 & 0 & 0 & 0 \\ 0 & 0 & 0 & 1 \\ 0 & 0 & 1 & 0 \end{pmatrix} \qquad T_{F_1} = \frac{1}{\sqrt{2}} \begin{pmatrix} 1 & 0 & 1 & 0 \\ 1 & 0 & -1 & 0 \\ 0 & 1 & 0 & 1 \\ 0 & 1 & 0 & -1 \end{pmatrix}$$

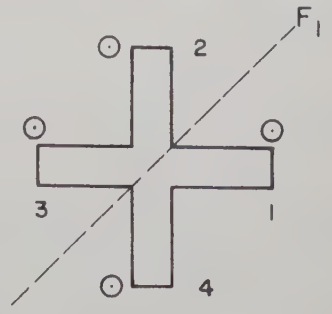

Natural Basis	$S = \begin{pmatrix} \mathcal{S}_{11} & \mathcal{S}_{12} & \mathcal{S}_{13} & \mathcal{S}_{14} \\ \mathcal{S}_{12} & \mathcal{S}_{22} & \mathcal{S}_{23} & \mathcal{S}_{24} \\ \mathcal{S}_{13} & \mathcal{S}_{23} & \mathcal{S}_{33} & \mathcal{S}_{34} \\ \mathcal{S}_{14} & \mathcal{S}_{24} & \mathcal{S}_{34} & \mathcal{S}_{44} \end{pmatrix}$	$S = \frac{1}{2} \begin{pmatrix} (\mathcal{A}_{11}+\mathcal{A}_{33}+2a_{13}) & (\mathcal{A}_{11}-\mathcal{A}_{33}) & (\mathcal{A}_{12}+\mathcal{A}_{34}+a_{14}+a_{23}) & (\mathcal{A}_{12}-\mathcal{A}_{34}-a_{14}+a_{23}) \\ (\mathcal{A}_{11}-\mathcal{A}_{33}) & (\mathcal{A}_{11}+\mathcal{A}_{33}-2a_{13}) & (\mathcal{A}_{12}-\mathcal{A}_{34}+a_{14}-a_{23}) & (\mathcal{A}_{12}+\mathcal{A}_{34}-a_{14}-a_{23}) \\ (\mathcal{A}_{12}+\mathcal{A}_{34}+a_{14}+a_{23}) & (\mathcal{A}_{12}-\mathcal{A}_{34}+a_{14}-a_{23}) & (\mathcal{A}_{22}+\mathcal{A}_{44}+2a_{14}) & (\mathcal{A}_{22}-\mathcal{A}_{44}) \\ (\mathcal{A}_{12}-\mathcal{A}_{34}-a_{14}+a_{23}) & (\mathcal{A}_{12}+\mathcal{A}_{34}-a_{14}-a_{23}) & (\mathcal{A}_{22}-\mathcal{A}_{44}) & (\mathcal{A}_{22}+\mathcal{A}_{44}-2a_{24}) \end{pmatrix}$
Transformed Basis	$S_{F_1} = \begin{pmatrix} \mathcal{A}_{11} & \mathcal{A}_{12} & a_{13} & a_{14} \\ \mathcal{A}_{12} & \mathcal{A}_{22} & a_{23} & a_{24} \\ a_{13} & a_{23} & \mathcal{A}_{33} & \mathcal{A}_{34} \\ a_{14} & a_{24} & \mathcal{A}_{34} & \mathcal{A}_{44} \end{pmatrix}$	$S_{F_1} = \frac{1}{2} \begin{pmatrix} (\mathcal{S}_{11}+\mathcal{S}_{22}+2\mathcal{S}_{12}) & (\mathcal{S}_{13}+\mathcal{S}_{14}+\mathcal{S}_{23}+\mathcal{S}_{24}) & (\mathcal{S}_{11}-\mathcal{S}_{22}) & (\mathcal{S}_{13}-\mathcal{S}_{14}+\mathcal{S}_{23}-\mathcal{S}_{24}) \\ (\mathcal{S}_{13}+\mathcal{S}_{14}+\mathcal{S}_{23}+\mathcal{S}_{24}) & (\mathcal{S}_{33}+\mathcal{S}_{44}+2\mathcal{S}_{34}) & (\mathcal{S}_{13}-\mathcal{S}_{23}+\mathcal{S}_{14}-\mathcal{S}_{24}) & (\mathcal{S}_{33}-\mathcal{S}_{44}) \\ (\mathcal{S}_{11}-\mathcal{S}_{22}) & (\mathcal{S}_{13}+\mathcal{S}_{14}-\mathcal{S}_{23}-\mathcal{S}_{24}) & (\mathcal{S}_{11}+\mathcal{S}_{22}-2\mathcal{S}_{12}) & (\mathcal{S}_{13}-\mathcal{S}_{14}-\mathcal{S}_{23}+\mathcal{S}_{24}) \\ (\mathcal{S}_{13}+\mathcal{S}_{23}-\mathcal{S}_{14}-\mathcal{S}_{24}) & (\mathcal{S}_{33}-\mathcal{S}_{44}) & (\mathcal{S}_{13}-\mathcal{S}_{23}-\mathcal{S}_{14}+\mathcal{S}_{24}) & (\mathcal{S}_{33}+\mathcal{S}_{44}-2\mathcal{S}_{34}) \end{pmatrix}$

(b) Symmetrical H-Plane Four-Port Junction F_3 Symmetry Plane

$$F_3 = \begin{pmatrix} 1 & 0 & 0 & 0 \\ 0 & 0 & 0 & 1 \\ 0 & 0 & 1 & 0 \\ 0 & 1 & 0 & 0 \end{pmatrix} \qquad T_{F_3} = \frac{1}{\sqrt{2}} \begin{pmatrix} \sqrt{2} & 0 & 0 & 0 \\ 0 & 0 & 1 & 1 \\ 0 & \sqrt{2} & 0 & 0 \\ 0 & 0 & 1 & -1 \end{pmatrix}$$

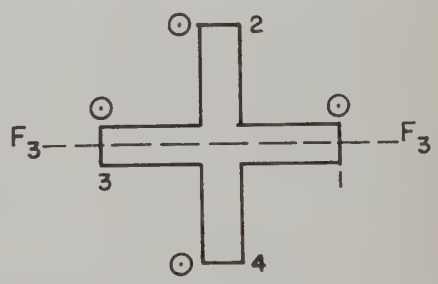

Natural Basis	$S = \begin{pmatrix} \mathcal{S}_{11} & \mathcal{S}_{12} & \mathcal{S}_{13} & \mathcal{S}_{14} \\ \mathcal{S}_{12} & \mathcal{S}_{22} & \mathcal{S}_{23} & \mathcal{S}_{24} \\ \mathcal{S}_{13} & \mathcal{S}_{23} & \mathcal{S}_{33} & \mathcal{S}_{34} \\ \mathcal{S}_{14} & \mathcal{S}_{24} & \mathcal{S}_{34} & \mathcal{S}_{44} \end{pmatrix}$	$S = \frac{1}{2} \begin{pmatrix} 2\mathcal{C}_{11} & \sqrt{2}(\mathcal{C}_{13}+c_{14}) & 2\mathcal{C}_{12} & \sqrt{2}(\mathcal{C}_{13}-c_{14}) \\ \sqrt{2}(\mathcal{C}_{13}+c_{14}) & (\mathcal{C}_{33}+\mathcal{C}_{44}+2c_{34}) & \sqrt{2}(\mathcal{C}_{23}+c_{24}) & (\mathcal{C}_{33}-\mathcal{C}_{44}) \\ 2\mathcal{C}_{12} & \sqrt{2}(\mathcal{C}_{23}+c_{24}) & 2\mathcal{C}_{22} & \sqrt{2}(\mathcal{C}_{23}-c_{24}) \\ \sqrt{2}(\mathcal{C}_{13}-c_{14}) & (\mathcal{C}_{33}-\mathcal{C}_{44}) & \sqrt{2}(\mathcal{C}_{23}-c_{24}) & (\mathcal{C}_{33}+\mathcal{C}_{44}-2\mathcal{C}_{34}) \end{pmatrix}$
Transformed Basis	$S_{F_3} = \begin{pmatrix} \mathcal{C}_{11} & \mathcal{C}_{12} & \mathcal{C}_{13} & c_{14} \\ \mathcal{C}_{12} & \mathcal{C}_{22} & \mathcal{C}_{23} & c_{24} \\ \mathcal{C}_{13} & \mathcal{C}_{23} & \mathcal{C}_{33} & c_{34} \\ c_{14} & c_{24} & c_{34} & \mathcal{C}_{44} \end{pmatrix}$	$S_{F_3} = \frac{1}{2} \begin{pmatrix} 2\mathcal{S}_{11} & 2\mathcal{S}_{13} & \sqrt{2}(\mathcal{S}_{12}+\mathcal{S}_{14}) & \sqrt{2}(\mathcal{S}_{12}-\mathcal{S}_{14}) \\ 2\mathcal{S}_{13} & 2\mathcal{S}_{33} & \sqrt{2}(\mathcal{S}_{23}+\mathcal{S}_{34}) & \sqrt{2}(\mathcal{S}_{23}-\mathcal{S}_{34}) \\ \sqrt{2}(\mathcal{S}_{12}+\mathcal{S}_{14}) & \sqrt{2}(\mathcal{S}_{23}+\mathcal{S}_{34}) & (\mathcal{S}_{22}+\mathcal{S}_{44}+2\mathcal{S}_{24}) & (\mathcal{S}_{22}-\mathcal{S}_{44}) \\ \sqrt{2}(\mathcal{S}_{12}-\mathcal{S}_{14}) & \sqrt{2}(\mathcal{S}_{23}-\mathcal{S}_{34}) & (\mathcal{S}_{22}-\mathcal{S}_{44}) & (\mathcal{S}_{22}+\mathcal{S}_{44}-2\mathcal{S}_{24}) \end{pmatrix}$

TABLE III

(c) SYMMETRICAL RECIPROCAL H-PLANE FOUR-PORT JUNCTION R_2 ROTATIONAL SYMMETRY (CONT'D)

$$R_2 = \begin{bmatrix} 0 & 0 & 1 & 0 \\ 0 & 0 & 0 & 1 \\ 1 & 0 & 0 & 0 \\ 0 & 1 & 0 & 0 \end{bmatrix} \qquad T_{R_2} = \frac{1}{\sqrt{2}} \begin{bmatrix} 1 & 0 & -1 & 0 \\ 0 & 1 & 0 & 1 \\ 1 & 0 & 1 & 0 \\ 0 & 1 & 0 & -1 \end{bmatrix}$$

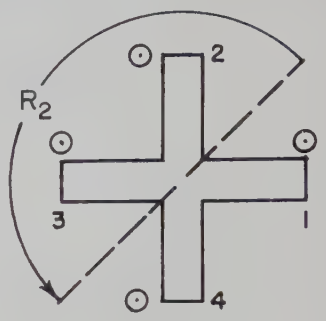

Natural Basis	$S = \begin{bmatrix} \mathcal{S}_{11} & \mathcal{S}_{12} & \mathcal{S}_{13} & \mathcal{S}_{14} \\ \mathcal{S}_{12} & \mathcal{S}_{22} & \mathcal{S}_{23} & \mathcal{S}_{24} \\ \mathcal{S}_{13} & \mathcal{S}_{23} & \mathcal{S}_{33} & \mathcal{S}_{34} \\ \mathcal{S}_{14} & \mathcal{S}_{24} & \mathcal{S}_{34} & \mathcal{S}_{44} \end{bmatrix}$	$S = \frac{1}{2} \begin{bmatrix} (\mathcal{G}_{11}+\mathcal{G}_{33}-2g_{13}) & (\mathcal{G}_{12}-\mathcal{G}_{34}+g_{14}-g_{23}) & (\mathcal{G}_{11}-\mathcal{G}_{33}) & (\mathcal{G}_{12}+\mathcal{G}_{34}-g_{14}-g_{23}) \\ (\mathcal{G}_{12}-\mathcal{G}_{34}+g_{14}-g_{23}) & (\mathcal{G}_{22}+\mathcal{G}_{44}+2g_{24}) & (\mathcal{G}_{12}+\mathcal{G}_{34}+g_{14}+g_{23}) & (\mathcal{G}_{22}-\mathcal{G}_{44}) \\ (\mathcal{G}_{11}-\mathcal{G}_{33}) & (\mathcal{G}_{12}+\mathcal{G}_{34}+g_{14}+g_{23}) & (\mathcal{G}_{11}+\mathcal{G}_{33}+2g_{13}) & (\mathcal{G}_{12}-\mathcal{G}_{34}-g_{14}+g_{23}) \\ (\mathcal{G}_{12}+\mathcal{G}_{34}-g_{14}-g_{23}) & (\mathcal{G}_{22}-\mathcal{G}_{44}) & (\mathcal{G}_{12}-\mathcal{G}_{34}-g_{14}+g_{23}) & (\mathcal{G}_{22}+\mathcal{G}_{44}-2g_{24}) \end{bmatrix}$
Transformed Basis	$S_{R_2} = \begin{bmatrix} \mathcal{G}_{11} & \mathcal{G}_{12} & g_{13} & g_{14} \\ \mathcal{G}_{12} & \mathcal{G}_{22} & g_{23} & g_{24} \\ g_{13} & g_{23} & \mathcal{G}_{33} & \mathcal{G}_{34} \\ g_{14} & g_{24} & \mathcal{G}_{34} & \mathcal{G}_{44} \end{bmatrix}$	$S_{R_2} = \frac{1}{2} \begin{bmatrix} (\mathcal{S}_{11}+\mathcal{S}_{33}+2\mathcal{S}_{13}) & (\mathcal{S}_{12}+\mathcal{S}_{14}+\mathcal{S}_{23}+\mathcal{S}_{34}) & (\mathcal{S}_{33}-\mathcal{S}_{11}) & (\mathcal{S}_{12}-\mathcal{S}_{14}+\mathcal{S}_{23}-\mathcal{S}_{34}) \\ (\mathcal{S}_{12}+\mathcal{S}_{23}+\mathcal{S}_{14}+\mathcal{S}_{34}) & (\mathcal{S}_{22}+\mathcal{S}_{44}+2\mathcal{S}_{24}) & (\mathcal{S}_{23}-\mathcal{S}_{12}-\mathcal{S}_{14}+\mathcal{S}_{34}) & (\mathcal{S}_{22}-\mathcal{S}_{44}) \\ (\mathcal{S}_{33}-\mathcal{S}_{11}) & (\mathcal{S}_{23}-\mathcal{S}_{14}-\mathcal{S}_{12}+\mathcal{S}_{34}) & (\mathcal{S}_{11}+\mathcal{S}_{33}-2\mathcal{S}_{13}) & (\mathcal{S}_{14}-\mathcal{S}_{12}) \\ (\mathcal{S}_{12}-\mathcal{S}_{14}+\mathcal{S}_{23}-\mathcal{S}_{34}) & (\mathcal{S}_{22}-\mathcal{S}_{44}) & (\mathcal{S}_{14}-\mathcal{S}_{12}) & (\mathcal{S}_{22}+\mathcal{S}_{44}-2\mathcal{S}_{24}) \end{bmatrix}$

(d) SYMMETRICAL H-PLANE FOUR-PORT JUNCTION R_1 ROTATIONAL SYMMETRY

$$R_1 = \begin{bmatrix} 0 & 0 & 0 & 1 \\ 1 & 0 & 0 & 0 \\ 0 & 1 & 0 & 0 \\ 0 & 0 & 1 & 0 \end{bmatrix} \qquad T_{R_1} = \frac{1}{2} \begin{bmatrix} 1 & 1 & 1 & 1 \\ 1 & -j & -1 & j \\ 1 & -1 & 1 & -1 \\ 1 & j & -1 & -j \end{bmatrix}$$

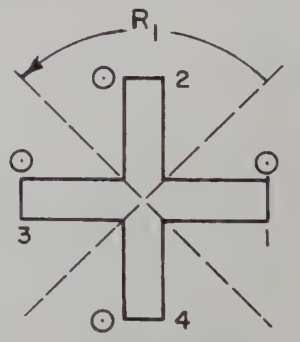

Natural Basis	$S = \begin{bmatrix} \mathcal{S}_{11} & \mathcal{S}_{12} & \mathcal{S}_{13} & \mathcal{S}_{14} \\ \mathcal{S}_{12} & \mathcal{S}_{22} & \mathcal{S}_{23} & \mathcal{S}_{24} \\ \mathcal{S}_{13} & \mathcal{S}_{23} & \mathcal{S}_{33} & \mathcal{S}_{34} \\ \mathcal{S}_{14} & \mathcal{S}_{24} & \mathcal{S}_{34} & \mathcal{S}_{44} \end{bmatrix}$	$\mathcal{S}_{11} = \frac{1}{4}[\mathcal{E}_{11} + \mathcal{E}_{33} + e_{24} + e_{42} + 2(e_{12} + e_{13} + e_{14} + e_{23} + e_{32}) + 2\mathcal{E}_{22}]$ $\mathcal{S}_{12} = \frac{1}{4}[\mathcal{E}_{11} - \mathcal{E}_{33} - j(e_{24} - e_{42}) + (1+j)(e_{12} - e_{23}) + (1-j)(e_{14} - e_{32})]$ $\mathcal{S}_{13} = \frac{1}{4}[\mathcal{E}_{11} + \mathcal{E}_{33} - (e_{24} + e_{42}) + 2e_{13} - 2\mathcal{E}_{22}]$ $\mathcal{S}_{14} = \frac{1}{4}[\mathcal{E}_{11} - \mathcal{E}_{33} - j(e_{42} - e_{24}) + (1+j)(e_{14} - e_{32}) + (1-j)(e_{12} - e_{23})]$ $\mathcal{S}_{22} = \frac{1}{4}[\mathcal{E}_{11} + \mathcal{E}_{33} - (e_{24} + e_{42}) - j2(e_{14} - e_{12} + e_{32} - e_{23}) - 2e_{13} + 2\mathcal{E}_{22}]$ $\mathcal{S}_{23} = \frac{1}{4}[\mathcal{E}_{11} - \mathcal{E}_{33} - j(e_{42} - e_{24}) + (1+j)(e_{32} - e_{14}) + (1-j)(e_{23} - e_{12})]$ $\mathcal{S}_{24} = \frac{1}{4}[\mathcal{E}_{11} + \mathcal{E}_{33} + e_{24} + e_{42} - 2e_{14} - 2\mathcal{E}_{22}]$ $\mathcal{S}_{33} = \frac{1}{4}[\mathcal{E}_{11} + \mathcal{E}_{33} + e_{24} + e_{42} + 2(e_{13} - e_{12} - e_{14} - e_{23} - e_{32}) + 2\mathcal{E}_{22}]$ $\mathcal{S}_{34} = \frac{1}{4}[\mathcal{E}_{11} - \mathcal{E}_{33} - j(e_{24} - e_{42}) + (1+j)(e_{23} - e_{12}) + (1-j)(e_{32} - e_{12})]$ $\mathcal{S}_{44} = \frac{1}{4}[\mathcal{E}_{11} + \mathcal{E}_{33} - (e_{24} + e_{42}) - j2(e_{12} - e_{14} + e_{23} - e_{32}) - 2e_{13} + 2\mathcal{E}_{22}]$
Transformed Basis	$S_{R_1} = \begin{bmatrix} \mathcal{E}_{11} & e_{12} & e_{13} & e_{14} \\ e_{12} & \mathcal{E}_{22} & e_{23} & e_{24} \\ e_{13} & e_{23} & \mathcal{E}_{33} & e_{34} \\ e_{14} & e_{24} & e_{34} & \mathcal{E}_{22} \end{bmatrix}$	$\mathcal{E}_{11} = \frac{1}{4}[\mathcal{S}_{11} + \mathcal{S}_{22} + \mathcal{S}_{33} + \mathcal{S}_{44} + 2(\mathcal{S}_{12} + \mathcal{S}_{13} + \mathcal{S}_{14} + \mathcal{S}_{23} + \mathcal{S}_{24} + \mathcal{S}_{34})]$ $e_{12} = \frac{1}{4}[\mathcal{S}_{11} - \mathcal{S}_{33} - j(\mathcal{S}_{22} - \mathcal{S}_{44}) + (1-j)(\mathcal{S}_{12} - \mathcal{S}_{34}) + (1+j)(\mathcal{S}_{14} - \mathcal{S}_{23})]$ $e_{13} = \frac{1}{4}[\mathcal{S}_{11} + \mathcal{S}_{33} - (\mathcal{S}_{22} + \mathcal{S}_{44}) + 2(\mathcal{S}_{13} - \mathcal{S}_{24})]$ $e_{14} = \frac{1}{4}[\mathcal{S}_{11} - \mathcal{S}_{33} - j(\mathcal{S}_{44} - \mathcal{S}_{22}) + (1+j)(\mathcal{S}_{12} - \mathcal{S}_{34}) + (1-j)(\mathcal{S}_{14} - \mathcal{S}_{23})]$ $\mathcal{E}_{22} = \frac{1}{4}[\mathcal{S}_{11} + \mathcal{S}_{22} + \mathcal{S}_{33} + \mathcal{S}_{44} - 2(\mathcal{S}_{13} + \mathcal{S}_{24})]$ $e_{23} = \frac{1}{4}[\mathcal{S}_{11} - \mathcal{S}_{33} - j(\mathcal{S}_{22} - \mathcal{S}_{44}) + (1+j)(\mathcal{S}_{23} - \mathcal{S}_{14}) + (1-j)(\mathcal{S}_{34} - \mathcal{S}_{12})]$ $e_{24} = \frac{1}{4}[\mathcal{S}_{11} + \mathcal{S}_{33} - (\mathcal{S}_{22} + \mathcal{S}_{44}) - j2(\mathcal{S}_{14} - \mathcal{S}_{34} - \mathcal{S}_{12} + \mathcal{S}_{23}) + 2(\mathcal{S}_{24} - \mathcal{S}_{13})]$ $e_{32} = \frac{1}{4}[\mathcal{S}_{11} - \mathcal{S}_{33} - j(\mathcal{S}_{44} - \mathcal{S}_{22}) + (1+j)(\mathcal{S}_{24} - \mathcal{S}_{12}) + (1-j)(\mathcal{S}_{23} - \mathcal{S}_{14})]$ $\mathcal{E}_{33} = \frac{1}{4}[\mathcal{S}_{11} + \mathcal{S}_{22} + \mathcal{S}_{33} + \mathcal{S}_{44} + 2(\mathcal{S}_{13} - \mathcal{S}_{12} - \mathcal{S}_{14} - \mathcal{S}_{23} + \mathcal{S}_{24} - \mathcal{S}_{34})]$ $e_{42} = \frac{1}{4}[\mathcal{S}_{11} + \mathcal{S}_{33} - (\mathcal{S}_{22} + \mathcal{S}_{44}) - j2(\mathcal{S}_{12} - \mathcal{S}_{23} - \mathcal{S}_{14} + \mathcal{S}_{34}) + 2(\mathcal{S}_{24} - \mathcal{S}_{13})]$

Asymmetry parameters associated with F_1, Table III(a):

$$a_{13} = \tfrac{1}{2}\alpha(p^2 - 1)$$
$$a_{14} = \tfrac{1}{2}\gamma(p^2 + 1)$$
$$a_{23} = \tfrac{1}{2}\gamma(p^2 - 1)$$
$$a_{24} = \tfrac{1}{2}\alpha(p^2 - 1). \quad (61)$$

Asymmetry parameters associated with F_2:

$$b_{13} = \tfrac{1}{2}\alpha(p^2 - 1)$$
$$b_{14} = -\tfrac{1}{2}\gamma(p^2 - 1)$$
$$b_{23} = \tfrac{1}{2}\gamma(p^2 - 1)$$
$$b_{24} = -\tfrac{1}{2}\alpha(p^2 - 1). \quad (62)$$

Asymmetry parameters associated with R_2, Table III(c):

$$g_{13} = g_{23} = g_{14} = g_{24} = 0. \quad (63)$$

Thus, the coupler, the scattering matrix of which had the form (60), has a symmetry (or asymmetry) equivalent to that shown in Fig. 4. For example, if

$$p = \exp\left(-j2\pi \frac{l}{\lambda_g}\right), \quad (64)$$

then the matrix (60) corresponds to that of a coupler which is perfectly symmetrical *except for lengths of guide* l indicated in Fig. 4. The implications as regard dimensional checks or compensating cuts to be made on the component are evident.

Orthogonality Relationships for Waveguides and Cavities with Inhomogeneous Anisotropic Media*

ALFRED T. VILLENEUVE†

Summary—**A modified reciprocity theorem forms the basis of development of orthogonality relationships for modes in waveguides and in cavities containing inhomogeneous, anisotropic media. In the lossless case certain of these may be interpreted in terms of power flow and energy storage. The special case of magnetized gyrotropic media is discussed for longitudinal and transverse magnetization.**

Introduction

RECENTLY the use of anisotropic materials has been the subject of numerous theoretical and experimental investigations.[1] Such materials are characterized in their macroscopic behavior by tensor permittivities or permeabilities. When these tensors are unsymmetric, the media may be termed "nonreciprocal" since the usual reciprocity theorem[2] does not apply to them. This nonreciprocal behavior finds applications in such devices as circulators, gyrators, load isolators and nonreciprocal phase shifters.[3]

One important special class of nonreciprocal media is that known as gyrotropic media, wherein application of a dc magnetic field causes the permittivity or permeability (hereafter referred to as constitutive parameters) to become an unsymmetric tensor. Two examples are gaseous plasma and ferromagnetic materials, especially low loss, magnetically-saturated ferrites.

Although the usual reciprocity theorem is not valid, a modified reciprocity theorem[4] does apply to anisotropic media. In this theorem, media characterized by transposed tensor constitutive parameters are employed in addition to the original media. In this paper, the modified reciprocity theorem forms a basis for the derivation of orthogonality relationships for modes in waveguides and cavities containing inhomogeneous, anisotropic media.

Let us denote the general form of the constitutive parameters in orthogonal coordinate systems as

$$[\epsilon] = \begin{bmatrix} \epsilon_{11} & \epsilon_{12} & \epsilon_{13} \\ \hat{\epsilon}_{12} & \epsilon_{22} & \epsilon_{23} \\ \hat{\epsilon}_{13} & \hat{\epsilon}_{23} & \epsilon_{33} \end{bmatrix} \quad [\mu] = \begin{bmatrix} \mu_{11} & \mu_{12} & \mu_{13} \\ \hat{\mu}_{12} & \mu_{22} & \mu_{23} \\ \hat{\mu}_{13} & \hat{\mu}_{23} & \mu_{33} \end{bmatrix}. \quad (1)$$

In this notation the careted symbols, $\hat{\epsilon}_{ij}$ and $\hat{\mu}_{ij}$, are the elements in the ith row and jth column of the constitutive parameter tensors for media characterized by the transposes of the above tensors. These media shall be referred to as "transposed media." In the case of gyrotropic media this has physical significance, since revers-

* Manuscript received by the PGMTT, March 10, 1959; revised manuscript received April 18, 1959. This work was supported by the Office of Ordnance Research, U. S. Army, Contract No. DA-30-115-ORD-861.

† Hughes Res. and Dev. Lab., Culver City, Calif.

[1] A complete list of references is impractical here and any attempt at making specific references would be difficult. For extensive lists of references the reader is referred to PROC. IRE, vol. 44, pp. 1229–1516; October, 1956.

[2] S. A. Schelkunoff, "Electromagnetic Waves," D. Van Nostrand Co., Inc., New York, N. Y., 1st ed., p. 478; 1943.

[3] C. L. Hogan, "The elements of non-reciprocal microwave devices," PROC. IRE, vol. 44, pp. 1345–1368; October, 1956.

[4] R. F. Harrington and A. T. Villeneuve, "Reciprocity relationships for gyrotropic media," IRE TRANS. ON MICROWAVE THEORY AND TECHNIQUES, vol. MTT-6, pp. 308–310; July, 1958.

ing the dc magnetic field transposes these tensors. Field quantities in the transposed media will be denoted by carets and a transposed tensor indicated by a tilde. Our discussion is based on the following form of the modified reciprocity theorem[4]

$$\oiint (\overline{H}_a \times \overline{E}_b - \overline{H}_b \times \widehat{\overline{E}}_a)\cdot d\overline{S} = \iiint \left[(\overline{J}_a \cdot \overline{E}_b - \overline{K}_a \cdot \overline{H}_b) - (\overline{J}_b \cdot \widehat{\overline{E}}_a - \overline{K}_b \cdot \widehat{\overline{H}}_a) \right] dv. \quad (2)$$

A second relation, similarly derived, which holds only for the lossless case and which will also be used subsequently is

$$\oiint (\overline{H}_a^* \times \overline{E}_b + \overline{H}_b \times \overline{E}_a^*)\cdot d\overline{S} = \iiint \overline{J}_a^* \cdot \overline{E}_b + \overline{K}_a^* \cdot \overline{H}_b + \overline{J}_b \cdot \overline{E}_a^* + \overline{K}_b \cdot \overline{H}_a^*] dv. \quad (3)$$

$\overline{J}$ and $\overline{K}$ are electric and magnetic source currents.

General Properties of Modes in Cylindrical Guides

In the following sections orthogonality relationships for modes in waveguides containing inhomogeneous anisotropic media will be discussed. For this discussion it is useful to have some knowledge of general relationships among the mode fields in the original media and in the transposed media. This section is devoted to a study of the field equations for such structures so that these relationships may be investigated.

Let the fields of the various modes be denoted as follows

$$\overline{E}_a = \overline{\mathcal{E}}_a e^{-\gamma_a z}, \qquad \overline{H}_a = \overline{\mathcal{H}}_a e^{-\gamma_a z}. \quad (4)$$

Here it has been assumed that the guide axis is parallel to the z axis and that the structure is uniform; *i.e.*, its material and electrical properties are independent of z (see Fig. 1). These will be referred to as "exponential

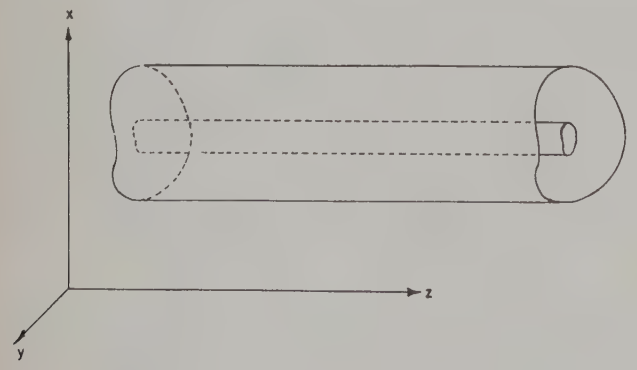

Fig. 1—Section of guide containing inhomogeneous anisotropic media.

modes" hereafter. The γ_a represent modes traveling or attenuating in either direction, depending on sign. Before proceeding it is convenient to express the constitutive parameter tensors in a form more suitable to cylindrical structures as follows:

$$[\mu] = \left[\begin{array}{cc|c} \mu_{11} & \mu_{12} & \mu_{13} \\ \hat{\mu}_{12} & \mu_{22} & \mu_{23} \\ \hline \hat{\mu}_{13} & \hat{\mu}_{23} & \mu_{33} \end{array}\right] = \left[\begin{array}{cc} [\mu_{1t}] & [\mu_{2t}] \\ [\tilde{\hat{\mu}}_{2t}] & [\mu_{2z}] \end{array}\right] \quad (5a)$$

$$[\epsilon] = \left[\begin{array}{cc|c} \epsilon_{11} & \epsilon_{12} & \epsilon_{13} \\ \hat{\epsilon}_{12} & \epsilon_{22} & \epsilon_{23} \\ \hline \hat{\epsilon}_{13} & \hat{\epsilon}_{23} & \epsilon_{33} \end{array}\right] = \left[\begin{array}{cc} [\epsilon_{1t}] & [\epsilon_{2t}] \\ [\tilde{\hat{\epsilon}}_{2t}] & [\epsilon_{2z}] \end{array}\right]. \quad (5b)$$

In these, the elements of the sub-matrices are those of the corresponding partitioned sections. In this notation the field equations become

$$-\nabla_t \times \overline{\mathcal{E}}_{at} = j\omega[\tilde{\mu}_{2t}]\overline{\mathcal{H}}_{at} + j\omega[\mu_{2z}]\bar{u}_z\mathcal{H}_{az} \quad (6a)$$

$$\bar{u}_z \times (\gamma_a \overline{\mathcal{E}}_{at} + \nabla_t \mathcal{E}_{az}) = j\omega[\mu_{1t}]\overline{\mathcal{H}}_{at} + j\omega[\mu_{2t}]\bar{u}_z\mathcal{H}_{az}, \quad (6b)$$

$$\nabla_t \times \overline{\mathcal{H}}_{at} = j\omega[\tilde{\hat{\epsilon}}_{2t}]\overline{\mathcal{E}}_{at} + j\omega[\epsilon_{2z}]\bar{u}_z\mathcal{E}_{az}, \quad (6c)$$

$$-\bar{u}_z \times (\gamma_a \overline{\mathcal{H}}_{at} + \nabla_t \mathcal{H}_{az}) = j\omega[\epsilon_{1t}]\overline{\mathcal{E}}_{at} + j\omega[\epsilon_{2t}]\bar{u}_z\mathcal{E}_{az}. \quad (6d)$$

where $\overline{\mathcal{E}}_{at} = \overline{\mathcal{E}}_a - \bar{u}_z\mathcal{E}_{az}$, etc. The differential operators may be considered identical with the usual three dimensional operators, since $\overline{\mathcal{E}}$ and $\overline{\mathcal{H}}$ are independent of z. The subscript t on them arises from convention. The boundary conditions at the guide walls are

$$-\hat{n} \times \overline{\mathcal{H}}_a = [y]\overline{\mathcal{E}}_a \quad (7)$$

where $\hat{n}$ is an outward normal and $[y]$ is a tensor admittance. In the transposed media the field equations take the form

$$-\nabla_t \times \widehat{\overline{\mathcal{E}}}_{bt} = j\omega[\tilde{\mu}_{2t}]\widehat{\overline{\mathcal{H}}}_{bt} + j\omega[\mu_{2z}]\bar{u}_z\widehat{\mathcal{H}}_{bz} \quad (8a)$$

$$\bar{u}_z \times (\hat{\gamma}_b\widehat{\overline{\mathcal{E}}}_{bt} + \nabla_t\widehat{\mathcal{E}}_{bz}) = j\omega[\tilde{\mu}_{1t}]\widehat{\overline{\mathcal{H}}}_{bt} + j\omega[\hat{\mu}_{2t}]\bar{u}_z\widehat{\mathcal{H}}_{bz}, \quad (8b)$$

$$\nabla_t \times \widehat{\overline{\mathcal{H}}}_{bt} = j\omega[\tilde{\epsilon}_{2t}]\widehat{\overline{\mathcal{E}}}_{bt} + j\omega[\epsilon_{2z}]\bar{u}_z\widehat{\mathcal{E}}_{bz}, \quad (8c)$$

$$-\bar{u}_z \times (\hat{\gamma}_b\widehat{\overline{\mathcal{H}}}_{bt} + \nabla_t\widehat{\mathcal{H}}_{bz}) = j\omega[\tilde{\epsilon}_{1t}]\widehat{\overline{\mathcal{E}}}_{bt} + j\omega[\epsilon_{2t}]\bar{u}_z\mathcal{E}_{bz}, \quad (8d)$$

subject to the boundary condition

$$-\hat{n} \times \widehat{\overline{\mathcal{H}}}_b = [y]\widehat{\overline{\mathcal{E}}}_b \quad (9)$$

at the walls.

In ref. 4 it is shown that for every γ_a in the original media there exists in the transposed media a propagation constant $\hat{\gamma}_a = -\gamma_a$, with fields which will be denoted $\widehat{\overline{\mathcal{E}}}_a$, $\widehat{\overline{\mathcal{H}}}_a$. In the general lossy case, there appears to be no simple relation between the fields corresponding to γ_a in the original media and those corresponding to $-\gamma_a$ in the transposed media. However, in the lossless case, the following relations hold for the tensor permeability and permittivity[5]

$$[\tilde{\mu}_{2t}] = [\tilde{\mu}_{2t}^*], \quad [\tilde{\mu}_{1t}] = [\mu_{1t}^*], \quad [\mu_{2z}] = [\mu_{2z}^*], \quad (10)$$

and, for traveling modes, $-\gamma_a = \gamma_a^*$. Thus, with the relationships

$$\widehat{\overline{\mathcal{E}}}_a = \pm\, \overline{\mathcal{E}}_a^* \quad \text{and} \quad \widehat{\overline{\mathcal{H}}}_a = \mp\, \overline{\mathcal{H}}_a^*, \quad (11)$$

the field of (8) in the transposed media become the complex conjugates of those of (6) in the original media. Either pair of signs may be selected, and, for convenience, the upper pair will be used in subsequent develop-

[5] This may be seen from energy considerations.

ments. The boundary conditions on the fields are satisfied by this since, for the lossless case,

$$[y] = j[b]. \tag{12}$$

Thus, it is seen that in the lossless case, for every traveling mode in the original media characterized by $\bar{\mathcal{E}}_a$, $\bar{\mathcal{H}}_a$ and γ_a, there exists in the transposed media a traveling mode characterized by $\hat{\bar{\mathcal{E}}}_a = \bar{\ }_a{}^*$, $\hat{\bar{\mathcal{H}}}_a = -\bar{\mathcal{H}}_a{}^*$ and $\hat{\gamma}_a = \gamma_a{}^* = -\gamma_a$. In the case of evanescent modes in lossless media, $\gamma_a{}^* = \gamma_a$ and the fields characterized by γ_a and $-\gamma_a$ are no longer simply related.

Application to Gyrotropic Media

Because of their useful properties, two special orientations of dc magnetization are commonly employed in nonreciprocal devices containing gyrotropic media. These are the cases of purely longitudinal and purely transverse dc magnetization. The longitudinal case will be considered first. The tensor permeability and permittivity now assume the form

$$[\mu] = \begin{bmatrix} \mu & -j\kappa & 0 \\ j\kappa & \mu & 0 \\ 0 & 0 & \mu_0 \end{bmatrix}; \qquad \epsilon = \begin{bmatrix} \epsilon & -j\eta & 0 \\ j\eta & \epsilon & 0 \\ 0 & 0 & \epsilon_z \end{bmatrix}, \tag{13}$$

and it is evident that

$$\begin{aligned} [\mu_{2t}] &= [\epsilon_{2t}] = [0] \\ [\tilde{\mu}_{2t}] &= [\tilde{\epsilon}_{2t}] = [0]. \end{aligned} \tag{14}$$

Under these conditions, the equations in (6) assume the simplified forms

$$-\nabla_t \times \bar{\mathcal{E}}_{at} = j\omega\mu_0 \bar{u}_z \bar{H}_{az} \tag{15a}$$

$$\bar{u}_z \times (\gamma_a \bar{\mathcal{E}}_{at} + \nabla_t \mathcal{E}_{az}) = j\omega[\mu_{1t}]\bar{\mathcal{H}}_{at}, \tag{15b}$$

$$\nabla_t \times \bar{\mathcal{H}}_{at} = j\omega[\epsilon_{2z}]\bar{\mu}_z \mathcal{E}_{az}, \tag{15c}$$

$$-\bar{u}_z \times (\gamma_a \bar{\mathcal{H}}_{at} + \nabla_t \mathcal{H}_{az}) = j\omega[\epsilon_{1t}]\bar{\mathcal{E}}_{at}. \tag{15d}$$

These are the equations of a field characterized by $\bar{\mathcal{E}}_{at}$, $\mathcal{E}_{az}$, $\bar{\mathcal{H}}_{at}$, $\mathcal{H}_{az}$, γ_a. However, substitution into Maxwell's equations shows that a field characterized by $\bar{\mathcal{E}}_{at}$, $-\mathcal{E}_{az}$, $-\bar{\mathcal{H}}_{at}$, $\mathcal{H}_{az}$ and $-\gamma_a$ also satisfies the equations (15). Examination of boundary conditions shows that they also are satisfied, and the above field is then a possible field in the untransposed media. Thus, when the dc magnetization is purely longitudinal (the anisotropy purely transverse) both $+\gamma_a$ and $-\gamma_a$ are eigenvalues of Maxwell's equations.

The Case of Transverse Magnetization

If the dc magnetization is purely transverse, other properties of the fields become evident. For this case, the permeability and permittivity tensors assume the forms

$$[\mu] = \left[\begin{array}{cc|c} \mu_{11} & \mu_{12} & \mu_{13} \\ \mu_{12} & \mu_{22} & \mu_{23} \\ \hline -\mu_{13} & -\mu_{23} & \mu_{33} \end{array}\right] = \begin{bmatrix} [\mu_{1t}] & [\mu_{2t}] \\ -[\tilde{\mu}_{2t}] & [\mu_{2z}] \end{bmatrix} \tag{16a}$$

$$[\epsilon] = \left[\begin{array}{cc|c} \epsilon_{11} & \epsilon_{12} & \epsilon_{13} \\ \epsilon_{12} & \epsilon_{22} & \epsilon_{23} \\ \hline -\epsilon_{13} & -\epsilon_{23} & \epsilon_{33} \end{array}\right] = \begin{bmatrix} [\epsilon_{1t}] & [\epsilon_{2t}] \\ -[\tilde{\epsilon}_{2t}] & [\epsilon_{2z}] \end{bmatrix}. \tag{16b}$$

Examination of (6) and (8) shows that, in this case, corresponding to the eigenvalue γ_a, the fields in the original media and the transposed media are related by

$$\begin{aligned} \hat{\bar{\mathcal{E}}}_{at} &= \bar{\mathcal{E}}_{at}, \quad \hat{\mathcal{E}}_{az} = -\mathcal{E}_{az}, \quad \hat{\bar{\mathcal{H}}}_{at} = -\bar{\mathcal{H}}_{at}, \\ \hat{\mathcal{H}}_{az} &= \mathcal{H}_{az}, \quad \hat{\gamma}_a = -\gamma_a. \end{aligned} \tag{17}$$

This may be thought of as a modified reflectional symmetry relating the original field to the transposed field. This relation, in conjunction with (11) in the lossless case, leads to

$$\begin{aligned} \bar{\mathcal{H}}_{at} &= \bar{\mathcal{H}}_{at}{}^* \\ \bar{\mathcal{E}}_{at} &= \bar{\mathcal{E}}_{at}{}^* \\ \mathcal{H}_{az} &= -\mathcal{H}_{az}{}^* \\ \mathcal{E}_{az} &= -\mathcal{E}_{az}{}^*. \end{aligned} \tag{18}$$

These equations state that the transverse field components are real and the longitudinal components are imaginary. This means that, *when the dc magnetization is purely transverse, and no loss is present, it is always possible to express the fields in terms of modes whose transverse fields are linearly polarized.*

The results of this section will be applied to simplify certain of the orthogonality relations to be examined.

Orthogonality Relationships for Cylindrical Guides

In the study of natural modes in closed cylindrical waveguides containing *homogeneous isotropic* media, it is found that the transverse and longitudinal field components satisfy certain orthogonality relationships.[6] Two general types of orthogonality may be considered; those involving vector products of electric and magnetic fields of the various modes, and those involving scalar products of the various mode fields. These orthogonality relationships may be summarized as

$$\iint_s (\bar{\mathcal{E}}_{bt} \times \bar{\mathcal{H}}_{at}) \cdot d\bar{S} = 0 \qquad \gamma_b \neq \pm \gamma_a \tag{19a}$$

$$\iint_s (\bar{\mathcal{E}}_{bt} \times \bar{\mathcal{H}}_{at}{}^*) \cdot d\bar{S} = 0 \qquad \begin{cases} \gamma_b \neq \pm \gamma_a \\ \gamma_b \neq \pm \gamma_a{}^* \end{cases} \tag{19b}$$

$$\iint_s \mathcal{E}_{bz}\mathcal{E}_{az} dS = \iint_s \bar{\mathcal{E}}_{bt} \cdot \bar{\mathcal{E}}_{at} dS = \iint_s \bar{\mathcal{E}}_b \cdot \bar{\mathcal{E}}_a dS$$

$$= \iint_s \mathcal{H}_{bz}\mathcal{H}_{az} dS = \iint_s \bar{\mathcal{H}}_{bt} \cdot \bar{\mathcal{H}}_{at} dS = \iint_s \bar{\mathcal{H}}_b \cdot \bar{\mathcal{H}}_a dS = 0$$

$$\gamma_b \neq \pm \gamma_a. \tag{19c}$$

[6] N. Marcuvitz, "Waveguide Handbook," Rad. Lab. Ser. McGraw Hill Book Co., Inc., New York, N. Y., vol. 10, 1st ed., p. 5; 1951.

and finally,

$$\iint_s \mathcal{E}_{bz}\mathcal{E}_{az}^* dS = \iint_s \bar{\mathcal{E}}_{bt}\cdot\bar{\mathcal{E}}_{at}^* dS = \iint_s \bar{\mathcal{E}}_b\cdot\bar{\mathcal{E}}_a^* dS$$
$$= \iint_s \mathcal{H}_{bz}\mathcal{H}_{az}^* dS = \iint_s \bar{\mathcal{H}}_{bt}\cdot\bar{\mathcal{H}}_{at}^* dS$$
$$= \iint_s \bar{\mathcal{H}}_b\cdot\bar{\mathcal{H}}_a^* dS = 0, \quad \gamma_b \neq \pm\gamma_a \quad \gamma_b \neq \pm\gamma_a^*. \tag{19d}$$

The integrations are performed over guide cross sections. Adler[7] refers to the first two expressions as "power orthogonality" and to the second two groups as "energy orthogonality." The power orthogonality relationships may be derived from the usual reciprocity relationships for isotropic media. The energy relationships appear to result from the fact that in guides containing homogeneous, isotropic media both $\mathcal{E}_z$ and $\mathcal{H}_z$ are solutions of the same scalar Helmholtz equation and satisfy certain boundary conditions at the walls.

General Orthogonality Relationships for Inhomogeneous Anisotropic Guides

When the guides contain *inhomogeneous*, isotropic media, the longitudinal field components no longer satisfy the scalar Helmholtz equation and the energy orthogonality relationships no longer hold in general.[8] However, the orthogonality relationship (19a) still holds as a result of reciprocity and reflectional symmetry. Eq. (19b) also holds in the lossless case. If, however, the media are also *anisotropic*, even the power orthogonality relationships must be modified. This is because the usual reciprocity no longer applies and the reflectional symmetry of the arrangement is usually lost. In this case, the modified reciprocity theorem forms the basis of the development. One may begin by considering a source-free region of closed cylindrical guide containing anisotropic media. All material and electrical properties are assumed to be independent of the longitudinal coordinate, which is chosen as z. The situation is as shown in Fig. 2. Under these conditions (2) becomes

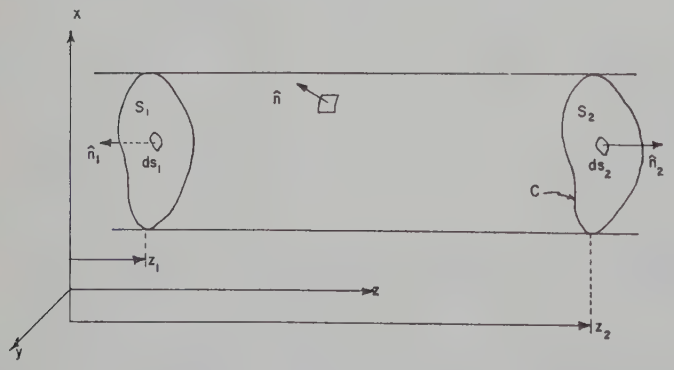

Fig. 2.

$$\oiint_s (\hat{\bar{H}}_b \times \bar{E}_a - \bar{H}_a \times \hat{\bar{E}}_b)\cdot d\bar{S} = 0. \tag{20}$$

The subscripts refer to possible waveguide modes, and the surface of integration is composed of the guide walls and the two cross sections of guide. $d\bar{S}$ is in the direction of the outward normal $\hat{n}$. Let the guide walls be tensor admittance sheets such that

$$-\hat{n} \times \bar{\mathcal{H}}_a = [y]\bar{\mathcal{E}}_a \tag{21a}$$
$$-\hat{n} \times \hat{\bar{\mathcal{H}}}_b = [y]\hat{\bar{\mathcal{E}}}_b. \tag{21b}$$

For the purposes of this paper the tensor $[y]$ will be restricted to the form

$$[y] = \left[\begin{array}{cc|c} y_{11} & y_{12} & 0 \\ y_{12} & y_{22} & 0 \\ \hline 0 & 0 & y_{zz} \end{array}\right] = \left[\begin{array}{cc} [y_{1t}] & [0] \\ [0] & [y_{2z}] \end{array}\right], \tag{22}$$

where the division is similar to that of $[\mu]$ and $[\epsilon]$ above. This form is chosen because it leads to symmetrical expressions and is sufficiently general for most purposes.[9] Under these circumstances, for exponential modes, (20) may be reduced to[10]

$$\iint_s (\hat{\bar{\mathcal{H}}}_{bt} \times \bar{\mathcal{E}}_{at} - \bar{\mathcal{H}}_{at} \times \hat{\bar{\mathcal{E}}}_{bt})\cdot d\bar{S} = N_b\delta_{\hat{\gamma}_b,-\gamma_a} \tag{23}$$

where N_b is a normalization constant and δ_{ij} is the Kronecker delta. The integration is over the guide cross section.

In the lossless case (3), can through an analogous procedure, be put into the following form:

$$\iint_s (\bar{\mathcal{H}}_{bt}^* \times \bar{\mathcal{E}}_{at} + \bar{\mathcal{H}}_{at} \times \bar{\mathcal{E}}_{bt}^*)\cdot d\bar{S} = M_b\delta_{\gamma_b^*,-\gamma_a} \tag{24}$$

where the guide walls are represented by a *lossless* symmetric tensor admittance of the same form as in (22). It may be seen from (11) that for traveling modes in lossless guide $M_b = -N_b$. It should be pointed out, however, that (24) is valid for both traveling and evanescent modes.

Eqs. (23) and (24) are the generalized power orthogonality relationships which hold for guides containing media characterized by tensor permeabilities or permittivities and subject to the appropriate boundary conditions.

Series Expansion of Fields

Through use of (23) it is possible to expand an arbitrary transverse field in terms of the transverse fields of exponential modes, assuming that these transverse fields form a complete set. The completeness, however, will not be discussed here. Under this assumption, an

[7] R. B. Adler, "Properties of Guided Waves on Inhomogeneous Cylindrical Structures," Res. Lab. of Elec., Mass. Inst. Tech., Cambridge, Tech. Rep. No. 102, pp. 28–29; May 27, 1949.
[8] *Ibid.*, pp. 12 and 29.
[9] *Ibid.*, pp. 16–17.
[10] This expression and a similar one for purely transverse anisotropy have been obtained by Bresler, Joshi and Marcuvitz from the point of view of the theory of linear operators rather than reciprocity. A. D. Bresler, G. H. Joshi, N. Marcuvitz, "Orthogonality Properties for Modes in Passive and Active Uniform Wave Guides," *J. Appl. Phys.*, vol. 29, pp. 794–798; May, 1958.

arbitrary transverse field may be expressed in series form as

$$\bar{\mathcal{E}}_t = \sum_n A_n \bar{\mathcal{E}}_{nt}; \qquad \bar{\mathcal{H}}_t = \sum_n A_n \bar{\mathcal{H}}_{nt}. \tag{25}$$

On forming the vector products $\hat{\bar{\mathcal{H}}}_{mt} \times \bar{\mathcal{E}}_t$ and $\bar{\mathcal{H}}_t \times \hat{\bar{\mathcal{E}}}_{mt}$, subtracting and integrating over the guide cross section, one gets

$$A_m = \frac{\iint_s (\hat{\bar{\mathcal{H}}}_{mt} \times \bar{\mathcal{E}}_t - \bar{\mathcal{H}}_t \times \hat{\bar{\mathcal{E}}}_{mt}) \cdot d\bar{S}}{N_m}, \tag{26}$$

where it has been assumed that the order of summation and integration may be interchanged. Thus, the coefficients of the expansion are determined.

Power Flow Relationships

Eq. (24) may be interpreted in terms of power flow in the guide. This may be seen by considering two distinct modes existing simultaneously in a closed guide. On forming the vector product of $\bar{E}$ and $\bar{H}$ and integrating the longitudinal component over the guide cross section, one arrives at the following result. *The net real power transmitted down a lossless guide is the algebraic sum of the power carried by the individual modes.* The same conclusion may not be drawn about the reactive power, however.

For the general case, (23) and (24) appear to be the only readily available orthogonality expressions. Due to lack of symmetry of $[\mu]$ and $[\epsilon]$, there seems to be no way of reducing them to single cross products as in the isotropic case. In special cases; *e.g.*, in gyrotropic media for special orientations of the dc magnetic field, the tensor properties discussed above provide some additional relationships. These are discussed in the following sections.

Longitudinal Magnetization of Gyrotropic Media

It was pointed out above that, for longitudinal dc magnetization of gyrotropic media, both γ_a and $-\gamma_a$ are eigenvalues of Maxwell's equations in cylindrical guides and reflectional symmetry exists. Through use of these properties, (23) may be further simplified since one then has the pair of relationships

$$\iint_s (\hat{\bar{\mathcal{H}}}_t \times \bar{\mathcal{E}}_{at} - \bar{\mathcal{H}}_{at} \times \hat{\bar{\mathcal{E}}}_{bt}) \cdot d\bar{S} = N_b \delta_{\hat{\gamma}_b, -\gamma_a} \tag{27a}$$

and

$$\iint_s (\hat{\bar{\mathcal{H}}}_{bt} \times \bar{\mathcal{E}}_{at} + \bar{\mathcal{H}}_{at} \times \hat{\bar{\mathcal{E}}}_{bt}) \cdot d\bar{S} = 0. \tag{27b}$$

Together, these yield the simple orthogonality relationship

$$\iint_s (\bar{\mathcal{H}}_{bt} \times \bar{\mathcal{E}}_{at}) \cdot d\bar{S} = -\iint_s (\bar{\mathcal{H}}_{at} \times \hat{\bar{\mathcal{E}}}_{bt}) \cdot d\bar{S} = \tfrac{1}{2} N_b \delta_{\hat{\gamma}_b, \pm\gamma_a}. \tag{28}$$

In the lossless case, (24) leads to the relationship

$$\iint_s (\bar{\mathcal{H}}_{bt}^* \times \bar{\mathcal{E}}_{at}) \cdot d\bar{S} = \iint_s (\bar{\mathcal{H}}_{at} \times \bar{\mathcal{E}}_{bt}^*) \cdot d\bar{S} = \tfrac{1}{2} M_b \delta_{\gamma_b^*, \pm\gamma_a}. \tag{29}$$

This last equation may be interpreted in terms of power flow as follows. *The net complex power transmitted down a lossless guide whose anisotropy is purely transverse is the algebraic sum of the complex powers of the individual modes.* This statement is more specific than could be made for the general case, since it now includes the *reactive* power. The general case included only the real power.

Transverse Magnetization of Gyrotropic Media

In view of the relationship between fields in the original and in the transposed media for transverse magnetization, the power orthogonality relationship (23) may be rewritten as

$$\iint_s [\bar{\mathcal{H}}_{bt} \times \bar{\mathcal{E}}_{at} + \bar{\mathcal{H}}_{at} \times \bar{\mathcal{E}}_{bt}] \cdot d\bar{S} = -N_b \delta_{\hat{\gamma}_b, -\gamma_a}. \tag{30}$$

This special case involves the fields in only the original media.

Energy Type Relationships

Through use of the field equations (6) and (8) and the application of various vector identities, it is possible to rewrite the preceding power orthogonality relationships in various other forms. Under certain conditions in the lossless case, these may be interpreted in terms of stored energy. The details are long and involved and again, only results are presented here for the special case of purely transverse anisotropy.[11] In this special case, the form of $[\mu]$ and $[\epsilon]$ make it possible to derive the relationship

$$\iint_s (\hat{\bar{\mathcal{E}}}_b \cdot [\epsilon] \cdot \bar{\mathcal{E}}_a + \hat{\bar{\mathcal{H}}}_b \cdot [\mu] \bar{\mathcal{H}}_a) dS + \frac{1}{j\omega} \oint_C \hat{\bar{\mathcal{E}}}_b \cdot [y] \bar{\mathcal{E}}_a dl = 0, \qquad \text{all } \hat{\gamma}_b, \gamma_a. \tag{31}$$

Here C is the perimeter of the guide cross section. In the lossless case, one gets the corresponding relationship

$$\iint_s \bar{\mathcal{E}}_b^* \cdot [\epsilon] \bar{\mathcal{E}}_a dS + \frac{1}{\omega} \oint_C \bar{\mathcal{E}}_b^* \cdot [b] \bar{\mathcal{E}}_a dl = \iint_s \bar{\mathcal{H}}_b^* \cdot [\mu] \bar{\mathcal{H}}_a dS, \qquad \text{all } \gamma_b^*, \gamma_a. \tag{32}$$

This equation may be interpreted in terms of mutual time-average electric and magnetic energies of two

[11] For details see in A. T. Villeneuve, "A study of Reciprocity Relationships For Gyrotropic Media," Res. Inst., Syracuse University, Syracuse, N. Y., Final Rept. No. EE509–589F; September, 1958.

modes, if one interprets the integral over C as the electric energy stored in the guide walls per unit length. With this interpretation, (32) states that *the mutual time average stored electric and magnetic energies of two modes are equal.*

From the foregoing, it is evident that when cylindrical guides contain *inhomogeneous, anisotropic* media, most of the usual orthogonality relationships are lost. Only a modified power orthogonality relationship remains in general. The energy orthogonality relationships are destroyed. However, when the anisotropy is purely transverse, the orthogonality relationships are similar to those which exist for the inhomogeneous, *isotropic* case.

Orthogonality Relationships for Closed Cavities

Next, orthogonality relationships for closed cavities containing inhomogeneous anisotropic media will be investigated. Consider such a closed cavity with perfectly conducting walls as in Fig. 3.

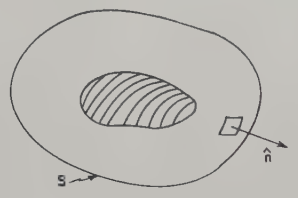

Fig. 3—Cavity with inhomogeneous anistropic media.

The usual orthogonality relationships among the modes[12] do not hold, except, possibly, in special cases. However, modified orthogonality relationships do exist. It has been demonstrated from the modified reciprocity theorem that the natural resonant frequencies of such a cavity are identical in both the transposed and the original media.[13] This forms the basis of the modified orthogonality conditions as follows. In the original cavity there exists a set of natural modes characterized by $\overline{E}_i$, $\overline{H}_i$ and ω_i, where $\omega_i = \omega_i' - j\omega_i''$ in general. In the cavity with media transposed (transposed cavity), one has modes characterized by $\widehat{\overline{E}}_i$, $\widehat{\overline{H}}_i$ and ω_i. Note that the ω_i are the same in both cases. The fields in the original cavity satisfy the equations

$$-\nabla \times \overline{E}_i = j\omega_i[\mu]\overline{H}_i \tag{33a}$$

$$\nabla \times \overline{H}_i = j\omega_i[\epsilon]\overline{E}_i \tag{33b}$$

$$\nabla \times [\mu]^{-1}\nabla \times \overline{E}_i = \omega_i^2[\epsilon]\overline{E}_i \tag{34a}$$

$$\nabla \times [\epsilon]^{-1}\nabla \times \overline{H}_i = \omega_i^2[\mu]\overline{H}_i \tag{34b}$$

subject to the boundary condition that the tangential component of $\overline{E}_i$ vanish at the walls. Similar equations are satisfied by $\widehat{\overline{E}}_i$ and $\widehat{\overline{H}}_i$ in the transposed case except that the tensor constitutive parameters are transposed.

In order to study the orthogonality relationships, one may proceed as follows. First, form the volume integral over the cavity

$$\iiint (\widehat{\overline{E}}_m \cdot \nabla \times [\mu]^{-1}\nabla \times \overline{E}_n - \overline{E}_n \cdot \nabla \times [\tilde{\mu}]^{-1}\nabla \times \widehat{\overline{E}}_m) dv. \tag{35}$$

By the use of vector identities, the divergence theorem, and (33) and (34), for both the original and transposed media and boundary conditions on $\overline{E}$, one arrives at the orthogonality relationship

$$\iiint \widehat{\overline{E}}_m \cdot [\epsilon]\overline{E}_n dv = \delta_{mn}, \tag{36}$$

where the fields have been normalized and δ_{mn} is the Kronecker delta. Through a similar procedure, one may also arrive at the result

$$-\iiint \widehat{\overline{H}}_n \cdot [\mu]\overline{H}_n dv = \delta_{mn}, \tag{37}$$

the $\overline{H}_n$ being automatically normalized when the $\overline{E}_n$ are normalized. In the lossless case, these reduce to

$$\iiint \overline{E}_m^* \cdot [\epsilon]\overline{E}_n dv = \iiint \overline{H}_m^* \cdot [\mu]\overline{H}_n dv = \delta_{mn}. \tag{38}$$

Eq. (38) shows that *in closed cavities containing lossless anisotropic media, the total electric or magnetic energy is the sum of the energies of the individual modes with no coupling terms between modes.* However, when loss is present, the above expressions do not necessarily hold and some mutual energy terms may be present.

It may be seen from the foregoing that orthogonality relationships for perfectly conducting cavities containing inhomogeneous anisotropic media are quite similar to those for isotropic media except that fields in the transposed cavity must be used in addition to those in the original cavity. Only in the lossless case can energy interpretations be given to these relationships, for in this case the fields in the original and in the transposed media are simply related.

ACKNOWLEDGMENT

The author wishes to acknowledge the suggestions and encouragement of Dr. R. F. Harrington, under whose direction this study was carried out.

[12] G. Toraldo di Francia, "Electromagnetic Waves," Interscience Publishers, Inc., New York, N. Y., 1st ed., p. 303; 1955.
[13] R. F. Harrington and A. T. Villeneuve, *op. cit.*

Mismatch Errors in Cascade-Connected Variable Attenuators*

G. E. SCHAFER AND A. Y. RUMFELT†

Summary—The treatment of mismatch errors is extended to cover variable attenuators cascade-connected in a system which is not free from reflections. The method of analysis is applicable to any number of cascaded attenuators, but only the analysis of two and three variable attenuators in cascade is presented. Graphs are given to aid in estimating the limits of mismatch error.

In an example, which is considered representative of rigid rectangular waveguide systems, the limits of error are: for two attenuators in cascade, 0.19 db in a 3-db measurement, and 0.17 db in a 40-db measurement; and for three attenuators in cascade, 0.25 db in a 40-db measurement, and 0.23 db in a 75-db measurement.

Introduction

ERRORS in attenuation caused by the interaction of reflections from generator, attenuator, and load mismatches are termed mismatch errors. Previous treatments of mismatch errors have considered variable or fixed single attenuators in systems with reflections[1,2] and cascaded fixed attenuators in reflection-free systems.[3] In cases where the variable attenuator to be calibrated has a very wide range (greater than 45 db), measurements are often made by using one or two previously calibrated attenuators cascade-connected with the test attenuator (a direct series substitution method). Therefore, the analysis is extended to cascaded variable attenuators in a system which is not free from reflections. Although the method of analysis employed is applicable to any number of variable attenuators in cascade, only the cases of two or three variable attenuators in cascade are presented. Graphs are presented which may be used to estimate the limits of mismatch error in these two cases. An example is given of the use of the graphs. Other sources of error such as the accuracy of the original calibrations, leakage, noise, etc., are not considered here but must be taken into account to obtain total limits of error in an actual calibration.

Theory

In a direct series-substitution method of measuring the attenuation[4] of a variable attenuator, the test attenuator is connected in series with a reference (previously calibrated or standard) attenuator. The total insertion loss of the series-connected pair of attenuators is adjusted to be the same at two different settings. The relative attenuation of the test attenuator is taken to be equal in magnitude to the relative attenuation of the reference attenuator. This is in error because the standard attenuator is connected to a mismatched attenuator, and also because the pair of attenuators are inserted in a mismatched system.

An expression can be derived for the insertion loss of the pair of attenuators connected in cascade. From this, an expression may be written for the difference between the total insertion loss and the sum of the individual attenuations. Inspection of this reveals that the error can be separated into two convenient parts. One of these has been previously worked out[3] in detail for fixed attenuators and is readily extended to variable attenuators, and the other is evaluated here by calculation of certain quantities associated with the combination of attenuators. This separation is performed in the following analysis.

At the initial settings of the attenuators, one may write the total insertion loss as

$$L_i = A_{ti} + A_{ri} + \epsilon_i, \tag{1}$$

where L_i is the total insertion loss at the initial settings of the attenuators, A_{ti} and A_{ri} are the attenuations of the test and reference attenuators at the initial settings, and ϵ_i is the difference between the insertion loss of the pair in cascade and the sum of the individual attenuations. At the final settings of the attenuators, a similar expression for the total insertion loss may be written as

$$L_f = A_{tf} + A_{rf} + \epsilon_f, \tag{2}$$

where the symbols have the same meaning as in (1) except that the subscript f refers to the final settings. The adjustments of the attenuators are made in this way to result in the initial and final total insertion losses being equal, $L_i = L_f$, from which

$$(A_{tf} - A_{ti}) = (A_{ri} - A_{rf}) + \epsilon_T, \tag{3}$$

where ϵ_T has been written for $\epsilon_i - \epsilon_f$. This means that the relative attenuation of the test attenuator may differ from the relative attenuation of the reference attenuator by ϵ_T. This is the desired error. However, a convenient separation may be made as follows. Rewrite (3) as

$$(A_{tf} + A_{rf}) - (A_{ti} + A_{ri}) = \epsilon_T. \tag{4}$$

Let A_i and A_f be the attenuation at the initial and final settings, respectively, of the combination of series-con-

* Manuscript received by the PGMTT, May 4, 1959; revised manuscript received, June 17, 1959.

† U. S. Dept. of Commerce, Natl. Bur. Standards, Boulder Labs., Boulder, Colo.

[1] R. W. Beatty, "Mismatch errors in the measurement of ultra-high frequency and microwave variable attenuators," *J. Research Natl. Bur. Standards*, vol. 52, pp. 7–9; January, 1954.

[2] C. G. Montgomery, ed., "Technique of Microwave Measurements," Mass. Inst. Tech. Rad. Lab. Ser., McGraw-Hill Book Co., Inc., New York, N. Y., vol. 11, Ch. 13; 1947.

[3] R. W. Beatty, "Cascade-connected attenuators," *J. Research Natl. Bur. Standards*, vol. 45, pp. 231–235; September, 1950.

[4] In this paper, attenuation is defined as the insertion loss in a reflection-free system. Thus, in measuring attenuation, one attempts to eliminate the reflections in the system, and then one measures the insertion loss.

nected attenuators considered as a single attenuator (called the combination attenuator in the remainder of the paper). These may differ from the sums of the individual attenuations by ϵ_{oi} and ϵ_{of}, respectively, and therefore one may write

$$A_f = A_{if} + A_{rf} + \epsilon_{of} \tag{5}$$

$$A_i = A_{ii} + A_{ri} + \epsilon_{oi}. \tag{6}$$

Substituting (5) and (6) into (4) yields

$$A_f - A_i + \epsilon_2 = \epsilon_T, \tag{7}$$

where ϵ_2 has been written for $\epsilon_{oi} - \epsilon_{of}$. The component ϵ_2 of the mismatch error is the difference between the attenuation of the combination attenuator and the sums of the attenuations of the individual attenuators. This component may be evaluated by an extension of the results of Ref. 3 to include the case of variable attenuators connected in cascade, and may be written as

$$\epsilon_2 = 20 \log_{10} \left| \frac{1 - {}^{(f)}S_{11}''{}^{(f)}S_{22}'}{1 - {}^{(i)}S_{11}''{}^{(i)}S_{22}'} \right|, \tag{8}$$

where the front superscripts (i) and (f) refer to the initial and final values, respectively; the primed S's are elements of the scattering matrices[5] of the individual attenuators, and the number of primes indicate the position of the attenuator as counted from the generator.

Eq. (7) may be written as

$$A_f - A_i = \epsilon_T - \epsilon_2 = \epsilon_1. \tag{9}$$

This form is equivalent to considering the combination attenuator as a single attenuator at two different attenuation settings, and ϵ_1 can therefore be evaluated as the mismatch error in a relative attenuation measurement with a single attenuator. This component of mismatch error has been treated by Beatty[1] and for this application may be written as

$$\epsilon_1 = 20 \log_{10} \left| \frac{(1 - {}^{(f)}\Gamma_1\Gamma_9)(1 - {}^{(f)}S_{22}\Gamma_L)}{(1 - {}^{(i)}\Gamma_1\Gamma_9)(1 - {}^{(i)}S_{22}\Gamma_L)} \right|, \tag{10}$$

where the front superscripts (i) and (f) refer to the initial and final values, respectively, and where Γ_1 is the input reflection coefficient of the combination attenuator when terminated with an equivalent detector having a reflection coefficient Γ_L. Also, Γ_G is the reflection coefficient of the equivalent generator, and S_{22} is an element of the scattering matrix, S, of the combination attenuator. It should be recalled that this expression gives smaller limits of mismatch error than the addition of the separate limits of mismatch error for attenuation at the initial and final settings.

The total error in cascading variable[6] attenuators in a mismatched system is then $\epsilon_1 + \epsilon_2$, where ϵ_1 is the error caused by interactions of reflections from the generator, combination attenuator, and the load, and ϵ_2 is the error caused by interactions of reflections from the individual attenuators.

The scattering matrix of the combination attenuator is used to evaluate the component ϵ_1 of the mismatch error according to (10). This is readily obtained in terms of the scattering matrices of the individual attenuators through use of the T matrices.[7] The T matrix for a combination of n cascade-connected attenuators may be written as

$$T = \prod_{k=n}^{k=1} T_k, \tag{11}$$

where the T_k are the matrices for the individual attenuators. This T matrix is the inverse of the A matrix used in Ref. 3. The scattering matrix, S, for the two-arm junction is related to the T matrix as follows:

$$S = \frac{1}{T_{22}} \begin{vmatrix} -T_{21} & 1 \\ 1 & T_{12} \end{vmatrix} \quad \text{and} \quad T = \frac{1}{S_{12}} \begin{vmatrix} S_{12}^2 - S_{22}S_{11} & S_{22} \\ -S_{11} & 1 \end{vmatrix}, \tag{12}$$

when reciprocity in the form $S_{pq} = S_{qp}$ is assumed. The necessary characteristics of the combination of attenuators needed to evaluate the error by (10) are Γ_1 and S_{22}. These may be obtained by use of (11) and (12), and the expression

$$\Gamma_1 = S_{11} + \frac{S_{12}^2\Gamma_L}{1 - S_{22}\Gamma_L}. \tag{13}$$

The results for two attenuators in cascade are

$$\Gamma_1 = S_{11}' + \frac{(S_{12}')^2 S_{11}''(1 - S_{22}''\Gamma_L) + (S_{12}')^2(S_{12}'')^2\Gamma_L}{(1 - S_{22}''\Gamma_L)(1 - S_{11}''S_{22}') - S_{22}'(S_{12}'')^2\Gamma_L}, \tag{14}$$

and

$$S_{22} = S_{22}'' + \frac{S_{22}'(S_{12}'')^2}{1 - S_{11}''S_{22}'}, \tag{15}$$

and for three attenuators in cascade, they are

$$\Gamma_1 = S_{11}' + \frac{(S_{12}')^2\{S_{11}''[(1 - S_{22}''S_{11}''')(1 - S_{22}'''\Gamma_L) - S_{22}''(S_{12}''')^2\Gamma_L] + S_{11}'''(S_{12}'')^2(1 - S_{22}'''\Gamma_L) + (S_{12}'')^2(S_{12}''')^2\Gamma_L\}}{(1 - S_{22}'''\Gamma_L)[(1 - S_{22}'S_{11}'')(1 - S_{22}''S_{11}''') - S_{22}'(S_{12}'')^2 S_{11}'''] - (S_{12}''')^2\Gamma_L[S_{22}''(1 - S_{11}''S_{22}') + S_{22}'(S_{12}'')^2]}, \tag{16}$$

and

$$S_{22} = S_{22}''' + \frac{(S_{12}''')^2\{S_{22}'(S_{12}'')^2 + S_{22}''(1 - S_{11}''S_{22}')\}}{(1 - S_{22}'S_{11}'')(1 - S_{11}'''S_{22}'') - S_{22}'S_{11}'''(S_{12}'')^2}, \tag{17}$$

[5] C. G. Montgomery, *op. cit.*, Ch. 14.

[6] The same analysis applies to cascaded-fixed, or a combination of fixed and variable attenuators in a mismatched system by using the appropriate forms of (8) and (10).

[7] C. G. Montgomery, R. H. Dicke, and E. M. Purcell, "Principles of Microwave Circuits," Mass. Inst. Tech. Rad. Lab. Ser., McGraw-Hill Book Co., Inc., New York, N. Y., vol. 8, Ch. 5; 1948.

where the primed S's are the scattering coefficients of the individual attenuators, where the number of primes indicates the position of the attenuator as counted from the generator end where Γ_L is the equivalent reflection coefficient of the detector, and where reciprocity in the form $S_{pq}=S_{qp}$ has been assumed.

Substitution of (14) and (15) into (10) gives the expression for the component ϵ_1 of the mismatch error for two variable attenuators in cascade. Similarly, substitution of (16) and (17) gives the corresponding expression for the case of three variable attenuators in cascade.

Assuming that the phases of the individual coefficients of (8) and (10) are not known and that they can have any possible value, the actual values of the error components cannot be determined, but limits may be found. Such a limit is a conservative figure, and a closer estimate of the actual error may be obtained if one determines the phases of the individual coefficients. The limits of ϵ_1 and ϵ_2 may be added to obtain limits of the mismatch error, ϵ_T, since the phases of the coefficients in (8) and (10) can take on values so that each component of mismatch error is simultaneously at its maximum possible value.

Graphical Presentation of Results

One of the factors taken into consideration, in constructing the graphs, was the ease of obtaining an estimate of the limits of the mismatch error. For this purpose, certain assumptions to be discussed were made concerning the scattering coefficients of the attenuators. Since many commercially available attenuators have similar voltage-standing-wave ratio (VSWR) characteristics, it will become evident that these assumptions caused very little loss in the generality of application. The following equalities were assumed:

$$|S_{11}'| = |S_{11}''| = |S_{11}'''| = |S_{22}'| = |S_{22}''| = |S_{22}'''| \tag{18}$$

and

$$|\Gamma_G| = |\Gamma_L|. \tag{19}$$

Furthermore, it was assumed that the phases of each coefficient in (14)–(17) and the S_{12}'s took on values at the initial and final settings of the attenuators which would give the maximum possible mismatch error (limits of mismatch error). This assumption yields a conservative estimate of the mismatch error.

The range of the limits of the mismatch error, ϵ_T, for two attenuators in cascade and for three attenuators in cascade are shown in Figs. 1 and 2, respectively. The sectors indicate how the limits of error vary with the number of decibels to be measured and with the VSWR of the attenuators for a number of specified equivalent generator and detector mismatches. Eq. (18) implies

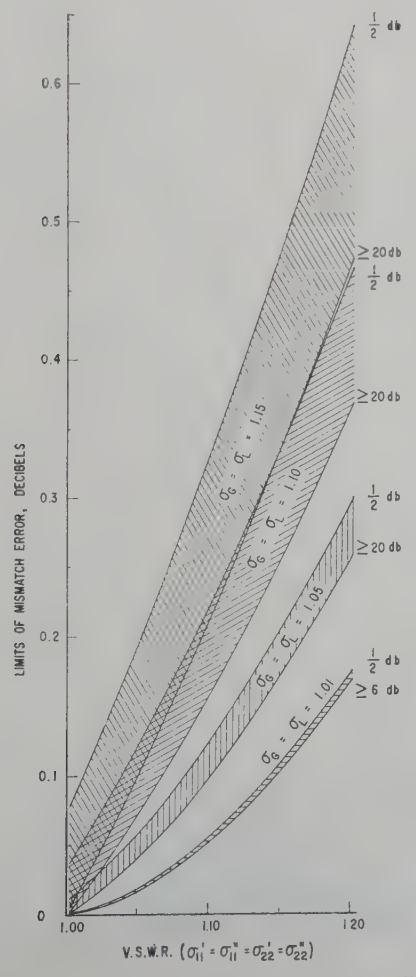

Fig. 1—Variation with range of measurement in limits of mismatch error, ϵ_T, for two variable attenuators in cascade.

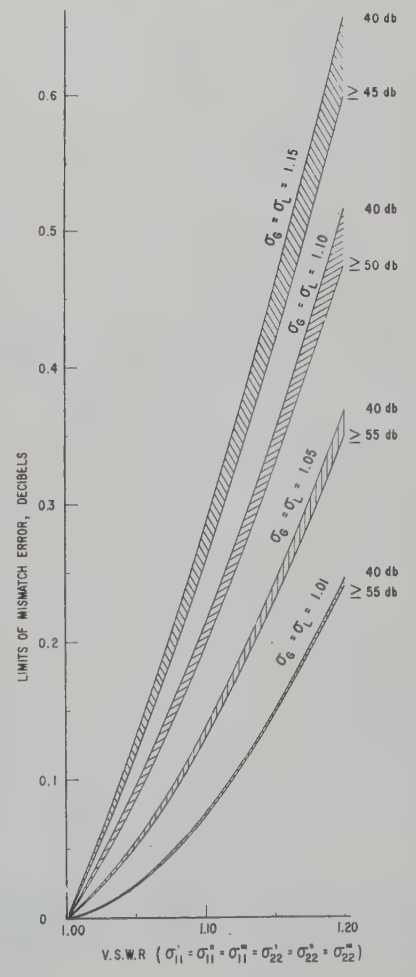

Fig. 2—Variation with range of measurement in limits of mismatch error, ϵ_T, for three variable attenuators in cascade.

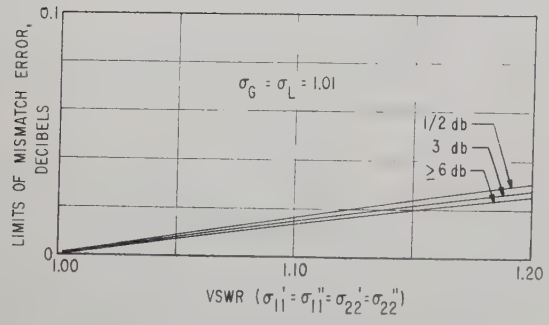

Fig. 3—Limits of component ϵ_1 of mismatch error for two attenuators with equal magnitudes of S_{11} and S_{22} cascaded in a system where $\sigma_G = \sigma_L = 1.01$.

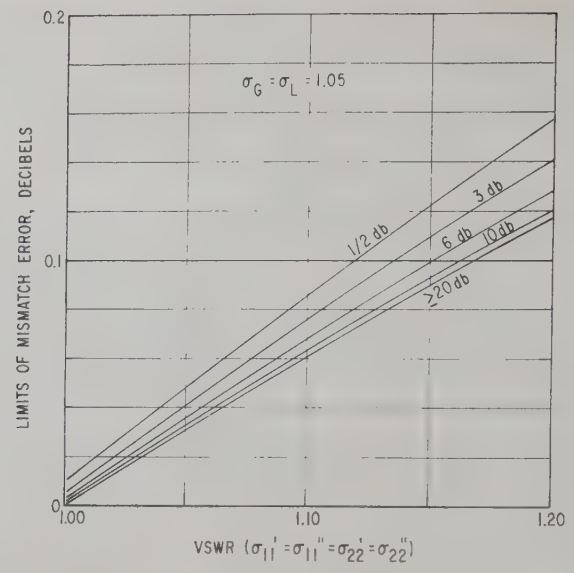

Fig. 4—Limits of component ϵ_1 of mismatch error for two attenuators with equal magnitudes of S_{11} and S_{22} cascaded in a system where $\sigma_G = \sigma_L = 1.05$.

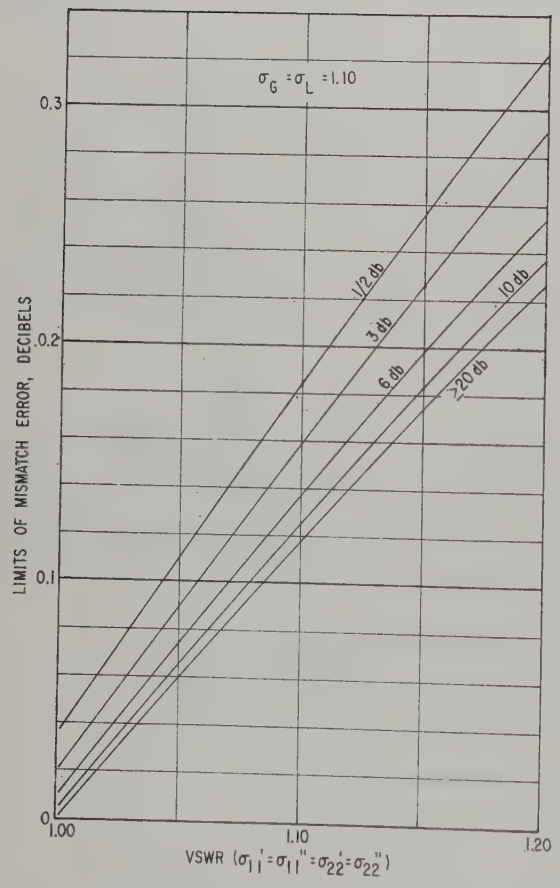

Fig. 5—Limits of component ϵ_1 of mismatch error for two attenuators with equal magnitudes of S_{11} and S_{22} cascaded in a system where $\sigma_G = \sigma_L = 1.10$.

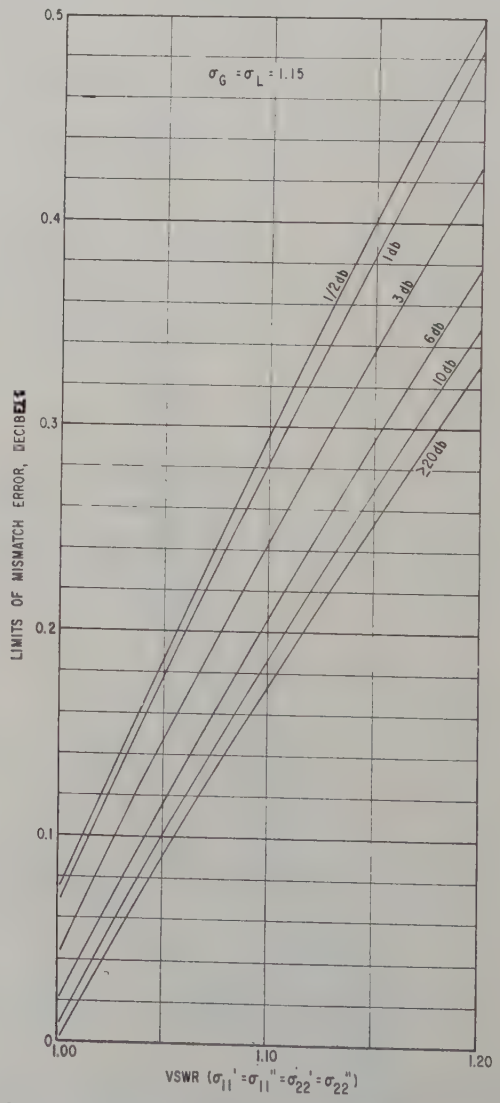

Fig. 6—Limits of component ϵ_1 of mismatch error for two attenuators with equal magnitudes of S_{11} and S_{22} cascaded in a system where $\sigma_G = \sigma_L = 1.15$.

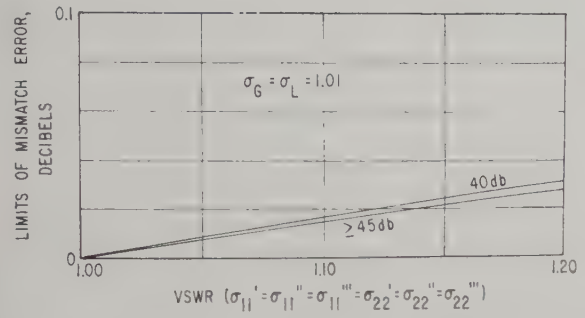

Fig. 7—Limits of component ϵ_1 of mismatch error for three attenuators with equal magnitudes of S_{11} and S_{22} cascaded in a system where $\sigma_G = \sigma_L = 1.01$.

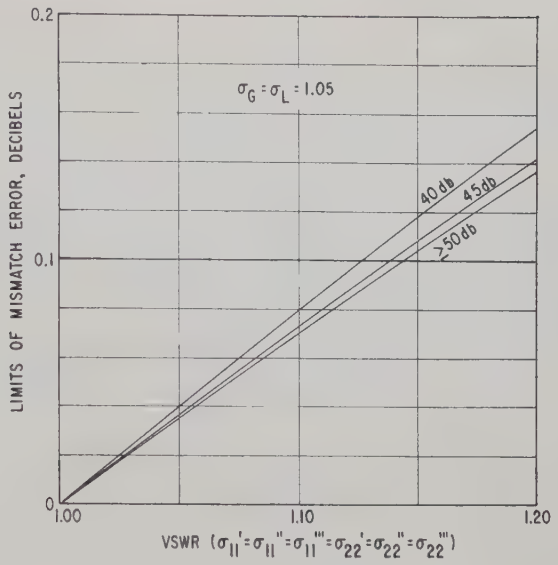

Fig. 8—Limits of component ϵ_1 of mismatch error for three attenuators with equal magnitudes of S_{11} and S_{22} cascaded in a system where $\sigma_G = \sigma_L = 1.05$.

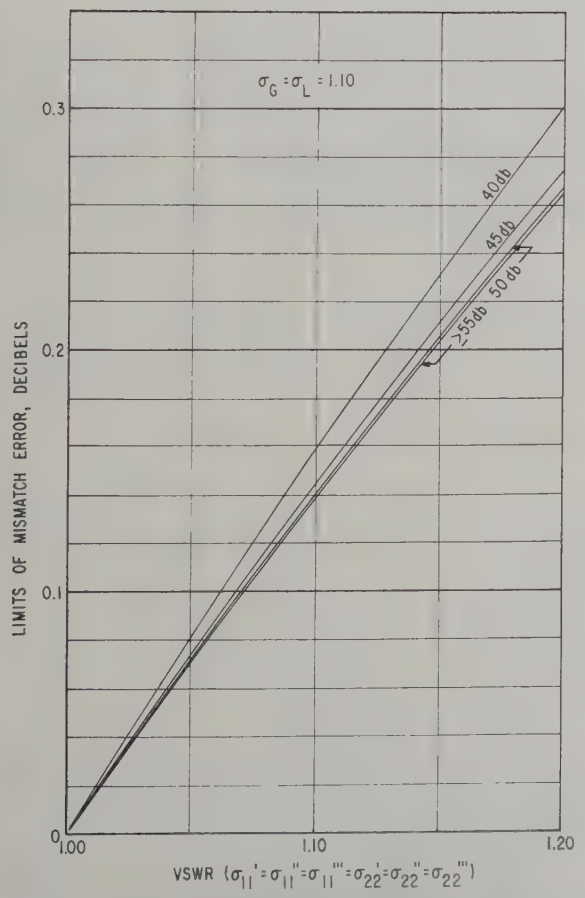

Fig. 9—Limits of component ϵ_1 of mismatch error for three attenuators with equal magnitudes of S_{11} and S_{22} cascaded in a system where $\sigma_G = \sigma_L = 1.10$.

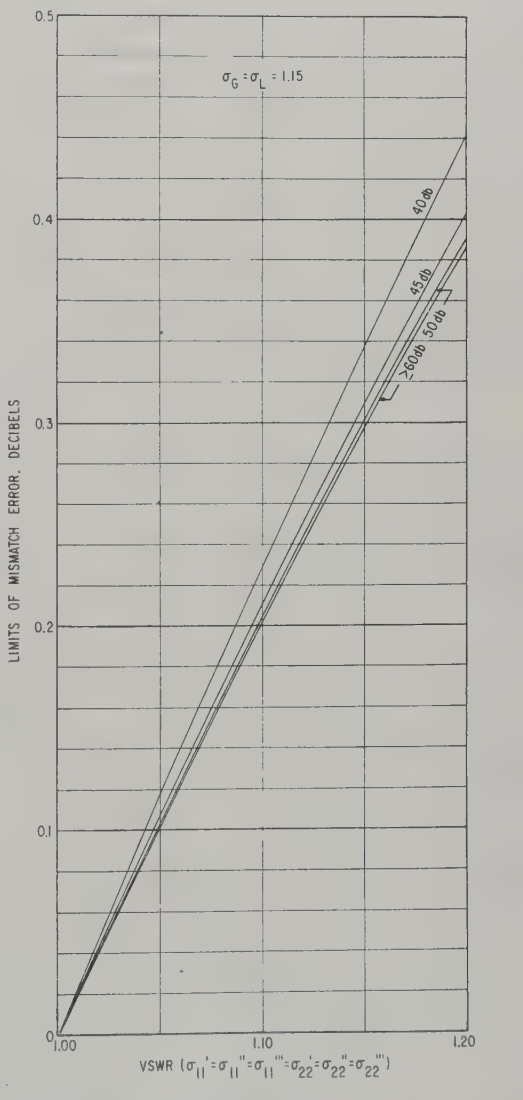

Fig. 10—Limits of component ϵ_1 of mismatch error for three attenuators with equal magnitudes of S_{11} and S_{22} cascaded in a system where $\sigma_G = \sigma_L = 1.15$.

that the VSWR corresponding to S_{11} or S_{22} of the attenuators, which is the abscissa, has been assumed to be the same and equal for the input and output of each attenuator. Each sector is labeled with the appropriate values of the VSWR associated with the equivalent generator and detector reflection coefficients which were assumed to be equal in (19). The ordinates are the limits of mismatch error. These figures are presented to illustrate the range of limits of mismatch error to be expected in the assumed situations.

Figs. 3–6 are a series of graphs of the limits of the component ϵ_1 of mismatch error for two attenuators in cascade with σ_G $(=\sigma_L)$ of 1.01, 1.05, 1.10, and 1.15, respectively. σ_G and σ_L are the VSWR's associated with the equivalent generator and detector reflection coefficients, respectively. The VSWR's used as the abscissas are the input and output VSWR's of the variable attenuators. It is assumed that these VSWR's are all equal. The parameter for the family of curves is the number of decibels to be measured by this technique.

Figs. 7–10 are an equivalent series of graphs of the limits of the component ϵ_1 of the mismatch error for the case of three attenuators in cascade. These are applicable for measurements of attenuation of 40 db or more.

Figs. 11 and 12 are graphs of the limits of the component ϵ_2 of the mismatch error for the cases of two and three attenuators in cascade. The abscissas are the VSWR's of the attenuators. The limits of error in this case are independent of the load and generator mismatches. For the case of three attenuators in cascade, Fig. 12 is constructed on the assumption that at least 20 db attenuation is in the middle attenuator at one of the attenuation settings, either the initial or the final.

Use of the Graphs

In order to use the graphs of Figs. 3–12 to estimate the limit of error, one must know the VSWR's of the attenuators and of the equivalent generator and detector, and the approximate number of decibels to be measured. For an example, consider a case where 1) the equivalent generator and detector VSWR's are 1.03 and 1.04, respectively; 2) the three attenuators have input and output VSWR's of 1.15 or less; and 3) the desired attenuation measurements are 3 db, 40 db, and 75 db, and the reference attenuators are calibrated up to 40 db. The values of the generator and detector VSWR's are used to determine which of the graphs of ϵ_1 is to be used. One selects the graph with the nearest available value of $\sigma_G(=\sigma_L)$ which is equal to, or greater than, the larger value of the actual load or generator VSWR. This will give a conservative estimate of the limits of error. In this example, the actual VSWR's of the generator and the detector are 1.03 and 1.04, respectively, and for the case of two attenuators in cascade, Fig. 4 would be selected, since it is constructed on the assumption that both of these are 1.05. Having selected the graph, the largest value of the VSWR at the input or output of the attenuators is the abscissa. Typical commercially-available attenuators for rectangular waveguide systems have maximum VSWR of 1.15 over their entire frequency and attenuation ranges. For a conservative estimate, then, one could use an abscissa of 1.15 unless the actual values of the VSWR are known to be different. The value of ϵ_1 is different for different values of attenuation. For a 3-db measurement it has the value 0.11 db, and for a 40-db measurement it is 0.09 db. Note that for measurements of attenuation of 20 db or greater the component ϵ_1 of the limits of error does not change within the resolution of the graphs.

One determines ϵ_2 from Fig. 11, and it depends only on the VSWR's of the attenuators, and not on the amount of attenuation or on the generator and load mismatches. For a VSWR of 1.15, ϵ_2 is 0.08 db. Addition of these two components, as determined from Figs. 4 and 11, yields the limits of mismatch error, ϵ_T, of 0.19

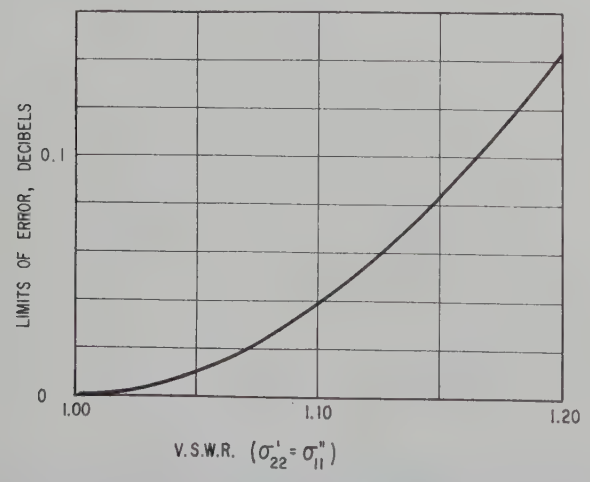

Fig. 11—Limits of component ϵ_2 of mismatch error for two attenuators with equal magnitudes of S_{11} and S_{22}.

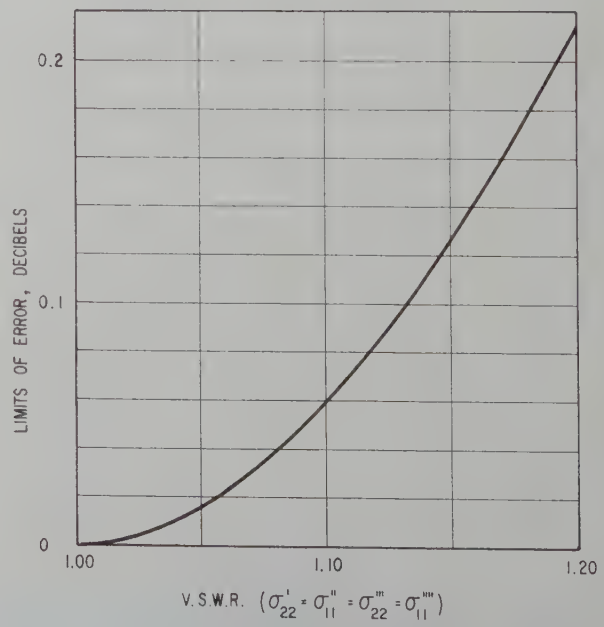

Fig. 12—Limits of component ϵ_2 of mismatch error for three attenuators with equal magnitudes of S_{11} and S_{22}.

db for a 3-db measurement and 0.17 db for a 40-db measurement.

If the three similar attenuators are connected in cascade and inserted in the system, Fig. 8 shows that ϵ_1 is now 0.12 db for a 40-db measurement and 0.10 db for a 75-db measurement, and Fig. 12 shows that ϵ_2 is 0.13 db for both measurements. Addition of these yields the limits of mismatch error, ϵ_T, of 0.25 db for a 40-db measurement and 0.23 db for a 75-db measurement. These examples are felt to be representative of conditions met in typical rectangular waveguide systems.

Conclusion

It can be seen that if maximum possible error is assumed, the mismatch error increases for smaller relative attenuation measurements.

The limit of mismatch error estimated by this method is a conservative figure since it is based on the assumption that all values of the coefficients have phases at the initial and final settings which give the maximum possible error. Thus, in an actual application, the mismatch errors are very probably less than those estimated in the examples.

A Nonreciprocal, TEM-Mode Structure for Wide-Band Gyrator and Isolator Applications*

E. M. T. JONES†, G. L. MATTHAEI†, AND S. B. COHN†

Summary—**The theoretical and experimental operation of a novel form of TEM transmission-line network capable of operation over octave bandwidths is described. This network consists, basically, of a parallel arrangement of two conductors and a ferrite rod within a grounded outer shield. The conductors may be connected in a two-port configuration which provides, in the absence of the ferrite rod, complete isolation from zero frequency to the cut-off frequency of the first higher mode. With an unmagnetized ferrite rod properly inserted, the broad-band isolation is virtually unaffected. When the rod is magnetized by an axial magnetic field, coupling occurs between the two ports by a process analogous to Faraday rotation.**

The device may be used as a broad-band gyrator, switch, or modulator, and with the addition of a resistance load, as an isolator. The bandwidth of these components is inherently limited only by the bandwidth capability of the ferrite material itself.

I. Qualitative Description of Operation

Gyrator Network

THE form of the nonreciprocal TEM transmission-linenet work that functions as a wide-band gyrator, switch, or modulator is illustrated in Fig. 1.[1–3] It consists of a pair of shielded, coupled transmission lines and an axially oriented ferrite pencil. This circuit behaves, in the absence of the ferrite rod, as an all-stop filter; *i.e.*, infinite attenuation theoretically exists between the two ports at all frequencies.[4] For the network to be an all-stop filter, it is necessary that one of the coupled lines be open-circuited and the other short-circuited, in the manner shown in the figure, and that the phase velocity of the even and odd modes on the coupled lines be the same. Both these conditions are satisfied when the ferrite is properly oriented in the plane of symmetry between the coupled lines. The proper position of the rod is quite independent of frequency, so that the composite structure has high attenuation over a wide band of frequencies.

When an axial magnetic field is applied to the ferrite rod, it rotates the plane of polarization of the linearly polarized transverse RF magnetic field existing along the ferrite rod, and energy is coupled between the input and output ports. When the axial field is increased to the point where the RF magnetic field is rotated by 90 degrees, virtually all the energy is transferred. When the cross section of the ferrite rod is small in terms of wavelength, and the operating frequency is far removed from the ferromagnetic resonance frequency, the rotation of the plane of polarization per unit length by the ferrite is essentially independent of frequency. Therefore, low insertion loss is experienced over a wide frequency range. Because the plane of polarization of the RF magnetic field is rotated in the same sense with respect to the positive direction of the biasing magnetic field, independent of the direction of propagation through the

* Manuscript received by the PGMTT, April 29, 1959; revised manuscript received, June 19, 1959.

† Div. of Engrg. Res., Stanford Res. Inst., Menlo Park, Calif.

[1] E. M. T. Jones, S. B. Cohn, and J. K. Shimizu, "A wide-band nonreciprocal TEM-transmission-line network," 1958 WESCON Convention Record, pt. 1, pp. 131–135.

[2] O. W. Fix, "A balanced-stripline isolator," IRE Convention Record, pp. 99–105; March, 1956.

[3] H. Boyet and H. Seidel, "Analysis of nonreciprocal effects in an N-wire ferrite-loaded transmission line," Proc. IRE, vol. 45, pp. 491–495; April, 1957.

[4] E. M. T. Jones and J. T. Bolljahn, "Coupled-strip-transmission-line filters and directional couplers," IRE Trans. on Microwave Theory and Techniques, vol. MTT-4, pp. 75–81; April, 1956.

device, it can be seen that the signal undergoes 180 degrees more phase shift while passing through in one direction that it does while passing through in the opposite direction. Thus, the device functions as a gyrator. It may also be used as a switch by abruptly changing the magnetizing field from zero to the strength that gives full transfer of energy, or it can be used as a modulator by continuously varying the field.

Isolator

The network configuration most suitable for use as an isolator is shown in Fig. 2. The diagrams at the bottom of the figure illustrate the manner in which the RF magnetic field at the axis of the ferrite rod is rotated in passing through the device in either direction. When a signal travels from left to right, the RF magnetic field is initially oriented at an angle ϕ_1, somewhat greater than 45 degrees to the horizontal. Since there is no voltage induced in the short-circuited line on the upper left, the resistive termination placed behind this line does not attenuate the signal. The RF magnetic field, on passing through the ferrite, is rotated through an angle ϕ_1 so that at the output it is horizontal. A signal entering

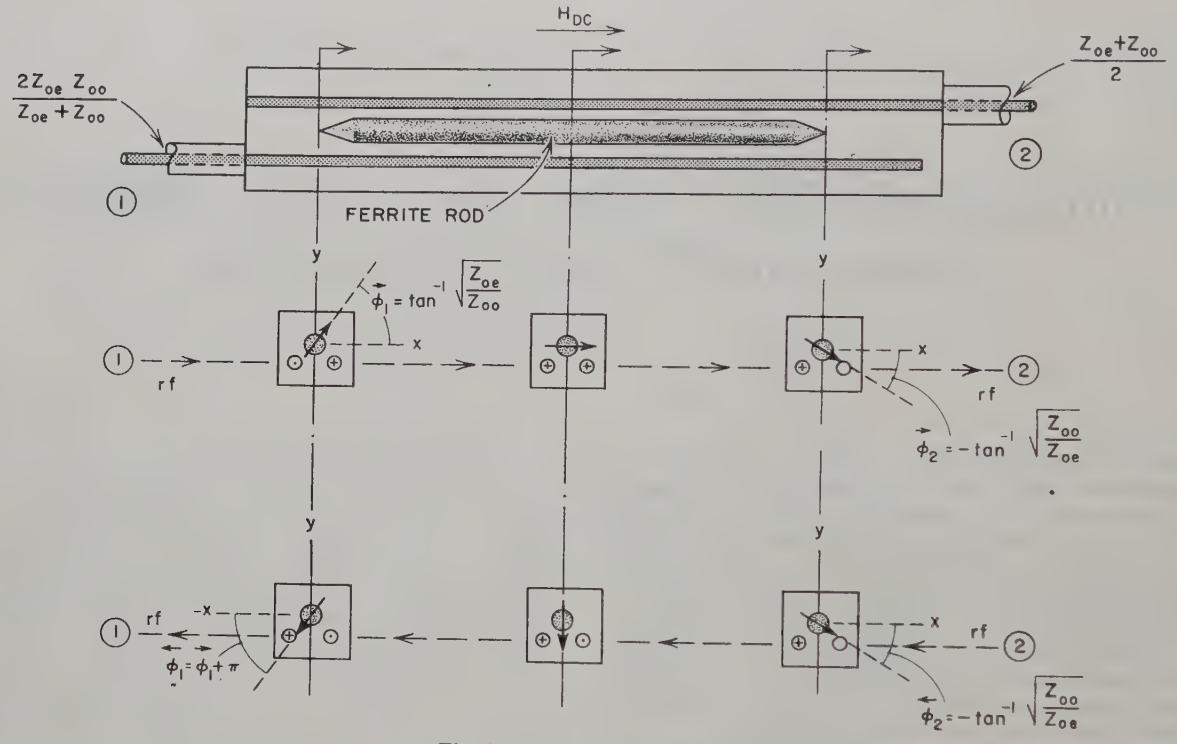

Fig. 1—Wide-band gyrator.

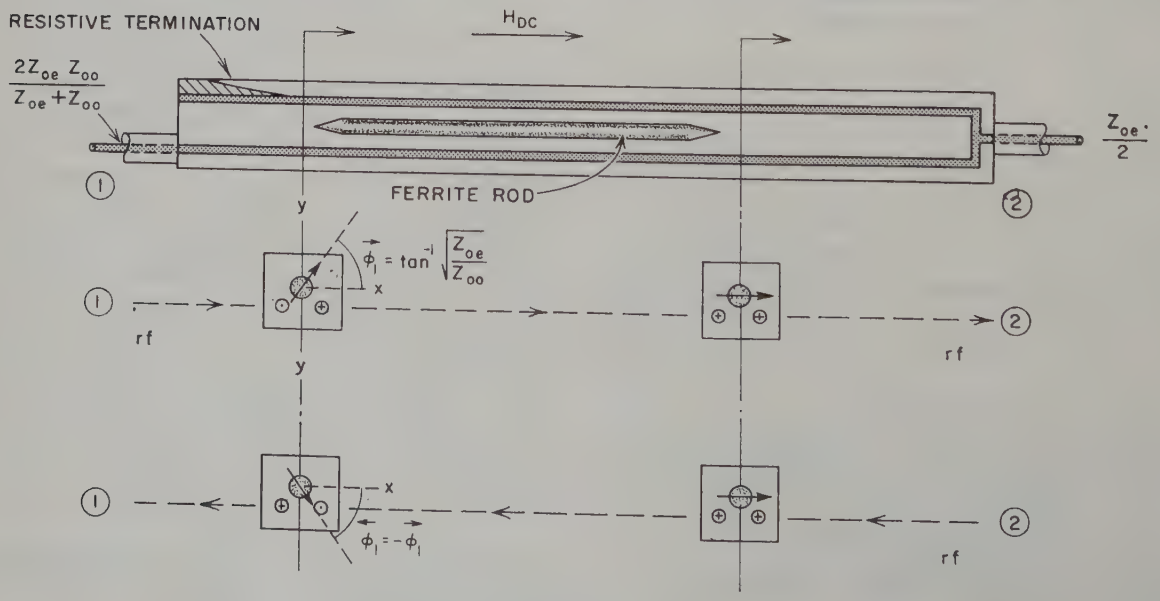

Fig. 2—Wide-band isolator.

from the right also has its RF magnetic field rotated ϕ_1 degrees as it passes through the ferrite so that all the power is transferred to the upper line where it is attenuated by the resistive termination at the left-hand end of the network.

II. Perturbation Analysis of Nonreciprocal Coupling Between a Pair of Shielded Conductors

A more detailed picture of the behavior of the various forms of the device may be obtained by analyzing the nonreciprocal coupling between shielded conductors using perturbation theory.[5] This theory is exact for ferrite rods having infinitesimal cross section areas, and is qualitatively correct for the ferrite rods used in practice. Application of this theory shows that with a lossless ferrite rod in position and unmagnetized, the propagation constant β_e' of the even mode is

$$\beta_e' - k_1 = \frac{\omega\mu_0\Delta s H_e^2\left[2\left(\frac{\epsilon-1}{\epsilon+1}\right)+2\left(\frac{\mu-1}{\mu+1}\right)\right]}{4I_e^2 Z_{oe}} \quad (1)$$

while the propagation constant β_0' of the odd mode is

$$\beta_0' - k_1 = \frac{\omega\mu_0\Delta s H_0^2\left[2\left(\frac{\epsilon-1}{\epsilon+1}\right)+2\left(\frac{\mu-1}{\mu+1}\right)\right]}{4I_o^2 Z_{oo}}. \quad (2)$$

In these expressions,

H_e = RF field existing at the axis of the ferrite, in the absence of the ferrite, when the device is excited in the even mode; *i.e.*, equal in-phase currents I_e flow on the conductors;

H_0 = RF magnetic field existing at the axis of the ferrite, in the absence of the ferrite, when the device is excited in the odd mode; *i.e.*, equal out-of-phase currents I_0 flowing in the center conductors;

Z_{oh} = characteristic impedance of one center conductor to ground with equal in-phase current I_e flowing in the center conductors;

Z_{oh} = characteristic impedance of one center conductor to ground with equal out-of-phase currents I_{oh} flowing in the center conductors;

k_1 = propagation constant of the unperturbed system, which is assumed lossless;

μ = relative initial permeability of the ferrite;

ϵ = relative dielectric constant of the ferrite;

$\mu_0 = 4\pi\times10^{-7}$ henries/meter;

ω = angular operating frequency; and

Δs = cross section area of ferrite rod, meter.[2]

In order that there be no reciprocal coupling between the conductors, the ferrite rod must be oriented so that the phase velocities of perturbed even and odd modes are equal. That is,

$$\beta_e' = \beta_o' = \beta. \quad (3)$$

Substitution of (1) and (2) into (3) yields the relation

$$\frac{H_e}{I_e\sqrt{Z_{oe}}} = \frac{H_o}{I_o\sqrt{Z_{oo}}}. \quad (4)$$

Eq. (4) shows that when the even and odd modes carry equal power, they will produce equal RF magnetic fields at the axis of the ferrite rod. However, equal even- and odd-mode currents do not produce equal fields at the center of the rod.

When the rod is biased with an axial field, the amount of nonreciprocal rotation θl of the plane of polarization of the wave in passing along the axis of the ferrite rod of length l, as well as the attenuation αl, can be determined by first resolving the wave into right- and left-hand circularly polarized components having the propagation constants $\alpha_+ + j\beta_+$ and $\alpha_- + j\beta_-$, respectively.

Making the usual approximation that $(\omega_{res}/\omega_0\tau)^2 \ll (\omega_{res}\pm\omega)^2$, one finds that

$$\theta l = \frac{(\beta_- - \beta_+)l}{2} = \frac{\omega l\mu_0\Delta s(H_e^2 + H_o^2)\omega\omega_m}{(4I_e^2 Z_{oe} + 4I_{oh}^2 Z_{oo})(\omega_{res}^2 - \omega^2)}, \quad (5)$$

and

$$\alpha l = \left(\frac{\alpha_+ + \alpha_-}{2}\right)l = \frac{\omega l\mu_0\Delta s(H_e^2 + H_o^2)\omega_m\omega}{(4I_e^2 Z_{oe} + 4I_{oh}^2 Z_{oo})\omega_o\tau}\left[\frac{\omega_{res}^2 + \omega^2}{(\omega_{res}^2 - \omega^2)^2}\right]. \quad (6)$$

The relation getween θl and αl takes the particularly simple form of

$$\alpha l = \frac{1}{\omega_0\tau}\left(\frac{\omega_{res}^2 + \omega^2}{\omega_{res}^2 - \omega^2}\right)\theta l. \quad (7)$$

In these expressions,

$\omega_m = \gamma 4\pi M$,

$4\pi M$ = saturation magnetization (gauss),

$\gamma/2\pi = 2.8$ mc/oersted,

$\omega_0 = \gamma H_{DC}$,

H_{DC} = applied internal field in the ferrite rod (oersteds),

$\omega_{res} = \omega_0 + \omega_m/2$,

$\tau = 2/\gamma\Delta H = T\omega/\omega_0$,

T = phenomenological relaxation time as defined by Lax,[5] and

ΔH = ferrite line width measured to the one-half amplitude points.

Eq. (7) shows that for a given total rotation θl, the total attenuation αl experienced by a signal is independent of the cross section geometry. In the experimental gyrator and isolator to be described later, the ferrite used is Ferramic R-1. This material has a line width ΔH of about 500 oersteds at an operating frequency of 9000 mc. This value of line width yields $\omega_0\tau = \omega T$ of about

[5] B. Lax, "Frequency and loss characteristics of microwave ferrite devices," Proc. IRE, vol. 44, pp. 1368–1386; October, 1956.

12.7 over a wide band of frequencies centered at 9000 mc. Hence, far from resonance the theoretical attenuation through the gyrator, which has a $\theta l = \pi/2$ radians, is about 1.07 db. The theoretical minimum forward attenuation through the isolator which has a θl of about 0.91 radian is 0.62 db. Inspection of (7) reveals that, at frequencies removed from the ferromagnetic resonance frequency, the rotation θl is independent of the operating frequency.

When the operating frequency approaches the resonance frequency, (5) shows that θl increases. However, (6) predicts an even greater increase in αl. For a given size of ferrite, the amount of rotation is proportional to the ratio of $H_o^2+H_e^2$ (the square of the total unperturbed RF field at the axis position of the ferrite) to $4I_e^2Z_{oe}+4I_o^2Z_{oo}$ (twice the total power transmitted along the ferrite-loaded structure). In general, it is very difficult to determine this ratio quantitatively; however, it has been done for the case of thin, flat, co-planar coupled strips using a conformal mapping technique. The results of this analysis show that this ratio increases as the gap between the coupled strips is decreased. At the same time, it is found that the position where the magnetic fields of the even and odd mode are equal for equal power in the two modes moves closer to the plane of the coupled strips as the gap between the strips is decreased. It seems likely that this behavior will obtain for other conductors having different cross section shapes.

III. Detailed Description of Operation

Gyrator

When the correct biasing field for gyrator action is applied to the ferrite rod shown in Fig. 1, perfect transmission is achieved through the network, assuming a reflectionless and lossless ferrite when the terminating impedances at Port 1 and Port 2 are equal to the input impedances at each of these ports when the opposite port is terminated in a matched load. The input impedance at Port 1 under these conditions can be readily computed by noting that a signal entering Port 1 excites even and odd modes on the coupled lines, having equal voltages $V/2$ since it is necessary to have zero voltage on the shorted line. Hence, the current flowing on the coupled line connected to Port 1 is $V/2[1/Z_{oe}+1/Z_{oo}]$, while that induced on the shorted line is

$$V/2[1/Z_{oe} - 1/Z_{oo}].$$

Therefore, the input impedance at Port 1 is

$$2Z_{oe}Z_{oo}/(Z_{oe} + Z_{oo}).$$

In a like manner, it is seen that a signal entering Port 2 excites even and odd modes having equal currents, I. Hence the voltage on the line connecting to Port 2 is $I(Z_{oe}+Z_{oo})$, while that induced on the open-circuited line is $I(Z_{oe}-Z_{oo})$. Therefore, the input impedance at Port 2 is $(Z_{oe}+Z_{oo})/2$.

The inclination angle ϕ of the RF magnetic field along the axis of the ferrite as a signal passes through the gyrator can be computed in the following fashion. When a signal is incident on Port 1[6] with voltage amplitude V, the amplitude of the even current $\vec{I}_{1e}$ is $V/2Z_{oe}$ on each of the coupled lines while the amplitude of the odd current $\vec{I}_{1o}$ is $-V/2Z_{oo}$. Referring to Fig. 1 and remembering the condition of (4), it is seen that the even current produces an x-directed component of magnetic field $\vec{H}_{1x}=\vec{H}_{1e}$ at the axis of the ferrite rod having an amplitude proportional to $1/\sqrt{Z_{oe}}$. The odd-mode current produces a y-directed component of magnetic field $\vec{H}_{1y}=\vec{H}_{1o}$ at the axis of the ferrite rod having an amplitude proportional to $1/\sqrt{Z_{oo}}$. Thus,

$$\tan \vec{\phi}_1 = \frac{\vec{H}_{1y}}{\vec{H}_{1x}} = \sqrt{\frac{Z_{oe}}{Z_{oo}}}. \tag{8}$$

As the signal passes through the magnetized ferrite, the plane of polarization of the field at the axis of the ferrite rod rotates clockwise; however, its magnitude $\sqrt{H_o^2+H_e^2}$ is unchanged. When the wave reaches the end of the ferrite rod adjacent to Port 2, it is necessary that $\vec{I}_{2e}=\vec{I}_{2o}=V/2\sqrt{Z_{oe}Z_{oo}}$ in order that all the signal power will pass out Port 2. Therefore, the inclination angle ϕ_2 is

$$\tan \vec{\phi}_2 = \frac{\vec{H}_{2y}}{\vec{H}_{2x}} = \sqrt{\frac{Z_{oo}}{Z_{oe}}}, \tag{9}$$

showing that the plane of polarization of the wave at the center of the ferrite is rotated 90 degrees in passing once through the gyrator. When a signal passes through the device from Port 2 to Port 1, the plane of polarization of the RF magnetic field is rotated in the same sense with respect to the biasing field, as shown in Fig. 1. Hence, as explained above, this device functions as a gyrator since a signal undergoes 180 degrees more phase shift in going through the device in one direction than the other.

Wide-Band Isolator

When the correct biasing field is applied to the ferrite rod shown in Fig. 2 for isolator action, zero forward loss is achieved, again assuming a lossless and reflectionless ferrite when the characteristic impedances of the lines connected to Port 1 and Port 2 are $2Z_{oe}Z_{oo}/(Z_{oe}+Z_{oo})$ and $Z_{oe}/2$, respectively. Furthermore, it is necessary that the termination within the isolator perturb the phase velocities of the even and odd modes equally, in order that there be no reciprocal coupling between the lines.

[6] The arrows indicate the direction of power flow through the device with reference to Fig. 1.

When a signal is incident on Port 1, the inclination angle $\vec{\phi}_1$ of the RF magnetic field at the axis of the ferrite rod is $\vec{\phi}_1 = \tan^{-1}\sqrt{Z_{oe}/Z_{oo}}$. As the signal passes through the isolator, the plane of polarization of the field at the axis of the rod is rotated until $\vec{\phi}_2$ is zero at Port 2. When a signal is incident on Port 2, the angle of inclination $\overleftarrow{\phi}_2$ of the field at Port 2 is again zero. As the signal passes through the device, the RF magnetic field is rotated in the same direction with respect to the biasing magnetic field so that the inclination angle $\overleftarrow{\phi}_1$ of the magnetic field at the center of the ferrite rod nearest Port 1 is $\overleftarrow{\phi}_1 = -\overleftarrow{\phi}_1$. This orientation of the magnetic field corresponds to zero RF voltage on the line connecting to Port 1 and maximum voltage on the line containing the termination, which is the optimum condition for a large absorption in the termination.

It is interesting to note that should the direction of the biasing magnetic field be reversed, a signal incident on Port 2 will propagate through the isolator and emerge unattenuated from Port 1. However, a signal incident on Port 1, after passing through the isolator, will set up both even and odd mode currents on the lines adjacent to Port 2. The energy in the even mode will pass out of Port 2 while the energy in the odd mode will be reflected at the T-junction and later, after retraversing the network, be absorbed in the termination. Thus, other factors being the same, the reverse loss is less for this orientation of biasing field than for the correct orientation of the biasing field shown in Fig. 1. However, as discussed in Section IV, measurements made on an isolator with a lossy ferrite indicated only a small difference in attenuation when the biasing field was reversed.

IV. Measured Performance

Gyrator Experimental Results

A photograph of the experimental model of the wide-band gyrator is shown in Fig. 3. Its measured performance is shown in Fig. 4. The cross section dimensions of the coupled strip lines and the Ferramic R-1 ferrite rod are also shown in Fig. 4. The over-all length of the coupled lines is 8 inches. The over-all length of the ferrite rod is 5.75 inches and each end is tapered over a length of 0.625 inch. The theoretical values of Z_{oe} and Z_{oo} are 139 ohms and 88 ohms, respectively. These values were computed from (24) and (25) of Jones and Bolljahn,[2] suitably modified to account for the increased self-capacitance of the lines caused by the presence of the vertical side walls of the outer conductor of the network. Tapered transitions were employed at either end of the gyrator to match it to the 50-ohm impedance level of the measuring equipment. The transition at Port 1 transformed between 50 ohms and $2Z_{oe}Z_{oo}/(Z_{oe}+Z_{oo}) = 108$ ohms, while the transition at Port 2 transformed between 50 ohms and $(Z_{oe}+Z_{oo})/Z = 114$ ohms.

With no dc biasing field applied, the insertion loss through the gyrator is greater than 20 db, except near the highest frequencies measured where it drops to 16 db. When the magnetic field is applied to obtain gyrator action, the insertion loss decreases to less than 2 db except at a few isolated points in the band. At the upper end of the band, the insertion loss averages about 1 db, in agreement with the results of the perturbation analysis. Although the data were not recorded, it is believed that the gyrator shown would operate satisfactorily down to frequencies as low as 5.5 kmc, since one of the experimental isolators described in the next section operated down to this frequency.

It is believed that the insertion loss of the gyrator, caused mainly by ferrite losses, could be greatly reduced by employing an yttrium iron garnet rod which has a line width of about 50 oersteds, rather than the Ferramic R-1 which has a line width of about 500 oersteds.

Isolator Experimental Results

An experimental isolator design was constructed having cross-sectional dimensions as shown in Fig. 5. In this case, the even- and odd-mode impedances are approximately $Z_{oe} = 148$ and $Z_{oo} = 90.4$ ohms. The input impedance at Port 1 in Fig. 2 is $2Z_{oe}Z_{oo}/(Z_{oe}+Z_{oo}) = 112.5$ ohms, while the input impedance at Port 2 is $Z_{oe}/2 = 74$ ohms. In order to match the 112.5-ohm impedance at

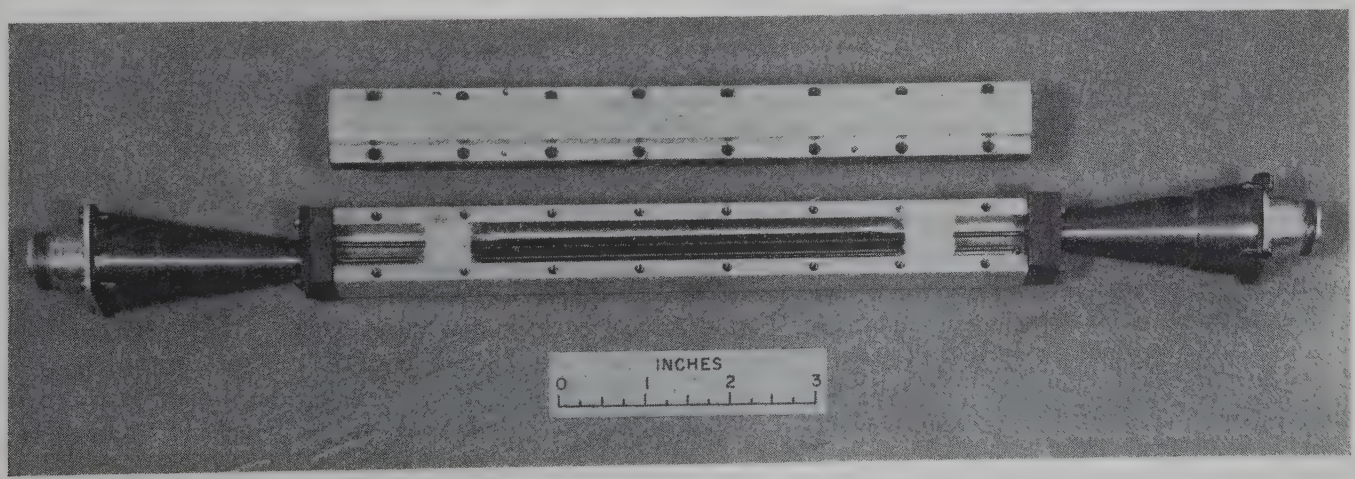

Fig. 3—Photograph of the wide-band gyrator.

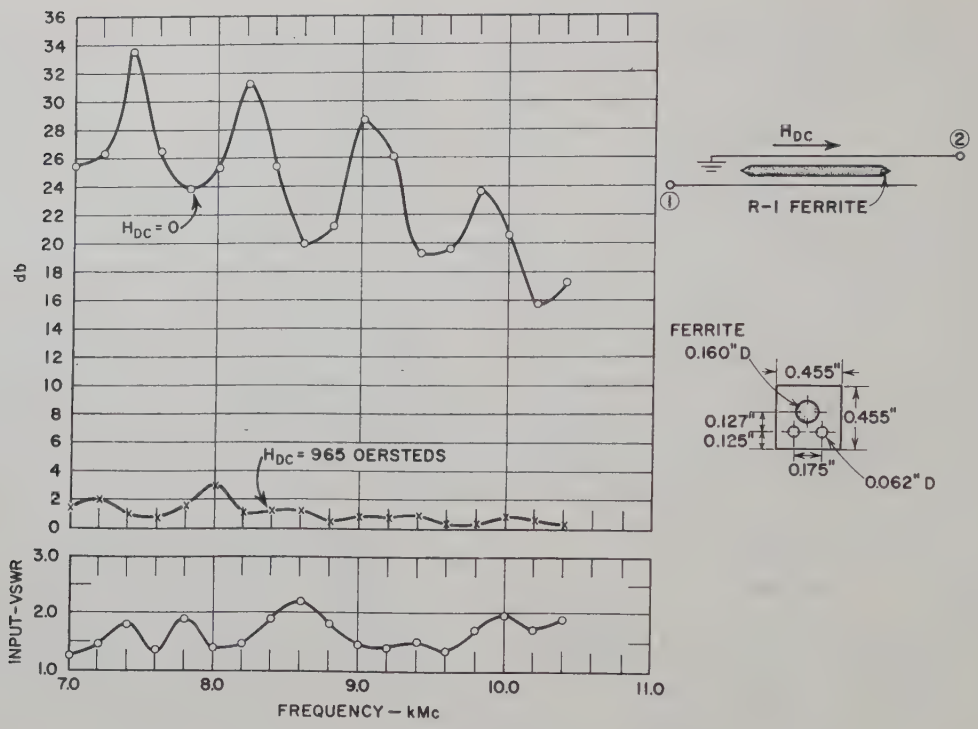

Fig. 4—Insertion loss of wide-band gyrator.

Port 1 to 50 ohms, a 2.4-inch taper section was used at that end. At Port 2, it was possible to achieve a good match by adjusting the position of the *Y*-junction with respect to the end wall, and by altering the diameter of the conductor between the junction and the end of the box. In order to test the VSWR of the transitions, long tapered sections of Polyiron were placed beside the conductors to act as terminations inside the box.

The isolator whose cross section is shown in Fig. 5 used a 0.147-inch diameter rod of Ferramic R-1 ferrite, 5.70 inches in over-all length, with each end tapered to a point in a distance of 1.2 inch. The ferrite rod was suspended within the outer shield by threads attached to metal pull rods and calibrated adjusting nuts so that it was possible to adjust the position of the ferrite rod while the isolator was in operation. Since the reverse loss is the most sensitive test of proper operation, the rod was positioned in such a way as to optimize the reverse loss characteristic. Because the thread system used for holding the rod was not very rigid, the rod position indicated in Fig. 5 can be regarded only as a close approximation.

The forward loss, shown in Fig. 5, of a signal traveling from Port 1 to Port 2, was measured with the biasing field oriented as shown in Fig. 2. The reverse loss was measured with the biasing field reversed. Within experimental error, the same result is obtained for the reverse loss with the biasing field oriented as shown in Fig. 2, but with the direction of propagation through the isolator reversed.

Fig. 5 shows that the device has high isolation; *i.e.*, reverse loss, over a considerable bandwidth. The forward loss is around 1.0 db over most of the band, with a few peaks reaching a maximum of 1.6 db. The VSWR at Port 1 and Port 2 was the same regardless of the *H*-field direction. The low VSWR at Port 2, which was observed for all biasing field strengths, is due to the fact that essentially all of the signal fed into Port 2 is absorbed either in the matched termination at Port 1 or in the matched internal termination. On the other hand, a low VSWR at Port 1 will only be obtained when the biasing field is adjusted to give the proper rotation. Therefore, it is believed that the relatively high VSWR observed at Port 1, when the isolator is adjusted for optimum reverse loss, indicates that the amount of "rotation" in the forward direction is different from that in the reverse direction, either because of reciprocal coupling or because of higher-order modes caused by the presence of the ferrite.

The data in Fig. 6 show the difference in decibels between the reverse and forward loss with the biasing field adjusted at each frequency to maximize the reverse loss. More biasing field is required at intermediate frequencies than at both the relatively low and the relatively high frequencies. At the lower frequencies it is possible that the proximity of ferromagnetic resonance diminishes the *H*-field required. The reduced biasing field required at the high frequencies may be due to increased concentration of energy in the ferrite rod.[7] It is probable that the rotation could be kept more constant with frequency for a given biasing field by introducing dielectric loading in the isolator box to draw away some of the energy from the ferrite rod at the higher frequencies.[7]

[7] E. A. Ohm, "Broad-band microwave circulator," IRE TRANS. ON MICROWAVE THEORY AND TECHNIQUES, vol. MTT-4, pp. 210–217; October, 1956.

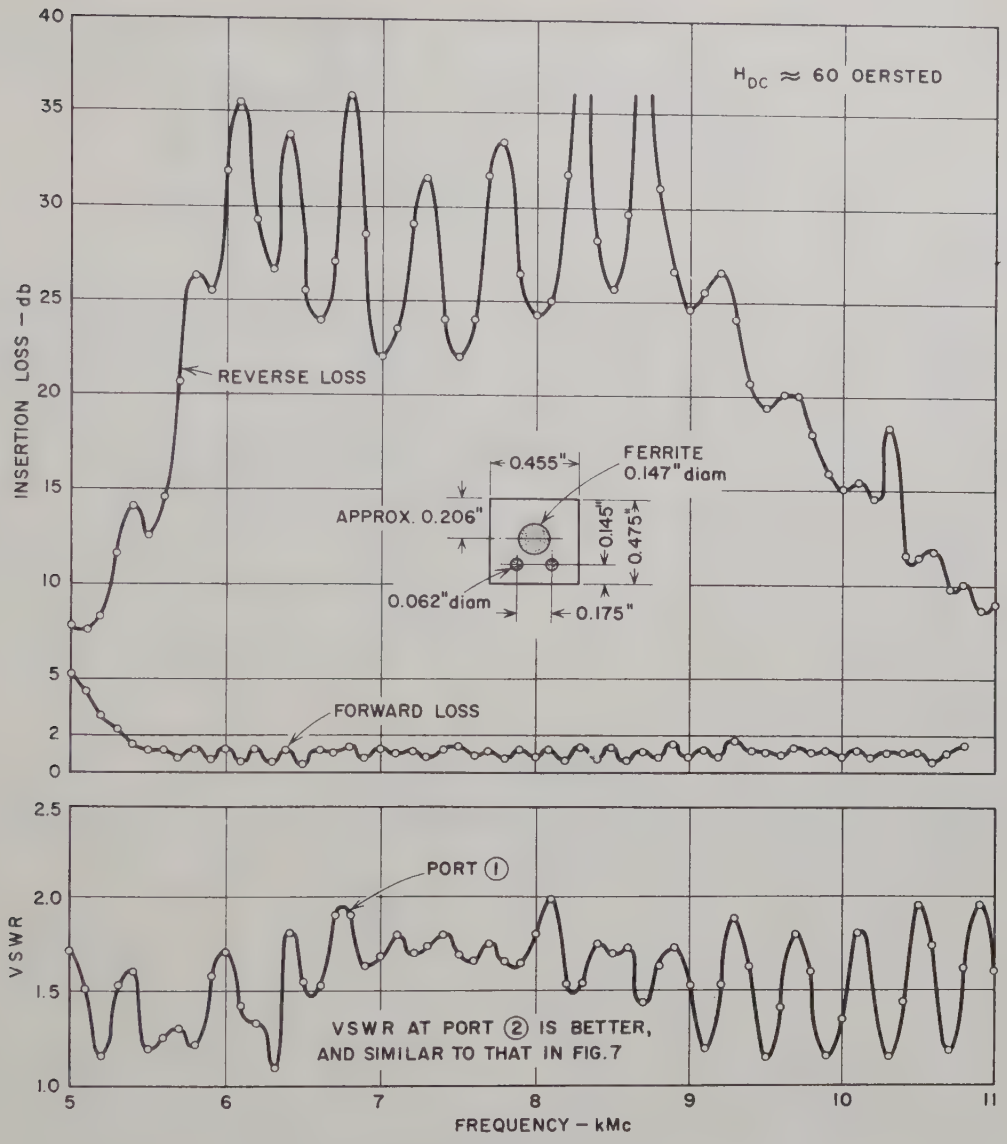

Fig. 5—Measured performance of a wide-band isolator using an R-1 ferrite rod 5.70 inches long with each end tapered to a point in a distance of 1.2 inches.

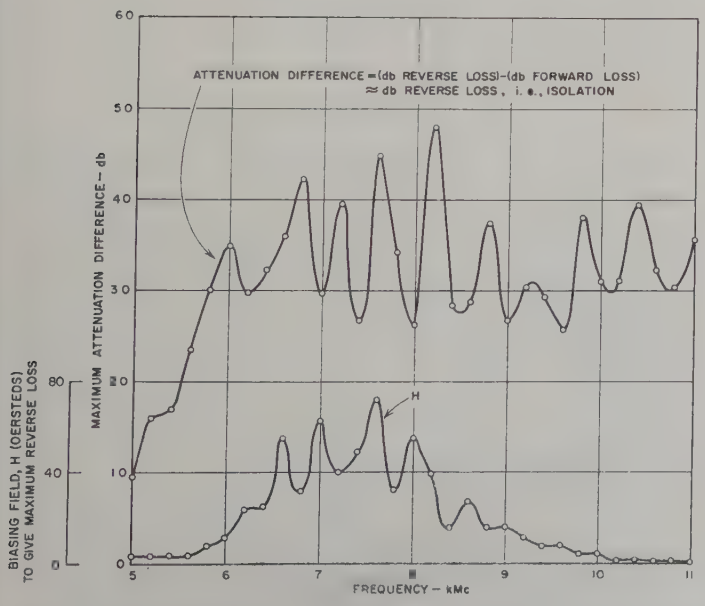

Fig. 6—Decibel difference between reverse and forward loss for the isolator in Fig. 5 when the biasing field is adjusted at each frequency to give the peak reverse loss.

The performance characteristics of an isolator using a smaller-diameter ferrite rod in an outer shield of reduced cross section appear in Fig. 7. The inserts used to reduce the outer shield cross section were tapered at the ends so as not to disturb the end impedance matches. The ferrite rod was Ferramic R-1, 0.100 inch in diameter, 6.00 inches in over-all length, with each end tapered to a point in a distance of 0.5 inch. The distance x in the cross section drawing in Fig. 7 was approximately 0.070 inch and was arrived at by adjusting for optimum reverse loss.

It is seen that the performance of this isolator is quite similar to that of the previously described isolator, except that the midband reverse loss is slightly lower. However, it is probable that the performance of this isolator could be improved by using a longer ferrite rod, since for frequencies beyond midband it was not possible to peak the reverse loss at a definite biasing field as was possible in the previous isolator. It was found possible to minimize the forward loss only at the lower frequencies, which again indicates that the rod was not long enough to give sufficient rotation at the higher frequen-

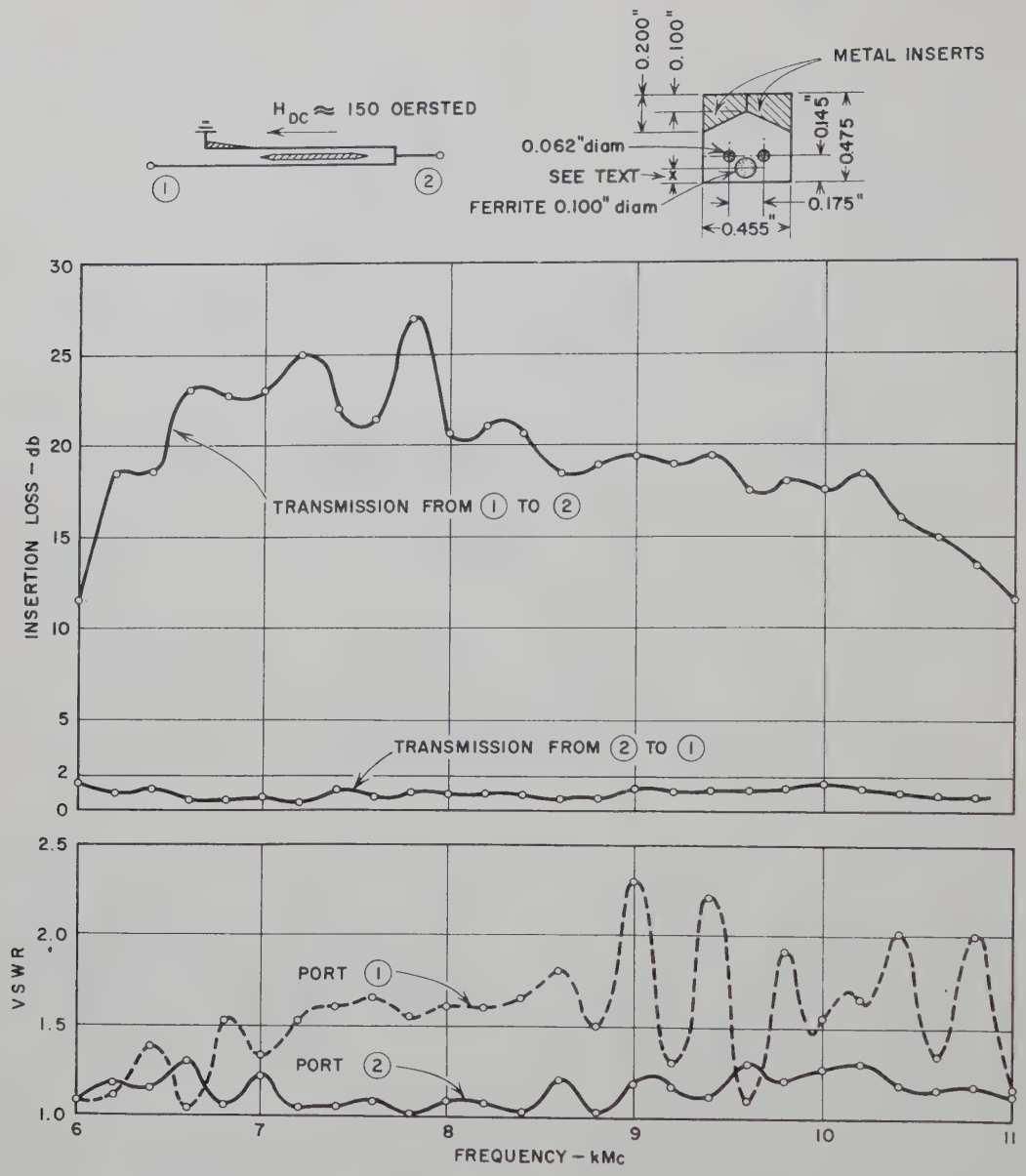

Fig. 7—Measured performance of a wide-band isolator using an R-1 ferrite rod 6 inches long with each end tapered to a point in a distance of 0.5 inch.

cies. At frequencies in the 7- to 8-kmc band, the optimum loss values ran around 0.5 db, or somewhat less, which agrees fairly well with the perturbation analysis and should be indicative of what optimum performance of the isolator would be. As seen from Fig. 7, the VSWR at Port 1 of the isolator is rather high, just as in the case of the previous isolator, while the VSWR at Port 2 is quite low. In this case, insertion loss data were taken for both directions of the *H*-field and for both directions of power flow. The differences in the measured data were quite small, although operation with the *H*-field, as shown, was slightly better in the forward loss characteristic.

Conclusion

The nonreciprocal TEM network described here can be used as a wide-band gyrator, isolator, switch, or modulator. The theoretical analysis of this network indicates that it should function over bandwidths even greater than an octave. Measurements on experimental versions of the network demonstrate that operation over almost an octave may be readily achieved in practice. If polycrystalline yttrium iron garnet is used in place of the R-1 ferrite, it is believed that low-loss operation can be achieved over even greater bandwidths.

High-Power Microwave Rejection Filters Using Higher-Order Modes*

JOSEPH H. VOGELMAN†

Summary—In order to obtain filters capable of handling very high power, the use of radial lines and uniform line discontinuities was investigated. Forty-five-degree tapers and uniform lines were used to design a high-power microwave filter capable of handling 700 kw at 15 pounds pressure in a 0.900 by 0.400 ID waveguide. In addition to the filtering which results from the discontinuities in the TE_{10} mode in the waveguide, high insertion loss elements are effected when the enlarged uniform line section is larger than the TE_{10} mode waveguide wavelength and when the length of the enlarged section is approximately $(2n-1)\lambda_g/4$. Extremely large insertion losses are possible by the cascading of these elements. Tuning, in the standard-size waveguide, has no effect on the insertion loss of the higher-mode enlarged waveguide at its resonant frequency. Empirical design formulas are evolved and the design procedure for band-rejection filters is given, using these high insertion loss elements.

Introduction

As the power of radar and communications transmitters increase and as their number continually becomes larger, the mutual interference between radars at the same site, or between radars and communications, reaches critical proportions. To eliminate the large power at spurious frequencies which are far removed from the assigned operating frequency band, it is essential to provide adequate filtering at high power on the transmission lines between the transmitters and the antennas. As an outgrowth of work done on high-power filters using radial transmission lines in combination with enlarged uniform transmission lines, it was found that the higher-order mode in the enlarged line would provide a useful high insertion loss element, which in combination with the filtering effect of the discontinuities in the fundamental TE_{10} mode, would provide a solution to the high-power microwave filtering problem. The basic filter section consists of a waveguide of rectangular cross section whose narrow dimension is expanded through a taper and then contracted through another taper to its original dimensions. The two tapers are separated by a length of an enlarged uniform line. The basic filter section (see Fig. 1) and its reactive characteristics have been described in a previous paper.[1] In this paper, this technique is extended to the case where higher-order modes can propagate in the enlarged uniform line in the filter section.

* Manuscript received by the PGMTT, May 13, 1959; revised manuscript received, June 19, 1959.

† Dynamic Electronics, Inc., Richmond Hill, N. Y. Formerly at Rome Air Development Center, Griffiss Air Force Base, N. Y.

[1] J. H. Vogelman, "High-power microwave filters," IRE TRANS. ON MICROWAVE THEORY AND TECHNIQUES, vol. MTT-6, pp. 429–439; October, 1958.

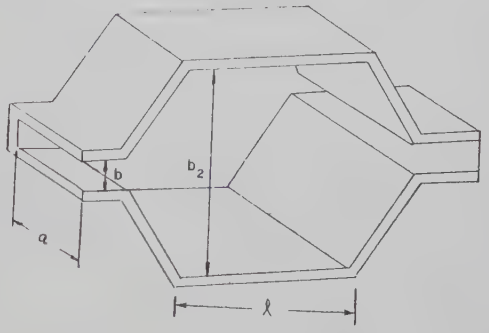

Fig. 1—Typical filter section with one side wall removed.

The High Insertion Loss Section

In filter sections (see Fig. 1) with enlarged center sections of a size where the height is greater than the waveguide wavelength in the standard TE_{10} mode waveguide, frequencies can be found where the insertion loss rises sharply to values in excess of 35 to 45 db for a single section. This has been experimentally investigated in an attempt to specify the conditions for its occurrence, in order to permit its use in the design of rejection filters. Experimental examinations of a large number of combinations of tapers to enlarged guides and corresponding abrupt steps to the same size guide produced a quantity of empirical data from which the following conclusions could be drawn.

1) The presence of the tapers contributed to the excitation of the higher-order modes which are necessary for the existence of the high insertion losses in the single section.

2) Of the modes capable of propagating in the enlarged waveguide (TE_{10}, TE_{11}, TE_{12}, TE_{01}, TE_{02}, TM_{11}, and TM_{12}), only the TE_{12} and TM_{12} modes can be considered as contributing to this resonant insertion loss.

3) Though the evidence is not conclusive, it is quite likely that it is the TE_{12} mode in which the high insertion loss elements operate.

4) The high insertion loss resonances show a relatively high Q (narrow bandwidth).

5) Discontinuities, or tuning in the standard waveguide on either the load or generator side of the filter section, do not affect the frequency of the high insertion loss and only produce minor changes in the value of the insertion loss itself.

6) The assumption of the TE_{12} mode in the enlarged waveguide permits the establishment of empirical design criteria leading to practical high insertion loss filters.

The Resonance Phenomena

A waveguide two-port structure is described in which each of the modes TE_{10}, TE_{12}, etc., form independent waveguide two-port structures coupled by ideal transformers at input and output ports to the main propagating mode line. One of the two-port structures carries the TE_{10} mode and can be treated as in Vogelman[1] except near the high insertion loss frequencies. When the TE_{12} mode becomes resonant, it extracts essentially all of the RF power from the fundamental mode-transmission line. For the TE_{12} mode, the enlarged waveguide section is terminated by a waveguide beyond cutoff at each end. Since neither the TE_{12} mode nor its related radial mode will propagate towards the standard waveguide for any distance, the energy coupled into this resonant cavity is dissipated in the metallic walls at resonance, producing a high insertion loss at that frequency. This concept was checked by the following experiment. A signal at resonance (*i.e.*, high insertion loss frequency) was fed through a slotted line in series with a directional coupler, a slide screw tuner, the filter, another directional coupler and a matched load. The magnitude of the insertion loss was measured with the slide screw tuner effectively out of the circuit. The VSWR was measured with the slotter line and the slide screw tuner adjusted to produce a VSWR of less than 1.05. The insertion loss was measured again. Without the tuner, the VSWR's that were measured were in the order of 5, or less, with insertion losses of >40 db. When the VSWR was reduced to less than 1.05, the insertion-loss measurement showed only a decrease of less than 1.5 db in all cases. This is the effect which is expected when a dissipative element is inserted in a transmission line. This experiment lends credence to the conclusion that the filter element at resonance in the TE_{12} mode is not reciprocal insofar as its mode-transformation properties are concerned; *i.e.*, it readily transforms TE_{10} power to the TE_{12} mode, but does not transform TE_{12} power back to the TE_{10} mode to any appreciable extent. In the case of multiple modes, the normal inductive or capacitive coupling of a resonant circuit to a transmission line cannot be used to describe the performance. A theoretical analysis of the equivalent circuit of the discontinuities between the enlarged uniform line and the radial line at each end and the reactance caused by the waveguide beyond cutoff radial lines was atttempted without success insofar as producing a relatively exact treatment of the high insertion loss phenomena was concerned. However, the analysis leads to the following qualitative conclusions.

1) The resonant length of the enlarged uniform line is reduced from one-half waveguide wavelength by the reactances of the discontinuities and the waveguide beyond cutoff at each end of the uniform line.

2) For short enlarged uniform lines, the interaction between the discontinuities at each end further shortens the required line length for resonance.

3) The section will resonate even when the line length of the enlarged uniform guide is reduced to zero because of the presence of the discontinuity reactances and the waveguides beyond cutoff.

Since an analytic solution was not possible, design formulas were empirically derived from the data experimentally obtained for enlarged waveguide sections.

General Design Considerations

A large number of filter sections, consisting of 45° tapers at the ends of an enlarged line, were constructed and tested to obtain empirical relations between the high insertion loss frequency and the dimensions of the cavity section. From the resultant data, the following empirical relationships were obtained.

1) The measured high insertion loss frequency occurs within one per cent of the value computed for a uniform enlarged waveguide length equal to a quarter wavelength for the TE_{12} mode, provided that this length is greater than one-half the cutoff wavelength.

2) When the enlarged waveguide length is reduced to zero, the high insertion resonance frequency is within three per cent, if the resonance is computed on the assumption that an equivalent length equal to the waveguide height is divided by $2\sqrt{2}$.

3) Linear interpolation can be used to compute the TE_{12} resonant wavelength for cavity length between zero and $\lambda_c/2$. This gives results which are within three per cent for lengths much shorter than $\lambda_c/2$ and closer to one per cent as the length approaches $\lambda_c/2$.

4) The Q of the TE_{12} resonance defined in terms of the bandwidth of the points 3 db down from the maximum insertion loss, is a function of the ratio of the TE_{12} resonant frequency to the cutoff frequency for that mode. Typical values of Q as determined in accordance with the preceding definition are as follows:

a) four to five thousand within one to two per cent of the cutoff frequency with a corresponding frequency-to-width ratio at 20-db insertion loss of approximately 200 to 300;

b) two thousand to twenty-five hundred within five to six per cent of the cutoff frequency with a corresponding frequency-to-width ratio at 20-db insertion loss of approximately 75 to 150;

c) four to five hundred for frequencies within twelve to thirteen per cent of the cutoff frequency with ratio at 20-db insertion loss of approximately 50 to 75;

d) two hundred and fifty to three hundred when the length of the enlarged line is reduced to zero, corresponding to a frequency-to-width ratio at 20-db insertion loss of 30 to 50;

e) the second-, third- and higher-order insertion-loss frequencies have correspondingly lower Qs.

Design Formulas

Fig. 1 shows the dimensions to be used in computing the resonant frequency of a high insertion loss filter section: l is the length of the enlarged section; a is the width of both the standard waveguide and the enlarged waveguide; b is the height of the standard waveguide, and b_2 is the height of the enlarged waveguide.

The notation λ_g and λ_c will refer to the waveguide wavelength and the cutoff wavelength of the enlarged uniform waveguide for the TE_{12} mode. The cutoff wavelength for the TE_{12} mode for a waveguide of width a and height b_2 is given by the formula[2]

$$\lambda_{c_{12}} = \frac{2a}{\sqrt{1 + (2a/b_2)^2}}. \tag{1}$$

Note: This mode cutoff occurs when the waveguide wavelength in the TE_{10} mode is equal to the height b_2.

The waveguide wavelength is obtained from the cutoff wavelength from the relationship

$$\lambda_g = \frac{\lambda}{\sqrt{1 - (\lambda/\lambda_{cnm})^2}} \tag{2}$$

which, for the TE_{12} mode, reduced to

$$\lambda_g = \frac{1}{\sqrt{1/\lambda^2 - 1/4a^2 - 1/b_2^2}} \tag{3}$$

for l_1 larger than $(2n-1)\lambda_c/2$ where n is the number of the resonance counting the resonances from lowest to higher frequencies. The required resonant dimension can be obtained from the resonant wavelength by the following relationship:

$$l_1 = (2n - 1)\lambda_g/4 \tag{4}$$

which combines with (3) to give

$$l_1 = \frac{2n - 1}{\sqrt{1/\lambda^2 - 1/4a^2 - 1/b_2^2}}. \tag{5}$$

Conversely, the resonant free-space wavelength is given in terms of the length, width and height by the following relationship:

$$\lambda_l = \frac{1}{\sqrt{\left(\frac{2n-1}{4l_1}\right)^2 + 1/4a^2 + 1/b_2^2}}. \tag{6}$$

Substituting

$$l_1 = (2n - 1)\lambda_{c_{12}}/2 \tag{7}$$

in (6) we obtain the criteria for the validity of (6); *i.e.*, that the TE_{12} resonant wavelength λ is smaller than λ_{lc} where λ_{lc} is given by

$$\lambda_{lc} = \frac{0.894427}{\sqrt{1/4a^2 + 1/b_2^2}}. \tag{8}$$

[2] N. Marcuvitz, "Waveguide Handbook," Mass. Inst. Tech. Rad. Lab. Ser., McGraw-Hill Book Co., Inc., New York, N. Y., p. 88; 1951.

The TE_{12} resonant wavelength for l_1 equal to zero is found to be

$$\lambda_{l_0} = \frac{1}{\sqrt{3/2b_2^2 + 1/4a_2^2}}. \tag{9}$$

If values of l_1 between zero and $\lambda_c/2$ are used, the resonance can be found by linear interpolation between the values obtained from (6) and (8) or from the relationship

$$\lambda_r = \sqrt{3.2}l_1\left(1 - \frac{\lambda_{l_0}}{\lambda_{lc}}\right) + \lambda_{l_0}. \tag{10}$$

For the second, third and subsequent resonances where the length of the enlarged section l_1 is less than $(2n-1)\lambda_c/2$ for the TE_{12} mode, the high insertion loss wavelength is obtained from

$$\lambda_r = \lambda_l + \left[1 - \frac{\lambda_l}{\lambda_{lc}}\right]\frac{\sqrt{3.2}l_1}{(2n - 1)}, \tag{11}$$

where λ_l is the value computed from (6). Eqs. (10) and (11) will give values of the high insertion loss wavelength to an accuracy of three per cent for the second, third and fourth TE_{12} resonance, provided that a/λ is greater than 1 or appropriate steps have been taken to suppress the TE_{20} mode in the standard-size waveguide.

Filter Design Procedure

A band-rejection filter using high insertion loss sections is specified in terms of the upper and lower cutoff frequencies of the pass band, the lowest high insertion loss frequency, and the minimum acceptable highest frequency of the attenuation band. The following symbols will be used.

- λ_a is the wavelength corresponding to the lower cutoff frequency of the pass band.
- λ_b is the wavelength corresponding to the upper cutoff frequency of the pass band.
- λ_{m_n} is the lowest frequency for the $(2n-1)\lambda_g/4$ resonance.
- λ_{M_n} is the highest frequency for the $(2n-1)\lambda_g/4$ resonance.

The procedure for designing a band-rejection filter consists of selecting a series of filter sections of the high insertion loss type such that the frequencies over which they reject form in combination a continuous frequency band of the desired width. The rejection bandwidth is divided into several parts, the lowest frequency part being covered by the filters operating in the first resonance, that is, in the $\lambda_g/4$ condition. The second band, which is continuous with the first, consists of the same filters operating in the $3\lambda_g/4$ mode and so forth. The first step in the design procedure is to select λ_{M_1}, the wavelength corresponding to the highest frequency of the rejection section in the $\lambda_g/4$ mode. If this value is

selected to be equal in wavelength to that resulting from the application of (8), the simplest design procedure results. The criteria for selection of λ_{M_1} (derived in Appendix I) are

$$0.894427\lambda_{m_1} \leq \lambda_{M_1} \leq 0.906765\lambda_{m_1}, \tag{12}$$

where λ_{m_1} is wavelength of lowest attenuation frequency. Normally, λ_{M_1} is selected close to the upper limit in order to produce individual sections of maximum rejection bandwidth. By manipulation of (8), we obtain the relationship for determining the height of the enlarged waveguide to be used in the filter design.

$$b_2 = \frac{1}{\sqrt{\dfrac{0.8}{\lambda_{M_1}} - \dfrac{1}{4a^2}}} \cdot \tag{13}$$

The length of the section l_1 corresponding to the wavelength λ_{M_1} is found from (5) and (13) to be

$$l_{M_1} = \frac{\lambda_{M_1}}{\sqrt{3.2}} \cdot \tag{14}$$

The length of the enlarged waveguide in the filter section for the lowest attenuation frequency is given by the relationship

$$l_{m_1} = \frac{1}{4\sqrt{\dfrac{1}{\lambda_{m_1}^2} - \dfrac{0.8}{\lambda_{M_1}^2}}} \cdot \tag{15}$$

Selection of λ_{M_1}, in accordance with the criteria of (12), insures that the resonances of the first, second, third, etc., type will overlap and form a continuous attenuation band provided that sufficient sections of lengths between l_{M_1} and l_{m_1} are incorporated to insure adequate attenuation over the band from λ_{m_1} to λ_{M_1}. Between 10 and 24 sections have been found to be adequate for filling the band between these two extremes. The exact number is dependent on the ripple in the attenuation curve which can be tolerated. As a first approximation, linear interpolation of the lengths between the two extremes has been found to be completely adequate if an adequate overlap is provided to account for tolerances. Alternately, sections spaced 0.5 to 1 per cent apart can be separately computed between λ_{m_1} and λ_{M_1}. The spacing between the high insertion-loss sections is computed from TE_{10} mode characteristics of the sections by the methods given by Vogelman.[1] This consists of computing quarter waveguide wavelength sections at the center frequency of the pass band between the equivalent steps corresponding to each of the high insertion loss sections. The resultant reflection loss at λ_a and λ_b is computed by the same method. If the insertion losses at the extremes of the pass band are too high, lengths of different values can be used to decrease these values at the expense of an increased insertion loss at the center frequency.

Filter Performance

Filters designed by the method described have been constructed and measured. Fig. 2 is an example of the filter performance when too few sections are selected.

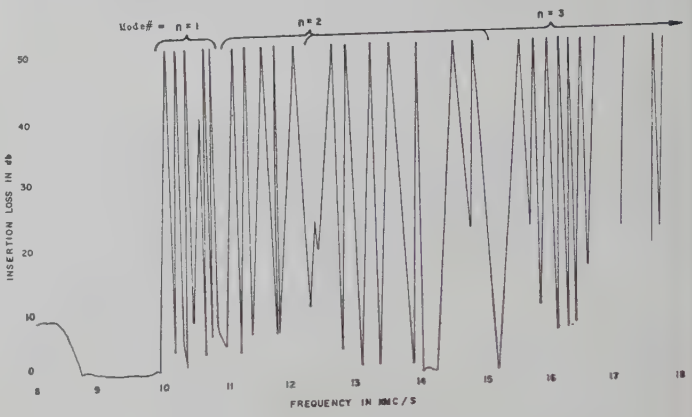

Fig. 2—Insertion loss performance of six-section filter.

The original calculations were intended to cover the band from 10,000 to 11,000 mc in 0.900×0.400 ID waveguide. The differences can be directly attributed to the mechanical tolerances and the 1 per cent accuracy of the equations. The 20-db insertion loss bandwidth of any section is between 75 and 100 mc for the lowest resonance mode ($n=1$). Dissymmetries in a section (as seen for section 4) result in a reduction of the peak attenuation of the section. For the higher resonance modes the dissymmetries are more pronounced and show themselves as splittings of the absorption curves and extraneous resonance peaks. When seven more sections were added to this filter, resonant at intermediate frequencies in the band between 10,000 and 11,000 mc, the depth of the nulls in the lowest resonance mode was never less than 10 db, and for frequencies above 12,000 mc, never less than 25 db. When the total number of sections was increased to 20, the attenuation at all frequencies from 10,000 to beyond 18,000 mc was greater than 40 db (Figs. 3 and 4). This filter was subjected to high power, with and without pressurization in the pass band at 9450 ± 50 mc with the following results.

No pressure: intermittent arcing at 350 kw.
15-pound pressure: no arcing at over 700 kw.

A single section was tested at its high insertion loss frequency at a power level of 50 kw. This is in excess of the reflected power that would cause magnetron breakdown. No breakdown in the filter occurred. Since this value is much higher than the spurious output of useable transmitter tubes, no further testing was considered necessary.

Conclusions

The procedure for designing high-power microwave rejection filters using higher-order modes has been described. These filters appear most promising as an aid in

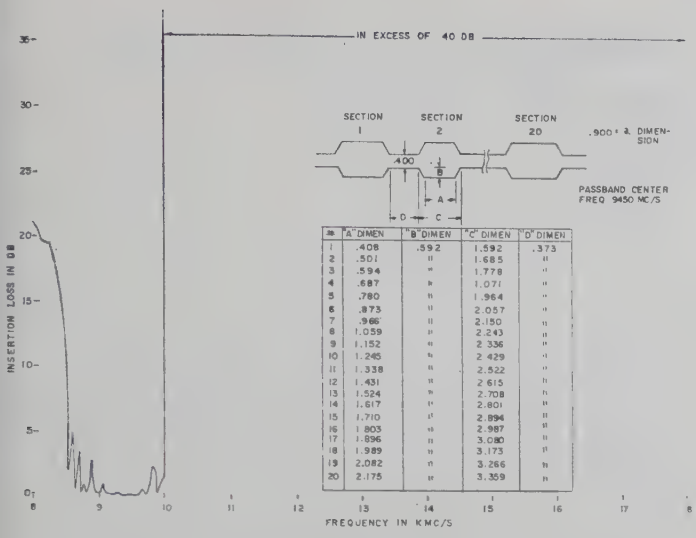

No.	A DIMEN	B DIMEN	C DIMEN	D DIMEN
1	.408	.592	1.592	.373
2	.501	"	1.685	"
3	.594	"	1.778	"
4	.687	"	1.871	"
5	.780	"	1.964	"
6	.873	"	2.057	"
7	.966	"	2.150	"
8	1.059	"	2.243	"
9	1.152	"	2.336	"
10	1.245	"	2.429	"
11	1.338	"	2.522	"
12	1.431	"	2.615	"
13	1.524	"	2.708	"
14	1.617	"	2.801	"
15	1.710	"	2.894	"
16	1.803	"	2.987	"
17	1.896	"	3.080	"
18	1.989	"	3.173	"
19	2.082	"	3.266	"
20	2.175	"	3.359	"

Fig. 3—Dimension and insertion loss performance of 20-section filter.

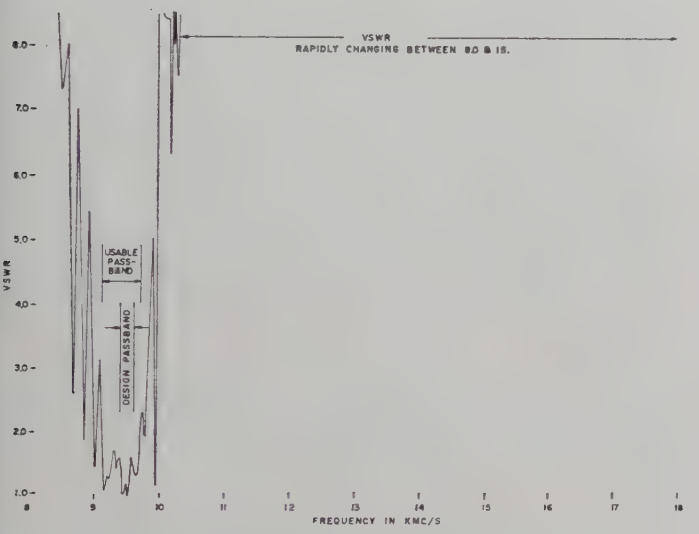

Fig. 4—VSWR performance of 20-section filter.

solving the major problems of radar-to-radar and radar-to-communications interference. In particular, the high insertion loss elements offer great promise in reducing the narrow-band spurious responses from radar magnetrons, since the elements can easily be cascaded to give insertion losses at particular frequencies of over 100 db and since the addition of matching structures for the pass band has no effect on the high insertion loss element. It has been found that cascading of filters designed in the manner indicated can give insertion losses as high as 120 db over a bandwidth of 40 per cent of the operating frequency. The power capability at frequencies in the pass band has proven to be equal to that encountered in normal waveguides with the usual quantity of joints and bends. This type of filter, though designed specifically for the high-power use, will find application in the low-power field where high insertion loss is required.

Appendix I

For a real solution, the value under the radical of (15) establishes the requirement that

$$\lambda_{M_1} \geq \lambda_{m_1}\sqrt{0.8}. \tag{16}$$

For the general case, for a continuous rejection band without holes

$$\lambda_{m_n} \geq \lambda_{M_{n-1}}; \qquad n \geq 2. \tag{17}$$

From (6) and (15),

$$\lambda_{m_n} = \frac{1}{\sqrt{\left(\frac{2n-1)^2}{4l_{m_1}}\right)^2 + \frac{0.8}{\lambda_{M_1}^2}}}$$

$$= \frac{1}{\sqrt{\left(\frac{2n-1}{\lambda_{m_1}^2}\right)^2 - 0.8(2n-1)^2 - 0.8}}. \tag{18}$$

From (6) and (14),

$$\lambda_{M_{n-1}} = \frac{1}{\sqrt{\left(\frac{2n-3}{4l_{M_1}}\right)^2 + \frac{0.8}{\lambda_{M_1}^2}}}$$

$$= \frac{\lambda_{M_1}}{\sqrt{0.2(2n-3)^2 + 0.8}}. \tag{19}$$

If (16) is to hold, then substituting (18) and (19) in (16),

$$\frac{1}{\frac{(2n-1)^2}{\lambda_{m_1}^2} - \frac{0.8(2n-1)^2 - 0.8}{\lambda_{M_1}^2}} \geq \frac{\lambda_{M_1}^2}{(0.2(2n-3)^2 + 0.8)}, \tag{20}$$

$$\frac{0.2(2n-3)^2 + 0.8(2n-1)^2}{(2n-1)^2}\ \lambda_{m_1} \geq \lambda_{M_1}, \tag{21}$$

$$\lambda_{M_n} \leq \sqrt{0.2\left(\frac{2n-3}{2n-1}\right)^2 + 0.8}\,\lambda_{m_1}; \quad n \geq 2. \tag{22}$$

The maximum restriction occurs when $2n-3/2n-1$ is a minimum; *i.e.*, when $n=2$.

Thus

$$\lambda_{M_1} \leq \sqrt{0.8222\cdots}\,\lambda_{m_1} \tag{23}$$

which proves (12).

A Method for Accurate Design of a Broad-Band Multibranch Waveguide Coupler*

K. G. PATTERSON†

Summary—A new approach is made to the problem of tapering the branch impedances for broad-band performance. A taper is proposed, which, for a 3-db branch coupler, is shown to give much better results in theory and practice than the currently used binomial taper.

Also, simple expressions are developed which enable the effects of waveguide junction discontinuities to be adequately corrected, thus allowing a greater accuracy in design to be achieved than was hitherto possible.

List of Symbols

λg_0 = Guide wavelength at the midband frequency.
f_0 = Midband frequency of a coupler.
A_k = Normalized voltage vector ($k=1$, 2, 3 or 4).
Γ = Reflection coefficient.
T = Transmission coefficient.
Z_n = nth branch guide impedance.
Z_n' = Corrected nth branch guide impedance.
$z_n = Z_n/Z_0$, where Z_0 = main guide impedance.
$z_n' = Z_n'/Z_0$.
$y_n = 1/z_n$.
g_n = nth element of normalized prototype network in farads or henries with respect to unity impedance level.
ρ, σ = Constants.
N = Total number of branches.
A, B, C, D = Matrix parameters.
j = Complex operator.
a = Broad dimension of all guides.
b_0 = Narrow dimension of main and auxiliary guides.
b_n = Narrow dimension of nth branch guide.
jB = Equivalent susceptance.
m^2 = Ideal transformer impedance ratio.
θ = Electrical line length in radians.
d_n, l_n = Displacement of reference planes.
L_n = Physical length of a branch guide.
D_{np} = Spacing between branch guide centers ($p = n \pm 1$).
λ = Free-space wavelength at a frequency f.
f = Frequency.
$\omega = 2\pi f$.
$\omega_0 = 2\pi f_0$.

* Original manuscript received by the PGMTT, March 27, 1959; revised manuscript received, June 22, 1959.
† Communication from the Staff of the Research Laboratories of the General Electric Co., Ltd., Wembly, England.

Introduction

SINCE 1945, a considerable number of papers have been written on the subject of directional couplers, notably by Riblet [1], Mumford [2], and Lippmann [3]; much of the theory presented therein is applicable to multi-element couplers employing branch lines or guides as coupling elements. These authors, however, were principally concerned with methods of analysis of the general multi-element coupler with ideal coupling elements; when practical design information on branch couplers is required, the engineer usually turns to the report by Harrison [5].

The section of Harrison's report [5] which deals with branch couplers is based on a report by Lippmann [4] which is not generally available, and which is restricted in its scope. The essential problem of optimum taper of branch impedances is given scant consideration, and the problem of correction for the discontinuity effects at the T-junctions is not accurately treated except for certain waveguide sizes where Lippmann's results [4] are quoted.

This paper is concerned with these two problems and is intended to fill in the gaps in the present design techniques with the presentation of some simple and generally applicable design equations.

Taper of Branch Impedances

The branch waveguide coupler comprises a main guide coupled to an auxiliary guide of equal size by a number of branch guides (Fig. 1). The branch guides are usually series-connected by T-junctions to the main and auxiliary guides; their narrow dimension may be varied

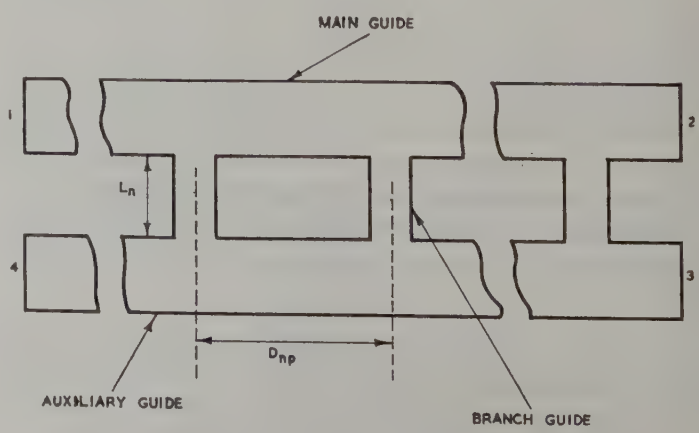

Fig. 1—Multibranch waveguide coupler, cross section.

according to the taper and coupling required; their broad dimension is made equal to that of the main and auxiliary guides. If the T-junctions are ideal; *i.e.*, there are no waveguide discontinuity effects, the length of a branch guide will be $\lambda g_0/4$, and the spacing between the corresponding points of adjacent guides will be $\lambda g/4$ at the midband or design frequency. When the ratio of input power to power coupled to the auxiliary guide is 3 db, such a coupler has all the properties of a hybrid junction.

There is a plane of symmetry between the main and auxiliary guides which bisects the branch guides transversely. Hence this type of coupler can be fully analyzed by the mode superposition method employed by Reed and Wheeler [7] and Young [8]. The substance of this method is that two related two-port circuits are derived from the coupler by first placing a magnetic and then an electric wall in the above mentioned plane of symmetry. One two-port circuit comprises a number of open-circuit stubs, and the other a number of short-circuit stubs, connected to the main or auxiliary guides (Fig. 2). At the midband frequency, these branch stubs will be $\lambda g_0/8$ long and spaced by $\lambda g_0/4$ between center lines. The performance of the coupler can now be expressed in terms of the properties of these derived two-port circuits. If the input to port 1 of the coupler is a voltage vector of unit amplitude, the emergent voltage vectors from the four ports of the coupler with each port properly matched are given by:

$$A_1 = \tfrac{1}{2}[\Gamma_- + \Gamma_+], \tag{1}$$

$$A_2 = \tfrac{1}{2}[T_- + T_+], \tag{2}$$

$$A_3 = \tfrac{1}{2}[T_- - T_+], \tag{3}$$

$$A_4 = \tfrac{1}{2}[\Gamma_- - \Gamma_+], \tag{4}$$

where the suffix $-$ refers to the short-circuit stub circuit, and the suffix $+$ refers to the open-circuit stub circuit.

Thus far, the development follows that of Reed and Wheeler [7]. At this point, the argument leading to the selection of a suitable taper can be taken up.

Each two-port circuit can be replaced by an equivalent network of lumped elements. The $\lambda g_0/8$ stubs can be simulated by the appropriate capacitance or inductance over small percentage bandwidths, as shown in the Appendix. The $\lambda g_0/4$ lengths between stubs act as impedance inverters; for simplification these will be assumed invariant with frequency. (This assumption is discussed later.) Hence the lumped networks of Fig. 3(a) and 3(b) are obtained, which are equivalent to the two-port circuits of Fig. 2(a) and 2(b) respectively, for N odd. An additional shunt element would be required for Fig. 3(a) and 3(b) for N even.

The networks of Fig. 3(a) and 3(b) are, respectively, high-pass and low-pass ladder networks. The elements of each network may be tapered according to well-known network theory [10] by the same proportionality, so that the insertion loss characteristic of each network is monotonic; *i.e.*, may be represented by a function of the form $1+x^{2N}$, where x is a frequency variable. Then, for small values of insertion loss, the magnitude of the input reflection coefficient will approximate closely to a monotonic characteristic of the form x^N. Thus for the low-pass network, $|\Gamma_-| \propto \omega'^N$, where ω' is given by (47), and for the high-pass network, $|\Gamma_+| \propto 1/\omega'^N$. The values of Γ_- and Γ_+ at f_0 for the networks equivalent to the coupler with branch impedance values given by (26) can be calculated from (14) and (21) to (23). They are

$$(\Gamma_-)_{f_0} = 0.0006(1 + j1)$$

$$(\Gamma_+)_{f_0} = 0.0006(1 - j1). \tag{5}$$

The criterion of coupler performance to be studied here is the directivity, which may be expressed as $|A_3/A_4|$. $|A_3|$ varies by <10 per cent over the 25 per cent frequency band of interest. This variation will not significantly affect the directivity. A_4 is given by (4) as the vector difference of Γ_- and Γ_+. Therefore:

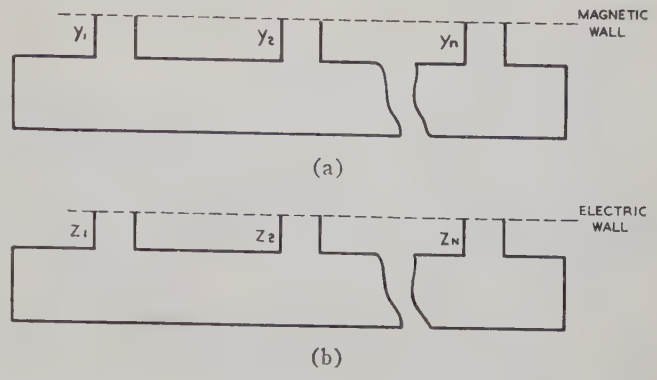

Fig. 2—Derived two-port circuits, cross sections.

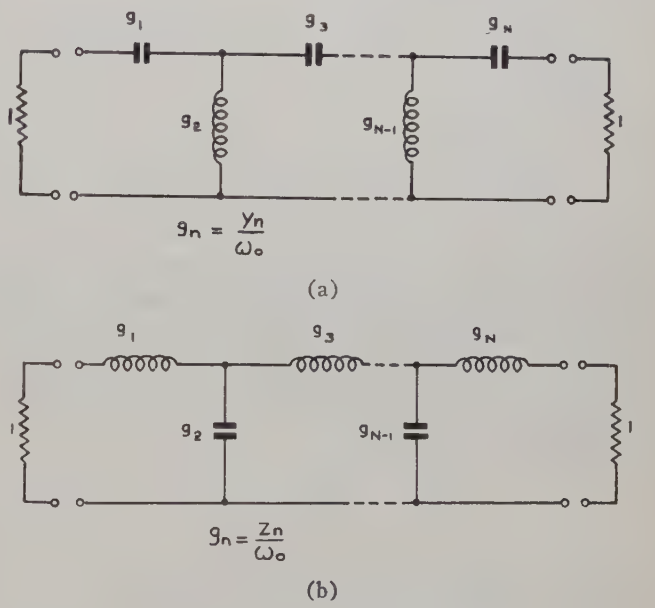

Fig. 3—Lumped element equivalent circuits.

$$|A_4| \geq \tfrac{1}{2}(|\Gamma_-| + |\Gamma_+|). \tag{6}$$

$|\Gamma_-|$ and $|\Gamma_+|$ can be written as:

$$|\Gamma_-| = |\Gamma_-|_{f_0}\left(\frac{\omega'}{\omega_0}\right)^N; \quad |\Gamma_+| = |\Gamma_+|_{f_0}\left(\frac{\omega_0}{\omega'}\right)^n, \tag{7}$$

where $|\Gamma_-|_{f_0} = |\Gamma_+|_{f_0} = 0.00085$, and $N = 5$.

Hence, (6) may be written as

$$|A_4| \leq 0.00042\left[\left(\frac{\omega'}{\omega_0}\right)^N + \left(\frac{\omega_0}{\omega'}\right)^N\right]. \tag{8}$$

For

$$\frac{f - f_0}{f_0} = 0.05, \qquad \frac{\omega'}{\omega_0} = 1.16, \qquad |A_4| \leq 0.0011$$

and directivity

$$\left|\frac{A_3}{A_4}\right| \geq 56 \text{ db for } \left|\frac{f - f_0}{f_0}\right| \leq 0.05.$$

These figures suggest that the so-called "maximally flat" taper when applied to 3-db branch couplers should give good results over the small frequency range for which the approximations are valid.

This taper is given by well-known network theory for the high-pass ladder network of Fig. 3(a), as

$$\frac{1}{g_n} = \rho \sin (2n - 1)\frac{\pi}{2N}, \tag{9}$$

and for the low-pass ladder network of Fig. 3(b), as

$$g_n = \rho \sin (2n - 1)\frac{\pi}{2N}, \tag{10}$$

where ρ is a constant determined by the equivalence of the lumped element networks to the waveguide circuits of Fig. 2. From either (9) or (10), the taper of branch impedances of the coupler is given by

$$Z_n = \sigma \sin (2n - 1)\frac{\pi}{2N}, \tag{11}$$

where σ is a constant determined by the coupling ratio of the branch coupler.

The main restriction to this argument lies in the assumption that the $\lambda g_0/4$ lengths between branches are frequency invariant. The results obtained, however, using the sine taper of (11) for 3-db couplers, suggest that the approximations here are not worse than those made by classical binomial theory [12] of weak coupling and frequency invariant coupling elements. However, it is not expected that the approximations made in the foregoing analysis should be valid outside the range

$$\left|\frac{\lambda g - \lambda g_0}{\lambda g_0}\right| < 0.1,$$

and it must be presumed that the wide useful range of

$$\left|\frac{\lambda g - \lambda g_0}{\lambda g_0}\right| < 0.2$$

obtained in the present instance with a sine taper is due to extra compensating effects not yet explained.

The theoretical characteristics of Figs. 4–6 were calculated with the aid of an electronic computer, following Reed and Wheeler's [7] method of analysis. Once the branch sizes are known—the analysis is straightforward, and there is no necessity to assume that branch length or branch spacing are frequency invariant. There is therefore no restriction in the theoretical calculations on that score, but the assumption is made that the T-junctions are ideal; *i.e.*, without reactive discontinuities. However, as is shown in the succeeding sections of this paper, the effects of these discontinuities can be largely corrected in a practical design, so that measured characteristics should agree fairly well with the theoretical ones. The measured characteristics shown in Fig. 4 are of a 3-db coupler designed by the methods of this paper, but there the extent of the correction for discontinuity effects has been limited by the physical requirement for equal branch lengths. The agreement between measured and theoretical performance in this instance is only fair.

Fig. 5 shows the theoretical performance of a five-branch 3-db coupler designed by Harrison's method [5] with binomially tapered voltage coupling coefficients, the resultant branch impedance taper being somewhat "sharper" than binomial. The theoretical performance of a 3-db coupler with binomial taper of the branch impedances, actual branch size being found by the method given later in this paper, is shown in Fig. 6. It will be seen that the input match has improved over that of Fig. 5. This is part of a general trend of improvement that takes place when the binomial taper is "flattened" towards the values given by the sine taper of (11). An important fact is that the theoretical directivity is not infinite at midband for any of the tapers discussed here, least of all for the binomial taper of Fig. 5. This is not an error in calculation, and may be easily checked by using (19) and (21)–(23). This deficiency is avoided in the design method employed by Reed and Wheeler [7] and Young [8], which has been further developed by Reed [9]. In this method, two branch impedance values are determined by applying the two essential midband conditions for coupling and for directivity. Thus the midband performance is assured, but no broad-band condition is applied.

It may be noted from Figs. 4–6 that the theoretical coupling characteristic shown as power division ratio, $|A_3/A_2|^2$, is not much affected by these changes of taper.

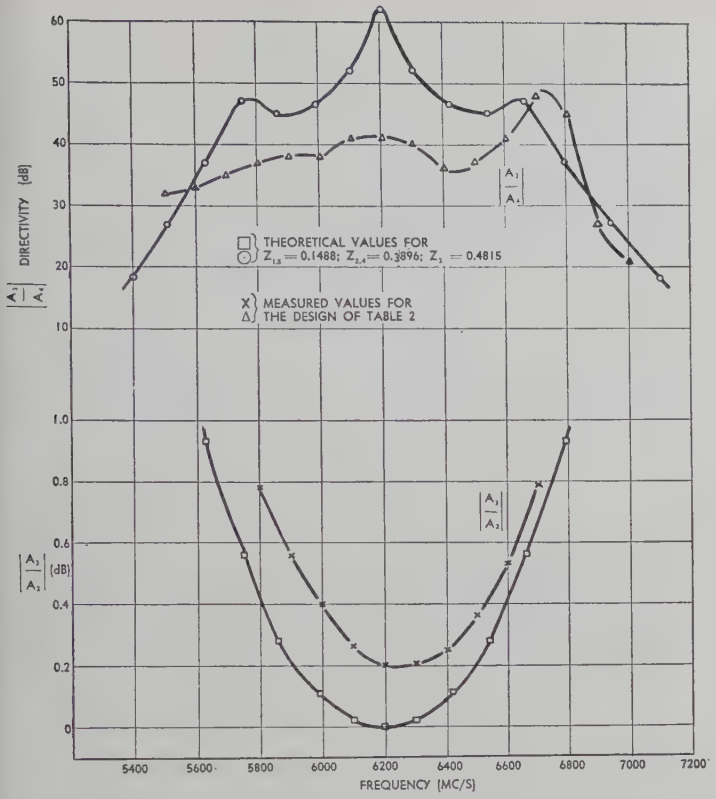

Fig. 4—Characteristics of branch coupler with sine taper.

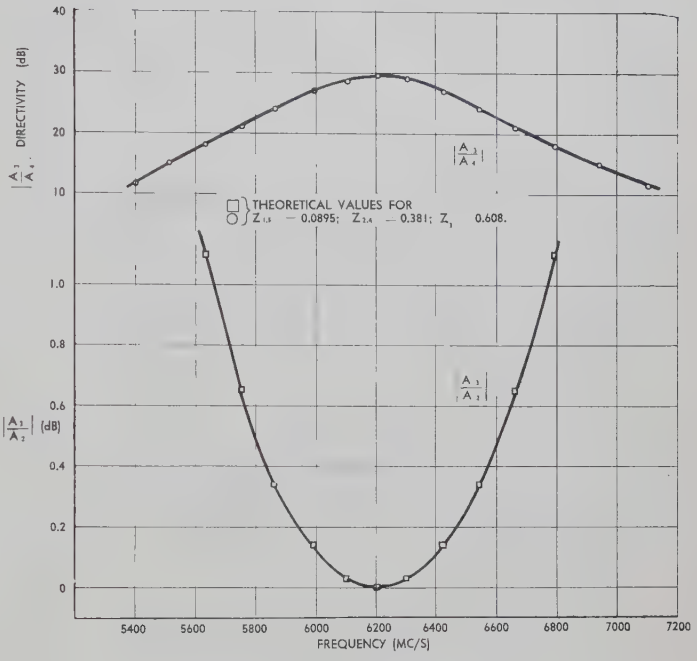

Fig. 5—Characteristics of branch coupler with binomial taper of voltage coupling coefficients.

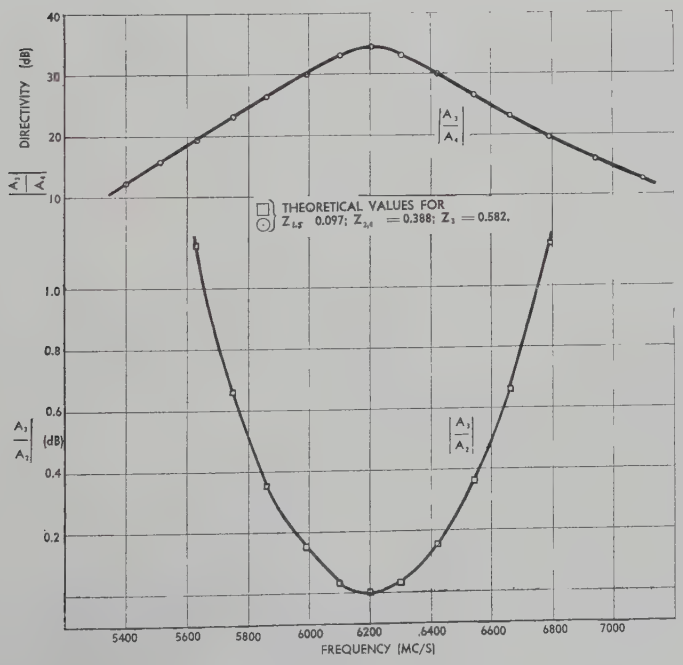

Fig. 6—Characteristics of branch coupler with binomial taper of branch impedances.

Exact Branch Impedance

The design methods of Harrison [5] and Crompton [6] consider the multi-element coupler as a cascaded series of two-element couplers. The coupling factor of the multi-element coupler is then found by a simple summation of the power coupled by the two-element couplers. This method cannot easily be applied to other than binomial couplers and is strictly applicable only if the total coupling is weak.

A more direct method, which avoids the above restrictions and is generally applicable, is possible. It is based on Reed and Wheeler's analysis, which can be developed in the following manner.

The transfer matrix of a lossless two-port circuit may be written as

$$\begin{bmatrix} A & jB \\ jC & D \end{bmatrix}, \tag{12}$$

taking Fig. 9 as a definition, so that the transmission and reflection coefficients of this circuit can be expressed as:

$$T = \frac{2}{A + jB + jC + D}, \tag{13}$$

$$\Gamma = \frac{A + jB - jC - D}{A + jB + jC + D}. \tag{14}$$

Let the matrix (12) apply in particular to the circuit of Fig. 2(a) with open-circuit stubs, at the midband frequency. Then the corresponding matrix of the circuit of Fig. 2(b) with short-circuit stubs can be shown to be

$$\begin{bmatrix} A & -jB \\ -jC & D \end{bmatrix}, \tag{15}$$

when there are an odd number of stubs. With an even number of stubs, both A and D change sign; the expressions for A_k are the same as for the odd-number case except for an interchange of A_2 and A_3.

The tapers considered here yield a circuit which is symmetrical end for end; hence,

$$A = D$$

and (1)–(4) can be developed as

$$A_1 = \frac{1}{R^2}(B^2 - C^2), \tag{16}$$

$$A_2 = \frac{2}{R^2}(A + D), \tag{17}$$

$$A_3 = \frac{2j}{R^2}(B - C), \tag{18}$$

$$A_4 = \frac{-j}{R^2}(A + D)(B + C);. \tag{19}$$

where

$$R^2 = (A + D)^2 + (B + C)^2.$$

The power balance at midband can now be expressed as

$$\left|\frac{A_3}{A_2}\right|^2 = \left|\frac{B + C}{A + D}\right|^2, \tag{20}$$

for the coupler with an odd number of branches, and as the reciprocal of this when there are an even number of branches.

As a specific example, the foregoing ideas will be applied to the design of a five-branch 3-db coupler.

Let the normalized branch impedances be, in order,

$$z_1 \quad z_2 \quad z_3 \quad z_2 \quad z_1.$$

When the component matrices are multiplied out, the elements of the matrix (12) are found to be, at f_0:

$$A = D = (z_1z_2 - 1)(z_2z_3 - 2) - 1, \tag{21}$$

$$B = (z_1z_2 - 1)(2z_1 + z_3 - z_1z_2z_3), \tag{22}$$

$$C = z_2(z_2z_3 - 2). \tag{23}$$

When the impedance taper is known, the matrix elements can be expressed in terms of z_1, or any one-branch impedance. The sine taper given by (11) applied to five branches gives

$$z_2 = 2.618z_1 \qquad z_3 = 3.236z_1. \tag{24}$$

Hence,

$$\left|\frac{A_3}{A_2}\right| = \left|z_1 \cdot \frac{5.236 - 22.18z_1^2 + 11.09z_1^4}{1.000 - 13.71z_1^2 + 22.18z_1^4}\right|. \tag{25}$$

For a 3-db coupler:

$$\left|\frac{A_3}{A_2}\right| = 1.000,$$

and (25) can be solved for z_1. It is not a difficult equation to solve, bearing in mind that only the smallest root (of the order of 0.1) is required. The method of iterative approximation is adequate. The resultant values for z_n are

$$\left.\begin{aligned} z_1 &= 0.1488 \\ z_2 &= 0.3896 \\ z_3 &= 0.4815 \end{aligned}\right\}. \tag{26}$$

These values will need to be corrected for the effect of the T-junction discontinuities. The necessary correction is given by (33), which can be stated as

$$z_n' = \frac{z_n}{m^2 \sin\theta}, \tag{27}$$

where z_n' is the corrected value and m^2, θ are found as shown later.

The narrow dimension b_n of the nth branch guide is found from the relation:

$$z_n' = \frac{b_n}{b_0}, \tag{28}$$

where b_0 is the narrow dimension of main and auxiliary guides.

Exact Branch Length

The existance of reactive discontinuity effects at the junction of a branch guide with main or auxiliary guides considerably modifies the performance of the branch guide. The effective size of a branch guide connected between two open E-plane junctions, which are commonly used in branch couplers, may be derived as follows.

Following Marcuvitz [11], the E-plane junction of Fig. 7(a) may be represented by the lumped equivalent network of Fig. 7(b), with suitable choice of reference planes T_1 and T_2. Values are given by Marcuvitz [11] for all the necessary parameters, but it has been pointed out to this author that the family parameter $b/\lambda g$ occurring inside the graphs of all Marcuvitz' E-plane curves should be altered to $2b/\lambda g$.

Let a branch guide of surge impedance Z_n' be connected between two such junctions and let the electrical length of the branch guide measured between the corresponding terminal planes T_1 of the junctions be θ radians. The lumped equivalent circuit of a branch guide can now be drawn, including the equivalent parameters of the junctions, the susceptances jB and ideal transformers of impedance ratio m^2, as shown in Fig. 8.

Defining the transfer matrix as in Fig. 9, the transfer matrix M_1 of the network of Fig. 8, assuming lossless components, is given by

$$M_1 = \begin{bmatrix} \cos\theta - BZ_n'' \sin\theta & jZ_n'' \sin\theta \\ j\left[2B\cos\theta + \left(\frac{1}{Z_n''} - B^2 Z_n''\right)\sin\theta\right] & \cos\theta - BZ_n'' \sin\theta \end{bmatrix}, \quad (29)$$

writing

$$Z_n'' \equiv m^2 Z_n'. \quad (30)$$

With discontinuity effects the branch guide would be of length $\lambda g_0/4$ and of surge impedance Z_n, for instance. The transfer matrix M_2 of the equivalent line network is

$$M_2 = \begin{bmatrix} 0 & jZ_n \\ \frac{j}{Z_n} & 0 \end{bmatrix}. \quad (31)$$

The matrices M_1 and M_2 become identical if

$$\cos\theta = BZ_n'' \quad (32)$$

and

$$Z_n'' = \frac{Z_n}{\sin\theta}. \quad (33)$$

This follows by equating A and B elements and substituting these results in the C elements.

Initially only Z_n, the surge impedance of a branch guide between ideal junctions, is known. However, the actual values required, Z_n' and θ, can be found quite easily by successive approximation using (30), (32), and (33). One or two iterations are usually sufficient.

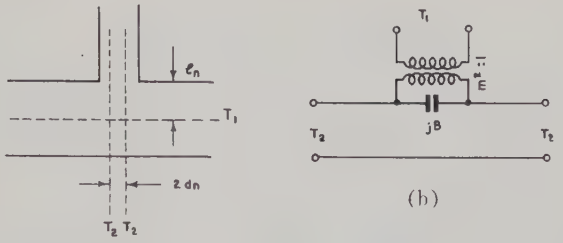

Fig. 7—Open E-plane waveguide junction (cross section), and lumped equivalent circuit.

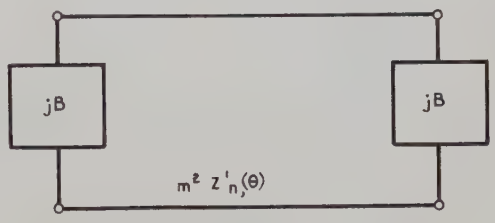

Fig. 8—Equivalent branch circuit.

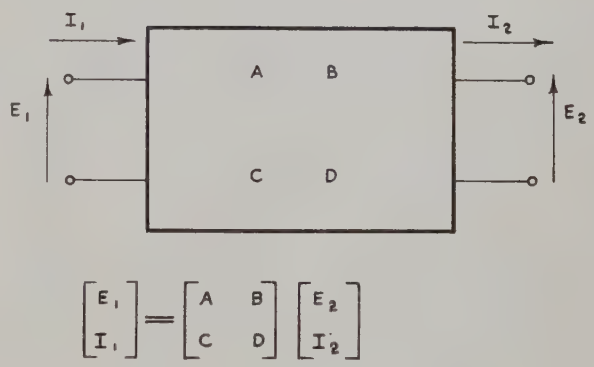

Fig. 9—Transfer matrix definition.

The exact length, L_n (Fig. 1), of a branch guide is given by

$$L_n = \frac{\lambda g_0}{2\pi}\theta_n - 2l_n, \quad (34)$$

where l_n is the displacement of the reference plane T_1 (Fig. 7).

The author has found that the lengths obtained by these means for the larger branch guides of a five-branch 3-db coupler are almost exact. The approximate expression given by Harrison [5] for the quantity L_n, *viz.*,

$$L_n = \frac{\lambda g_0}{4} - \frac{2b_n}{\pi}\left(1 + \log_e \frac{b_0}{2b_n}\right), \quad (35)$$

has been found to predict values which are 6 per cent short.

Branch Spacing

Little manipulation is required to obtain this quantity. The spacing D_{np} between center lines of adjacent branch guides is given by

$$D_{np} = \frac{\lambda g_0}{4} + d_n + d_p, \tag{36}$$

where $p = n \pm 1$ and $2d_n$ is the distance between the reference planes T_2 (Fig. 7), of the nth branch guide junction.

Comparison of Theoretical and Practical Design

A five-branch coupler was designed by the foregoing methods with main and auxiliary guide dimensions of 1.372 inches × 0.622 inch. The branch impedances followed the sine taper of (11). For comparison with a coupler actually constructed, the coupling loss at the midband frequency of 6200 mc has been made 2.90 db; *i.e.*, the power division ratio $|A_3/A_2|^2 = 0.22$ db. This necessitates a recalculation of the values for z_n given by (26). These become

$$\left.\begin{aligned} z_1 &= 0.1513 \\ z_2 &= 0.3958 \\ z_3 &= 0.4892 \end{aligned}\right\}. \tag{37}$$

The final calculated dimensions are given in Table I.

TABLE I

($\lambda g_0/4 = 0.661$ inch)

n	z_n'	L_n (inches)	D_{np} (inches)
1, 5	0.156	0.572	0.669
2, 4	0.435	0.499	0.679
3	0.556	0.484	—

In order to simplify the mechanical design, it is common practice to make all branch arms the same length, choosing a power-weighted average of the correct branch lengths; *i.e.*,

$$\frac{\sum z_n^2 L_n}{\sum z_n^2}.$$

For the design of Table I, this common length would be about 0.496 inch. In an actual five-branch coupler with the dimensions given in Table II designed with a sine taper of branch impedances, the branch length required to center the power division characteristic at 6200 mc was found to be 0.496 inch. The agreement is fortuitous; an error of at least 1 per cent might be expected. The measured power division ratio, $|A_3/A_2|^2$, was 0.2 db at midband, 6200 mc.

The practical values of branch impedance should be related to the theoretical values of (37) by the previously used relation (33), restated as

$$z_n' = \frac{z_n}{\sin 2\pi L_n/\lambda g_0}, \tag{38}$$

where L_n is given the same value for each branch of 0.496 inch, and z_n is given by (37). Hence at the midband frequency of 6200 mc:

$$z_n' = \frac{z_n}{0.924}. \tag{39}$$

This is a short cut on the design (27), the parameter m^2 having been eliminated together with its associated line length l_n.

TABLE II

($\lambda g_0/4 = 0.661$ inch)

n	z_n'	$z_n/0.924$	L_n (inches)	D_{np} (inches)
1, 5	0.165	0.163	0.496	0.668
2, 4	0.436	0.428	0.496	0.679
3	0.536	0.529	0.496	—

The actual value of z_n' required differs by 2 per cent or less from the value predicted by (39).

Fig. 4 shows the directivity and coupling characteristics of a coupler made to the dimensions given in Table II and measured with all output ports terminated by loads with less than 0.005 reflection coefficient.

With incomplete correction of junction discontinuity effects, due to using a common branch length, the measured performance would not be expected to equal the theoretical performance. Nevertheless, it is considerably better than the theoretical performance of the binomial couplers.

Conclusion

A considerable improvement, which is particularly applicable to 3-db couplers, can easily be made on the currently used binomial design of branch couplers.

The practical values of Table II differ from the predicted values by <2 per cent in branch length and about 2 per cent in branch impedance. This is equivalent to <1 per cent difference in midband frequency, and about 0.3 db in power division ratio, $|A_3/A_2|^2$, at midband.

Appendix

Lumped Element Equivalence

The normalized input reactance z_i of a short-circuit waveguide stub may be expressed as

$$z_i = z_n \tan \theta/2.$$

Differentiating with respect to frequency f,

$$\frac{dz_i}{df} = \frac{z_n}{2} \sec^2 - /2 \cdot \frac{d\theta}{d\lambda g} \cdot \frac{d\lambda g}{d\lambda} \cdot \frac{d\lambda}{df}, \tag{40}$$

and since

$$\frac{d\theta}{d\lambda g} = -\frac{\theta}{\lambda g}, \tag{41}$$

$$\frac{d\lambda g}{d\lambda} = \left(\frac{\lambda g}{\lambda}\right)^3, \tag{42}$$

$$\frac{d\lambda}{df} = -\frac{\lambda}{f}, \tag{43}$$

then

$$\frac{dz_i}{df} = \frac{z_n}{2}\sec^2\theta/2 \cdot \frac{\theta}{f} \cdot \left(\frac{\lambda g}{\lambda}\right)^2. \tag{44}$$

When $f=f_0$ (6200 mc),

$$\left(\frac{\lambda g}{\lambda}\right)^2 \approx 2 \quad \text{and} \quad \theta = \frac{\pi}{2},$$

$$\left(\frac{dz_i}{df}\right)_{f=f_0} = \frac{\pi z_n}{f}. \tag{45}$$

Thus, to a first-order approximation valid over a small frequency range around f_0, the slope of z_i is linear and positive with frequency, and hence the short-circuit stub can be represented as an inductance L_n, in conjunction with a certain frequency variable, ω', given by

$$L_n = \frac{z_n}{\omega} \text{ (henries, with respect to unity impedance level)}, \tag{46}$$

$$\omega' = \omega_0\left(1 + \pi\frac{\omega - \omega_0}{\omega_0}\right). \tag{47}$$

A similar argument applies to the open-circuit stubs, the slope of the input admittance being linear and positive with frequency to a first-order approximation so that the open-circuit stub can be represented as a capacity C_n, in conjunction with the frequency transformation of (47). C_n is given by

$$C_n = \frac{y_n}{\omega_0} \text{ (farads, with respect to unity impedance level)}. \tag{48}$$

Bibliography

[1] H. J. Riblet, "A mathematical theory of directional couplers," Proc. IRE, vol. 35, pp. 1307–1313; November, 1947.
[2] W. W. Mumford, "Directional couplers," Proc. IRE, vol. 35, pp. 160–165; February, 1947.
[3] B. A. Lippmann, "Theory of Directional Couplers," Mass. Inst. Tech. Radiation Lab. Rept. 860; 1945.
[4] B. A. Lippman, "Equivalent Circuit Analysis of Directional Couplers," Mass. Inst. Tech. Radiation Lab. Rept. 41; March 1, 1945.
[5] R. J. Harrison, "Design Considerations for Directional Couplers," Mass. Inst. Tech. Radiation Lab. Rept. 724; 1945.
[6] J. W. Crompton, "A contribution to the design of multi-element directional couplers," *Procl IEE (London)*, vol. 104, pt. C, pp. 398–402; 1957. (Monograph No. 230R.)
[7] J. Reed, and G. J. Wheeler, "A method of analysis of symmetrical four port networks," IRE Trans. on Microwave Theory and Techniques, vol. MTT-4, pp. 246–252; October, 1956.
[8] L. Young, "Branch guide couplers," *Proc. NEC*, vol. 12, pp. 723–732; 1956.
[9] J. Reed, "The multiple branch waveguide coupler," IRE Trans. on Microwave Theory and Techniques, vol. MTT-6, pp. 398–403; October, 1958.
[10] S. B. Cohn, "Direct coupled resonator filters," Proc. IRE, vol. 45, pp. 187–196, February, 1957.
[11] N. Marcuvitz, "Waveguide Handbook," McGraw-Hill Book Co., Inc., New York, N. Y., p. 339; 1948.
[12] A. T. Starr, "Radio and Radar Technique," Sir Isaac Pitman and Sons, London, Eng., p. 163; 1953.

Correspondence

The Analogy between the Weissfloch Transformer and the Ideal Attenuator (Reflection Coefficient Transformer) and an Extension to Include the General Lossy Two-Port*

Weissfloch's transformer theorem states that at certain pairs of reference planes a lossless two-port can be represented by an ideal transformer. There are many proofs of this important theorem. One of the most interesting is due to Bolinder,[1] who uses properties of the bilinear transformation. For lossless two-ports, the transformations will belong to the Fuchsian[2] group. This means that the isometric[1,2] circles are orthogonal to the principal circle. In the reflection coefficient plane (where Bolinder proves the theorem), the principal circle is the unit circle. The fixed points of the transformation will be on the unit circle or in a pair inverse with respect to the unit circle. Bolinder then uses lengths of lossless line to move the fixed points to the positions $\Gamma = \pm 1$. In the impedance plane this corresponds to fixed points of 0 and ∞. Therefore the transformation can be written as $Z' = k^2 Z$ and the transformer theorem is proven. The transformation through the two-port at any pair of reference planes, in either the reflection coefficient or the impedance plane, can be done by inversion in the isometric circles and a reflection in the line of symmetry,[3] as described by Ford[2] and Bolinder.[1]

The reflection coefficient transformer-(ideal attenuator), described by Altschulter and Kahn,[4] has a scattering matrix

$$S = \begin{pmatrix} 0 & K \\ K & 0 \end{pmatrix}$$

where K is a real number and, for an attenuator, less than unity. The transformation in the reflection coefficient plane is $\Gamma' = K^2\Gamma$, while in the impedance plane the corresponding relation is

$$Z' = \frac{\dfrac{Z(1+K^2)}{2K} + \dfrac{(1-K^2)}{2K}}{\dfrac{Z(1-K^2)}{2K} + \dfrac{1+K^2}{2K}}.$$

The fixed points of this transformation are ± 1 in the impedance plane and 0 and ∞ in the reflection coefficient plane. Both transformers produce hyperbolic transfor-

* Received by the PGMTT, February, 1959; revised, March, 1959.

[1] E. F. Bolinder, "Impedance and polarization—ratio transformations by a graphical method using the isometric circles," IRE Trans. on Microwave Theory and Techniques, vol. MTT-4, pp. 176–180; July, 1956.

[2] L. R. Ford, "Automorphic Functions," 2nd ed., Chelsea Publishing Co., New York, N. Y.; 1951.

[3] If the transformation is loxodromic, a rotation must be added.

[4] H. M. Altschulter and W. K. Kahn, "Nonreciprocal two-ports represented by modified Wheeler networks," IRE Trans. on Microwave Theory and Techniques, vol. MTT-4, pp. 228–233; October, 1956.

mations, since the trace of the normalized transformation is real and its magnitude is greater than two.[5] At the proper reference planes (where the transformations are the same), problems involving one of the two-ports *per se* in the impedance plane can be solved considering the other two-port in the reflection coefficient plane. It should be pointed out that analogy will fail when the reference planes are moved, because for the loss-less two-port the transformation is always nonloxodromic, while for the ideal attenuator the transformation will become, in general, loxodromic. It is also of interest to note that the fixed points of the reflection coefficient transformer are independent of the choice of reference planes.

In the general case of a lossy two-port, it is shown in the Appendix that pairs of reference planes can be found where the transformation is nonloxodromic. At these reference terminals the lossy two-port will be analogous to the lossless two-port which has the same fixed points in the reflection coefficient plane and which has the same multipliers of the transformations in canonical[2] form. This is true for all hyperbolic transformations where the two fixed points (the iterative impedances) have the same magnitude, all parabolic transformations (which have only one fixed point), and all elliptic transformations where the phase angles of the fixed points are equal. This class of transformation includes all symmetric networks with positive resistive components. Therefore, for this special class of lossy networks (eacj at its proper pair of reference planes) the transformations belong to the Fuchsian group. Therefore, any of the several lossy networks can be "replaced" (in the sense that it has the same transformation) by an "analogous" lossless network. If the fixed points in the impedance plane for a hyperbolic transformation do not have equal magnitude, then a transformation is used to map the fixed points in the impedance plane into fixed points in the new W plane with magnitude equal to unity and for convenience equal to ± 1. In this W plane, the analogy with the lossless two-port in the Γ plane holds. Similarly, for the elliptic transformation, the fixed points in the impedance plane are moved to points inverse with the unit circle and an "analogous" elliptic lossless network can be found. Therefore, it has been shown that any lossy two-port can be "replaced" by an "analogous" lossless network.

An Alternate Viewpoint

If the constructions for the isometric circle method becomes unwieldy because of the unbounded nature of Euclidean space, the impedance and/or the reflection coefficient planes can be transformed into the Cayley-Klein diagram (projective chart), which has hyperbolic measure. The required transformations are described by Bolinder[6] and Deschamps.[7] The transformation of impedances through lossless networks has been treated by Bolinder.[6] By analogy, the transformation of reflection coefficients through the "equivalent lossless" network is identical. Of course, it may be found by the user that the extended method (using the Cayley-Klein Diagram) is simpler. This may be true if Deschamps'[7] hyperbolic protractor is available.

Example

The symmetrical resistive network (reflection coefficient transformer) shown will be considered in an illustration of the method (see Fig. 1). The resistance values were chosen to locate the fixed points (iterative impedances) at ± 1 on the unit circle. If this were not the case, the impedance level could be adjusted. The input impedance is found to be:

$$Z' = \frac{\sqrt{2}Z + 1}{Z + \sqrt{2}}.$$

If this is compared with relation (1) of the Appendix, an analogous transformation,

$$\Gamma' = \frac{\sqrt{2}\Gamma + 1}{\Gamma + \sqrt{2}},$$

may be written if

$$S_{11} = \frac{1}{\sqrt{2}} \qquad S_{12} = \frac{1}{\sqrt{2}} \qquad S_{22} = -\frac{1}{\sqrt{2}}.$$

It is noted that the analogous network is lossless, since its scattering matrix is unitary. While the original network is a transformer in the Γ plane, the analogous network is a transformer in the Z plane, whose Z matrix does not exist. Its A, B, C, D matrix is

$$\begin{pmatrix} \sqrt{2}+1 & 0 \\ 0 & \sqrt{2}-1 \end{pmatrix}.$$

Appendix

In general,

$$\Gamma' = \frac{\dfrac{(S_{12}^2 - S_{11}S_{22})\Gamma}{S_{12}} + \dfrac{S_{11}}{S_{12}}}{-\dfrac{S_{22}\Gamma}{S_{12}} + \dfrac{1}{S_{12}}} = \frac{a\Gamma + b}{c\Gamma + d}$$

$$(ad - bc) = 1$$

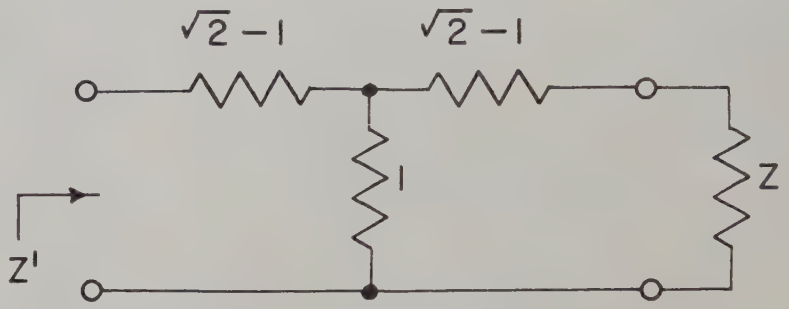

Fig. 1—Reflection coefficient transformer with arbitrary load.

where

$$S_{11} = |S_{11}|\, e^{j\Phi_{11}}$$
$$S_{12} = |S_{12}|\, e^{j\Phi_{12}}$$
$$S_{22} = |S_{22}|\, e^{j\Phi_{22}}.$$

Now, if we move reference planes 1 and 2 by electrical distances θ_1 and θ_2 along lossless lines, respectively,[8]

$$S_{11}' = |S_{11}|\, e^{j(\Phi_{11}+2\theta_1)}$$
$$S_{12}' = |S_{12}|\, e^{j(\Phi_{12}+\theta_1+\theta_2)}$$
$$S_{22}' = |S_{22}|\, e^{j(\Phi_{22}+2\theta_2)}.$$

Let $\psi = \theta_1 + \theta_2$ (an electrical length of transmission line), and compute $a+d$

$$a + d = \frac{|S_{12}|^2 e^{j(2\Phi_{12}+2\psi)} - |S_{11}S_{22}|\, e^{j(\Phi_{11}+\Phi_{22}+2\psi)} + 1}{|S_{12}|\, e^{j(\Phi_{12}+\psi)}}.$$

For the transformation to be nonloxodromic, $a+d$ has to be real. Setting the imaginary part to zero, the result is

$$\tan\psi = \frac{(1 - |S_{12}|^2)\sin\Phi_{12} + |S_{11}S_{22}|\,\sin(\Phi_{11} + \Phi_{22} - \Phi_{12})}{(|S_{12}|^2 - 1)\cos\Phi_{12} - |S_{11}S_{22}|\,\cos(\Phi_{11} + \Phi_{22} - \Phi_{12})}.$$

D. J. R. Stock
L. J. Kaplan
Electrical Engrg. Dept.
New York University
New York, N. Y.

[5] There is an exception when either k or K is unity, but this is lossless uniform line, which is a trivial case.

[6] E. F. Bolinder, "Graphical methods for transforming impedances through lossless networks by the Cayley-Klein diagram," *Acta Pol.* Elec. Engrg. Series, vol. 7, no. 5; 1956.

[7] G. A. Deschamps, "New chart for the solution of transmission-line and polarization problems," IRE Trans. on Microwave Theory and Techniques, vol. MTT-1, pp. 5–13; March, 1953.

[8] C. G. Montgomery, R. H. Dicke, and E. M. Purcell, "Principles of Microwave Circuits," McGraw-Hill Book Co., Inc., New York, N. Y.; 1948.

Comments* on "Some Notes on Strip Transmission Line and Waveguide Multiplexers"[1]

Use of two tuning screws through the ground planes of a strip-line cavity resonator can excite the parallel plane TEM mode unless both screws are equidistant from the center conductor, rendering this method of tuning quite unattractive. A single tuning screw parallel to and midway between the ground planes is the better way of tuning a stripline cavity resonator.

The implication that a Tchebycheff response shape is preferable to the Butterworth response shape merely on the sole criteria of sharper skirt selectivity is debatable. Butterworth filters are simpler to design, have more favorable phase responses, and are easier to align. Furthermore, Butterworth filters are superior when designing narrow band filters for minimum insertion loss.[2]

We are currently using direct-coupled waveguide resonant cavity filters and have found them to be quite satisfactory. These filters employ five cavity resonators with bandwidths of about 3 per cent in frequency (This corresponds to a filter Q of 33.) Use of quarter-wave coupled cavities would increase over-all filter length by a factor of two, while use of quarter-wave coupled resonant elements would result in intolerable filter insertion losses. It should also be noted that quarter-wave coupled waveguide filters usually employ nominal $\frac{3}{4}\lambda_g$ connecting lines, since use of $\lambda_g/4$ connecting lines and centered inductive coupling posts will cause appreciable higher-mode interaction between adjacent resonators. No general statement can be made concerning the relative merits of direct-coupled and quarter-wave coupled filters. Percentage bandwidth, physical size, construction cost, and other factors must be carefully considered in each specific filter application.

Richard M. Kurzrok
Surface Communications Systems Lab.
RCA Defense Electronic Products Div.
New York, N. Y.

* Received by the PGMTT, March 18, 1959.

[1] D. Alstadter and E. O. Houseman, Jr., 1958 WESCON Convention Record, pt. 1, pp. 54–69.

[2] J. J. Taub and B. F. Bogner, "Design of three-resonator dissipative band-pass filters having minimum insertion loss," Proc. IRE, vol. 45, pp. 681–687; May, 1957.

The Representation of Impedances with Negative Real Parts in the Projective Chart*

In a previous note [1] the authors considered the representation of active networks in the reflection coefficient chart. The projective chart [2] is obtained from a stereographic projection onto a unit sphere and then from an orthographic projection from the sphere. It is immediately obvious that reflectances whose magnitude is greater than unity will lie within the unit circle of the projective chart. Therefore, each will coincide with another reflectance whose magnitude is less than unity.

From intuitive reasoning it is apparent the reflectances which share the same point in the projective chart are $re^{j\phi}$ and $(1/r)e^{j\phi}$. To show this analytically one determines the hyperbolic distance in the projective chart as proportional to the logarithm of the cross ratio. When the points[1] r and $1/r$ are transformed algebraically, the cross ratios are negatives (but both are real) and the hyperbolic distance of the reflectance whose magnitude is greater than unity is complex. The imaginary component of the distance arises because of the ultra-infinite end point of the measured distance. The real parts of both distances are equal, since the projective chart cannot indicate the j direction which is perpendicular to the plane of the projective chart (they are the same point). This may be seen by using the Riemann sphere as described by Bolinder [3] to visualize that the positive and negative resistance values are on different halves of the sphere and that the orthographic projection is perpendicular to the dividing equator and hence cannot differentiate between real conjugate impedances or reflectances which are inverse with respect to the unit circle. The equivalence between the inverse reflectances can also be seen by constructions in the plane by using the circle of inversion [4]. This leads to a modification of the β transformation of Deschamps which is shown in Fig. 1.

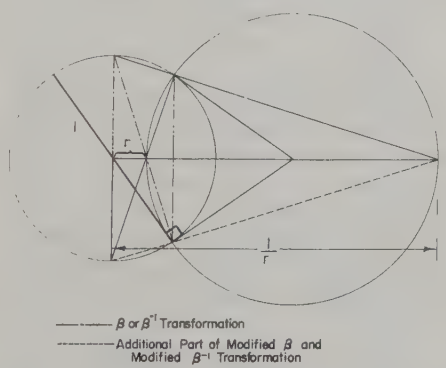

Fig. 1—Modified β and modified β^{-1} transformation.

Therefore, it is seen that the projective chart can be used to represent active networks by using the points of the real conjugate of the impedance or the reflectance that is inverse with respect to the unit circle.

References

[1] L. J. Kaplan and D. J. R. Stock, "An extension of the reflection coefficient chart to include active networks," IRE Trans. on Microwave Theory and Techniques, vol. MTT-7, pp. 298–299; April, 1959.

[2] G. A. Deschamps, "New chart for the solution of transmission-line and polarization problems," IRE Trans. on Microwave Theory and Techniques, vol. MTT-1, pp. 5–13; March, 1953.

[3] E. F. Bolinder, "General method of analyzing bilateral two-part networks from three arbitrary impedance measurements," *Ericsson Technics*, vol. 14, no. 1, pp. 3–37; 1958.

[4] J. de Buhr, "Eine neue methode zur bearbeitung linearer vierpole," *FTZ-Fernmeldetech Z.*, vol. 8, pp. 200–204, April, 1955; pp. 335–340; June, 1955.

* Received by the PGMTT, April 28, 1959.

[1] The phase angle ϕ will not affect the distance from the center.

D. J. R. Stock
L. J. Kaplan
Electrical Engrg. Dept.
New York University
New York, N. Y.

Design Calculations for UHF Ferrite Circulators*

The recent advances in low-noise amplifier work for communications systems has created an additional demand for circulators; in this case, to prevent receiver noise from returning to the low-noise amplifier. In the range of frequencies greater than 2000 mc, ferrite circulators have been developed in circular and rectangular waveguides. However, in the UHF region, which is a range of frequencies of increasing interest and importance in communications, ferrite circulators present a problem in the sense that ordinary waveguides needed in this range are prohibitively large for practical use. Button[1] of Lincoln Laboratory and Seidel[2] of Bell Telephone Laboratories have pointed a way around this difficulty by considering a TEM structure (a coax) loaded antisymmetrically with dielectric material and ferrite. This configuration provides for the longitudinal component of RF magnetic field necessary for nonreciprocity in the phase constant.[2] The essentially TEM nature of the device allows use of reasonably small, practical cross-sectional areas. The parallel-plate analog analysis presented in Button's paper leads to a transcendental equation for the phase constant which we present below for convenience, together with an example of the structure (see Fig. 1).

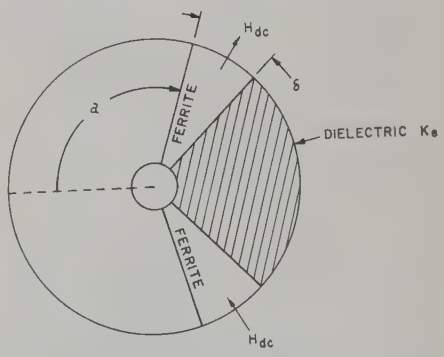

Fig. 1—Cross section of coaxial phase shifter.

* Received by the PGMTT, May 4, 1959.

[1] K. J. Button, *J. Appl. Phys.*, vol. 29, p. 998; June, 1958.

[2] H. Seidel, *J. Appl. Phys.*, vol. 28, p. 218; February, 1957.

$$L = 2(a+\delta) + \frac{2}{k_d}\tan^{-1}\left(\frac{-M}{N}\right) \qquad (1)$$

$$M = (\beta^2 G^2 - k_m^2\rho^2)\cos k_a a \sin k_m\delta - k_a \sin k_a a[k_m\rho\cos k_m\delta + j\beta G \sin k_m\delta]$$

$$N = k_d[k_a \sin k_a a \sin k_m\delta - \cos k_a a(k_m\rho\cos k_m\delta - j\beta G \sin k_m\delta)]$$

$$G = \rho/\theta$$

$$\rho = \frac{\mu}{\mu^2-\kappa^2}$$

$$\theta = -j\mu/\kappa$$

$$\mu = 1+\frac{4\pi M_S\gamma f_0}{f_0^2-f^2};\quad \kappa = \frac{4\pi M_S\gamma f}{f_0^2-f^2};$$

$$f_0 = \gamma H_{dc}$$

H_{dc} = static magentic field applied to ferrite
$\gamma = 2.8\times10^6$ cps-oersted
f_0 = ferrite resonant frequency
f = RF frequency
$4\pi M_S$ = saturation magnetization of the ferrite
δ = ferrite slab thickness
$2a$ = width of empty region
L = mean value of circumference of inner and outer conductors of coax

$$k_d^2 = \frac{\omega^2}{c^2}K_e - \beta^2$$

$\omega = 2\pi f$
c = speed of light in vacuum
K_e = dielectric constant of dielectric slab
β = phase constant

$$k_a^2 = \frac{\omega^2}{c^2} - \beta^2$$

$$k_m^2 = \frac{\omega^2}{c^2}\frac{K_f}{\rho} - \beta^2$$

K_f = dielectric constant of ferrite

We carried out computer solutions of the transcendental equation (1) for the differential phase shift $\beta_+ - \beta_-$ in the frequency range 400–440 mc. Our operating conditions were chosen in the following way. Calculations were made by Button[1] on a 2000-mc coaxial ferrite phase shifter. We scaled,[3] in a very approximate way, his operating conditions down to 400 mc. Thus we chose a ferrite slab thickness $\delta = 2$ cm (corresponding to Button's choice 0.425 cm), an empty space region $2a = 26$ cm vs Button's 5.7 cm, a ferrite magnetization 450 gauss vs Button's 800 gauss (procurement of required 200-gauss ferrite is not presently possible, so we chsse the lowest reasonable value for $4\pi M_S$), and a dc magnetic field of 100 oersteds vs Button's 275 oersteds. We chose a large dielectric constant $K_e = 15$ in order to attain large nonreciprocal phase shift. The dielectric constant of the ferrite was taken to be 10. Eq. (1) was then solved for $\beta_+ - \beta_-$ as a function of L for three sets of a, δ: $a = 15$ cm, $\delta = 2$ cm; $a = 15$ cm, $\delta = 1.6$ cm; $a = 13$ cm, $\delta = 2$ cm. The results are shown in Fig. 2 at 400 mc for $H_0 = 100$ oersteds. Practical coax is designed with a mean circumference of 33.9 cm and for this value, Fig. 2 shows the largest differential phase shift will occur for the set $a = 13$ cm, $\delta = 2$ cm (even larger $\Delta\beta$ will occur for still smaller a).

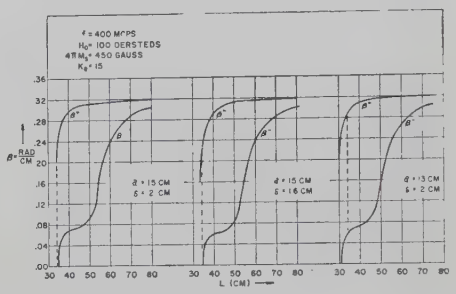

Fig. 2.

Keeping $a = 13$ cm, $\delta = 2$ cm, we then varied the dc field H_0 between 50 and 152 oersteds and also varied f between 400 and 440 mc and solved (1) for $\beta_+ - \beta_-$ for these varying conditions. Fig. 3 shows typical results, β_+ and β_- vs L, when $H_0 = 145$ oersteds and f is varied. This graph yields $\Delta\beta$ vs f for a given L (33.9 cm) and a given H_0. Allowing H_0 to take on different values then leads to Fig. 4, which shows $\Delta\beta$ vs f for 3 dc fields. From this figure, we see that best broadbanding is obtained for a dc field $H_0 = 145$ oersteds. The $\Delta\beta$ attained for these conditions is about 0.250 radian/cm leading to a circulator ($l\Delta\beta = \pi$ radians; l = length of circulator) about 5 inches long. The variation in $\Delta\beta$ in the 400 to 440-mc range for the 145-oersted field is about ± 1.3 per cent. This degree of broadbanding in $\Delta\beta$ leads to a minimum of 33-db isolation between circulator arms.

To summarize, Button's theory for the coax configuration when applied to the 400- to 440-mc band leads to the following design parameters (see Fig. 1):

ferrite slab thickness $\delta = 2$ cm
air region $= 2a = 26$ cm
ferrite magnetization = 450 gauss
dc magnetic field = 145 oersteds
mean circumference of coax = 33.9 cm
dielectric constant = 15
length of coax = 5 inches
isolation between arms $\geq$ 33 db over the band

It should be mentioned that 1) a more exhaustive investigation of the a and δ parameters might lead to larger $\Delta\beta$ and therefore even more compact structure, 2) the above design parameters can serve as the basis for

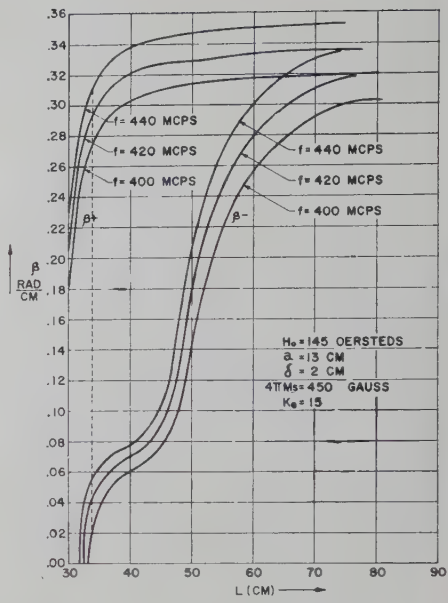

Fig. 3.

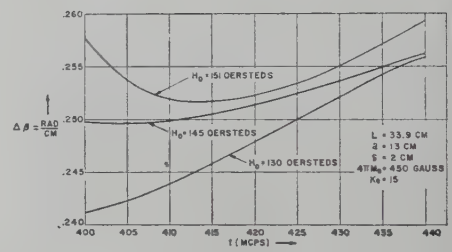

Fig. 4.

design of coax circulators in other frequency bands by scaling.

It also should be mentioned that the theory used here predicts nothing about the insertion loss of the device. However, we may note that the resonance condition for this structure [obtained by letting $\beta \to \infty$ in the transcendental equation (1)] is $\mu + \kappa = -1$ or $f_{resonance} = \gamma(H_{dc} + 2\pi M)$. Thus for $H_0 = 145$ oersteds, $2\pi M = 225$ gauss, and

$$\gamma = 2.8\times10^6 \frac{\text{cycles}}{\text{second oersted}},$$

we have $f_{resonce} \approx 1000$ mc, well above the operating range 400 to 440 mc. Thus, the device should have reasonably small insertion loss.

We should like to thank Dr. Button for access to a prepublication copy of his work and for several stimulating discussions with him. He was also kind enough to read this paper and offer criticisms and suggestions before publication. The programming and calculations were performed by Mrs. S. Zucker of RCA, and her competent work is gratefully acknowledged.

H. Boyet
S. Weisbaum
I. Gerst
Surface Communications Div.
RCA
Defense Electronic Products
New York, N. Y.

[3] S. Weisbaum and H. Seidel, *Bell Sys. Tech J.*, vol. 35, p. 877; July, 1956.

Discussion on Optimum Bead Spacing*

Mr. Dettinger's article[1] on the optimum spacing of bead supports in coaxial transmission lines is too sanguine as to the performance which will result. He states that an array of M beads arranged according to his theory will result in a total reflection coefficient of no more than $\sqrt{M}\Gamma_0$ where Γ_0 is the reflection of one bead. In his Fig. 5 he shows a chart of the reflection of four beads equally spaced and the reduced reflection which he hopes will result from application of his rule. The case where there are four beads will result for equal spacing in a maximum value of $4\Gamma_0$, and from his theory for progressive spacing it should be possible to arrange the beads so that the maximum possible reflection is only $2\Gamma_0$.

Assume that the reflection of each bead in Fig. 1 is very small so that the total reflection of the array of beads can be found by simple vector addition of the reflections of the individual beads. Also assume that the reflection from each bead is invariant with frequency and the differences in bead spacing a and b are constant with frequency. Then the reflection patterns of Figs. 2 and 5 of Mr. Dettinger's article become equivalent to plotting the pattern as a function of phase angle ϕ instead of frequency.

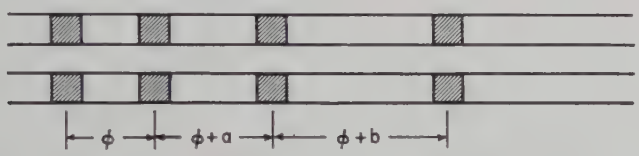

Fig

If now the value of the total reflection coefficient Γ_t as a function of ϕ is computed and this value is squared it will be found that the average value of this power reflected computed for one cycle is exactly $M\Gamma_0^2$. In this case $M=4$ but the statement is true for any M and is independent of a and b. Now let us imagine that we are able to space an assembly of beads so that the total reflection coefficient has a constant value over a cycle of ϕ. Of course this constant value of reflection coefficient would have to be $\sqrt{M}\Gamma_0$. But this is just the value of reflection coefficient which Mr. Dettinger claims is the *peak* for his spacing.

JOHN REED
Wayland Laboratory
Raytheon Co.
Wayland, Mass.

Author's Comment[2]

I am sorry that the objectives of my paper were not clear to Mr. Reed. My goal was to reduce the envelope of reflection peaks in a limited frequency band for a long coaxial transmission line made up of many identical sections. The idea of the limited band was discussed in the text and figures, but was not explicitly restated in the summary or in the conclusions.

Mr. Reed has presented a concept regarding the average reflection from any number of beads arbitrarily dispersed along a line. This concept is only incidentally related to the subject of my paper, in that it considers neither the actual envelope of reflection peaks nor the possibility of reducing the envelope in a limited frequency band by the use of a controlled dispersal of beads in each section.

However, he has raised a philosophical issue. The question might be stated—Can the maximum value of a varying function be equal to its average value under any circumstances? I believe that the answer is yes in the special case where the maxima are measured in a frequency band which is narrow in comparison with the band over which the average is computed. This happens to be the very case we are considering. The bandwidth of reduced reflection envelope is necessarily limited by the requirement that the progressive increment remain close to its nominal design value, whereas the average reflection would be computed over a much wider band. Therefore, I believe that the two concepts are not inconsistent. Instead, Mr. Reed's work has yielded the interesting observation that the reflection may "pile up" in other parts of the frequency band.

It is perhaps necessary to point out that in his second sentence Mr. Reed has misstated my formula for the predicted reduction of reflection envelope. The relation he gives, $\sqrt{M}\Gamma_0$, is a simplified form obtained only for the case where M, the number of beads per section, is equal to N, the total number of beads in the array; in short, for one section. The general form would be $N\Gamma_0/\sqrt{M}$. This formula is not intended to apply to the case of one section and would require modification for that use.

As was indicated in my paper, a complete mathematical analysis of the progressive dispersal across a wide frequency band has not been achieved. It has been suggested that the solution may be arrived at through conventional antenna array theory. I hope to carry this through when time permits. In the meantime, I should welcome any contribution of another worker, such as Mr. Reed, to the mathematical solution of a relation which has been verified experimentally.

DAVID DETTINGER
Wheeler Labs.
Great Neck, N. Y.

* Received by the PGMTT, March, 1959.
[1] D. Dettinger, "The optimum spacing of bead supports in coaxial line at microwave frequencies," 1957 IRE CONVENTION RECORD, vol. 5, pt. I, pp. 250–253.
[2] Received by the PGMTT, April, 1959.

Concerning Riblet's Theorem*

I would like to add yet another comment[1,2] concerning Riblet's theorem.[3] Ozaki's impedance function

$$Z(p) = \frac{2p^2 + 2p + 4}{3p + 1} \tag{1}$$

which satisfies an equation of the form

$$m_1(p)m_2(p) - n_1(p)n_2(p) = C(1 - p^2)^n \tag{2}$$

(with $C=4$ and $n=1$), can be realized in many ways, of which only four are shown in Fig. 1. [Type (b) was the only one given by Ozaki and his numerical solution was incorrect.]

As is well known in lumped constant network theory, for a driving point impedance $Z(p)$ to be physically realizable, the degrees of its numerator and denominator polynomials can differ by at most unity. The same property carries over to resistor-transmission-line circuits by Richards' transformation.[4] It follows from Riblet's proof[3] of his theorem, that a rational impedance function $Z(p)$ which is positive real and satisfies an equation of the form (2) can be realized as a cascade of n equal-line sections terminated in a resistance and possibly one stub, as in Ozaki's example. As with the three circuits (a), (b) and (c) of Fig. 1, it can be seen that in general, if one stub appears at the termination, it can be moved in whole or in part, and placed at any one junction or shared out between several junctions anywhere along the cascade of lines. (Of course the characteristic impedances of the cascaded lines will change as the stubs are passed over them, but there will always be just n cascaded line sections, whereas the number of stubs may be changed.) The form $Z(p)$ determines the *minimum* number of stubs required, and Riblet's theorem may be generalized as follows:

> "The necessary and sufficient conditions that a rational function of p, written in its lowest form,
>
> $$Z(p) = \frac{m_1(p) + n_1(p)}{m_2(p) + n_2(p)}$$
>
> with m_1 and m_2 even, and n_1 and n_2 odd polynomials in p, be the input impedance of a cascade of n transmission line sections of equal length θ, terminated in a resistance with at most one study of length θ, are
>
> 1) $Z(p)$ must be a positive real function of p;
> 2) $m_1m_2 - n_1n_2 = C(1 - p^2)^n$.
>
> The numerical difference between the degrees of (m_1+n_1) and (m_2+n_2) is equal to the minimum number of stubs involved."

* Received by the PGMTT, May 22, 1959.
[1] H. Ozaki, "On Riblet's theorem," IRE TRANS. ON MICROWAVE THEORY AND TECHNIQUES, vol. MTT-6, pp. 331–332; July, 1958.
[2] H. J. Riblet, "Comments on Ozaki's comments," IRE TRANS. ON MIROWAVE THEORY AND TECHNIQUES, vol. MTT-7, pp. 297–298; April, 1959.
[3] H. J. Riblet, "General synthesis of quarter-wave impedance transformers," IRE TRANS. ON MICROWAVE THEORY AND TECHNIQUES, vol. MTT-5, pp. 36–43; January, 1957.
[4] P. I. Richards, "Resistor-transmission-line circuits," PROC. IRE, vol. 36, pp. 217–220; February, 1948.

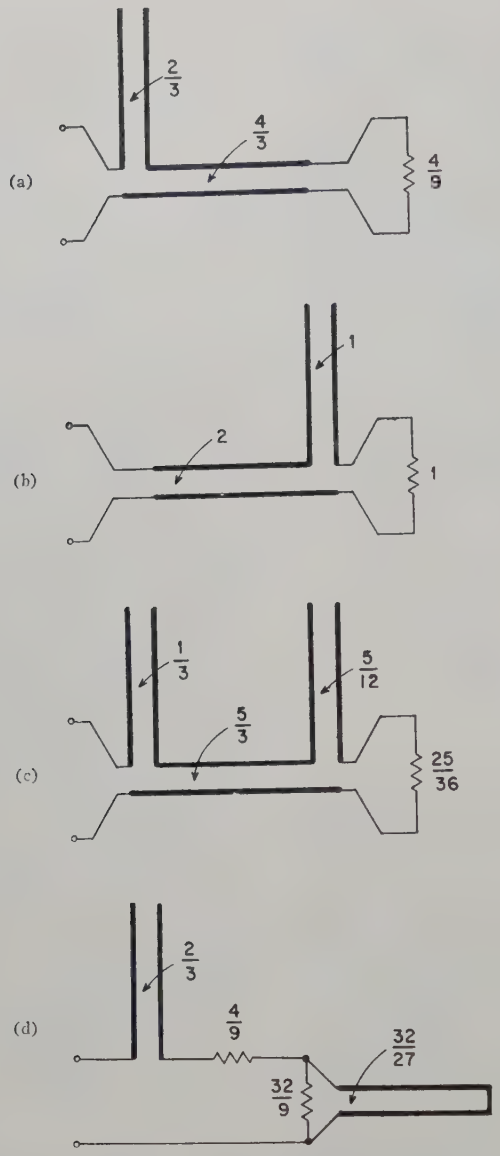

Fig. 1—Four circuits with the same input impedance (1). All lines are of length θ; all numbers are either resistances or characteristic impedances of lines.

The theorem thus stated specifically excludes common factors of (m_1+n_1) and (m_2+n_2). As Riblet has pointed out,[2] this results in a mathematical loss of generality, which however is physically trivial, since no measurement can distinguish between two one-ports consisting, respectively, of a resistance R, and a resistance R preceded by a length of transmission line of characteristic impedance R.

A final comment on terminology. In my paper[5] on the same subject, I specified "homogeneous" transformers without clearly defining this term, and would like to make up this omission now.

Definition: A homogeneous waveguide is one in which the guide wavelength is independent of position.

As a corollary, an inhomogeneous waveguide is one in which the guide wavelength varies with position; *i.e.*, it is not uniformly dispersive. The quarter-wave transformers which are the subject of this discussion and of the references mentioned so far are all homogeneous transformers. There has been little need in the past to distinguish between homogeneous and inhomogeneous quarter-wave transformers (as defined above), as no theory existed for the latter. However, inhomogeneous quarter-wave transformers have recently been analyzed,[6] and the above terminology was introduced to distinguish between these two situations.

Leo Young
Electronics Div.
Westinghouse Electric Corp.
Baltimore, Md.

[5] L. Young, "Tables for cascaded homogeneous quarter-wave transformers," IRE Trans. on Microwave Theory and Techniques, vol. MTT-7, pp. 233–237; April, 1959.

[6] L. Young, "Design of microwave stepped transformers with applications to filters," Dr. Eng. dissertation, The Johns Hopkins University, Baltimore, Md.; 1959.

Broad-Band Stub Design*

Mr. Muehe's results for broad-band stubs,[1] while going beyond that of previous investigators, are similar to my design curves published earlier without detailed derivation.[2] The main difference is that my curves were based on a formula involving the bandwidth as defined by the lowest and highest frequencies of *zero* reflection. Mr. Muehe's analysis is therefore superior to my simpler approach; my design curves erred on the safe side in predicting a slightly smaller bandwidth.

Leo Young
Electronics Div.
Westinghouse Electric Corp.
Baltimore, Md.

* Received by the PGMTT, May 15, 1959.

[1] C. E. Muehe, "Quarter-wave compensation of resonant discontinuities," IRE Trans. on Microwave Theory and Techniques, vol. MTT-7, pp. 296–297; April, 1959.

[2] L. Young, "Coaxial stub design," *Electronics*, vol. 30, p. 188; July 1, 1957.

Attenuation of the HE_{11} Mode in the *H*-Guide*

The properties of the lowest order hybrid mode of the *H*-guide line have been analyzed by Tischer in a number of papers.[1–3] This type of transmission line has also been under investigation at this laboratory for some time and a number of discrepancies exist between our analysis and those of Tischer.

The geometry of this line is shown in Fig. 1. For comparison purposes, the coordinates and notation introduced by Tischer will be used throughout this letter.

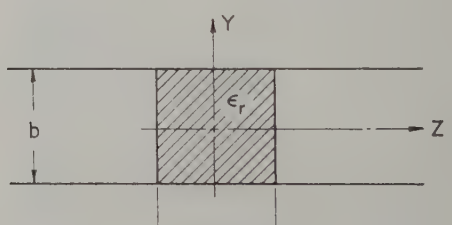

Fig. 1—Cross section of the *H*-guide line. The positive x-axis is into the paper.

In Tischer[1,2] the dielectric slab is considered thin and as a result, 1) dielectric losses are neglected, and 2) in the derivation of the expression for the wall losses the power flow in the dielectric slab and the losses in the portion of the walls contacting

* Received by the PGMTT, May 15, 1959.

[1] F. J. Tischer, "Microwellenleitung mit geringen verlusten" (Waveguides with small losses), *Arch. elekt. Uebertragung*, vol. 7, pp. 592–596; December, 1953.

[2] F. J. Tischer, "The *H*-guide, a waveguide for microwaves," 1956 IRE Convention Record, pt. 5, pp. 44–47.

[3] F. J. Tischer, "Properties of the *H*-guide at microwaves and millimeter waves," 1958 WESCON Convention Record, pt. 1, pp. 4–12.

the dielectric slab are neglected. The resulting equation for the attenuation due to the loss in the walls is a good approximation for a thin slab but it is not generally correct.

The analysis conducted at this laboratory yields the following equations for the attenuation due to the wall and dielectric loss respectively:

$$\alpha_w = \frac{\frac{2R_s}{bZ_0}\pi^3\left(\frac{a}{\lambda_0}\right)^3\left(\frac{\lambda_0}{2b}\right)^2\epsilon_r}{\sqrt{\pi^2\left(\frac{a}{\lambda_0}\right)^2\left[\epsilon_r-\left(\frac{\lambda_0}{2b}\right)^2\right]-\left(k_d\frac{a}{2}\right)^2}} \cdot \left\{\frac{k_d\frac{a}{2}\tan k_d\frac{a}{2}+\sin^2 k_d\frac{a}{2}+\epsilon_r\cos^2 k_d\frac{a}{2}}{\left[\pi^2\epsilon_r\left(\frac{a}{\lambda_0}\right)^2-\left(k_d\frac{a}{2}\right)^2\right]k_d\frac{a}{2}\tan k_d\frac{a}{2}+\pi^2\epsilon_r\left(\frac{a}{\lambda_0}\right)^2\left(\sin^2 k_d\frac{a}{2}+\epsilon_r\cos^2 k_d\frac{a}{2}\right)}\right\} \quad (1)$$

$$\alpha_d = \frac{\left[\pi^2\epsilon_r\left(\frac{a}{\lambda_0}\right)^2-\left(k_d\frac{a}{2}\right)^2\right]\tan\delta}{a\sqrt{\pi^2\left(\frac{a}{\lambda_0}\right)^2\left[\epsilon_r-\left(\frac{\lambda_0}{2b}\right)^2\right]-\left(k_d\frac{a}{2}\right)^2}} \cdot \left\{\frac{\pi^2\epsilon_r\left(\frac{a}{\lambda_0}\right)^2 k_d\frac{a}{2}\tan k_d\frac{a}{2}+\left[\pi^2\epsilon_r\left(\frac{a}{\lambda_0}\right)^2-2\left(k_d\frac{a}{2}\right)^2\right]\sin^2 k_d\frac{a}{2}}{\left[\pi^2\epsilon_r\left(\frac{a}{\lambda_0}\right)^2-\left(k_d\frac{a}{2}\right)^2\right]k_d\frac{a}{2}\tan k_d\frac{a}{2}+\pi^2\epsilon_r\left(\frac{a}{\lambda_0}\right)^2\left(\sin^2 k_d\frac{a}{2}+\epsilon_r\cos^2 k_d\frac{a}{2}\right)}\right\}, \quad (2)$$

where α_w and α_d are the wall and dielectric attenuation foactors in nepers/meter if a, b, and λ_0 are in meters, R_s is the surface resistance of the conducting walls, $\tan\delta$ is the loss tangent of the dielectric slab, Z_0 is the impedance of free space, and k_d is the transverse wave number for the z-direction in the dielectric filled region. k_d is related to the dielectric constant (ϵ_r), the dielectric slab width (a), and the free space wavelength (λ_0) by the following transcendental equation:

$$\left(k_d\frac{a}{2}\right)^2\left[\frac{\tan^2 k_d\frac{a}{2}}{\epsilon_r^2}+1\right] = (\epsilon_r-1)\pi^2\left(\frac{a}{\lambda_0}\right)^2. \quad (3)$$

Eq. (3) is obtained by satisfying the boundary conditions at the dielectric-air interfaces and requiring that the axial propagation constant be the same in the air and dielectric regions. Graphical techniques have been used to determine $[k_d(a/2)]$ as a function of (a/λ_0) and ϵ_r. For the lowest hybrid mode (HE_{11}), $[k_d(a/2)]$ is constrained to be within the following interval.

$$0 \le \left(k_d\frac{a}{2}\right) \le \frac{\pi}{2}.$$

If $(\epsilon_r-1)\pi^2(a/\lambda_0)^2$ is very small, then $[k_d(a/2)]$ becomes a very small angle and the following approximation may be used for (3).

$$\left(k_d\frac{a}{2}\right)^2 \approx (\epsilon_r-1)\pi^2(a/\lambda_0)^2. \quad (4)$$

Using (4), the following thin slab limiting value for α_w and thin slab approximation for α_d are obtained.

$$\lim_{a\to 0}\alpha_w = \frac{2R_s}{bZ_0}\cdot\frac{(\lambda_0/2b)^2}{\sqrt{1-(\lambda_0/2b)^2}} \quad (5)$$

$$\alpha_d = \frac{2\pi^3(\epsilon_r-1)(a/\lambda_0)^2}{\epsilon_r^2\lambda_0\sqrt{1-(\lambda_0/2b)^2}}\tan\delta,$$

$$\text{for } (\epsilon_r-1)\pi^2\left(\frac{a}{\lambda_0}\right)^2 \ll 1. \quad (6)$$

It is of interest to comment on the other extreme condition in which $(\epsilon_r-1)\pi^2(a/\lambda_0)^2$ is very large and $[k_d(a/2)]$ approaches $\pi/2$. In that case (3), (1) and (2) become, respectively,

$$\left(k_d\frac{a}{2}\right)^2\tan^2 k_d\frac{a}{2} \approx \epsilon_r^2(\epsilon_r-1)\pi^2(a/\lambda_0)^2 \quad (7)$$

$$\lim_{a\to\infty}\alpha_w = \frac{2R_s}{bZ_0}\cdot\frac{(\lambda_0/2b)^2}{\sqrt{\epsilon_r-(\lambda_0/2b)^2}} \quad (8)$$

$$\lim_{a\to\infty}\alpha_d = \frac{\pi\epsilon_r}{\lambda_0\sqrt{\epsilon_r-(\lambda_0/2b)^2}}\tan\delta. \quad (9)$$

It should be noted that (5) and (8) are, respectively, the expressions for the wall loss attenuation of a completely air-filled and a completely dielectric-filled parallel plane transmission line in which the lowest order TE mode is propagating. This serves as a good check on the validity of (1), since the HE_{11} mode approaches the field configuration of this TE mode when the space between the conducting walls is uniformly loaded.

If the same thin slab and thick slab approximations are applied to the equations for α_w in Tischer,[1,2] it is found that the thin slab approximations agree but the thick slab approximations do not.

In a more recent publication,[3] Tischer outlines a method of deriving equations for α_w and α_d, in which the dielectric slab need not be thin. The final expression for α_w, which he presents, does not agree with (1). Furthermore if the thin and thick slab approximations are applied to his equation, it is found that they do not agree with either the limiting expressions presented here [(5) and (8)] or with those determined from his earlier publications.[1,2] In addition, the various curves of α_w as a function of slab width in Tischer's most recent publication[3] do not agree with each other. In this most recent work of Tischer's, no equation is presented for the attenuation due to the loss in the dielectric; however, a curve of α_d vs slab width is presented for a particular line. This curve does not agree with the corresponding curve computed from (2). The two curves of α_d vs slab width are shown here in Fig. 2. Also shown here is a curve of α_w as computed from (1).

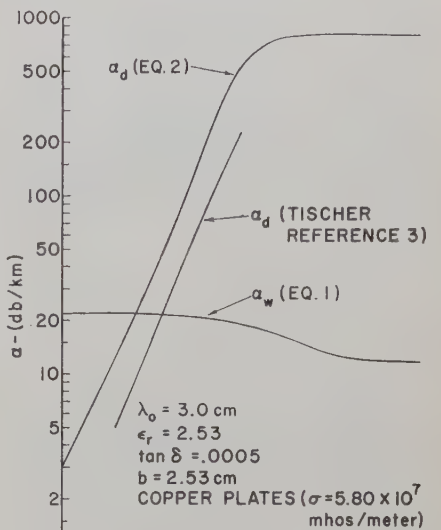

Fig. 2—Attenuation due to wall loss and dielectric loss as a function of dielectric slab width.

These curves show that except for very thin dielectric slabs (assuming typical values for $\tan\delta$) the dielectric loss is the principal contributor to the total attenuation. Eq.s (2) and (6) show that, if either very thin slabs or very low dielectric constant materials are used, the dielectric loss can be comparable to or less than the very low wall loss. In that case there will be a range of frequencies in which the highly desirable property of decreasing attenuation with increasing frequency will exist. The price for this advantage is that the fields in the air space will decay very slowly with increasing distance from the dielectric slab. Therefore, the conducting planes will have to be extended in the z-direction.

The HE_{11} mode on this line has also been analyzed by Moore and Beam.[4] Their equations for the field components of this mode are erroneous, however, in that they do not show that the transverse magnetic field which is parallel to the conducting planes is everywhere zero. This fact had been reported by Tischer and was confirmed by this writer.

It should be noted that although the HE_{11} mode is the lowest order hybrid mode of this line, it is not the dominant mode.

[4] R. A. Moore and R. E. Beam, "A duo-dielectric parallel plane waveguide," *Proc. NEC*, vol. 12, pp. 689–705; April, 1957.

There is a class of TE modes which can propagate on this line.[5,6] The TE_{10} mode is the dominant mode of this structure. These TE modes should not be confused with the prior-mentioned TE modes which can only propagate in a uniformly-loaded parallel-plane line.

Tischer has shown that a conducting plane can be placed at the plane $z=0$ and not affect the field configuration of the HE_{11} mode. This conducting plane completely suppresses all of the TE modes which are symmetric about the $z=0$ plane (TE_{10}, TE_{30}, etc.). If in addition the slab width is such that

$$\frac{a}{\lambda_0} < \frac{1}{2\sqrt{\epsilon_r - 1}},$$

the TE_{20} and all higher order antisymmetric TE modes cannot propagate. The HE_{11} mode will then be the dominant mode of the resulting trough line. The attenuation due to the loss in this added conducting plane will not, however, decrease with increasing frequency.

MARVIN COHN
Radiation Lab.
The Johns Hopkins University
Baltimore, Md.

[5] M. Cohn, "Parallel plane waveguide partially filled with a dielectric," PROC. IRE, vol. 46, pp. 1952–1953; December, 1958.
[6] M. Cohn, "Propagation in a dielectric-loaded parallel plane waveguide," IRE TRANS. ON MICROWAVE THEORY AND TECHNIQUES, vol. MTT-7, pp. 202–208; April, 1959.

Author's Comment[7]

It was interesting to learn that my proposal of 1952 for a new waveguide, the *H*-guide, found such attention, and that it became the subject of investigation at several places.

Concerning discrepancies mentioned in the above letter of Cohn, it is suggested that one should consider that approximate solutions, in general, depend on the neglections introduced and may not be called either correct or incorrect.

The equations for the attenuation of the *H*-guide dealt with in the above letter are quite complicated. One part of the attenuation constant, contributed by the wall losses, follows for comparison. The neglections, on which the approximations are based, are indicated.

The equations are valid for the waveguide of infinite height which is excited in the fundamental hybrid mode. They are approximations based on the field distribution in a lossless guide:

$$\alpha_w = \frac{R_s\left(\frac{\omega\epsilon_0\pi}{b\Gamma k_a}\right)^2}{\frac{b}{2}\left(\frac{\omega\epsilon_0}{\Gamma}\right)\left(1+\frac{\omega^2\epsilon_0\mu_0}{k_a{}^2}\right)} m; \quad (1)$$

$$m = \frac{\cos^2\psi + \frac{k_a}{k_d}[\psi + \sin\psi\cos\psi]}{\cos^2\psi + \frac{k_a}{\epsilon_r k_d}[\psi + \sin\psi\cos\psi]}, \quad (2)$$

where

$$\psi = k_d\frac{a}{2}.$$

For small values of a, where the wall currents and the Poynting vector become approximately independent of z inside the dielectric (varying with $\cos k_d z$, where $k_d z \ll 1$), $m \to 1$, and it is the same as if the losses in the walls inside the dielectric and the power transmitted in this region were neglected.

Eq. (1) becomes, after transformation,

$$\alpha_w = \frac{2R_s}{bZ_0}\left(\frac{\lambda_0}{2b}\right)^2 \frac{1}{\sqrt{1-\left(\frac{\lambda_0}{\lambda_{c0}}\right)^2}} \cdot\left[1+\left(\frac{k_a\lambda_0}{2\pi}\right)^2\right]^{-1} \cdot\left[1+\left(\frac{k_a\lambda_0}{2\pi}\right)^2\left(\frac{\lambda_{g0}}{\lambda_0}\right)^2\right]^{-1/2}, \quad (3)$$

which is (16) of the publication cited by Cohn.[3]

A limiting value for $\alpha_w = \alpha_0$ is obtained if $a \to 0$.

$$\alpha_0 = \frac{2R_s}{bZ_0}\left(\frac{\lambda_0}{2b}\right)^2 \frac{1}{\sqrt{1-\left(\frac{\lambda_0}{\lambda_{c0}}\right)^2}}, \quad (4)$$

which is the attenuation of the rectangular waveguide of infinite height excited in the TE_{10} mode. Typographical errors occurred in the above cited publication in the exponents of the equations for α_0 and (16).

Discrepancies seem still to exist between Cohn's (1) and the above (1) and (2), but no errors could be detected in our equation for α_w.

Due to lack of time and manpower in our case, I have to leave the honor of investigating and detecting this discrepancy to somebody else.

Mr. Chen Pang Wu's assistance in the calculations and checks is appreciated.

F. J. TISCHER
Dept. of Electrical Engrg.
The Ohio State University
Columbus, Ohio

[7] Received by the PGMTT, June 22, 1959.

Mr. Cohn's Reply[8]

In Dr. Tischer's above letter, I am in complete agreement with his corrected (3), since it is clearly labeled as an approximation for a thin dielectric slab. With regard to his more general equations, (1) and (2), discrepancies between our results certainly do exist. I submit that it is a necessary (though not sufficient) condition that the limiting values of α_w for $a \to 0$ and $a \to \infty$ should agree respectively with the well-known solutions for the attenuation of an infinitely-high rectangular waveguide which is air filled and dielectric filled. Eqs. (1) and (2) in Dr. Tischer's letter do not satisfy the thick slab limiting condition.

MARVIN COHN

[8] Received by the PGMTT, June 25, 1959.

Experimental Determination of Wavelength in Dielectric-Filled Periodic Structures*

Let it be required to determine the guided wavelength in a dielectric-filled periodic structure, such as a corrugated wall or serrated waveguide. The accepted travelling probe technique requires a slot in the broad wall of the guide and a groove in the dielectric material. Even if the errors introduced by these modifications could be tolerated, other effects render this technique unsuitable. One of these is a surface-wave effect which results in a measured wavelength higher than the one in the guide and lower than the free-space value. If the structure is dissipative, such as a serrated guide, more difficulties arise.

A suggested solution to this experimental problem is based on Deschamps' method of determining the elements of the scattering matrix.[1] All that is needed is the value of the argument of the transfer coefficient $S_{12}e^{i\theta}$ where $\theta + 2\pi n$ is the electrical length of the sample and n is an integer.

Suppose now that θ has been measured at two frequencies, f and $f+\delta f$, where $\delta f/f$ is of the order of 10^{-3}. Let the guided wavelengths in the two measurements be λ_g and $\lambda_g + \delta\lambda_g$, respectively, and let L be the length of the sample. Then,

$$\lambda_g(\theta + 2\pi n) = 2\pi L \quad (1a)$$

$$(\lambda_g + \delta\lambda_g)(\theta + \delta\theta + 2\pi n) = 2\pi L \quad (1b)$$

Implied in (1b) is the fact that θ is a continuous function of f which is true for periodic structures whose period is small compared with the guided wavelength. It appears that we have on hand two second-order equations in three unknowns: n, λ_g and $\delta\lambda_g$. But by expressing $\delta\lambda_g$ in terms of λ_g, f, and δf we can obtain one third order equation in n. It is expedient to use a method of numerical solution, because once an approximate solution has been arrived at, the exact value of n becomes the nearest integer.

We represent the structure by an equivalent dielectric constant ϵ and write

$$\lambda_g = \frac{\lambda}{\sqrt{\epsilon - \frac{\lambda^2}{\lambda_c{}^2}}} \quad (2)$$

$$\lambda = \frac{c}{f} \quad (3)$$

where λ and λ_c are the free-space and cut-off wavelength in the unloaded guide respectively.

To a first approximation we have

$$\delta\lambda_g = \frac{d\lambda_g}{d\lambda}\cdot\frac{d\lambda}{df}\cdot\delta f. \quad (4)$$

From (2) and (3) we have

$$\frac{d\lambda_g}{d\lambda} = \left(\epsilon - \frac{\lambda^2}{\lambda_c{}^2}\right)^{-1/2} + \frac{\lambda^2}{\lambda_c{}^2}\left(\epsilon - \frac{\lambda^2}{\lambda_c{}^2}\right)^{-3/2}$$

and

* Manuscript received by the PGMTT, April 24, 1959; revised manuscript received, May 21, 1959.
[1] G. A. Deschamps, "Determination of reflection coefficients and insertion loss of a waveguide junction," *J. Appl. Phys.*, vol. 24, pp. 1046–1050; August, 1953.

$$\frac{d\lambda}{df} = -\frac{\lambda}{f}.$$

Substituting into (4) we obtain

$$\frac{\delta\lambda_g}{\lambda_g} = -\left(1+\frac{\lambda_g^2}{\lambda_c^2}\right)\frac{\delta f}{f}. \qquad (5)$$

Substituting again from (1a) and (5) into (1b) we obtain

$$\left\{1-\left(1+\frac{4\pi^2L^2}{(\theta+2\pi n)^2\lambda_c^2}\right)\frac{\delta f}{f}\right\} \cdot \frac{2\pi L(\theta+\delta\theta+2\pi n)}{\theta+2\pi n} = 2\pi L.$$

Or putting

$$\theta+2\pi n = x; \qquad \frac{4\pi^2L^2}{\lambda_c^2} =$$

we obtain

$$\frac{\delta f}{f}x^3 - x^2\delta\theta\left(1-\frac{\delta f}{f}\right) + x\xi\frac{\delta f}{f} + \delta\theta\xi\frac{\delta f}{f} = 0. \qquad (6)$$

In view of the fact that n is an integer, no error is introduced by the approximation involved in (4). The accuracy of the method depends solely on the accuracy to which θ and L have been measured. On the other hand, f must be measured to an accuracy just sufficient for an unambiguous determination of n from (6).

Accuracy in the measurement of θ is assured by a high-quality slotted line and variable-short-circuit and it is suggested that no less than 10 points be measured for each frequency to assure the accurate plotting of the iconocentre of the transformed unit circle.

The above described method has been successfully applied to the measurement of the propagation constant in a serrated waveguide filled with polystyrene.

EFRAIM WEISSBERG
Scientific Dept.
Ministry of Defence
Hakirya, Tel Aviv, Israel

An Automatic Microwave Dielectrometer*

The dielectric constant of low-loss dielectric materials can be measured accurately, rapidly, and automatically by proper utilization of an automatic microwave impedance instrument of the type which presents its output in Smith Chart form; *i.e.*, the magnitude and phase of the reflection coefficient. The method employed is essentially a modification of the slotted line technique which was originally described by Roberts and Von Hippel,[1] the difference

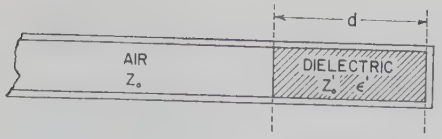

Fig. 1—Dielectric slug in short circuited section of waveguide.

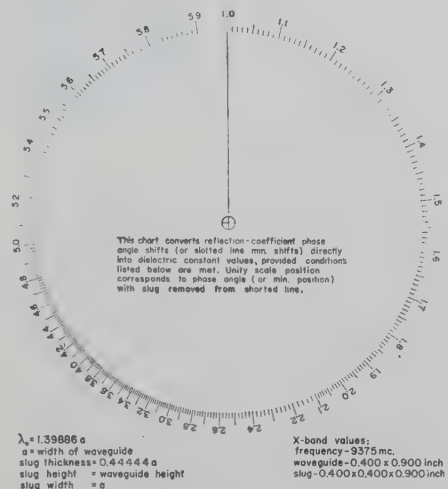

Fig. 2—Example of a direct reading dielectric constant scale.

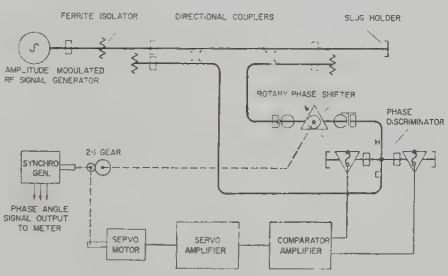

Fig. 3—Schematic diagram of an automatic dielectrometer.

being that the slotted line is replaced by an automatic impedance instrument with a direct reading scale.

A sample of the dielectric to be measured is accurately cut in the form of a slug which fills the waveguide in its transverse dimensions and is positioned against a reference short circuit, as shown in Fig. 1. From the derived relationship for this case available in the literature,[2] it will be found that the change in a slotted line minimum position, caused by insertion of the dielectric slug, can be related to the dielectric constant of the slug by

$$x = \frac{\lambda_g}{2\pi}\tan^{-1}\left[\frac{\lambda_g'}{\lambda_g}\tan\left(\frac{2\pi d}{\lambda_g'}\right)\right] - d$$

where

x = "min-shift" distance (minimum position without sample minus that with sample)
λ_g = wavelength in air-filled waveguide
λ_g' = wavelength in dielectric-filled waveguide
d = length of sample.

The particular expression for λ_g' will contain the dielectric constant, of course. Upon replacing the slotted line with an automatic impedance instrument which measures reflection coefficient, it becomes desirable to convert the "min-shift" distance, x, to the associated change in reflection coefficient phase angle, Δ_ϕ,

$$\Delta_\phi = \frac{4\pi x}{\lambda_g}.$$

One can then calculate values of Δ_ϕ for various values of dielectric constant, assuming fixed values for λ_g and d, and can construct circular scales which read directly in dielectric constant. An example of such a scale is shown in Fig. 2, calculated for 0.400 $\times$0.400$\times$0.900 inch slugs in X-band waveguide at a frequency of 9375 mc. It is assumed that the relative permeability is unity and that λ_g' is given by the TE_{10} mode expression

$$\lambda_g' = \frac{\lambda_0}{\sqrt{\epsilon' - \left(\frac{\lambda_0}{2a}\right)^2}}$$

where

λ_0 = free space wavelength,
ϵ' = dielectric constant (relative)
a = width of waveguide.

Scales such as this convert reflection coefficient phase angle shifts directly into dielectric constant values, thereby permitting automatic indication. If variations in slug length or frequency are desired, a family of such scales can be constructed to cover the particular sets of conditions involved.

To use the scale, replace the Smith Chart with it on whatever output device the impedance instrument utilizes, usually an oscilloscope or a linear polar recorder. Next, align the unity scale position with the phase angle indicated for the reference short circuit by itself. Then simply insert the slugs against the short circuit and either record or read off the dielectric constant values.

The accuracy of this type of dielectrometer is dependent upon the accuracy with which the automatic impedance instrument can follow changes in reflection coefficient phase angle at a given frequency. Results comparable to those obtained from slotted-line measurements require a phase angle accuracy of about ± 0.5 degrees. Instruments of this order of accuracy have been built,[3] utilizing a servo driven Fox type rotary phase shifter as the principal element in the phase measuring circuit.

If an automatic dielectrometer is desired, but an automatic impedance instrument does not happen to be available for such use, then the arrangement shown in Fig. 3 is suggested. It is based upon the reference impedance instrument.[3]

WILLIAM F. GABRIEL
Microwave Antennas and Components Branch
U. S. Naval Res. Lab.
Washington, D. C.

* Received by the PGMTT, June 12, 1959; revised, July 15, 1959.

[1] S. Riberts and A. von Hippel, "A New Method for Measuring Dielectric Constant and Loss in the Range of Centimeter Waves," Electrical Engrg. Dept., Mass. Inst. Tech., Cambridge, Mass.; March, 1941.

[2] C. G. Montgomery, "Technique of Microwave Measurements," Rad. Lab. Ser., McGraw-Hill Book Co., Inc., New York, N. Y., vol. 11, Ch. 10, p. 627, (71); 1947.

[3] W. F. Gabriel, "Automatic Microwave Impedance Recorder, X-Band Pototype Model," U. S. Naval Res., Lab. Rept. No. 5295, Washington, D. C.; May, 1958.

Design Note on a Serrated Choke*

The serrated choke described by Dr. Kiyo Tomiyasu and J. J. Bolus[1] is a very effective device to employ whenever long cuts or gaps are present on the walls of rectangular waveguide. This communication is concerned with the application of a serrated choke to an X-band waveguide ring switch,[2] wherein the waveguide was split longitudinally at opposite corners to form a rotor section and a stator section.

The final choke design arrived at is shown in Fig. 1. It consists of 0.050×0.050-inch square pins of 0.330-inch length spaced 0.040 inch apart, with a gap of 0.015 inch between the pins and the adjacent choke surface. The reason for using such a small gap was to obtain as low an impedance as possible from the quarter-wavelength open-ended two-wire line stubs formed by the pins and the adjacent choke surface. The mechanical configuration involved was chosen so as to permit the choke to be easily and accurately cut by standard machining methods into the same piece of metal which forms the walls of the half-waveguide section, thus eliminating the need for any tedious soldering or adjustment of individual pins. Another advantage of this design is that the metallic surfaces are continuous (no cracks) at all points of high current density, thus permitting higher RF power capacity. The point of attachment of a choke cover and the gap necessary to permit relative movement of the two half-waveguide sections both occur in the low current density region of the choke. Fig. 2 shows aluminum X-band experimental test sections which were constructed for the purpose of evaluating the machined serrated choke. RF tests conducted upon such a section 37 inches in length showed a loss of only 0.1 db per foot, a power handling capacity in excess of 200 kw peak, and no main-guide interference from choke channel propagation over the frequency band of 8200 to 10,000 mc.

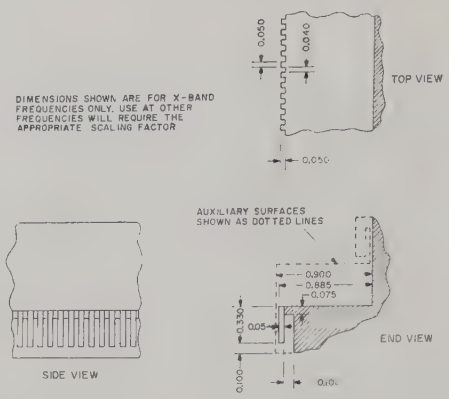

Fig. 1—X-Band serrated choke design.

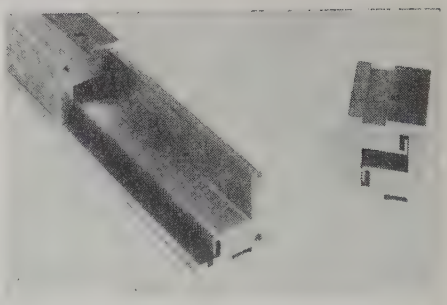

Fig. 2—Experimental test sections of serrated choke machined from aluminum castings.

WILLIAM F. GABRIEL
Microwave Antenna and
Components Branch
U. S. Naval Res. Lab.
Washington, D. C.

* Received by the IRE, July 15, 1959.

[1] K. Tomiyasu and J. J. Bolus, "Characteristics of a new serrated choke," IRE TRANS. ON MICROWAVE THEORY AND TECHNIQUES, vol. MTT-4, pp. 33–36; January, 1956.

[2] W. F. Gabriel, G. D. Peeler, H. P. Coleman, and D. H. Archer, "Volumetric Scanning GCA Antenna Design," Naval Res. Lab., Washington, D. C., Rept. No. 5019, pp. 34–48; November, 1957.

Contributors

Morris Cohen was born in Brooklyn, N. Y., on March 31, 1925. He attended RCA Institutes, Brooklyn, N. Y., from 1947 to 1949, graduating in 1949. He received the B.E.E. and M.E.E. degrees from the Polytechnic Institute of Booklyn, N. Y., in 1954 and 1958.

M. COHEN

From 1950 to 1955, he was a research assistant at the Microwave Research Institute, Polytechnic Institute of Brooklyn. From 1955 to 1956 he was employed as a microwave engineer in the microwave components section of the Polarad Electronics Corp., Long Island City, N. Y. In 1956, he joined the Polytechnic Research and Development Company, Brooklyn, N. Y., and at present he is a section head in the microwave research department, engaged in the design and development of microwave components and systems.

Mr. Cohen is an associate member of Sigma Xi.

Seymour B. Cohn (S'41–A'44–M'46–SM'51) was born in Stamford, Conn., on October 21, 1920. He received the B.E. degree in electrical engineering from Yale University, New Haven, Conn., in 1942. The M.S. degree in communication engineering in 1946, and the Ph.D. degree in engineering sciences and applied physics, in 1948, were awarded by Harvard University, Cambridge, Mass.

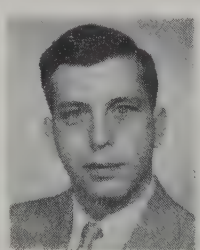

S. B. COHN

From 1942 to 1954 he was employed as a special research associate by the Radio Research Laboratory of Harvard University, also representing that laboratory as a technical observer with the U. S. Army Air Force in the Mediterranean theater of operations. He worked at Sperry Gyroscope Company, Great Neck, N. Y., from 1948 to 1953, where he held the position of research engineer in the microwave instruments and components department. Since February, 1953, he has been with the Stanford Research Institute, Menlo Park, Calif., as head of the Microwave Group, and, since 1957, as manager of the Electromagnetics Laboratory.

Dr. Cohn is a member of Tau Beta Pi and Sigma Xi.

❖

A. F. Harvey was born in Monmouthshire, England, on March 21, 1910. He received the B.Sc. degree in electrical engineering from the University College of Wales, Cardiff, in 1930, and the D.Phil. degree from Oxford University, Oxford, Eng., in 1940.

A. F. HARVEY

From 1930 to 1932, he was a college apprentice with Metropolitan-Vickers, Manchester. During the next six years he was on the technical staff of, successively, General Electric Co., Wembley; Johnson and Phillips, London;

and the Royal Aircraft Establishment, Farnborough. Since 1940, he has served at what is now the Royal Radar Establishment, Malvern. His work has been concerned mainly with ultra-high and microwave frequencies, in which fields he holds several patents and has published many survey papers and a book. He has also made original contributions on waveguides, electron tubes, millimeter-wave components and ferrite devices.

Dr. Harvey was for several years chairman of the R.C.R.D. and R.C.S.C. waveguide committees and also of the NATO working group on waveguides. He is a member of the IEE.

❖

E. M. T. Jones (S'46–A'50–SM'56) was born in Topeka, Kans., in 1924. He received the B.S. degree in electrical engineering from Swarthmore College, Swarthmore, Pa., in 1944 and the M.S. and Ph.D. degrees in electrical engineering from Stanford University, Stanford, Calif., in 1948 and 1950, respectively. He was a radar maintenance officer in the U. S. Navy from 1944 to 1946. From 1948 to 1950, he was a research associate at Stanford University, working on the microwave local oscillator project. In 1950, he joined the staff of Stanford Research Institute, Menlo Park, Calif., and in 1957 he became head of the Microwave Group of the Electromagnetics Laboratory.

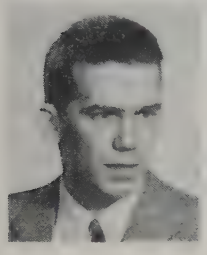

E. M. T. Jones

Dr. Jones is a member of Sigma Tau and RESA.

❖

Walter K. Kahn (S'50–A'51–M'56–SM'59) was born on March 24, 1929, in Mannheim, Germany, and came to the United States in 1938. He completed his undergraduate studies at the Cooper Union School of Engineering, New York, N. Y., receiving the B.E.E. degree in 1951. He received the M.E.E. degree from the Polytechnic Institute of Brooklyn, N. Y., in 1954.

W. K. Kahn

In 1951, he was employed at the Wheeler Laboratories, New York, where he was engaged in microwave radar system development. After receiving the M.E.E. degree, he joined the staff of the Microwave Research Institute of the Polytechnic Institute of Brooklyn, N. Y., where he is presently studying general diffraction theory and propagation in multimode waveguides.

Mr. Kahn is a member of Sigma Xi.

George L. Matthaei (S'49–A'52–M'57) was born in Tacoma, Wash., on August 28, 1923. After leaving college for three years of military service, he returned to the University of Washington, Seattle, and received the B.S. degree in electrical engineering in 1948. He then did graduate work at Stanford University, Stanford, Calif., and received the Ph.D. degree in electrical engineering in 1952.

G. L. Matthaei

While at Stanford, he was a research assistant in the Electronics Research Laboratory where he did research on network synthesis. In 1951, he joined the faculty of the Division of Electrical Engineering of the University of California at Berkeley, where he was an assistant professor. He continued research on network synthesis and supervised graduate student research in that field. From 1955 to 1958 he was a member of the technical staff of the Ramo-Wooldridge Corporation, Los Angeles, Calif., and was engaged in system analysis and research on microwave components. In September, 1958, he joined the staff of Stanford Research Institute, Menlo Park, Calif., where he is presently a senior research engineer in the electromagnetics laboratory. His work is concerned with research on microwave components.

Dr. Matthaei is a member of Sigma Xi, Tau Beta Pi, and the Tensor Club of Great Britain.

❖

Kenneth G. Patterson was born in London, England, on February 22, 1925. He studied radio techniques and physics at Queen Mary College, London, from 1944 to 1946.

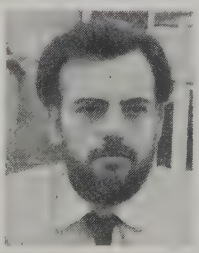

K. G. Patterson

In 1946 he joined the Research Laboratories of the Electrical and Musical Industries, Ltd., Hayes, Middlesex, where he worked on pulse circuitry for television. Since 1952 he has been employed at the Research Laboratories of the General Electric Company, Ltd., North Wembley, Middlesex, working on the development of microwave filters and couplers.

❖

Raymond Redheffer was born on April 17, 1921, in Chicago, Ill. He received the B.S., M.S., and in 1948, the Ph.D. degree from Massachusetts Institute of Technology, Cambridge, Mass.

From 1942 to 1946 at the M.I.T. Radiation Laboratory, and from 1946 to 1948 at the Research Laboratory of Electronics, he was engaged in transmission-line theory and microwave measurement techniques. His interest in antennas led to the design of a machine for computing Fourier transforms which was later built by the Navy.

R. Redheffer

Dr. Redheffer was Benjamin Pierce Instructor at Harvard, Cambridge, Mass., from 1948 to 1950, a National Science Foundation Senior Postdoctoral Fellow at Göttingen, Germany in 1956, and in 1957 he was a Fulbright Research Fellow at Vienna, Austria.

Since 1950 Dr. Redheffer has been an associate professor of mathematics at the University of California at Los Angeles.

❖

Anne Y. Rumfelt (M'57) was born in Washington, D. C., on July 15, 1924. She received the B.S. and M.S. degrees in physics from the University of Michigan, Ann Arbor, in 1946 and 1951, respectively.

A. Y. Rumfelt

She was with the National Bureau of Standards, Washington, D. C., from 1946 to 1950, and with the Research Center of the Minneapolis-Honeywell Regulator Co., Hopkins, Minn., from 1951 to 1953. In 1954, she rejoined the National Bureau of Standards, Boulder, Colo., where she is presently engaged in work on microwave attenuation standards.

Mrs. Rumfelt is a member of the American Physical Society.

❖

George E. Schafer (SM'57) was born in Lincoln, Neb., on April 27, 1922. He received the B.A. degree in physics from Macalester College, St. Paul, Minn., in 1943, the M.A. degree in physics from the University of Minnesota, Minneapolis, in 1949, and the Ph.D. degree in physics from the University of Colorado, Boulder, in 1958.

G. E. Schafer

He served as a weather officer in the Air Force from 1943 to 1946, taught physics from 1948 to 1950, and joined the National Bureau of Standards, Boulder, Colo., in 1951. He is presently engaged in work on microwave attenuation and field-strength standards.

Dr. Schafer is a member of the American

Physical Society, American Association of Physics Teachers, Colorado and Wyoming Academy of Science, RESA, and Sigma Xi.

❖

A. T. Villeneuve (S'52–A'53) was born on March 14, 1930, in Syracuse, N. Y. He received the B.E.E. degree from Manhattan College, New York, N. Y., in June, 1952. From 1952 until 1955 he served as a research assistant at Syracuse University, Syracuse, N. Y., where he received the M.E.E. degree in February, 1955, and the Ph.D. degree in February, 1959. He was an instructor and assistant professor of electrical engineering at Syracuse from 1955 to 1959. At present Dr. Villeneuve is with the Antenna Research Department of the Microwave Laboratory, Hughes Aircraft Company. His experience includes theoretical and experimental work on antennas and microwave devices as well as theoretical research in electromagnetic problems.

A. T. Villeneuve

He is a member of Sigma Xi and Eta Kappa Nu.

❖

Joseph H. Vogelman (M'46–SM'49–F'59) was born in New York City, N. Y., on August 18, 1920. He received the B.S. degree in 1940 from the City College of New York, and received the M.S. and Ph.D. degrees in 1948 and 1957 from the Polytechnic Institute of Brooklyn, N. Y., both in electrical engineering.

J. H. Vogelman

In 1945, after several years at the Signal Corps Radar Laboratory at Ft. Hancock and Belmar, N. J., he joined the staff of the Watson Laboratories in Red Bank, N. J., where he served as chief of the Development Branch until 1951, responsible for research and development of test equipment and microwave components and techniques. In 1951, he moved to the Rome Air Development Center, Griffiss Air Force Base, N. Y. From 1951 to 1953, he was chief scientist in the general engineering laboratory and consultant on UHF and SHF theory and techniques to the U. S. Air Force. From 1953 to 1956, he was chief of the electronic warfare laboratory, directing all research and development in ground based electronic warfare for the USAF. From 1956 to June, 1959 he has been technical director of the Communications Directorate with responsibility for the Air Force research and development effort in ground based and ground to air communications. He is now director of research and development at Dynamic Electronics—New York, Inc.

Dr. Vogelman is a Fellow of the American Association for the Advancement of Science, a member of Eta Kappa Nu, Sigma Xi, the AIEE, and the Armed Forces Communications and Electronics Association.

Call for Papers for 1960 PGMTT Symposium

On May 9–11, 1960, at the Coronado Hotel, Coronado (San Diego), Calif., the IRE Professional Group on Microwave Theory and Techniques will hold the 1960 PGMTT National Symposium. The San Diego Chapter will be the sponsoring host.

Prospective authors are requested to submit papers in the areas related to:

Microwave Components
Microwave Systems
Microwave Physics.

One-hundred-word abstracts in triplicate and 500-word summaries in triplicate should be sent before January 15, 1960 to:

Dr. David B. Medved, *Chairman*
Technical Program Committee
1960 PGMTT Symposium
Convair, A Division of General Dynamics
Mail Zone 6-172
P. O. Box 1950
San Diego 12, Calif.

All papers are to be submitted in English. Authors should advise the Technical Program Committee if any paper will have been presented elsewhere or published prior to the symposium.

The 1960 Symposium Committee Chairmen are:

Chairman—D. Proctor Convair, Astronautics, Division of General Dynamics
Financial Chairman—B. I. Small, Naval Electronics Laboratory
Technical Program—D. B. Medved, Convair, Division of General Dynamics
Facilities—H. D. Dickstein, Convair, Division of General Dynamics
Records Chairman—W. E. Moore, Convair, Division of General Dynamics
Publicity—H. B. Babbitz, Convair, Division of General Dynamics
Women's Activities Chairman—Mrs. E. K. Abbey.

Index to
IRE Transactions
on
Microwave Theory and
Techniques
Volume MTT-7, 1959

IRE Transactions on Microwave Theory and Techniques

Index to Volume MTT-7, 1959

Contents

Volume MTT-7, Number 4, October, 1959

Index to Authors

Index to Subjects

NOTICE TO ADVERTISERS

•

Effective immediately the IRE TRANSACTIONS ON MICROWAVE THEORY AND TECHNIQUES will accept display advertising. For full details contact Tore N. Anderson, Advertising Editor, PGMTT TRANSACTIONS, 1539 Deer Path, Mountainside, N.J.

AVAILABLE BACK ISSUES OF IRE TRANSACTIONS ON MICROWAVE THEORY AND TECHNIQUES

Publication	Prices		
	Group Members	IRE Members	Non-* Members
Vol. MTT-2, No. 3, Sept., 1954	$1.10	$1.65	$3.30
Vol. MTT-3, No. 1, Jan., 1955	$1.50	$2.25	$4.50
Vol. MTT-3, No. 4, July, 1955	$1.60	$2.40	$4.80
Vol. MTT-4, No. 1, Jan., 1956	$1.65	$2.45	$4.95
Vol. MTT-4, No. 3, July, 1956	$1.25	$1.85	$3.75
Vol. MTT-4, No. 4, Oct., 1956	$1.85	$2.75	$5.55
Vol. MTT-5, No. 2, April, 1957	$1.90	$2.85	$5.70
Vol. MTT-5, No. 3, July, 1957	$1.15	$1.70	$3.45
Vol. MTT-5, No. 4, Oct., 1957	$1.20	$1.80	$3.60
Vol. MTT-6, No. 1, Jan., 1958	$2.65	$3.95	$7.95
Vol. MTT-6, No. 2, April, 1958	$2.50	$3.75	$7.50
Vol. MTT-6, No. 3, July, 1958	$2.00	$3.00	$6.00
Vol. MTT-6, No. 1, Oct., 1958	$2.50	$3.75	$7.50
Vol. MTT-7, No. 1, Jan., 1959	$3.75	$5.60	$11.25
Vol. MTT-7, No. 2, April, 1959	$2.20	$3.30	$6.60
Vol. MTT-7, No. 3, July, 1959	$1.65	$2.45	$4.95

*Colleges, Universities, Subscription Agencies, and All Libraries may purchase at IRE Member rate.

THERE'S MORE TO A D-B BROADBAND WAVEMETER THAN JUST THE DIAL!

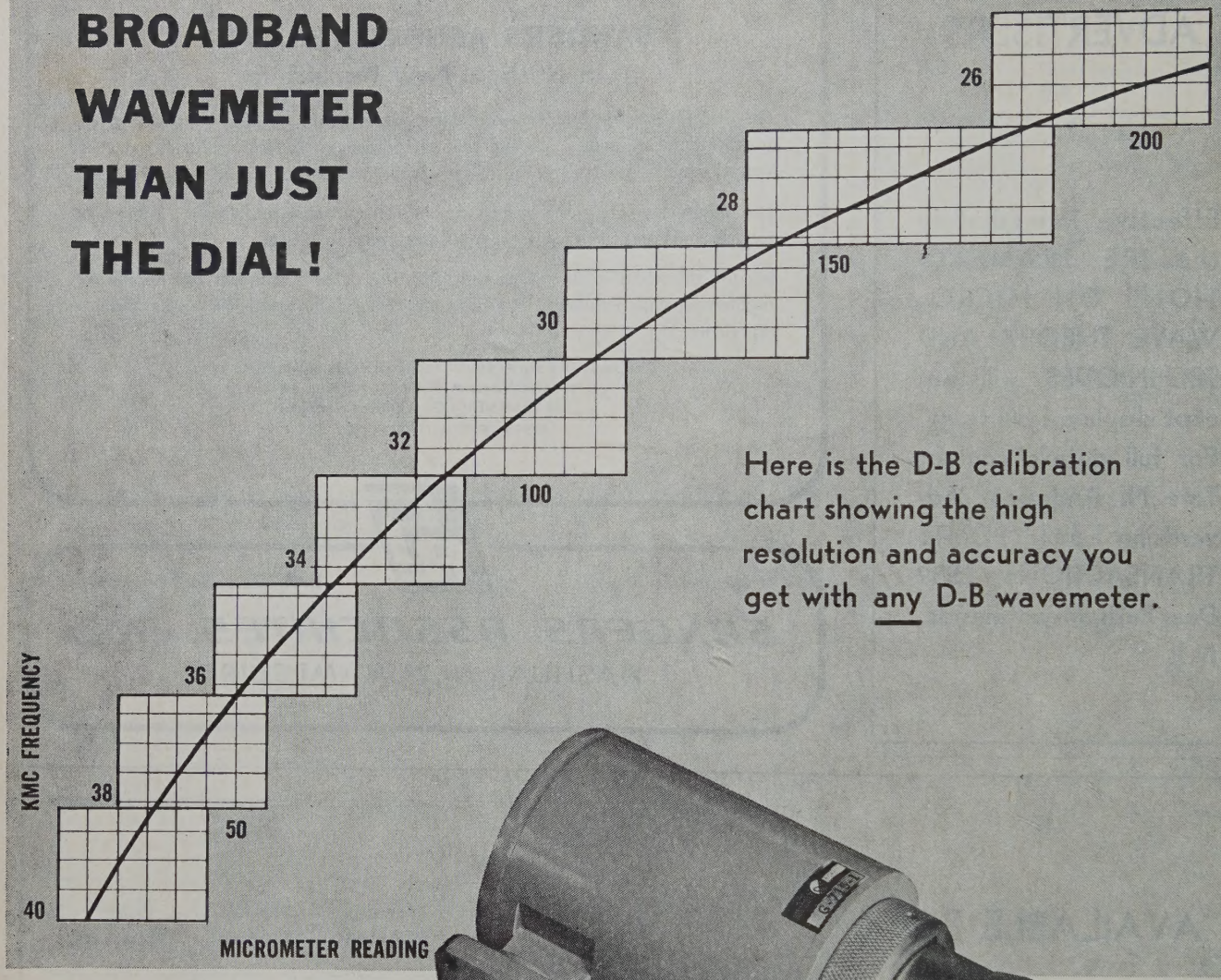

Here is the D-B calibration chart showing the high resolution and accuracy you get with any D-B wavemeter.

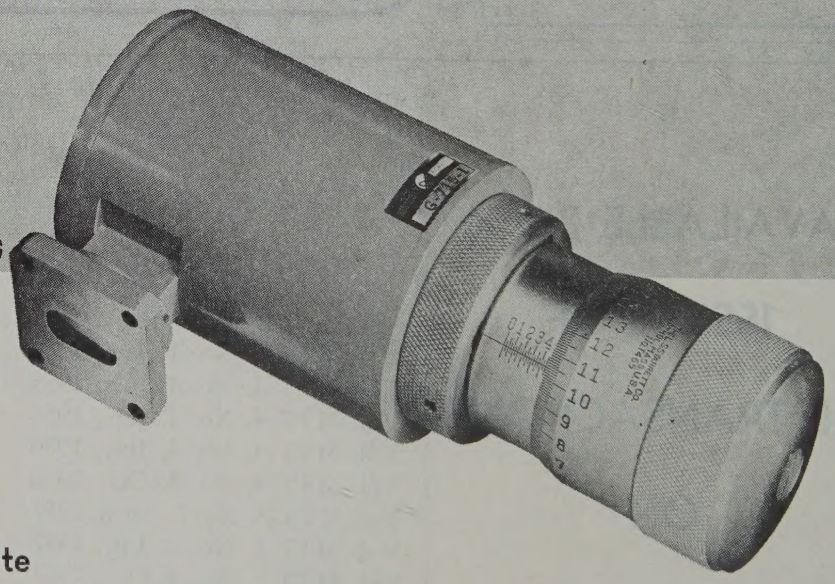

Twelve models cover from 2.6 KMC to 140 KMC. Write for complete data in Bulletin D-B 715.

DE MORNAY BONARDI

DE MORNAY-BONARDI

780 SOUTH ARROYO PARKWAY • PASADENA, CALIF.

INSTITUTIONAL LISTINGS

The IRE Professional Group on Microwave Theory and Techniques is grateful for the assistance given by the firms listed below, and invites application for Institutional Listing from other firms interested in the Microwave field.

AIRTRON, INC., A Division of Litton Industries, 200 East Hanover Ave., Morris Plains, N.J.
Designers and Producers of Complete Line of Microwave Electronic and Aircraft Components

COLLINS RADIO CO., Texas Division, Dallas, Tex.
Complete Microwave and Transhorizon Communication Systems

ITT LABORATORIES, 500 Washington Ave., Nutley 10, N.J.
Line-of-Sight and Over-the-Horizon Microwave Systems; Test Equipment and Components

LITTON INDUSTRIES, Electron Tube Div., 960 Industrial Rd., San Carlos, Calif.
Magnetron, Klystrons, Carcinotrons, TWT's, Backward Wave Oscillators, Gas Discharge Tubes, Noise Sources

MICROWAVE CHEMICALS LABORATORY, INC., 282 Seventh Ave., New York 1, N.Y.
Single Crystals and Polycrystalline Y.I.G. and Related Ferrites Designed for Your Devices

MICROWAVE DEVELOPMENT LABS., INC., 92 Broad St., Babson Park 57, Mass.
Designers, Developers and Producers of Microwave Components and Assemblies, 400 mc to 70 kmc

WHEELER LABORATORIES, INC., Great Neck, N.Y.; Antenna Lab., Smithtown, N.Y.
Consulting Services, Research & Development, Microwave Antennas & Waveguide Components

The charge for an Institutional Listing is $50.00 per issue or $140.00 for four consecutive issues. Applications for Institutional Listings and checks (made out to the Institute of Radio Engineers) should be sent to Tore N. Anderson, PGMTT Advertising Editor, 1539 Deer Path, Mountainside, N.J.

NOTICE TO ADVERTISERS

Effective immediately the IRE TRANSACTIONS ON MICROWAVE THEORY AND TECHNIQUES will accept display advertising. For full details contact Tore N. Anderson, Advertising Editor, PGMTT TRANSACTIONS, 1539 Deer Path, Mountainside, N. J.

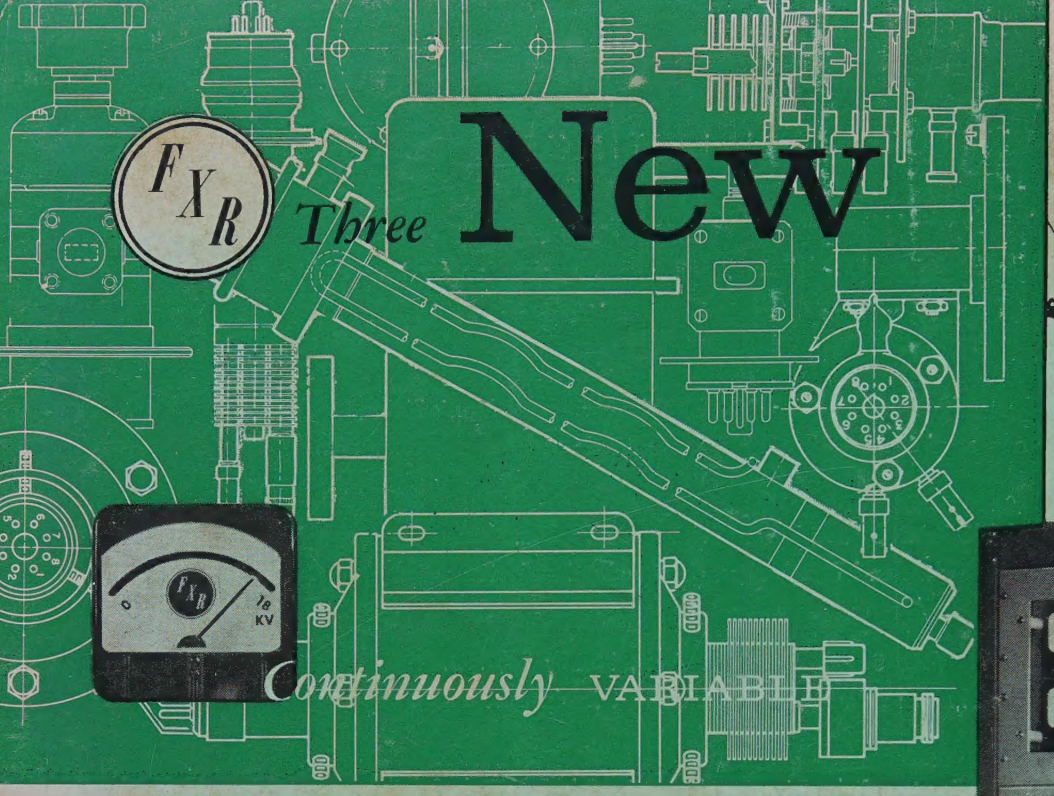

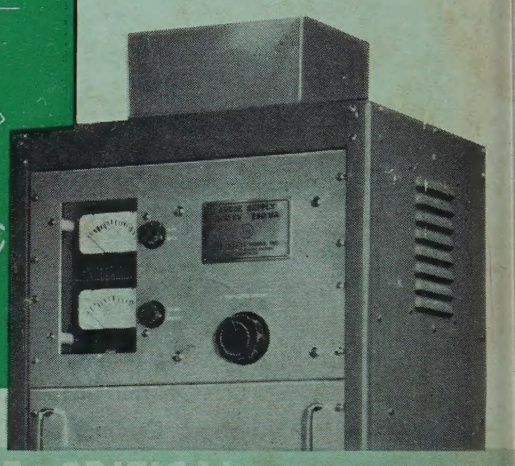

WHERE PERFORMANCE STANDARDS ARE CRITICAL...

HIGH-VOLTAGE REGULATED POWER SUPPLIES*

- EXCEPTIONAL REGULATION—BETTER THAN 0.1% WITH A 10% FLUCTUATION OF PRIMARY POWER.
- LOW RIPPLE.
- BUILT-IN FOCUS, FILAMENT AND MAGNET SUPPLIES.
- RF INSULATION TECHNIQUES INCORPORATED TO MINIMIZE PICK-UP AND CORONA NOISE.

1 *FXR Model Z850A*
- 0 to 12 KV
- 150 MA
- Ripple, 4 MV

2 *FXR Model Z851A*
- 0 to 10 KV
- 250 MA
- Ripple, 5 MV

3 *FXR Model Z852A*
- 0 to 18 KV
- 1 AMP
- Ripple, 5 MV

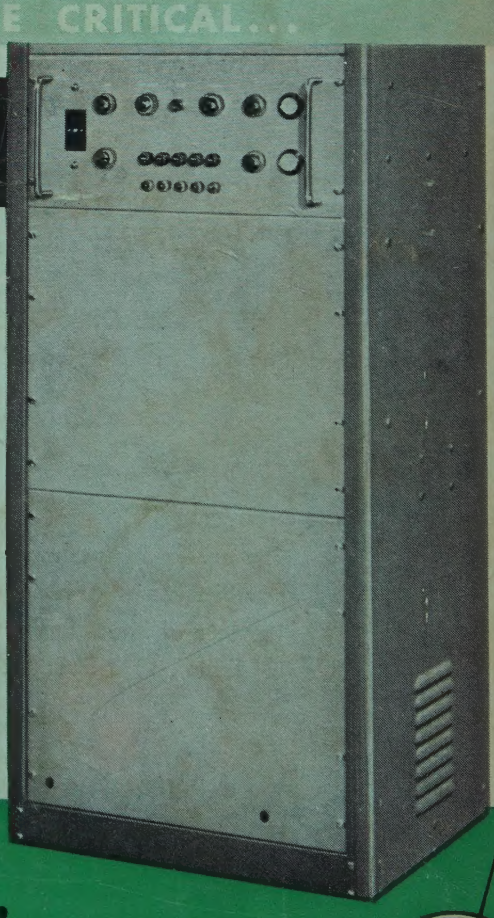

shown here, FXR Model Z850A

* Newest representatives of FXR's commercial line of high-voltage power supplies.

WRITE OR CALL TODAY.

FXR, Inc.

formerly F-R MACHINE WORKS, Inc.

DESIGN • DEVELOPMENT • MANUFACTURE •

26-12 BOROUGH PLACE
WOODSIDE 77, N. Y.
Phone: AStoria 8-2300

FXR pioneers in the design and manufacture of custom and standard high-power pulse modulators.

PRECISION MICROWAVE EQUIPMENT • HIGH-POWER MODULATORS • RADAR COMPONENTS • ELECTRONIC TEST EQUIPMENT